# A study of CD4+ follicular helper T cells in the follicular lymphoma microenvironment and normal germinal centres

Townsend, William Mathew

*Awarding institution:*
King's College London

# A study of CD4+ follicular helper T cells in the follicular lymphoma microenvironment and normal germinal centres

MD Thesis

William Mathew Townsend

Student number: 1255904

First Supervisor: Dr Andrea Pepper

Second Supervisor: Professor Stephen Devereux

## Abstract

Follicular lymphoma is a common B cell malignancy which usually follows an indolent course but it is a heterogeneous disease and there are no biomarkers that can accurately predict outcome or prognosis at the time of diagnosis. There is now clear evidence that the microenvironment plays an important role in the pathogenesis of this disease and the composition of the microenvironment has been linked to prognosis with variable results. The biological basis for the influence of the microenvironment and the contribution of individual cell types remain unclear. In this research we focus on CD4+ T cell subsets, in particular T follicular helper cells and characterise their number, phenotype and distribution in follicular lymphoma with comparisons to normal germinal centres in reactive lymph nodes. We also investigate if T follicular helper cells have a role in promoting B cell proliferation, and induction of AID, whether B and T cells form immunological synapses in follicular lymphoma, and if there is evidence of antigen specificity in the T-cell receptor repertoire.

## Acknowledgements:

This research was funded by grants awarded by Bloodwise and The British Society for Haematology in conjunction with The Roger Counter Foundation. I would like to thank the funders for supporting our vision.

I am so grateful to many people who have helped me to perform and complete this work.

I could not have done this work without the support of my wife Jo and our wonderful children Annie and Rose who were born during the time I worked on this. Thank you for your patience with me while I spent long hours working on this.

Steven Devereux and Andrea Pepper have been fantastic supervisors and I thank them in particular for their work, advice, inspiration, friendship and guidance. I also thank the many friends and colleagues that I met whilst working at the Rayne Institute for the help and advice they gave me as well as their friendship and endless supply of coffee and cakes.

Lastly I thank Prof Duncan and Mr McEvoy and their teams at Queen Square who got me well again which allowed me to complete this work.

# Contents

**Table of Figures:**

**Table 0-1 List of abbreviations**

| Abbreviation | Meaning |
|---|---|
| AID | Activation Induced Cytidine Deaminase |
| BCL2 | B cell lymphoma 2 |
| BCR | B cell receptor |
| BTK | Bruton's Tyrosine Kinase |
| CHOP | Cyclophosphamide Doxorubicin Vincristine Prednisolone |
| CI | Confidence Interval |
| cHL | Classical Hodgkin Lymphoma |
| CLL | Chronic Lymphocytic Leukaemia |
| CR | Complete remission |
| cSMAC | central supramolecular activation cluster |
| CSR | Class Switch Recombination |
| CVP | Cyclophosphamide Vincristine Prednisolone |
| DAPI | 4',6-diamidino-2-phenylindole dihydrochloride |
| DLBCL | Diffuse Large B cell Lymphoma |
| EFS | Event free survival |
| FDC | Follicular Dendritic Cell |
| FDG-PET | Fluorodeoxyglucose positron emission tomography |
| FFPE | Formalin Fixed Paraffin Embedded |
| FISH | Fluorescence In Situ Hybridisation |
| FL | Follicular Lymphoma |
| FLIPI | Follicular lymphoma prognostic index |
| FOXP3 | Forkhead Box Protein 3 |
| GC | Germinal Centre |
| GEP | Gene expression profile |
| HPF | High Power Field |
| HR | Hazard Ratio |
| ICOS | Inducible co-stimulator |
| IGH | Immunoglobulin Heavy Chain |
| IHC | Immunohistochemistry |
| LDH | Lactate dehydrogenase |
| LUT | Look Up Table |
| MALT | Mucosa Associated Lymphoid Tissue |
| MHC | Major Histocompatibility Complex |
| NHL | Non Hodgkin Lymphoma |
| OS | Overall survival |
| PBS | Phosphate buffered saline |
| PCR | Polymerase Chain Reaction |
| PD1 | Programmed Cell Death 1 |
| PFS | Progression free survival |
| PI3K | Phosphatidylinositol-4,5-bisphosphate 3-kinase |
| PKC-θ | protein kinase c theta |
| PMT | photomultiplier tube |
| PR | Partial remission |

| | |
|---|---|
| pSMAC | peripheral supramolecular activation cluster |
| ROI | Region of interest |
| SHM | Somatic Hypermutation |
| TAM | Tumour associated macrophages |
| TBS | Tris buffered saline |
| TCR | T cell receptor |
| $T_{FH}$ | T Follicular Helper Cell |
| $T_{FR}$ | T follicular regulatory cell |
| $T_{reg}$ | T regulatory cell |
| TTF | Time to treatment failure |
| TTP | Time to progression |
| ULN | Upper limit of normal |
| W&W | Watch and Wait |
| WHO | World Health Organisation |
| β2MCG | Beta 2 microglobulin |

# Chapter 1 Introduction

## 1.1 Follicular Lymphoma

### 1.1.1 Introduction to follicular lymphoma

Follicular lymphoma (FL) is the second commonest subtype of non-Hodgkin lymphoma (NHL) worldwide accounting for approximately 20% of all lymphoma diagnoses (Harris, Swerdlow et al. 2008) with an annual incidence of approximately 1800 new cases in the UK per year (Haematological Malignancy Research Network 2014). FL is a neoplasm of germinal centre (GC) B-cells typically characterised by the presence of the chromosomal translocation t(14;18)(q32;q21) which leads to deregulation of the proto-ongogene *BCL-2* (Rowley 1988, Harris, Swerdlow et al. 2008). The disease is described as indolent but it is has a highly variable course; whilst some patients never require treatment, rapid progression and the development of refractory disease or histological transformation are all also well recognised and it is difficult to predict outcome or prognosis at the time of diagnosis (Smith 2013). Despite improvements in treatment over recent years, FL remains a largely incurable malignancy. It is increasingly apparent that the driving force for the survival and proliferation of the malignant B cells in FL is not limited to intrinsic events within the tumour cells but is also dependent on signals from, and interactions with non-malignant cells infiltrating the tumour microenvironment.

It is hoped that better understanding of the role of the microenvironment in the pathogenesis of FL will lead to better prognostic markers and ultimately, new targets for therapy.

### 1.1.2 Pathology, immunophenotype, and cytogenetics of follicular lymphoma

FL is a malignancy of GC B cells, it predominantly affects the lymph nodes but the spleen, bone marrow, peripheral blood and other extra-nodal sites can also be involved. The lymph node architecture is typically effaced by enlarged follicles which resemble normal GCs although, in contrast to GCs, the mantle zones are reduced or absent, and the demarcation between highly proliferative

dark zones containing many centroblasts and less proliferative light zones composed mainly of centrocytes is lost and there are fewer tingible body macrophages in FL than in normal GCs (Harris, Swerdlow et al. 2008, Leich, Ott et al. 2011, Kridel, Sehn et al. 2012, Victora and Nussenzweig 2012).

The number of centroblasts – large round cells with prominent nucleoli - counted per high power field (x40 objective) within follicles forms the basis of the histological grading of FL in the World Health Organisation (WHO) classification of tumours of haematopoietic and lymphoid tissues (Table 1-1) (Harris, Swerdlow et al. 2008). Grades 1-2 are considered the same in terms of clinical outcome and are treated identically; accordingly there is no distinction between grade 1 and 2 disease in the current classification system. Grade 3 FL is separated into grade 3a and grade 3b, in grade 3b FL the FDC network is absent and there are solid sheets of centroblasts with no centrocytes present, whereas in grade 3a disease, the FDC networks are disrupted and occasional centrocytes are retained. Clinical evidence suggests that the outcome of grade 3a FL is similar to that of grade 1-2 disease and it is managed in the same way (Wahlin, Yri et al. 2012). Grade 3b FL, however, has an aggressive course analogous to DLBCL and is clinically treated as such (Salaverria and Siebert 2011). 80-90% of all cases of FL are grade 1-2. The bone marrow is involved in approximately 50% of patients and the pattern of infiltration is characteristically paratrabecular (Solal-Celigny, Roy et al. 2004).

**Table 1-1 World Health Organisation Grading of Follicular Lymphoma**

| Grading | Definition |
|---|---|
| **Grade 1-2 (low grade)*** <br>- Grade 1 <br>- Grade 2 | **0-15 centroblasts per hpf** <br>- 0-5 centroblasts per hpf <br>- 6-15 centroblasts per hpf |
| **Grade 3** <br>- Grade 3a <br>- Grade 3b | **>15 centroblasts per hpf** <br>- Centrocytes present <br>- Solid sheets of centroblasts |
| *Grade 1 and 2 usually reported as “Grade 1-2” <br>If diffuse areas containing >15 centroblasts per HPF are present, the diagnosis is reported as DLBCL with follicular lymphoma. <br>hpf = high power field | |

The malignant B-cells express the B-cell antigens CD19, CD20, CD22, and CD79a and surface immunoglobulin is usually present, typically IgM. The immunoglobulin heavy chain variable genes (IgVH) show ongoing somatic hypermutation reflecting the GC origin of the malignant cells (Leich, Ott et al. 2011). BCL-2 (as a result of the t(14:18) translocation), BCL-6, and CD10 are usually positive. CD5, which is aberrantly expressed on the surface of CLL and mantle cell lymphoma B cells, is not expressed in FL. Of note, BCL-2 is not expressed in the B-cells of normal GCs. The expression of CD10 is variable; expression is stronger in the malignant cells of the follicles than the interfollicular, bone marrow, or peripheral blood malignant cells, similarly, BCL-6 is often low in interfollicular malignant cells (Harris, Swerdlow et al. 2008). Follicular dendritic cells (FDCs) forming meshworks within the follicles can be identified by CD21 or CD23 staining which highlights the follicular structure (Harris, Swerdlow et al. 2008, Kridel, Sehn et al. 2012). The proliferation index, measured by Ki67 staining reflects the histological grade and is typically <20% in grade I-2 FL and >20% in grade 3 disease (Samols, Smith et al. 2013, Kedmi, Hedvat et al. 2014).

The characteristic cytogenetic abnormality in FL is the chromosomal translocation t(14;18) resulting in over-expression of the anti-apoptotic proto-oncogene, *BCL-2* (B-cell lymphoma-2) by bringing it into proximity with the immunoglobulin heavy chain gene on chromosome 14. *BCL-2* is over-expressed in approximately 80-90% of grade 1-2 FL but is less commonly identified in grade 3 disease where other translocations are more often found (Harris, Swerdlow et al. 2008, Leich, Ott et al. 2011). There is considerable variation in the reported incidence of *BCL-2* negative FL. The difference in reported rates of BCL-2 negativity is in part explained by different mutations in the *BCL-2* gene leading to loss of the epitopes to which the most commonly used immunohistochemistry BCL-2 antibodies react, and when antibodies to alternative epitopes are used, expression can be identified in 20% of cases that were negative with the first antibody (Marafioti, Copie-Bergman et al. 2013). Nevertheless, there remains a small proportion of FL cases in which BCL-2 is not over expressed as there is no translocation involving this gene. Fluorescence *in-situ* hybridisation (FISH) can be used to confirm t(14;18) status although this is not routinely performed in most cases. In some BCL-2 negative cases, 3q27 *BCL-6*

translocations can instead be identified (Marafioti, Copie-Bergman et al. 2013). Further genetic events that have been identified in FL include mutations in the epigenetic modifiers *EZH2*, *CREBBP* and *MLL2*, loss of function mutations in *TNFRSF14*, and mutations in the apoptosis regulator *FAS* (Kridel, Sehn et al. 2012, Shaffer, Young et al. 2012).

### 1.1.3 Pathogenesis of follicular lymphoma

The malignant cells of FL are B cells that form follicles resembling GCs, express the GC markers CD10 and BCL-6, have somatically mutated immunoglobulin variable genes and a gene expression profile of centrocytes or centroblasts. Taken together, these findings demonstrate that FL arises through the malignant transformation of GC-derived B cells (Kuppers 2005, Kridel, Sehn et al. 2012, Shaffer, Young et al. 2012).

The translocation t(14;18) leads to deregulated, constitutive expression of *BCL-2* which gives a strong anti-apoptotic signal to the B cells so promoting their survival. This occurs as a result of defective RAG-mediated VDJ recombination leading to a double stranded break at the immunoglobulin heavy chain gene (IGH) on chromosome 14 and a break in the *BCL-2* locus on chromosome 18. Given that VDJ recombination occurs early in normal B cell development in the bone marrow, it is thought that this first step in the development of FL occurs at an early phase of naïve B cell development in the bone marrow (Kuppers 2005, Kridel, Sehn et al. 2012). It is proposed that naïve B cells carrying the t(14;18) translocation and therefore over-expressing BCL-2, leave the bone marrow and migrate to secondary lymphoid organs where they are able to undergo the GC reaction in the same way as normal B cells. Normal GC B cells do not express BCL-2, and die by apoptosis if their B cell receptor (BCR) is non-functional. B cells with t(14;18) fail to undergo apoptosis and therefore have a survival advantage over normal B cells (Roulland, Faroudi et al. 2011).

Although the t(14;18) translocation leads to failure of apoptosis of B-cells, there is evidence that this alone is not sufficient to lead to the development of FL. Firstly, circulating peripheral blood mononuclear cells (PBMCs) carrying the t(14;18) translocation with the same breakpoints as seen in

FL can be identified in healthy individuals who have no evidence of FL (Limpens, Stad et al. 1995, Schuler, Dolken et al. 2009, Roulland, Kelly et al. 2014). The reported incidence is between 50% and 70% of normal populations with the translocation identified by PCR in approximately 1 in $10^5$ circulating PBMCs, the frequency of this increases with age (Rabkin, Hirt et al. 2008, Schuler, Dolken et al. 2009, Hirt, Weitmann et al. 2013). Evidence from transgenic mouse models also indicates that the t(14;18) translocation is insufficient to cause FL. In mice with the *IgH-BLC-2* fusion onco-gene, B cell expansion and lymphoid hyperplasia were seen, but overt FL did not develop. Some mice did however develop high grade NHL but additional cytogenetic abnormalities such as *c-myc* translocations were identified in these mice, suggesting that a second 'hit' after t(14:18) is required for the development of lymphoma (McDonnell and Korsmeyer 1991). Further evidence that the t(14;18) translocation is in itself insufficient to lead to the development of FL comes from the observation that over-expression of BCL-2 cannot be identified in some cases of FL, even when different antibodies and FISH studies are used, see section 1.1.2 above.

Until recently, an increased pre-disposition to FL was not described in healthy individuals with circulating t(14;18) cells but a recent study involving 520,000 healthy subjects revealed that people with a high frequency of circulating t(14;18) cells (greater than 1 in $10^4$) had a 23-fold increased risk of subsequently developing FL, sometimes many years later (Roulland, Kelly et al. 2014). The other key observation that emerged from this important study is that the same *IGH-BCL-2* break points were present in the original peripheral blood samples of circulating t(14;18) cells and the tumour biopsies of individuals who subsequently developed FL many years later, so indicating the presence of a 'founder clone' of pre-malignant B cells. The clinical significance of this finding is not yet known and screening for people carrying t(14;18) is neither practical or desirable at present, but these findings clearly support the notion that the t(14;18) translocation is an early step in the complex pathogenesis of FL but that further events or influences are required for the disease to develop.

It has recently been demonstrated that normal B cells undergo multiple cycles of entry and egress to and from GCs (Victora and Nussenzweig 2012). This has led to the suggestion that circulating t(14;18) cells similarly undergo multiple GC cycles and it is during these repeated cycles that they acquire further genetic alterations and mutations leading to the development of FL under the influence of activation induced cytidine deaminase (AID), the enzyme required for class switch recombination and somatic hypermutation (Roulland, Sungalee et al. 2013, Sungalee, Mamessier et al. 2014). AID has previously been shown in a mouse model to be important for the development of GC derived lymphomas and has also been implicated in the transformation of FL to high grade disease indicating that it plays an important role in disease development (Pasqualucci, Bhagat et al. 2008, Pasqualucci, Khiabanian et al. 2014). See section 1.2 below.

The pathophysiology of histological transformation is poorly understood but is likely to involve genetic and epi-genetic events as well as involvement of the microenvironment. In many cases, transformation involves the accumulation of additional cytogenetic mutations through clonal evolution. Additional mutations in transformed disease typically involve cell cycle regulation or DNA damage responses and include upregulation of *MYC*, mutation of *TP53,* genetic or epigenetic inactivation of the CDKN2A/p16 tumour suppressor gene, or additional translocations involving *BCL-6* (Pasqualucci, Khiabanian et al. 2014). There is also evidence to support a role for the microenvironment in inducing transformation, for example, a predominantly follicular location of FOXP3+ T regulatory cells has been identified as a risk factor for the development of transformed disease in one study (Farinha, Al-Tourah et al. 2010). Furthermore, aberrant somatic hypermutation, mediated by AID has been implicated in some cases of transformation (Pasqualucci, Khiabanian et al. 2014).

As with some other forms of lymphoma e.g. mucosa associated lymphoid tissue (MALT) lymphomas, there is indirect evidence that chronic infection may play a role in the development of FL. The evidence for antigenic activation includes the identification of auto-reactive BCRs in some patients with FL,

somatic hypermutation with a pattern consistent with antigenic selection, and the generation of carbohydrate-linking motifs (Coelho, Krysov et al. 2010, Ame-Thomas and Tarte 2014).

There is now a large body of evidence that supports the hypothesis that the tumour microenvironment has an important role in the pathophysiology of FL. This is discussed in detail in section 1.6 below.

### 1.1.4 Epidemiology

The median age at time of diagnosis of FL is 64 years and it is rare in childhood, it has an approximately equal sex distribution (Harris, Swerdlow et al. 2008). There is considerable geographical variation in incidence; in Europe and North America, FL is the 2$^{nd}$ commonest lymphoma after DLBCL but in Asia the incidence is up to 10 times lower. There are approximately 1800 new cases per year (or 3.1 per 100,000 population) in the UK (Haematological Malignancy Research Network 2014). The long natural history of the disease, and increasing survival give rise to a high prevalence which is likely to increase further as outcomes continue to improve and as the population ages (Sant, Minicozzi et al. 2014).

### 1.1.5 Clinical features

FL is often described as 'indolent', or 'low-grade'. This reflects the slow rate of progression observed in the majority of cases and the fact that some patients do not require treatment for many years after diagnosis. It is known from studies of untreated asymptomatic patients that up to 19% of patients with asymptomatic advanced stage disease never require therapy and spontaneous remissions in untreated patients are also well recognised (Horning and Rosenberg 1984, Ardeshna, Smith et al. 2003). However, the indolent label can be misleading as the disease progresses rapidly in some patients and it belies the fact that, for most patients, FL is an incurable condition characterised by responses to initial therapy but with inevitable relapses. Both the response rate and length of remissions are observed to decline with subsequent lines of therapy and in many cases the disease ultimately becomes refractory to further therapy or transforms to high grade disease (Johnson, Rohatiner et al. 1995).

Presentation of FL is most commonly with lymphadenopathy which may be asymptomatic or may cause local symptoms or rarely (compared to high grade disease) organ compromise. In the largest retrospective review of patients which included 4167 patients enrolled in clinical trials, 78% had advanced stage, 22% early stage, 19% had constitutional 'B' symptoms (weight loss, night sweats or fever), 52% had bone marrow involvement, and 38% had areas of extranodal disease (other than bone marrow) (Solal-Celigny, Roy et al. 2004). These clinical characteristics were broadly verified in a prospective review of 942 patients (Federico, Bellei et al. 2009). It should be noted that these characteristics are not wholly representative of all patients presenting with FL as they only included patients who required active treatment and were enrolled in clinical trials.

There is an associated risk of transformation to high grade lymphoma, most commonly DLBCL but occasionally Burkitt Lymphoma. The risk is approximately 3% per year or 15-28% at 10 years (Montoto, Davies et al. 2007). There is considerable variation in the reported rates of transformation in part due to differences in the definition of transformation (whether histologically confirmed or clinically suspected) and variations in clinical practice with regard to performing biopsies to histologically verify transformation. Transformation has a very poor prognosis with a median time from histological transformation to death of 1.2 years in one retrospective study although the outcome for patients treated with contemporary immunochemotherapy is likely to be better than this (Montoto, Davies et al. 2007).

### 1.1.6 Clinical staging and baseline investigations

FL is clinically staged according to the Ann Arbor staging system which was originally devised for the staging of Hodgkin Lymphoma (Lister, Crowther et al. 1989). Stage is determined by the number and distribution of involved lymph nodes, the involvement of extranodal sites of disease and the presence or absence of a number of modifying factors (Table 1-2). Stage I-$II_A$ is early stage disease while $II_B$-IV is classified as advanced stage. Approximately 80-90% of patients present with advance stage disease; accordingly, early stage disease is infrequently seen.

Accurate staging is of vital importance for prognostication and also for planning treatment, especially for determining whether patients with apparent early stage disease are truly early stage, or whether there are any distant lymph nodes or extranodal sites of disease that would lead to upstaging. Staging routinely involves bone marrow biopsy and cross-sectional imaging of the neck, chest, abdomen, and pelvis. Functional imaging by [18F]-fluorodeoxyglucose positron emission tomography (FDG-PET) is increasingly being used, especially in the staging of early stage disease where it has been shown to up-stage (i.e. identify advanced stage disease) 18-30% of patients (Meignan, Barrington et al. 2014).

**Table 1-2 The Ann Arbor Staging system for Lymphoma**

| Stage | Definition |
|---|---|
| I | Involvement of one lymph node region only |
| II | Involvement of 2 or more lymph node regions on the same side of the diaphragm |
| III | Involvement of lymph node regions on both sides of the diaphragm |
| IV | Extranodal involvement beyond that indicated by the subscript 'E' |
| **Subscripts/modifying factors:** | |
| A | Absence of 'B' symptoms |
| B | 'B' symptoms present (weight loss of >10% body weight over 6 months, fever >38$^0$C, or night sweats) |
| E | Direct extranodal spread from an adjacent lymph node that is limited in extent |
| X | Disease bulk (>10cm in maximal diameter, or mediastinal mass >1/3 thoracic diameter) |

### 1.1.7 Predicting prognosis in FL

Determining prognosis in FL is currently based on a number of clinical and laboratory parameters. The most commonly used scoring system is the Follicular Lymphoma International Prognostic Index (FLIPI) which incorporates age (>60 vs. ≤60 years), stage (III-IV vs. I-II), number of involved nodal groups (>4 vs. ≤4), anaemia (Haemoglobin <120g/l vs. ≥120g/l), and serum LDH (>upper limit of normal vs. ≤ upper limit of normal range), see Table 1-3, and Figure 1-1. The FLIPI score was developed from retrospective analysis of data and uses overall survival (OS) as its end point. Patients are divided into 3 risk groups,

low risk (FLIPI 0-1) with 10 year OS of 71%, intermediate risk (FLIPI 2) with 10 year OS 51%, and high risk (FLIPI 3-5) with 10 year OS 36% (Solal-Celigny, Roy et al. 2004). Despite a number of drawbacks, including the fact that the FLIPI score was developed from retrospective data from patients treated before the introduction of rituximab, it remains the most widely used prognostic tool and is useful in clinical trials for describing the distribution of high risk and low risk patients in the population, and therefore allowing comparison of trials in this heterogeneous disease.

**Table 1-3 Overall survival by group defined by the follicular lymphoma international prognostic index (FLIPI).**

| FLIPI Score | Risk Group | Proportion of patients (%) | 5 year overall survival (%) | 10 year overall survival (5%) |
|---|---|---|---|---|
| 0-1 | Low | 36 | 90.6 | 70.7 |
| 2 | Intermediate | 37 | 77.6 | 50.9 |
| 3-5 | High | 27 | 52.5 | 35.5 |

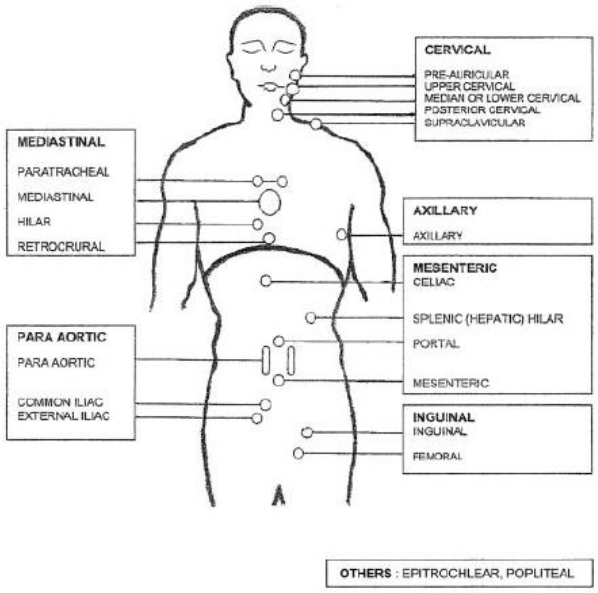


**Figure 1-1 Diagram detailing the number of nodal areas used to calculate the FLIPI score (Figure reproduced from Solal-Celigny, Roy et al. 2004).**

An updated prognostic score, The FLIPI 2, has been developed prospectively using PFS as the primary outcome measure. The FLIPI2 score determines risk according to age (>60 vs. ≤60 years), haemoglobin (<120g/l vs. ≥120g/l), bone marrow infiltration (present vs. absent), β2MCG (>upper limit of normal

(ULN) vs. ≤ULN), and greatest diameter of largest involved lymph node (>6cm vs. ≤6cm). Patients with a FLIPI2 score of 0 are low risk and have a 3-year PFS of 91%, score 1-2 is intermediate risk with a 3-year PFS of 69%, and score 3-5 is high risk with a 3-year PFS of 51% (Federico, Bellei et al. 2009).

It is likely that the mutational status of genes implicated in the pathogenesis of FL will be incorporated into risk stratification systems in the near future. One such approach that has already been proposed is the M7 FLIPI score. In this risk stratification score, the mutational status of 7 genes, *EZH2*, *ARID1A*, *MEF2B*, *EP300*, *FOXO1*, *CREBBP* and *CARD11* are added to a prognostic model that also incorporates the FLIPI score and the patient's performance status. This has been shown to be highly predictive of 5-year failure free survival and overall survival but is not yet in standard clinical practice (Pastore, Jurinovic et al. 2015).

Depth of response to treatment has also been used to provide prognostic information with evidence to show that patients achieving a complete remission (CR) to treatment have significantly longer duration of response than patients achieving only partial remission (PR) (Marcus, Imrie et al. 2008, Bachy, Brice et al. 2010). It is possible that new techniques for determining response including FDG-PET and determining the level of molecular response by quantifying the burden of circulating t(14;18) cells will prove useful in assessing response to treatment and provide prognostic information after first line treatment. However such methods would not provide baseline information at the time of diagnosis to guide initial management decisions.

Therefore there is a need for better predictors of prognosis, to date there are few biological parameters that are useful in this regard (with the exception of haemoglobin, LDH, and β2MCG which are incorporated into the FLIPI and FLIPI2 scores) and it is hoped that better understanding of the tumour microenvironment will allow improved identification of good and poor risk groups; factors in the microenvironment that impact prognosis are discussed below in section 1.6.

### 1.1.8 Current clinical management of FL

Choosing the optimal management for patients with newly diagnosed FL depends on accurate determination of clinical stage and assessing the requirement for active treatment.

#### 1.1.8.1 Treatment of early stage disease

Early stage FL represents only about 20% of all new FL diagnoses. It is important to identify this group of patients because the treatment intent and treatment modality are different to advanced stage disease; whereas it is anticipated that most treatments in advanced stage FL will not be curative, true early stage FL can be cured with radiotherapy alone. The current standard of care for early stage FL is 24 Gray involved field radiotherapy (Hoskin, Kirkwood et al. 2014, Specht 2014). This approach leads to excellent outcomes with 49% PFS at 10 years. If relapse does occur, it typically occurs outside of the original radiotherapy field suggesting that the disease was in fact disseminated at time of treatment but was not detectable, and it is therefore likely that patients with stage I-II disease confirmed by FDG-PET may have better PFS with localised radiotherapy although there is no prospective data to support this. Late relapses beyond 10 years are extremely rare in early stage FL treated with this approach (Campbell, Voss et al. 2010).

#### 1.1.8.2 Treatment of advanced stage asymptomatic disease

For patients with advanced stage disease (stage IIb-IV) who are asymptomatic, there is no proven benefit of early initiation of chemotherapy over observation alone (Ardeshna, Smith et al. 2003). A period of observation or 'watchful waiting' is often employed in asymptomatic patients, withholding treatment until such a time as it is required due to progressive disease, increasing symptoms, or falling peripheral blood counts. Interestingly, when this approach is followed, 19% of patients never require therapy.

The approach of not treating asymptomatic patients was originally adopted due to the failure of treatments to prolong survival and to delay exposure to potentially toxic chemotherapy but, in the modern treatment era where survival is improving and treatments are becoming less toxic (leading to

fewer treatment-related deaths and secondary malignancies) this paradigm is being challenged. In a recent trial, patients with advanced stage, asymptomatic disease were randomised to receive no treatment or the anti-CD20 monoclonal antibody, rituximab alone with no cytotoxic chemotherapy. This demonstrated, perhaps unsurprisingly, that patients receiving single-agent rituximab had a longer time to initiation of next treatment than the observed cohort but longer follow up is required to determine the effect of this on response to subsequent therapies, survival, and other long term outcome measures (Ardeshna, Qian et al. 2014).

#### 1.1.8.3 Treatment of symptomatic advanced stage follicular lymphoma

To determine whether a patient with advanced stage disease needs to start treatment, the GELF (Groupe d'Etude des Lymphomes Folliculaires) criteria are widely used. According to these criteria, patients with any site of disease >7cm in maximal diameter, ≥3 nodal sites each ≥3cm in diameter, B symptoms, splenic enlargement, or cytopenias should be considered for active treatment, whereas patients with none of these factors can often be managed with 'watchful waiting'. These criteria are also frequently used as inclusion criteria in clinical trials of induction therapy to ensure that all patients have a clinical indication to start treatment.

Until 2005, there were no advances in the treatment of advanced stage symptomatic FL that improved overall survival. In 2005 a trial was published that demonstrated a significant improvement in overall survival through the addition of the anti-CD20 monoclonal antibody rituximab to combination chemotherapy. Rituximab has subsequently revolutionised the treatment of FL and other CD20 positive NHLs (Marcus, Imrie et al. 2005).

Rituximab was first demonstrated to have activity in FL when used as a single-agent in the relapsed or refractory setting (Maloney, Grillo-Lopez et al. 1997) and was also found to be highly active as a single agent in the front-line setting where 4 x weekly doses of 375mg/$m^2$ gave an overall response rate of 73% (Colombat, Salles et al. 2001). Subsequent trials assessed the addition of rituximab to existing chemotherapy regimens. Marcus et al demonstrated that the addition of rituximab to CVP

(cyclophosphamide, vincristine and prednisolone) combination chemotherapy in the first-line treatment of advanced stage FL led to significant improvements in all outcome measures assessed including longer time to treatment failure (TTF), CR rate, time to progression (TTP), response duration and OS. The 4-year OS in the R-CVP arm was 83% compared to 77% in the CVP arm (P = 0.029) and this represents a landmark in the treatment of FL, Figure 1-2 (Marcus, Imrie et al. 2005, Marcus, Imrie et al. 2008).

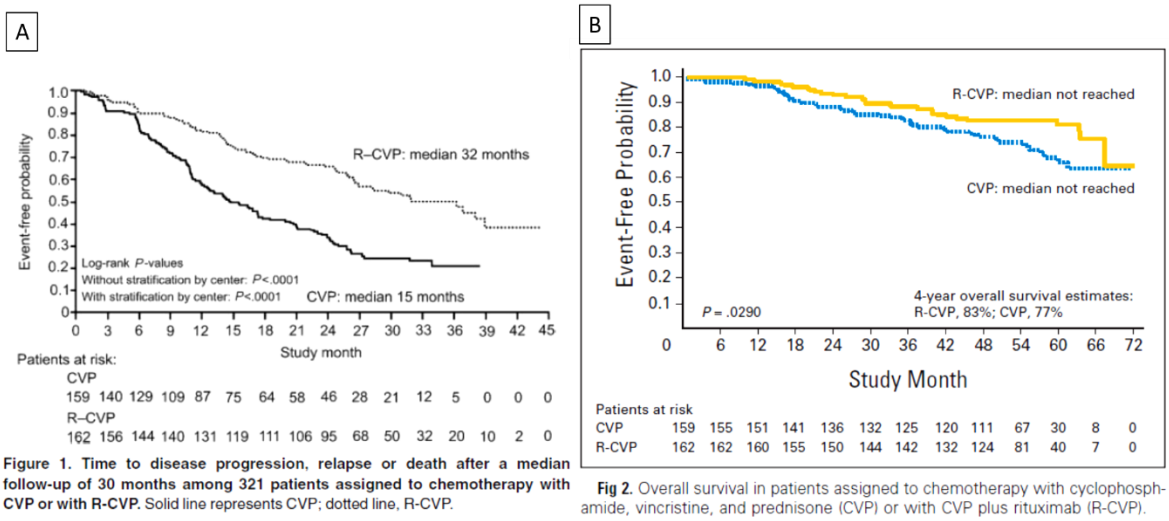


**Figure 1. Time to disease progression, relapse or death after a median follow-up of 30 months among 321 patients assigned to chemotherapy with CVP or with R-CVP.** Solid line represents CVP; dotted line, R-CVP.

**Fig 2.** Overall survival in patients assigned to chemotherapy with cyclophosphamide, vincristine, and prednisone (CVP) or with CVP plus rituximab (R-CVP).

**Figure 1-2 Outcomes from the CVP versus R-CVP trial.** (A) Time to disease progression. (B) Overall survival showing improvement in outcome with the addition of rituximab (Marcus, Imrie et al. 2005, Marcus, Imrie et al. 2008)

Several further studies have conclusively demonstrated the benefit of adding rituximab to chemotherapy with significant improvement in both PFS and OS (Hiddemann, Kneba et al. 2005) (Herold, Haas et al. 2007) (Salles, Mounier et al. 2008). The optimal chemotherapy regimen to use in conjunction with rituximab has until recently been open to debate with little evidence to suggest the superiority of any particular regimen. However, evidence is emerging that treatment with more intensive regimens such as R-CHOP delivers better outcomes than R-CVP and there is data from one randomised trial suggesting that bendamustine in combination with rituximab (BR) may be superior even to CHOP with lower toxicity too. Accordingly, BR has been widely adopted as first line therapy although it should be noted that there is little data on BR followed by rituximab maintenance (Morschhauser, Seymour et al. 2011) (Federico, Luminari et al. 2011, Rummel, Niederle et al. 2013).

As described above, FL is largely incurable with a disease course characterised by recurrent relapses and progressively shorter remissions (Johnson, Rohatiner et al. 1995). This has led to searches for effective ways of maintaining remission in patients who respond to treatment. Previously, maintenance therapy with interferon was found to be partially effective but poorly tolerated and difficult to administer (Baldo, Rupolo et al. 2010). Given its proven efficacy in induction and its favourable toxicity profile, the role of rituximab as maintenance therapy was investigated. It has now been demonstrated that rituximab maintenance is effective at prolonging remissions after initial single agent rituximab (Ghielmini, Schmitz et al. 2004, Martinelli, Schmitz et al. 2010), after CVP chemotherapy (Hochster, Weller et al. 2009), after rituximab-containing chemotherapy (R-CHOP) in the relapsed setting (van Oers, Van Glabbeke et al. 2010), and after rituximab-containing chemotherapy in previously untreated patients (Salles, Seymour et al. 2011).

The landmark trial for rituximab maintenance as part of first line therapy was conducted by the French study group GELA (Group d'Etude des Lymphomes de l'Adulte). In the PRIMA study, 1217 previously untreated patients with advanced stage FL received 1 of 3 rituximab-containing induction regimens with responding patients (1019, 84%) randomised to maintenance rituximab (every 2 months for 2 years) or observation only. At a median of 36 months follow-up, the rate of progression was significantly lower in the maintenance arm, PFS 74.9% vs. 57.6%, HR 0.55 (95% CI 0.44-0.68, $p<0.0001$) Figure 1-3. More patients in the maintenance arm have achieved CR than the observation arm but no difference in OS has been identified to date (Salles, Seymour et al. 2011). This trial has led to the widespread use of rituximab maintenance following first-line treatment with immunochemotherapy.

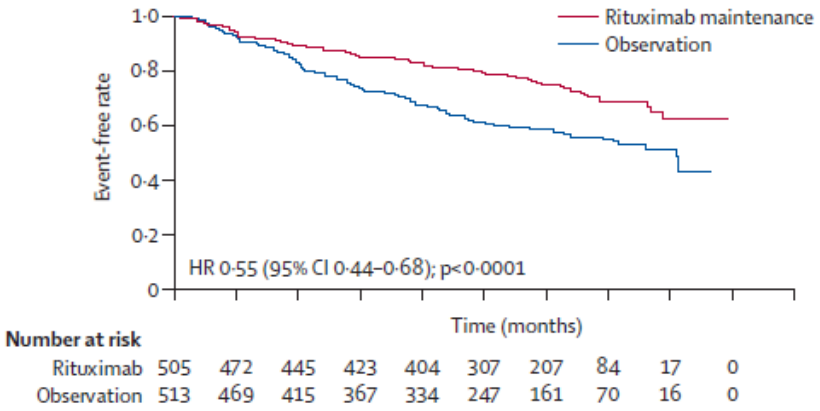


**Figure 1-3 Results of the PRIMA trial.** Improvement in PFS with maintenance rituximab versus observation alone (Salles, Seymour et al. 2011)

High dose therapy followed by autologous stem cell transplantation or allogeneic haematopoietic stem cell transplant are not typically used in first line therapy but are reserved for relapsing patients with aggressive disease who are fit enough (and young enough) to tolerate these intensive treatment strategies (Montoto, Corradini et al. 2013).

#### 1.1.8.4 Novel agents and future treatment strategies

Attempts to improve on the results achieved with rituximab plus chemotherapy followed by rituximab maintenance are ongoing and the aims are twofold; to improve outcome through prolonged PFS and to reduce exposure to cytotoxic agents so reducing short and long term toxicity.

Novel agents that may be added to the rituximab plus chemotherapy backbone include the immunomodulatory agent lenalidomide which may have a role in maintenance, and the proteasome inhibitor bortezomib although the precise place of these agents in the treatment of patients with newly diagnosed FL have not been formally demonstrated at present (Merli, Ferrario et al. 2013, Wang, Fowler et al. 2013, Craig, Hanna et al. 2014, Evens, Smith et al. 2014, Tuscano, Dutia et al. 2014). There are several new anti CD20 monoclonal antibodies that are being assessed in clinical trials including ofatumumab and GA101 (obinutuzumab). Obinutuzumab is a glycoengineered anti CD20 monocloncal antibody, with a different mechanism of action to rituximab; it induces lower levels of complement-dependent cytotoxicity, but greater antibody-dependent cellular cytotoxicity and

phagocytosis, and higher levels of direct B-cell killing. Emerging clinical trial data in low grade NHL and CLL appear to demonstrate superior outcomes with obinutuzumab compared to rituximab although longer follow up will be required to see whether an early PFS advantage translates into an overall survival benefit (Mossner, Brunker et al. 2010, Czuczman, Fayad et al. 2012, Czuczman, Hess et al. 2012, Radford, Davies et al. 2013, Salles, Morschhauser et al. 2013, Cartron, de Guibert et al. 2014, Marcus, Davies et al. 2017).

Exciting results are being achieved in various B cell malignancies by targeting the downstream signalling of the BCR with agents such as the PI3K inhibitor idelalisib or the BTK inhibitor ibrutinib and results from early stage clinical trials of these agents in low grade NHL are very promising (Gopal, Kahl et al. 2014). Inhibition of *BCL-2* with compounds such as the small molecule inhibitor Venetoclax (ABT-199) also shows great promise (Advani, Buggy et al. 2013, Fowler and Davis 2013, Gopal, Kahl et al. 2014, Ng and Davids 2014).

In addition, there are some emerging therapies that directly influence the microenvironment; most applicable to this research is the development of anti-PD1 antibodies such as nivolumab, pembrolizumab, and pidilizumab. Pidilizumab was shown to have considerable clinical efficacy when used in combination with rituximab in patients with relapsed FL perhaps through restoration of the anti-tumour immune response (Westin, Chu et al. 2014). However development of this compound has recently been halted after it was disclosed that its mechanism of action may after all not be through PD-1 inhibition; there is at time of writing uncertainty about this and the implications for the trials already performed using this drug in FL are unclear. The response of FL to PD-1 inhibition with nivolumab is less marked than in classical Hodgkin Lymphoma (Ansell, Lesokhin et al. 2015).

It is highly likely that in the near future, treatment for advanced stage FL will comprise of immunotherapy (rituximab or another anti-CD20 antibody) and novel, non-chemotherapy agents alone or in combination but numerous clinical trials with long follow-up will be required to determine the optimal combinations, doses and duration of these agents in induction and maintenance therapy.

## 1.2 The normal germinal centre reaction

As described in section 1.1.2 above, there are a number of similarities between the physical structure of the malignant follicles found within the involved lymph nodes of patients with FL and normal GCs in reactive lymph nodes and there is good evidence that FL arises from GC-derived B cells.

One of the aims of this research is to investigate to what extent the interactions between malignant B cells and T cells in the FL microenvironment recapitulate the interactions between normal B and T cells in the GC reaction in reactive lymph nodes.

GCs are the site of VDJ recombination, somatic hypermutation (SHM), class switch recombination (CSR), and B cell selection and clonal expansion in response to antigenic stimulation. These are the processes by which the human adaptive immune system is able to produce immunoglobulins highly specific to an almost infinite number of possible antigens. The diversity generated through these mechanisms are far in excess of what would be expected with a relatively limited genome (Victora and Nussenzweig 2012).

In the normal GC reaction, naïve B cells are exposed to antigen by follicular dendritic cells (FDCs) in the secondary lymphoid tissue. On engaging antigen via their BCR, the B cells are activated and the antigen is internalised before being expressed on the cell surface in conjunction with Major Histocompatibility Complex (MHC) class II. GC B cells are critically dependent on specific T cell help for full activation, survival, proliferation and differentiation, see Figure 1-4.

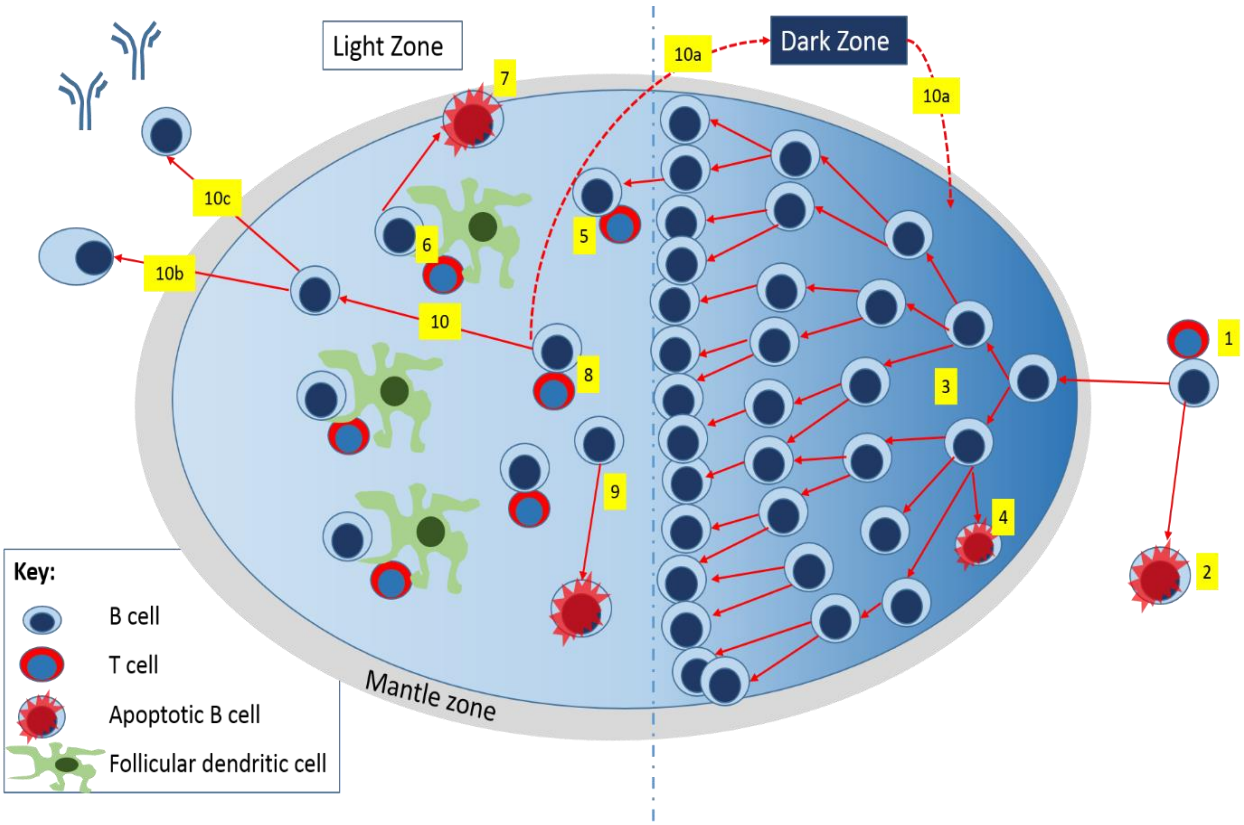


**Figure 1-4 Schematic representation of key events in the germinal centre reaction. Figure made by W. Townsend, adapted from figures in: Victora 2012 and Kuppers 2005.**

1. B cells with the highest affinity for T cells are permitted entry to the GC
2. B cells not expressing a BCR or with low affinity do not enter the GC and undergo apoptosis
3. In the dark zone, B cells rapidly proliferate and undergo somatic hypermutation under the influence of AID
4. B cells with low or absent BCR expression undergo apoptosis
5. Upregulation of the chemokine receptor CXCR5 permits entry to the light zone
6. B cells interact with antigen presented on the surface of follicular dendritic cells
7. B cells with low antigen affinity undergo apoptosis
8. B cells present antigen to a limiting number of CD4+ helper T cells. B cells with the highest antigen affinity react preferentially at the expense of B cells with lower affinity in a rate limiting step (competitive selection)
9. B cells not receiving T cell help undergo apoptosis
10. B cells with high affinity and receiving T cell help have 3 potential fates:
    a. Upregulation of CXCR4 permits re-entry to the dark zone where they undergo further rounds of proliferation, mutation and selection
    b. Exit from the GC to a plasma cell fate
    c. Exit from the GC to a memory B cell fate

- Note that these processes in the GC reaction are not linear, some B cells undergo many cycles of selection in the light zone and cycling back to the dark zone for further proliferation and mutation of their BCRs in order to expand the repertoire of BCRs and attain B cells of higher affinity.

Within the GC, T helper cells with a specific T cell receptor (TCR) engage B cells via their TCR which recognises the MHC-linked antigenic peptide on the B cell surface. Interaction of the tumour necrosis factor family member CD40 on B-cells with its ligand CD40L expressed on CD4+ T cells provides one of the vital co-stimulatory signals that the B cells require. The importance of T cells to the GC reaction and therefore to the generation of high affinity antibody in response to antigen is highlighted by the observations from mouse models that athymic mice are unable to produce GCs and that blockade of CD40-CD40L interaction leads to termination of the GC reaction (Victora and Nussenzweig 2012). In humans, loss-of-function mutations in CD40 or CD40L lead to failure of GC reactions and low-affinity, non-class-switched antibody responses with accompanying high susceptibility to infections (Allen, Armitage et al. 1993, Ferrari, Giliani et al. 2001, Victora and Nussenzweig 2012).

The interaction of antigen-expressing B cells with a specific subset of CD4+ helper T cells, T follicular helper cells ($T_{FH}$) promotes B cell survival, proliferation, SHM, and CSR to generate the high-affinity response to the antigenic stimulus.

Central to the process of generating a repertoire of B cells with a vast range of BCR specificities are the processes by which the genes encoding the BCR of naïve B cells in the GC undergo rearrangement. The key regions to the genes encoding the BCR are the Variable, Diversity, and Joining regions (V,D, and J). Initial diversity of the BCR is generated through the multitude of different combinations of these regions under the control of recombination activation genes (RAG), but this leads only to a relatively limited repertoire of BCRs, limited by the number of genes encoding each V,D, and J regions. Further diversity is generated through somatic hypermutation (SHM) of those B cells with the highest affinity after VDJ recombination in a process called affinity maturation. SHM, and class switch recombination occur under the influence of the DNA modifying enzyme AID in the dark zone of GCs. AID deaminates cytidine residues to uracyl in single strand DNA in the variable region at a very high frequency. This unique process leads to the generation of a vast number of different BCRs so that, by

chance it is likely that some BCRs with very high affinity for the antigen will be generated, the B cells expressing the highest affinity BCRs are then selected to proliferate.

Because AID leads to breaks in DNA, its' off-target action has been proposed to lead to mutations in genes other than immunoglobulin variable regions or double stranded breaks leading to translocations, both of which have been implicated in lymphomagenesis (Pasqualucci, Bhagat et al. 2008, Nussenzweig and Nussenzweig 2010).

GCs can be clearly identified on conventional histology of secondary lymphoid tissue and it is possible to visually distinguish two discrete zones within the GC on haematoxylin and eosin stained sections; a dark zone where B cells undergo rapid proliferation and expansion and a light zone composed mainly of non-proliferating centrocytes and antigen-presenting FDCs.

It is now apparent that GCs are dynamic structures and the GC B cells migrate between the dark and light zones, furthermore there is also evidence that the GC T cells are able to migrate both within and between GCs (Shulman, Gitlin et al. 2013). In the light zone, they bind antigen and present it together with MHC class II to $T_{FH}$ cells (see below). GC B cells with high-affinity BCRs receive help signals from $T_{FH}$ cells and migrate from the light zone to the dark zone of the GC where they proliferate and undergo SHM and CSR under the influence of AID. After undergoing SHM and CSR, the GC B cells then migrate back to the light zone for further interaction with $T_{FH}$ cells, to select those B cells with highest affinity BCRs. The B cells with highest affinity BCRs receive further 'help' from $T_{FH}$ cells to undergo further proliferation, mutation and additional selection to continually ensure that only the highest affinity B cells are selected, Figure 1-4.

Through these repeated rounds of selection, proliferation and mutation under $T_{FH}$ cell help and control, a high affinity antibody response is generated (Victora and Nussenzweig 2012, Shulman, Gitlin et al. 2013).

## 1.3 T follicular helper cells

The ability to mount a rapid and effective immune response on exposure to a novel or previously identified antigen is pivotal to the human adaptive immune system (Crotty 2014).

As described above, GCs are essential structures at the centre of the adaptive immune system where B cells undergo somatic hypermutation, class switch recombination, selection and ultimately proliferation. Central to this process is interaction between B cells and CD4+ T cells, and without T cell help, the GC reaction would fail, antibody production would be non-specific and there would be heightened susceptibility to infection (Allen, Armitage et al. 1993, Ferrari, Giliani et al. 2001, Victora and Nussenzweig 2012, Crotty 2014).

Follicular helper T cells ($T_{FH}$) are highly specialised CD4+ T cells usually restricted to the follicles of secondary lymphoid tissue, they are essential for providing B cell help and for propagating the GC reaction.

Differentiation of naïve T cells to $T_{FH}$ is dependent on cognate interaction with B cells and there is evidence that the quality of this interaction determines differentiation of naïve CD4+ T cells into $T_{FH}$ with only those T cells with highest antigen affinity developing into $T_{FH}$ (Fazilleau, Mark et al. 2009). The differentiation of naïve T cells remains only partially understood and much remains to be elucidated to fully understand this complex process (King 2009, Crotty 2014).

It is increasingly apparent that the relationship between $T_{FH}$ cells and GC B cells is mutually beneficial; without GC B cells presenting antigen in conjunction with MHC class II, naïve T cells would not receive signals for differentiation to a $T_{FH}$ phenotype. Likewise, without $T_{FH}$ cell help, GC B cells would not survive and proliferate. It has been shown that GC size is correlated with the availability of $T_{FH}$ cell help, and the amount of $T_{FH}$ cell help may therefore be a critical rate-limiting step in the GC reaction (Rolf, Bell et al. 2010, Victora and Nussenzweig 2012).

### 1.3.1 $T_{FH}$ phenotype

There is no single antigen or transcription factor that identifies $T_{FH}$ cells, instead they can only be identified by the presence or absence of a combination of cell surface proteins and transcription factors. They have a complex phenotype and are characterized by very high surface expression of the T cell inhibitory protein, programmed cell death 1 (PD1, PDCD1, CD279), the CD28 family member ICOS (T-cell inducible costimulatory molecule), the chemokine receptor CXCR5, and the transcription factor B cell lymphoma 6 (BCL6). Additionally they express the chemokine CXCL13, and the growth factors IL-21 and IL-4.

The reason for, or cause of the very high level of surface expression of programmed cell death 1 (PD1 - CD279), an immunoreceptor tyrosine-based inhibitory motif (ITIM) - containing inhibitory molecule on $T_{FH}$ cells is not fully understood at present (King 2009). One theory for the high level expression of this immunomodulatory protein is that it may regulate and slow the rate of $T_{FH}$ cell proliferation in GCs upon TCR signalling (Crotty 2014). T cells within the GC are constantly exposed to antigen and would ordinarily proliferate on TCR activation but since one of the primary functions of GCs is to promote B cells to rapidly proliferate, the $T_{FH}$ cells present within the GCs may express high levels of PD1 to slow their own rate of proliferation. Without PD1 expression, $T_{FH}$ cells would potentially proliferate uncontrollably which could have a detrimental effect on the ability to mount an effective adaptive immune response to antigen challenge (Crotty 2014).

PD1 expression is not unique to $T_{FH}$ cells and has previously been suggested to be a marker of exhausted T cells; whilst this appears to be the case for cytotoxic T cells, it remains unclear if the same is true for CD4+ T helper cells (Haynes, Allen et al. 2007).

The chemokine receptor CXCR5 is also highly expressed by $T_{FH}$ cells which, together with their lack of chemokine receptor 7 (CCR7) expression – the main chemotactic receptor for the T cell zone - facilitates their egress from the T cell rich zone of the lymph node and permits their entry into the CXCL13-rich B cell follicles and GCs along a CXCL13 gradient (King 2009). CXCR5 expression is not

limited to $T_{FH}$ cells, it is expressed by many cells within the GC and so is not helpful on its own for defining this cellular subset within a GC. Unlike other subsets in which CXCR5 is only transiently expressed, $T_{FH}$ cells maintain a persistently high level of CXCR5 expression (King 2009).

Expression of the T cell co-stimulatory molecule ICOS is essential for $T_{FH}$ cell differentiation. Upon ligation with ICOS-ligand which is highly expressed on GC B cells, naïve T cells receive further signals to differentiate to $T_{FH}$ cells. Signalling through ICOS is also required for $T_{FH}$ cell survival and, in its absence in $ICOS^{-/-}$ mice, GC formation is grossly diminished (Fazilleau, Mark et al. 2009, Nutt and Tarlinton 2011, Linterman, Liston et al. 2012). Continued signalling through ICOS may be essential for perpetuating BCL6 expression and therefore maintaining the $T_{FH}$ phenotype and function (Kroenke, Eto et al. 2012, Crotty 2014). It has also been demonstrated that ICOS-mediated PI3 kinase signalling is a vital step in regulating the number of $T_{FH}$ cells and their production of cytokines (Gigoux, Shang et al. 2009, Rolf, Bell et al. 2010).

### 1.3.2 $T_{FH}$ differentiation

A further key feature of $T_{FH}$ cells is their expression of the repressive transcription factor BCL6 which has been shown to be essential for $T_{FH}$ differentiation (Johnston, Poholek et al. 2009, Crotty 2014). It is interesting to note that whilst it appears that $T_{FH}$ cells and GC B cells have an absolute requirement for each other to survive, they share a common transcription factor in BCL6.

T helper cell differentiation is determined largely by the expression of transcription factors with each T helper lineage having a 'master controller' or lineage specific transcriptional factor programme. For example expression of the forkhead box protein 3 transcription factor (FOXP3) leads to differentiation to a T regulatory cell phenotype and function, GATA-binding protein 3 (GATA3) expression leads to a $T_H2$ phenotype, T-bet (TBX21) leads to $T_H1$ differentiation, and retinoic acid receptor - $ROR_Yt$ leads to $T_H17$ differentiation. Rather than being a definitive, 'one-way' process, T helper cell differentiation is now increasingly thought of as a 'plastic' process reliant on the continued expression of transcription

factors and other proteins but changes in expression of these may lead to a change in phenotype, function and lineage (King 2009).

$T_{FH}$ cell differentiation is dependent on the transcription factor BCL6. BCL6 is also present in GC B cells in secondary lymphoid tissue as well as in GC-derived B cell lymphomas such as FL and many cases of DLBCL. BCL6 expression in $T_{FH}$ cells is thought to lead to suppression of other transcription factors such as $ROR_{\gamma}t$, T-bet, and Blimp-1 preventing differentiation to $T_H2$ and $T_H17$ and other T helper cell fates whilst also promoting the development of $T_{FH}$ characteristics such as CXCR5 expression (Johnston, Poholek et al. 2009, King 2009). MAF is another transcription factor which, together with BCL6 is essential for $T_{FH}$ differentiation (King 2009, Kroenke, Eto et al. 2012).

### 1.3.3 $T_{FH}$ cell function

As described above in section 1.2 on the normal GC reaction, $T_{FH}$ cells are absolutely essential for GCs to develop and function. They supply the essential signals required for the survival and proliferation of GC B-cells and may trigger expression of AID, which initiates somatic hypermutation (SHM) and class switch recombination (CSR) leading to the development of a class-switched, high affinity antibody response.

$T_{FH}$ are able to regulate GC size, limit the ability of B cells with low affinity BCRs from entering the GC, and stimulate the survival and proliferation of GC B cells with the highest affinity BCRs and highest amount of antigen expressed on their surface with MHC class II. Thereby $T_{FH}$ cells ensure that the GC reaction leads to the generation and selection of B cells with the highest possible antigen specificity (Johnston, Poholek et al. 2009, Good-Jacobson, Szumilas et al. 2010, Victora and Nussenzweig 2012, Crotty 2014).

The signals that $T_{FH}$ cells provide to GC B cells come from both cell surface receptors and via cytokines. For example, $T_{FH}$ cells have high expression of CD40 ligand (CD40L), interleukin 21 (IL-21), and interleukin 4 (IL-4) which provide key 'help' signals to GC B cells to survive and to promote B cell

proliferation. Upon ligation of ICOS, $T_{FH}$ cells are stimulated to produce IL-21 and IL-4 which are important in inducing IgG1 class switch recombination.

Since $T_{FH}$ cells have such a pronounced ability to stimulate GC B cell expansion, it is important that they only select the GC B cells with the highest affinity BCRs. Accordingly, negative regulatory checks are in place to prevent uncontrolled 'help' being given to GC B cells with low affinity BCRs which, if allowed to proceed unchecked would lead to the generation of ineffective, low affinity antibody production. One such regulatory check is the signalling lymphocyte activation molecule SLAMF6, which is upregulated in $T_{FH}$ cells and signalling through which leads to loss of $T_{FH}$-GC B cell adhesion and abrogation of $T_{FH}$ help (Crotty 2014). The high surface expression of PD1 on $T_{FH}$ cells may also serve as a further inhibitory process by limiting the proliferation of the $T_{FH}$ cells themselves (Crotty 2014). Further regulation of $T_{FH}$ cells is achieved through the action of T follicular regulatory cells ($T_{FR}$) which are thought to attenuate the immune response either by interacting with and suppressing the $T_{FH}$ cells or by directly inhibiting GC B cells with an autoreactive BCR (Linterman, Pierson et al. 2011, Crotty 2014), $T_{FR}$ are further discussed in sections 1.3.4 and 1.6.2.1 below.

### 1.3.4 T follicular regulatory cells

T follicular regulatory cells ($T_{FR}$) are a subset of CD4+ T cells that have a similar phenotype to $T_{FH}$ but are distinct from $T_{FH}$ and have a role in controlling the GC response.

$T_{FR}$ are CD4+, CXCR5+, $PD1^{Hi}$ cells and like $T_{FH}$ they are positive for the transcription factor Bcl-6 and are dependent on B-cell interaction for their development. Unlike $T_{FH}$ however, $T_{FR}$ are FOXP3+ and originate from Thymic FOXP3+ precursors.

$T_{FR}$ have been shown in vitro to have suppressive effects and are able to limit the number of $T_{FH}$ and GC B cells so controlling the size and rate of the GC reaction. In the absence of $T_{FR}$, an excess of B cells lacking antigen specificity has been observed. The mechanisms through which $T_{FR}$ regulate the GC are

not established at present but it is likely that they have a directly suppressive effect on $T_{FH}$ cells (Linterman, Pierson et al. 2011).

### 1.3.5 $T_{FH}$ in disease states

As described above, $T_{FH}$ are essential for generating a high affinity antibody response and defects in, or absence of $T_{FH}$ cells leads to a dramatically attenuated immune response to infection and ineffective vaccination.

$T_{FH}$ cells have been implicated in a range of autoimmune diseases such as systemic lupus erythematosus (SLE), rheumatoid arthritis, Sjogren's syndrome and other connective tissue disorders. In these conditions, increased numbers of circulating $T_{FH}$ cells can be identified in the peripheral blood and it is possible that uncontrolled or poorly regulated $T_{FH}$ response leads to autoantibody generation in these disorders (Simpson, Gatenby et al. 2010, Ma, Zhu et al. 2012, Ahearne, Allchin et al. 2014).

In addition to having a role in autoimmune diseases, infection and response to vaccination, $T_{FH}$ cells may have a role in allergy and have also been recently reported to be important in some solid organ malignancies as well as lymphomas.

A correlation between the number of $T_{FH}$ cells, an associated gene expression profile of $T_{FH}$ cells and good clinical outcome has been reported in breast cancer and colorectal cancer (Bindea, Mlecnik et al. 2013, Gu-Trantien, Loi et al. 2013). The reason why enrichment of $T_{FH}$ cells infiltrating the tumour of solid organ malignancies should be associated with improved outcome has not been elucidated but it is interesting to consider why this may be.

In research into breast cancer, histopathological studies have revealed the presence of B cell follicle-like structures, so called ectopic lymphoid infiltrates at the border of the tumour, and the $T_{FH}$ cells are found within these structures (Gu-Trantien, Loi et al. 2013). Therefore it may be that the increased number of $T_{FH}$ cells identified in patients with good outcome reflects the fact that in those patients, a robust anti-tumour immune response has been established rather than that the $T_{FH}$ cells themselves

are directly providing anti-tumour signals (Bindea, Mlecnik et al. 2013, Crotty 2014). Further work is needed to unravel this interesting finding.

Conversely, in FL $T_{FH}$ cell infiltration has been associated with adverse outcome (Richendollar, Pohlman et al. 2011). This needs to be interpreted with caution due to technical limitations of the research and contradictory findings from other groups as described in greater detail below in section 1.6 (Carreras, Lopez-Guillermo et al. 2009, Wahlin, Aggarwal et al. 2010, Yang, Grote et al. 2015) but why this should be the reverse of the situation observed in breast and colorectal cancer is important to consider.

Whilst in the solid organ malignancies we can hypothesise that $T_{FH}$ cell infiltration represents part of an effective anti-tumour immune response - with $T_{FH}$ cells providing appropriate B cell support to mount an immune response to the tumour, in FL, the malignant cells themselves are derived from and share many features with GC B cells, and the tumour shares many features of normal GCs.

$T_{FH}$ cell infiltration in FL may therefore provide FL B cell support as in normal GCs with $T_{FH}$ cell help leading to increased proliferation and survival of the malignant B cells. If this theory is correct, increased numbers of $T_{FH}$ cells may be associated with adverse outcome in this GC-derived B cell malignancy.

### 1.3.6 Summary of the role of $T_{FH}$ cells and rationale for studying them in FL:

Given the similarities between GC and FL follicles, and the central role of $T_{FH}$ cells in the GC reaction, this research focussed on the role of $T_{FH}$ cells in FL and investigated similarities and differences between the malignant follicles of FL and the GCs of reactive lymph nodes.

In particular we were interested to determine if there is any evidence that $T_{FH}$ cells provide FL B cells with support or a proliferative advantage.

## 1.4 PD1, PD-L1, immune tolerance, immune checkpoints and their role in oncogenesis

Programmed cell death 1 (PD1, PDCD1, CD279) is an immunoglobulin superfamily transmembrane protein, expressed by many T cells upon activation (Ishida, Agata et al. 1992, Ahearne, Allchin et al. 2014, Hawkes, Grigg et al. 2015). The key role of the PD1 pathway in the normal physiological state is proposed to be to control the immune response to avoid an excessive, potentially damaging host response to antigenic challenge, and to promote self-tolerance and prevent autoimmunity; as such it operates as an 'immune checkpoint' (Pardoll 2012). Immune checkpoints mainly act through cell surface receptors interacting with surface-bound ligands (Zou 2005). There are many other such immune checkpoints but, alongside PD1, Cytotoxic T-lymphocyte associated antigen 4 (CTLA4) is the other immune checkpoint that is at present most clinically relevant to cancer immune-biology and represents a therapeutic target against which drugs are currently available (Pardoll 2012, Eyre and Collins 2015).

As described above in section 1.3.1, PD1 is very highly expressed on $T_{FH}$ cells. It is thought that this is to prevent $T_{FH}$ cell proliferation in GCs to control the number of $T_{FH}$ cells in a site where one of their key roles is to promote B cell proliferation and to maintain tight control of GC B cell selection (Crotty 2014).

In the normal healthy state, in addition to being expressed on $T_{FH}$ cells, PD1 is expressed predominantly on antigen presenting cells including B cells and other activated T cells as well as being expressed on T cells that have become exhausted or anergic. This phenomenon has especially been noted in CD8+ T cells on exposure to chronic viral infection. It is thought that this 'exhausted' state can be reversed by PD1 inhibition has been proposed that this mechanism is involved in tumour-induced immune suppression (Barber, Wherry et al. 2006, Eyre and Collins 2015).

There are two known endogenous ligands for PD-1, PD-L1 (CD274) and PD-L2 (CD273) which are variably expressed on antigen presenting cells, including some GC B cells, macrophages, and dendritic

cells (Hawkes, Grigg et al. 2015). Upon ligation with PD-L1 or PD-L2, T cells expressing PD1 downregulate intracellular phosphoinositide-3 kinase activity as well as other stimulatory pathways leading to reduced cytokine production, and reduced TCR-mediated T cell proliferation (Eyre and Collins 2015, Hawkes, Grigg et al. 2015).

One of the hallmarks of cancers is their ability to avoid detection and eradication by the immune system by evading immune surveillance (Hanahan and Weinberg 2011). There has been a recent explosion of interest in how cancers evade immune surveillance which has been fuelled by greater understanding of 'immune checkpoints' such as PD1 and CTLA4 and the emergence of novel therapeutic strategies that seek to unlock these immune checkpoints, co called 'immune checkpoint inhibitors' (Pardoll and Drake 2012, Eyre and Collins 2015).

There is now good evidence that in many malignancies the tumour itself is able to influence its microenvironment and accordingly the immune landscape in which it is found. One way in which cancers are able to influence the immune response is through up-regulation of immune checkpoints such as PD1 on the immune cells infiltrating the microenvironment. This renders the CD8+ cytotoxic T-cells ineffective and exhausted and so attenuates the anti-tumour immune response.

Another way that cancers are able manipulate the microenvironment to evade immune surveillance is through up-regulation of the PD1 ligands, PD-L1 or PD-L2 on the malignant cells themselves (Blank, Gajewski et al. 2005). PD-L1 has been found to be highly overexpressed in many solid organ malignancies (Quezada and Peggs 2013, Pyo, Kang et al. 2016). When cytotoxic T cells come into contact with the malignant cells expressing a PD1 ligand, signalling through PD1 leads to downregulation of phosphoinositide-3 kinase activity and other stimulatory pathways in the T cells leading to reduced cytokine production, and reduced TCR-mediated T cell proliferation (Eyre and Collins 2015, Hawkes, Grigg et al. 2015). Hence, the tumour downregulates the anti-tumour immune response. Increased levels of PD-L1 expression on malignant cells has been associated with adverse prognosis in some solid organ malignancies including but not limited to malignant melanoma, breast

cancer, and gastric cancer (Wu, Zhu et al. 2006, Nomi, Sho et al. 2007, Hino, Kabashima et al. 2010, Hawkes, Grigg et al. 2015).

### 1.4.1 PD-L1 expression in lymphoma

Since lymphomas are malignancies of the immune system, the role of PD1, the expression of its ligands PD-L1 and PD-L2 and the effects of its inhibition are different and more complex than in solid organ malignancies (Hawkes, Grigg et al. 2015).

Unlike in many solid organ malignancies, expression of PD-L1 and PD-L2 is less pronounced in lymphoma and there is considerable heterogeneity in expression both within and between lymphoma sub-types. This heterogeneity and the fact that PD1 may be expressed on 'normal' cells of the immune system (as found in the normal GC reaction) as well as on lymphoma cells goes some way to explaining why there has been considerable variation in the reported influence of PD1 expression on prognosis in lymphoma (Eyre and Collins 2015, Hawkes, Grigg et al. 2015).

In most lymphomas, the malignant cells themselves rarely express PD1, the exceptions being angioimmunoblastic T cell lymphoma (AITL) and some cases of CLL (Xerri, Chetaille et al. 2008, Ahearne, Allchin et al. 2014). The expression of PD1 on AITL cells is interesting as it has been proposed that the cell of origin in AITL is a $T_{FH}$ cell (Xerri, Chetaille et al. 2008).

Whilst malignant lymphoma cells rarely express PD1, tumour infiltrating T lymphocytes with high surface expression of PD1 have been reported in FL, DLBCL, Burkitt lymphoma, primary mediastinal DLBCL, and Hodgkin lymphoma, especially the nodular lymphocyte predominant sub-type (Hawkes, Grigg et al. 2015). This is an area of considerable interest and complexity. PD1 may be expressed on $T_{FH}$ cells as in normal GCs and these certainly represent a significant proportion of PD1+ CD4+ T cells infiltrating the microenvironment of GC derived lymphomas including FL, however PD1 can also be expressed in other T cell subsets as well as in exhausted T cells (Barber, Wherry et al. 2006), and in these cells, PD1 expression may reflect a tumour-driven down-regulation of the anti-tumour immune

response (Eyre and Collins 2015, Hawkes, Grigg et al. 2015). Thus, in lymphoma, PD1 may be expressed on exhausted, dysfunctional, anergic tumour infiltrating T lymphocytes and also on active CD4+ T cell subsets such as $T_{FH}$ cells. This complexity partially explains the difficulties and discrepancies in using PD1 as a prognostic biomarker in lymphoma (see section 1.6.2.1 below) and also adds a layer of complexity when considering the mechanism of action of PD1 inhibitors in the treatment of lymphoma.

Despite high levels of PD1 expression by tumour infiltrating T lymphocytes in many sub-types of B cell NHL, there is only low level of expression of the ligands PD-L1 and PD-L2 in these conditions and the ligands have not been identified on the malignant cells themselves (Hawkes, Grigg et al. 2015).

In Hodgkin lymphoma and primary mediastinal DLBCL however, high levels of PD-L1 have been reported on the malignant cells. Expression of PD-L1 in these conditions is proposed to be mediated by the 9p24 mutation leading to increased copy numbers of the genes encoding the PD1 ligands. Furthermore, EBV-driven lymphomas have been demonstrated to have upregulated PD-L1 expression as an aberrant effect of the EBV genome (Green, Monti et al. 2010, Green, Rodig et al. 2012, Chen, Chapuy et al. 2013, Hawkes, Grigg et al. 2015). It is proposed that in these conditions the tumour cells themselves have upregulated PD-L1 expression to downregulate the anti-tumour immune response so conferring a survival advantage for the malignant cells. This is especially interesting in classical Hodgkin Lymphoma as it has been appreciated for many years that this condition is typified by impaired T cell mediated immunity, and it is now apparent that this may be driven by the tumour cells through upregulation of PD-L1 (Ansell, Lesokhin et al. 2015).

## 1.5 Immune checkpoint inhibition: PD1 blockade as a therapeutic option in malignancy

Blockade of immune checkpoints with antibodies to PD1 or CTLA4 is an exciting emerging therapeutic option in many cancers with particularly marked benefits recorded in non-small cell lung cancer,

malignant melanoma, pancreatic cancer and a number of other solid organ malignancies (Pardoll 2012, Quezada and Peggs 2013, Hawkes, Grigg et al. 2015).

The effect of blockade of PD1 or PD-L1 is downregulation of PD1 expression on lymphocytes infiltrating the tumour with associated improvement in the anti-tumour immune response including slowing of tumour growth and tumour 'rejection'. This has led to marked clinical benefits in a range of solid organ malignancies including dramatic prolongation of overall survival in metastatic malignant melanoma whether used as a single agent, in combination with chemotherapy or in combination with the anti-CTLA4 antibody, Ipilimumab, another checkpoint inhibitor (Hamid, Robert et al. 2013, Postow, Chesney et al. 2015, Robert, Long et al. 2015).

At present there are 3 selective, humanised anti-PD1 inhibitors in use and more are in development. The PD1 inhibitors currently in use are pidilizumab, nivolumab, and pembrolizomab.

Side effects of PD1 inhibition are largely predictable given that the role of the PD1 – PD-L1 axis is to control the immune response to prevent autoimmunity and excessive response to detected antigens. Reported toxicities and side effects include immune-mediated toxicities such as inflammatory colitis, hepatitis, dermatitis, uveitis, thyroid disorders and pneumonitis. Although these complications are relatively common (up to 41%), they are usually mild (toxicity grade 1-2) and overall these drugs are well tolerated (Topalian, Hodi et al. 2012, Hawkes, Grigg et al. 2015). When used in combination with an anti-CTLA4 antibody in the treatment of malignant melanoma, there was predictably an increase in incidence of these toxicities (Postow, Chesney et al. 2015).

Whilst the field of PD1 / PD-L1 inhibition is revolutionising the management of many solid-organ malignancies, the complexity of PD1 and its ligands' expression in lymphomas and differences compared to solid organ malignancies mean that there has been a lag in testing these agents in lymphoma. Nevertheless there is now considerable interest and many clinical trials are either in process or have already reported in various lymphoma sub-types.

An initial phase 1 clinical trial assessed a single intravenous dose of the PD1 inhibitor Pidilizumab in a range of haematological malignancies (Berger, Rotem-Yehudar et al. 2008). The maximum tolerated dose (MTD) was not established in this trial, and although this phase 1 trial was not primarily designed to assess efficacy there was one patient with advanced stage FL who experienced a CR after a single dose of anti-PD1 therapy which was maintained for at least 1 year which is a remarkable response. A further phase 1 clinical trial of Nivolumab showed a response rate of 40% amongst patients with FL (Hawkes, Grigg et al. 2015).

Subsequent trials in FL include a phase 2 clinical trial assessing Pidilizumab in combination with rituximab in 30 patients with relapsed FL (Westin, Chu et al. 2014, Eyre and Collins 2015). In this single-arm trial the ORR was 66% with a CR rate of 52%, interestingly some responses were delayed. The response rate is impressive but is hard to interpret as single-agent rituximab has a good response rate even in previously treated patients. Nevertheless it represents an exciting new therapeutic approach that should be evaluated further in randomised trials.

Anti-PD1 therapy has also been assessed in DLBCL with variable results. Pidilizumab has been assessed in a phase 2 clinical trial as consolidation therapy post autologous stem cell transplantation (Armand, Nagler et al. 2013). This showed a modest improvement in PFS compared to historical controls and 50% of patients who had residual disease post-transplant had a further reduction in disease burden following anti-PD1 therapy.

The most exciting results of anti-PD1 therapy in lymphoma reported to date have been in the treatment of classical Hodgkin lymphoma (cHL). In a phase 1 clinical trial of Nivolumab in patients with heavily pre-treated cHL, an amazingly high rate of response of 87% with 17% of patients achieving CR despite the fact that many of these patients had previously relapsed after ASCT (Ansell, Lesokhin et al. 2015). Although this is a small data set and the follow-up is short this represents a very high response rate in a group of patients with typically very poor prognosis. The higher response rates in

cHL than other lymphomas may represent the increased expression of PD-L1 on the malignant cells in cHL compared to the low level of expression on the malignant cells of other lymphoma sub-types.

## 1.6 The FL microenvironment

The tumour microenvironment is increasingly appreciated to be of great importance in the pathophysiology of many types of malignancy. Interactions between the tumour and the microenvironment assist tumour cells to grow, proliferate, and evade immune destruction. This is now recognised as one of the key hallmarks of cancer (Hanahan and Weinberg 2011, Hanahan and Coussens 2012).

The cells comprising the microenvironment in FL are a variety of immune regulatory cells including subsets of CD4+ T cells, CD8+ T cells, FDCs, tissue macrophages, and mast cells. Non-malignant cells account for up to 50% of the tumour mass. It is apparent that the interaction between FL cells and their microenvironment is a dynamic two-way process; the microenvironment is able to deliver either pro-survival or anti-tumour signals to the FL cells which in turn are also able to influence the composition of the microenvironment (Ame-Thomas and Tarte 2014).

In the normal GC reaction, differentiation, survival and proliferation of B cells is dependent on interactions with CD4+ T cells so it can be hypothesised that, since FL arises from GC B cells that reside and proliferate in follicles which have some similarities to normal GCs, similar interactions between B and T cells are important in the pathogenesis of FL. This hypothesis is supported by the observation that FL cells die rapidly by apoptosis *in vitro*, but can be rescued from apoptosis by the activation of CD40 which is present on both GC B cells and malignant FL cells. As the ligand for CD40 is found on T cells, it can be speculated that FL B cells are dependent on interaction with T cells *in vivo* for their survival (Johnson, Watt et al. 1993). Further circumstantial evidence that FL is linked to the host immune system is gained from the observation that, in a proportion of patients who are managed on a 'watch and wait' policy, lymph nodes sometimes regress without treatment - the reason for this is not clear but it may indicate an immune response against the tumour (Horning and Rosenberg 1984).

In DLBCL, gene expression profiling (GEP) has revealed that the malignant cells have distinctive gene expression profiles that strongly determines prognosis (Lenz, Wright et al. 2008). It has also been demonstrated that GEP of whole tumour specimens can predict prognosis in FL but here it is the molecular features of the non-malignant cells infiltrating the tumour that determines prognosis rather than genetic signatures intrinsic to the malignant cells. Dave *et al* performed oligonucleotide micro-array based GEP on tumour samples from patients with newly diagnosed FL, first using a training set of 95 patient samples to identify good and poor prognostic signals, and then testing this on a separate cohort of 96 patient samples. They identified 2 different host immune response profiles which were predictive of overall survival. Immune response 1 was characterised predominantly by expression of T cell genes and was associated with a good prognosis, whereas the immune response 2 profile showed over expression of genes expressed by tissue macrophages and or follicular dendritic cells and was associated with poor prognosis (Dave, Wright et al. 2004). This study provided important information to support the hypothesis that the microenvironment plays a role in FL and, by sorting cells into CD19+ and CD19- populations showed that it was the signal from infiltrating T cells and macrophages that was associated with prognosis. This finding was corroborated in work by Glas *et al* who showed that the different immune response profiles could not only predict survival but also the risk of transformation (Glas, Knoops et al. 2007). It has also been shown that PCR of selected genes could be used as a surrogate for GEP in identifying these prognostic groups (Byers, Sakhinia et al. 2008). These findings were an important step in understanding that FL is an immunologically active disease and that prognosis may be determined by the level of T cell infiltration and the number of tumour associated macrophages. However, this has not yet translated into a practical prognostic tool due to the cost and complexity of the methods involved. In addition, GEP studies on whole tissues do not give information about the specific cell types, their localisation and distribution.

Subsequent research into the role of the microenvironment in the pathogenesis of FL or investigating the prognostic significance of its composition has typically used either immunohistochemistry (IHC) on tissue sections or flow cytometry on disaggregated tumour biopsies.

To date, studies investigating the prognostic significance of the microenvironment have yielded disparate results. There are many reasons for this but chief amongst them are the heterogeneity in outcome in patients with FL, the use of different clinical endpoints, and the lack of a standard treatment in FL which makes interpreting outcome difficult. Technical issues also underpin the disparity in results. Whilst traditional IHC techniques can characterise the cells in the microenvironment, their numbers, distribution, and, if dual labelling is performed, their proximity to other cells, it is insufficiently sensitive to discriminate between the various complex cell types implicated. It has also been shown that there can be poor reliability and inter-user agreement on IHC interpretation (Sander, de Jong et al. 2014).

Multi-parameter flow cytometry on disaggregated lymph node samples overcomes the limitation of IHC because many antigens or proteins can be simultaneously labelled and analysis can be standardised to a certain extent but it does not allow architectural information to be obtained (e.g. the distribution of cell types with regard to the follicles).

### 1.6.1 Tumour associated macrophages in the FL microenvironment

Consistent with the GEP studies described above which identified that a GEP showing increased expression of tissue macrophage genes in the tumour was associated with poor prognosis, a number of studies using IHC suggested that increased macrophage infiltration was associated with worse prognosis. Farinha and colleagues constructed tissue microarrays on 99 biopsy specimens from patients treated uniformly in a clinical trial between 1987 and 1993. They found that patients with >15 CD68+ tumour associated macrophages (TAM) per high power field (hpf) had a significantly shorter overall survival than patients with <15 TAMs per hpf (Farinha, Masoudi et al. 2005, Byers, Sakhinia et al. 2008). The adverse impact of increased TAMs was also identified in an IHC study of 194 patients treated in a randomised trial between 2000 and 2002 (Canioni, Salles et al. 2008). In this study, increased TAMs were associated with adverse prognosis, especially if they were localised within the follicles (follicular) rather than in interfollicular areas. The patients in this trial were randomised to

receive chemotherapy with, or without rituximab. Importantly, in patients treated with rituximab, the adverse prognostic impact of increased TAMs was lost. The reason for this is not entirely clear but it can be speculated that rituximab reverses the apparent negative effect of increased TAMs because it relies on macrophages for tumour cell deletion and therefore is most efficacious when there are more macrophages in the tumour microenvironment (de Jong, Koster et al. 2009, de Jong and Fest 2011).

Treatment received was also found to affect the prognostic significance of TAMs in a study in which tissue microarrays were constructed on 61 samples from patients treated between 1993 and 1997 as part of a trial comparing two chemotherapy regimens (CVP versus fludarabine). In this study it was found that a dense infiltrate of TAMs conferred favourable prognosis if treated with CVP whereas it was associated with a worse prognosis in patients treated with fludarabine (de Jong, Koster et al. 2009). Other studies have concluded that TAMs either have no association with prognosis, or indeed have an opposite effect to that described above, or that the association between TAMs and prognosis depends on treatment received (Alvaro, Lejeune et al. 2006, Lee, Clear et al. 2006, Taskinen, Karjalainen-Lindsberg et al. 2007, de Jong, Koster et al. 2009).

These conflicting results show the difficulty in correlating markers related to the tissue microenvironment to clinical outcome, and the importance of interpreting these findings carefully. These studies used different clinical endpoints (OS vs. EFS vs. PFS), and included patients with different clinical characteristics who received heterogeneous treatments. IHC also relies on observer interpretation and despite efforts to automate image analysis and eliminate bias, it is still shown to be unreliable in some instances (Sander, de Jong et al. 2014). Nevertheless, it can be inferred that increased TAMs as demonstrated by IHC was a marker of worse clinical outcome in patients treated with traditional chemotherapy but, in patients treated with rituximab-containing regimens, this adverse effect is overcome, or even reversed. As most patients today are treated with rituximab-based therapy, increased TAMs can't be seen as a valid indicator of poor prognosis.

### 1.6.2 T cells in the FL microenvironment

It has long been appreciated that T cells infiltrate the tumour in FL, these are predominantly CD4+ (75%) with approximately 25% CD8+ and their location is predominantly interfollicular rather than follicular. The GEP study described above demonstrated that T cells in the tumour microenvironment were an important predictor of prognosis with stronger T cell gene expression (immune response 1) associated with better prognosis but this does not account for the types of T cell implicated or their distribution (Dave, Wright et al. 2004). As with IHC-based research into TAMs, studies linking the numbers and location of various T cell subsets to prognosis have yielded sometimes contradictory results.

#### 1.6.2.1 CD4+ T cells in FL

CD4+ T cells (T helper cells) have a vital role in protecting GC B cells from apoptosis. This is achieved through direct cell contact between the B cells via a number of receptor-ligand interactions including CD40 (on B cells) and CD40 ligand (CD154) on CD4+ T cells, and it is apparent that the same process is important in FL B cell survival (Carbone, Gloghini et al. 2009).

Investigating the number and distribution of CD4+ cells in FL has yielded contradictory results in IHC based studies with a high number of CD4+ T cells located within follicles associated with either prolonged survival (Lee, Clear et al. 2006) or worse survival (Glas, Knoops et al. 2007, Wahlin, Aggarwal et al. 2010) in three studies of heterogeneously treated patients. Accordingly, attention has turned to investigating the importance of CD4+ T cell subsets. Two classes of CD4+ T cells thought to play an important role in the pathogenesis of FL are T follicular helper T cells ($T_{FH}$) and regulatory T cells ($T_{regs}$).

IHC studies have investigated the significance of PD1+ cells in the FL microenvironment. In a study of 100 patients with FL, single parameter staining for PD1 was performed and images were quantitatively analysed (Carreras, Lopez-Guillermo et al. 2009). They found that PD1+ cells were mainly restricted to the follicles, and that the absolute number of PD1+ cells was decreased in grade 3 compared to grade 1-2 disease. They also reported that an increased number of PD1+ cells was associated with better

prognosis. These findings were confirmed in a separate study (Wahlin, Aggarwal et al. 2010), but in further work, increased follicular PD1+ cells were associated with inferior outcome (Richendollar, Pohlman et al. 2011). These studies all used single parameter staining and therefore were unable to identify the different populations of cells expressing PD1.

Studies on disaggregated FL lymph node specimens have confirmed the presence of $T_{FH}$ in FL. Identifying $T_{FH}$ as CD4+, CD25-, PD1+, ICOS+, CXCR5+, Pangault and colleagues found that $T_{FH}$ cells accounted for approximately 30-35% of all CD4+ cells in disaggregated FL lymph nodes which was no different to tonsils but was significantly higher than in whole disaggregated reactive lymph nodes. They went on to characterise these cells in detail and found that they expressed high levels of IL-4 (higher than tonsil-derived $T_{FH}$), demonstrated that $T_{FH}$ derived IL-4 was implicated in STAT6-dependent FL B cell activation, and proposed that this may favour FL B cell survival and proliferation (Pangault, Ame-Thomas et al. 2010, Ame-Thomas, Le Priol et al. 2012). In a separate study they were able to demonstrate that FL $T_{FH}$ cells express very high levels of PD1, have the capacity to rescue FL B cells from apoptosis *in vitro*, do not have regulatory function, and express a high level of CD40 ligand which contributes to the malignant B cell survival (Ame-Thomas, Le Priol et al. 2012).

By contrast, it has also been proposed that CD4+ PD1+ T cells in FL represent exhausted, anergic T cells with defects in function and *in vitro* studies have demonstrated that T cells in FL have impaired immune synapse formation compared to T cells in normal subjects (Ramsay, Clear et al. 2009, Myklebust, Irish et al. 2013).

Thus, CD4+ PD1+ cells infiltrating FL may consist of different populations; functional $T_{FH}$ cells that confer an active pro-tumour signal to the FL B cells through expression of CD40L and secretion of IL-4, and dysfunctional, exhausted PD1+ T cells that lack the function of $T_{FH}$ cells. These dysfunctional PD1+ T cells are postulated to support B cell growth through inhibition of the anti-tumour immune response.

Regulatory T cells ($T_{regs}$) are important in regulating T cell activation and maintaining immune tolerance. They are characterised by the expression of CD4, CD25, and the transcription factor FOXP3 (forkhead box protein 3). In FL, $T_{regs}$ have been demonstrated to inhibit the anti-tumour immune response through suppression of CD4 and CD8 T cell activation and proliferation (Yang, Novak et al. 2006, Glas, Knoops et al. 2007, Ame-Thomas and Tarte 2014). In reactive lymph nodes, $T_{regs}$ are mainly located outside of the GCs but they have been identified within the follicles in FL. IHC studies have assessed the relevance of FOXP3+ cells to prognosis in FL and interestingly it was found in one study that it is the distribution of FOXP3 rather than the absolute number that is important with a follicular or perifollicular pattern associated with poor prognosis whilst a diffuse pattern was associated with improved prognosis (Farinha, Al-Tourah et al. 2010).

There are various subsets of cells that express FOXP3 and a subset termed T follicular regulatory ($T_{FR}$) cells has recently been identified in FL. These are cells with a phenotype between $T_{FH}$ and $T_{regs}$, expressing CD4, CD25, ICOS, FOXP3 and CXCR5 which permits their follicular localisation. It is thought that they may inhibit the anti-tumour response although the mechanism for this is unclear at present (Linterman, Pierson et al. 2011, Ame-Thomas, Le Priol et al. 2012).

#### 1.6.2.2 CD8+ T cells in FL

Anti-tumour activity has been demonstrated by cytotoxic CD8+ T cells infiltrating the FL microenvironment. Accordingly, increased CD8+ T cell infiltration has been associated with improved outcome in IHC studies (Alvaro, Lejeune et al. 2006, Wahlin, Aggarwal et al. 2010, Laurent, Muller et al. 2011). In a study using multi-parameter labelling and confocal microscopy on frozen biopsy specimens, functional granzyme B containing cytotoxic T cells were found to form lytic synapses with FL B cells at the follicular border but were rarely found within the follicles (Laurent, Muller et al. 2011).

### 1.6.3 Influence of the tumour on the composition of the microenvironment

In addition to the effects of the microenvironment on the pathogenesis and prognosis of the tumour, it is now clear that this is a two-way process with evidence that the tumour is able to influence the

microenvironment in order to escape immune surveillance. Evidence for this includes the findings that malignant B cells are able to increase the number of immunosuppressive FOXP3+ $T_{regs}$ in the tumour environment by chemotaxis and migration through the secretion of CCL22 (Yang, Novak et al. 2006) or by inducing the conversion of conventional CD4+ T cells to become functional FOXP3+ $T_{regs}$ (Ai, Hou et al. 2009). It has also been demonstrated that healthy peripheral blood T cells co-cultured *in vitro* with malignant B cells acquire defective immune synapse formation (Ramsay, Clear et al. 2009), and that the gene expression profile of healthy T cells is changed on co-culture with FL B cells through both direct cellular contact and through soluble factors resulting in T cell functional impairment (Kiaii, Clear et al. 2013). In addition it has been demonstrated that both tumour associated neutrophils and cancer associated fibroblasts (CAFs) contribute to the generation of a pro-tumour cell niche in FL and other GC-derived lymphomas although the mechanisms by which this is achieved are not yet fully elucidated (Gregoire, Guilloton et al. 2015).

### 1.6.4 Summary of the FL microenvironment

It is clear that the microenvironment is important in the pathogenesis of FL, that it can impart pro-tumour and anti-tumour signals to the malignant B cells, and that the tumour cells themselves are able to influence their environment to escape immune surveillance. It is also increasingly clear that this is a complex phenomena and it is likely that it is the balance between these pro- and anti-tumour factors alongside the intrinsic molecular and genetic features of the malignant cells that ultimately determines the behaviour of the disease in a given individual at a particular time point in the disease course.

Some of the techniques used to date to explore this are not sufficiently sensitive on their own to understand the interactions between the tumour and the microenvironment. We refined a technique using multiparameter immunofluorescent labelling and confocal microscopy on tumour biopsy specimens that we believe will help to answer some of these questions. This technique has many advantages over traditional IHC which cannot resolve complex cellular subsets and, compared to flow

cytometry on disaggregated lymph node samples, this technique permits disease architecture and spatial relationships to be explored. These and other advantages of using multiparameter immunofluorescent confocal microscopy on FFPE LN samples are described in greater detail below.

## 1.7 Immunohistochemistry, multi-colour immunofluorescent labelling and confocal microscopy

Archived formalin fixed paraffin embedded (FFPE) biopsy material is an immensely valuable research resource. Some of the benefits of using FFPE material are that it can be stored easily and cheaply for a very long period of time, long follow up data for archived samples is often available, and, in patients who have relapsed, paired samples from time of diagnosis and relapse can be compared. Immunohistochemistry (IHC) is the most commonly used research tool on archived FFPE material, but it is also possible to extract RNA and DNA to perform gene expression profiling studies, or sequencing of genes implicated in the pathogenesis of the disease. However traditional IHC, using a primary antibody followed by a secondary antibody and a peroxidase complex with visualisation by a chromogenic substrate under a light microscope, has a number of limitations. Firstly, this technique is usually limited to visualising one protein at a time; two antibodies can be used simultaneously but this is complex and does not typically yield accurate co-localisation data. Secondly, the resolution of light microscopy is limited by the thickness of the sections. Thirdly, the quantitative analysis of images obtained from IHC is limited (Robertson, Savage et al. 2008).

An alternative approach to traditional IHC staining of FFPE tissue sections is to use immunofluorescent labelling. When visualised under an epifuorescence microscope, tissue autofluorescence and the inability to eliminate light emitted from the entire depth of the specimen can prevent meaningful analysis of immunofluorescently labelled FFPE sections especially when staining more than one protein simultaneously therefore this technique has not been widely used. However, these problems can be overcome by imaging immunofluorescently labelled sections with a confocal laser scanning microscope (Conchello and Lichtman 2005, Robertson, Savage et al. 2008).

A method of simultaneously staining multiple proteins with primary antibodies and fluorescently conjugated secondary antibodies detected with a confocal laser scanning microscope has been developed and it has been demonstrated to be able to obtain high quality images from FFPE material (Patten, Buggins et al. 2008, Robertson, Savage et al. 2008). This method has been used to detect 3 antibodies simultaneously with the 4$^{th}$ available channel usually being used for a nuclear stain, commonly 4',6-diamidino-2-phenylindole, dihydrochloride (DAPI).

Confocal laser scanning microscopes have a number of significant advantages over standard epifluorescence microscopes that ultimately result in the generation of images with much reduced background fluorescence. The principle benefit of confocal microscopy is the ability to generate images from specific focal depths whilst removing or blocking out-of-focus light, this is known as optical sectioning. The other key difference of a confocal microscope is that it generates an image by scanning, this means that, rather than acquiring all of the image from illuminating a section simultaneously (as in a light microscope or wide field epifluorescence microscope), the section is scanned by exciting points of the section with each laser in sequence and then building up the image from the information gathered at each point whilst blocking or masking light emitted from all other parts of the section.

These two factors combined, optical sectioning and scanning mean that the images generated by a confocal microscope are of very high contrast and have a much lower level of background fluorescence than conventionally acquired fluorescent images.

The ability to form optical sections within a tissue section also permits the collection of images in the vertical Z axis which can be reconstructed into 3D series known as Z-series or Z-stacks which is particularly useful for investigating cellular interactions or the colocalisation of two or more antigens within cells (Conchello and Lichtman 2005, Robertson, Savage et al. 2008).

Using a laser scanning confocal microscope equipped with lasers emitting light at 4 distinct wavelengths permits the development of a staining protocol that uses 3 primary antibodies which are then detected with 3 fluorescently labelled secondary antibodies plus a fluorescent nuclear counterstain, or, theoretically 4 primary antibodies can be detected with 4 fluorescently labelled secondary antibodies if no nuclear counterstain is used. The fluorescently labelled secondary antibodies each have an excitation threshold and they should be chosen to match the wavelength of the light emitted by the lasers on the microscope. Following excitation by the lasers, the fluorochromes emit light at a slightly higher wavelength (emission peak) which is detected by photomultiplier tubes (PMTs). A series of filters prevents out-of-focus light, or light that it not within the emission spectra of the fluorochromes from reaching the PMTs.

When designing multiple labelling experiments it is important to consider the excitation and emission spectra of the fluorescently labelled secondary antibodies. The excitation spectra of the different fluorochromes must be sufficiently different not to be excited by the same laser, and the maximum emission wavelengths must be well resolved with minimal spectral overlap, and fall within the wavelengths of the filters used with the microscope (see example in Figure 1-5).

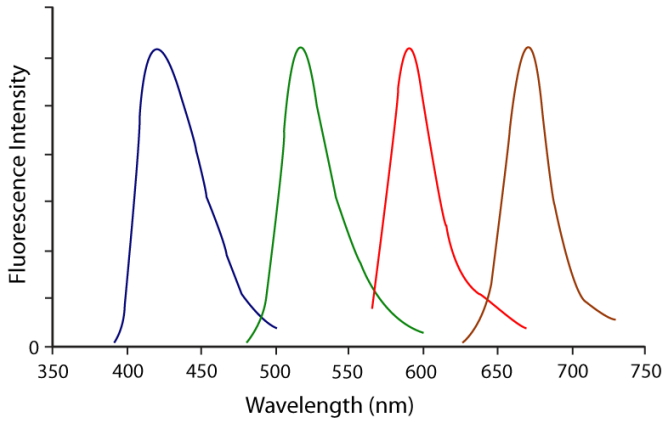


**Figure 1-5. Example of emission spectra.** Approximate emission spectra of DyLight 405 (blue), Alexa Fluor 488 (green), Alexa Fluor 555 (red), and Alexa Fluor 647 (brown) showing that the emission peaks of these 4 fluorochromes are well resolved with minimal spectral overlap. Reproduced from Jackson Immuno Research Laboratories

## 1.8 T cell receptor repertoire

The ability of T cells to recognise antigen bound to the major histocompatibility complex (MHC) is critical for an effective immune response. T cells recognise antigen through their surface-bound T cell receptor (TCR) which forms a complex together with CD3. The TCR is made up of two chains linked together by a disulphide bond, the two chains are either alpha and beta (α, β) or less frequently gamma and delta (γ,δ).

In order to be able to recognise near-limitless potential antigens, the TCR genes, like the BCR, diversify by random rearrangement and recombination of the variable domains, V, D, and J. The linkage areas between these domains are known as hypervariable regions and the greatest diversity is generated in the third hypervariable region, CDR3.

T cells undergo a process of positive or negative selection in the thymus depending on their TCR affinity. Up to 95% of T cells are negatively selected either due to either an ineffective, low affinity TCR or due to high affinity for auto-antigen. Further selection occurs in the secondary lymphoid tissue by interaction with antigen presenting cells.

Skewing of the repertoire of TCRs occurs as a result of particular TCR V gene usage in response to different antigens. The TCR repertoire of tumour infiltrating T lymphocytes has previously been investigated in a number of different solid organ malignancies. This research using high throughput sequencing of the TCRs has demonstrated that in some cancers there is relative skewing of the TCRs of tumour infiltrating lymphocytes compared to circulating T cells indicating perhaps a local response within the tumour to specific, as yet unidentified antigens (Emerson, Sherwood et al. 2013, Sherwood, Emerson et al. 2013).

The TCR repertoire of T cells infiltrating the FL tumour microenvironment has not been previously investigated, and we hypothesised that, since there are many similarities between the malignant follicles of FL and GCs of reactive LNs, the TCR repertoire of intra-follicular FL T cells may be restricted in response to a specific antigen.

## 1.9 Aims and Objectives

The goal of this research is to investigate the hypothesis that interactions in the neoplastic follicles in FL mirror those that occur in the normal GC reaction.

Since CD4+ $T_{FH}$ cells play such a key role in the normal GC reaction, and many of the features of the normal GC are retained in FL, in this research we focus on the location, phenotype and possible role of $T_{FH}$ cells in the pathogenesis of FL.

Specific aims of the research are to:

- Characterise the phenotype and precise location of CD4+ $T_{FH}$ cells infiltrating the microenvironment of FL using multi-colour immunofluorescent confocal microscopy *in situ* in formalin fixed paraffin embedded lymph node tissue sections
- Investigate to what extent the CD4+ T cell subsets and their distribution in FL are similar to the normal GC
- Investigate whether $T_{FH}$ cells are involved in promoting the proliferation of malignant B cells
- Investigate if $T_{FH}$ cells are associated with induction of AID in malignant B cells
- Investigate whether the CD4+ T cells in FL show evidence of antigen specificity
- Undertake preliminary investigation to determine if the composition of the CD4+ T cell population is associated with any clinico-pathological characteristics of the disease

# Chapter 2 Materials and Methods

## 2.1 Ethics

Ethical approval was applied for and granted for the collection and analysis of archived formalin fixed paraffin embedded (FFPE) tissue biopsy specimens from patients with lymphoproliferative disorders or reactive lymphadenopathy.

The histological material was surplus to clinical requirements, anonymised, and linked with a relevant clinical dataset.

The ethics committee determined that individual patient consent was not required for this work on archived, anonymised material. The research ethics registration number is 13/NW/0040.

## 2.2 Patient samples

Potential samples were identified from the database of the department of histopathology at King's College Hospital. Patients with a diagnosis of FL, CLL, or reactive lymphadenopathy with adequate surplus FFPE tissue blocks were included. Biopsies were either from the time of original diagnosis or taken at time of relapse. In cases of relapsed disease, only cases in which no systemic treatment had been received for at least 12 months prior to biopsy were included. Linked clinical information was collected according to the dataset in Table 2-1, all patient-data was kept anonymised.

**Table 2-1 Clinical dataset of information for patients with FL**

| Parameter | Value / units |
|---|---|
| Diagnosis | FL / CLL / reactive LN |
| Gender | Male / Female |
| Age at time of biopsy | Years |
| Biopsy site | Cervical / Supraclavicular / Axillary / Mediastinal / Mesenteric / Retroperitoneal / Inguinal / Extranodal |
| Biopsy taken at diagnosis or relapse? | Diagnosis / Relapse |
| Histological grade | Grade 1 / 2 / 3a / 3b |
| Stage at time of diagnosis | I / II / III / IV |
| FLIPI score | 0-5 |
| FLIPI 2 score | 0-5 |
| Initial management | Observation only / radiotherapy only / chemotherapy / immunochemotherapy / other |
| Treatment outcome | CR / CRu / PR / SD / PD / unknown / other |
| Time to event outcome (next treatment, progression, transformation, death) | Months |
| Current disease status | Alive in remission / alive with relapse / dead (death due to lymphoma) / dead (death not due to lymphoma) |

## 2.3 Sample preparation

### 2.3.1 Cutting sections, de-paraffinisation, and antigen retrieval

FFPE lymph node blocks were cooled on ice for at least 30 minutes prior to sectioning, blocks were then cut into sections of either 4µm or 12µm thickness on a rotary microtome (Slee Mainz, Cut 4060). Thick sections (12µm) were used for detailed co-localisation studies; for all other studies, thin sections (4µm) were used. Sections were floated onto warm water at 40°C and mounted onto Poly-L-Lysine coated microscope slides (VWR). Slides were dried on a hotplate at 70°C for 30 minutes before further drying at room temperature overnight.

Tissue sections were deparaffinised in two changes of xylene (Fisher scientific) in a fume cupboard for five minutes each then rehydrated in changes of graded ethanol. Rehydration was in 100% ethanol for 10 minutes followed by two changes of 96% ethanol for 10 minutes each, and 10 minutes in each of 70% and 50% ethanol. After this, the sections were washed in water.

Heat induced epitope retrieval was performed before immunohistochemical staining to unmask epitopes that had been cross linked by the formation of methylene bridges during the fixation of the specimens. Antigen retrieval was performed in pH 6.1 citrate buffer with 0.05% Tween 20 or pH 9.0 Tris-EDTA with 0.05% Tween 20. The antigen retrieval solution was heated to boiling in a pressure cooker and the slides were then transferred in a metal rack from water to the boiling solution using forceps. The lid of the pressure cooker was locked and, once full pressure had been achieved, 3 minutes were timed. After this, the pressure was released and the lid removed, the slides were cooled by the addition of cool water.

### 2.3.2 Multiple immunofluorescent labelling of formalin fixed tissue sections

After antigen retrieval, slides were washed in water and rehydrated in phosphate buffered saline (PBS) for 30 minutes. The slides were removed from the PBS and the tissue sections were circumscribed with a hydrophobic barrier pen (ImmEdge) without allowing the tissue to dry out.

Next, the slides were blocked with 5% normal donkey serum diluted in PBS for 1 hour at room temperature. The species of the blocking antibody was the same as the species in which the secondary antibodies were raised. In all experiments described in this report, donkey serum was used as all secondary antibodies in immunofluorescent labelling experiments were raised in donkey. Blocking with serum helps to prevent non-specific secondary antibody binding to the tissue section and reduces Fc receptor binding of both primary and secondary antibodies.

The donkey serum was drained off the slides but not washed and relevant combinations of primary antibodies diluted in PBS were carefully pipetted onto the sections within the area circumscribed by

the hydrophobic barrier pen. 0.025% Triton X-100 was added to the PBS to reduce surface tension and ensure that the tissue sections were completely covered to prevent drying out of the specimens.

The primary antibodies used, the manufacturers, and the concentrations at which they were used are listed in Table 2-2. Numerous combinations of primary antibodies were used but all primary antibodies used on each section were raised in different species; no experiments using two primary antibodies from the same species were performed.

The slides were incubated with the primary antibodies for 2 hours at room temperature or overnight at 4°C in a humidified chamber. Overnight incubation at low temperature was preferable as it permitted the use of a lower concentration of some antibodies and was associated with a lower level of non-specific background staining. The concentrations of antibodies listed in Table 2-2 are for overnight incubation at 4°C. The total volume of diluted antibody combination depended on the size of the tissue section being stained, 100-200µl for small sections and 400µl for large sections was adequate; it was important to ensure that the section was completely covered to prevent drying out during incubation.

**Table 2-2 Primary antibodies for immunofluorescent labelling**

| Antigen | Species | Manufacturer | Clonality | Clone | Product code | Dilution |
|---|---|---|---|---|---|---|
| CD3 | Rat | Abcam | Monoclonal | CD3-12 | Ab11089 | 1:200 |
| ICOS | Rabbit | Abcam | Monoclonal | SP98 | Ab105227 | 1:100 |
| Ki67 | Rabbit | Abcam | Polyclonal | - | Ab833 | 1:100 |
| PKC-theta | Rabbit | Abcam | Polyclonal | - | Ab131503 | 1:100 |
| T-bet | Rabbit | Abcam | Monoclonal | EPR9302 | Ab154200 | 1:200 |
| pSTAT6 | Rabbit | Abcam | Polyclonal | - | Ab28829 | 1:100 |
| CD8 | Rabbit | Abcam | Monoclonal | EP1150Y | Ab93278 | 1:400 |
| PD1 | Goat | R&D systems | Polyclonal | - | AF1086 | 1:50 |
| Ki67 | Mouse | Leica Novocastra | Monoclonal | MM1 | NCL-L-Ki67-MM1 | 1:100 |
| CD20cy | Mouse | Dako | Monoclonal | L26 | M0755 | 1:400 |
| BCL-6 | Mouse | Dako | Monoclonal | PG-B6p | M7211 | 1:50 |
| CD4 | Mouse | Leica Novocastra | Monoclonal | 4B12 | NCL-CD4-368 | 1:50 |
| AID | Mouse | Invitrogen | Monoclonal | ZA001 | 39-2500 | 1:200 |
| FOXP3 | Mouse | Abcam | Monoclonal | 236A/E7 | Ab20034 | 1:100 |
| PD-L1 | Rabbit | Spring Bioscience | Monoclonal | SP142 | M442RUO | 1:200 |

After primary antibody incubation, slides were thoroughly washed in 3 changes of PBS for 10 minutes each (30 minutes total). The relevant combination of fluorescently conjugated secondary antibodies (total volume 100-400µl depending on section size) was then carefully pipetted onto the tissue within the area circumscribed by the hydrophobic barrier pen and the slides were incubated in the dark at room temperature for 2 hours. The secondary antibodies used, the manufacturers, and the concentrations at which they were used are listed in Table 2-3.

The secondary antibodies were all raised in donkey and were directed against the species in which the primary antibodies were raised. For example, if 3 primary antibodies were used, raised in mouse, goat,

and rabbit then the secondary antibodies used were donkey anti-mouse, donkey anti-goat, and donkey anti-rabbit. When choosing the secondary antibodies, as well as ensuring that there was no species cross reactivity, it was also important to ensure that the fluorochromes were well separated to prevent spectral overlap, see section 1.7 above.

After secondary antibody incubation, slides were thoroughly washed in 3 changes of PBS for 10 minutes each in the dark. If a nuclear counter stain was required, DAPI (Cell Signalling Technology) was diluted to 0.4µg/ml in PBS, pipetted onto the tissue within the area circumscribed by the hydrophobic barrier pen and incubated for 10 minutes in the dark before washing in PBS. DAPI could not be used in conjunction with any secondary antibody conjugated to the DyLight 405 fluorochrome as they are excited by the same laser and their maximum emission wavelengths are similar (DAPI emission maximum 461nm, Alexa Fluor 405 emission maximum 420nm).

**Table 2-3 Fluorescently conjugated secondary antibodies**

| Host species | Target | Fluorochrome | Manufacturer | Product Code | Dilution | Excitation Peak (nm) | Emission Peak (nm) |
|---|---|---|---|---|---|---|---|
| Donkey | Rat IgG (H+L) | DyLight 405 | Jackson | 712-475-150 | 1:200 | 400 | 421 |
| Donkey | Rabbit IgG (H+L) | DyLight 405 | Jackson | 711-475-152 | 1:200 | 400 | 421 |
| Donkey | Rabbit IgG (H+L) | Alexa Fluor 488 | Jackson | 711-545-152 | 1:200 | 493 | 519 |
| Donkey | Rat IgG (H+L) | Alexa Fluor 488 | Jackson | 712-545-153 | 1:200 | 493 | 519 |
| Donkey | Mouse IgG (H+L) | Alexa Fluor 555 | Life Technologies | A31570 | 1:200 | 555 | 565 |
| Donkey | Goat IgG (H+L) | Alexa Fluor 647 | Jackson | 705-605-003 | 1:200 | 651 | 667 |
| Donkey | Rat IgG (H+L) | Alexa Flour 647 | Jackson | 712-605-150 | 1:200 | 651 | 667 |

Slides were briefly dried at room temperature in the dark (approximately 10-30 minutes depending on tissue size) and then mounted with 0.13-0.16mm thickness coverslips (VWR) using ProLong Gold

Antifade (Invitrogen) to reduce the rate of bleaching of the fluorescently conjugated secondary antibodies. Slides were cured in the dark for at least 24 hours prior to microscopy.

It was important to ensure that the tissue sections were not allowed to dry between the start of the deparaffinisation process until after DAPI staining. It was also important to protect the slides from prolonged light exposure once the immunofluorescent secondary antibodies had been added. Slides were stored after microscopy in the dark at 4°C and were imaged within 2 weeks of staining.

### 2.3.3 Controls

Negative controls were run in parallel with all staining experiments. Negative controls were tissue sections incubated with PBS without the addition of any primary antibodies but all of the fluorescently conjugated secondary antibodies (with or without DAPI) that were used in the positive slides. Negative controls were performed to determine whether fluorescence detected in the stained sections was genuine or was due to non-specific binding of the fluorescently labelled secondary antibodies or tissue autofluorescence.

Sections for negative controls were cut from the same blocks as the experimental sections and all stages of preparation were performed simultaneously with the experimental sections. When testing new secondary antibodies, or to determine the level of autofluorescence of the tissue, a double negative control slide was prepared which had no primary or secondary antibodies but had otherwise been processed in the same way as the stained sections.

When testing new combinations of antibodies it was important to ensure that there was no cross reactivity or spectral overlap by running single stained control slides which were stained with only one primary antibody in turn but all relevant secondary antibodies, this allowed us to assess whether the primary antibody staining had successfully worked and to determine whether fluorescence was only observed in the channel of the species-specific fluorescently conjugated secondary antibody. Where necessary, positive control slides were run in parallel. Tissue for positive controls were reactive lymph

nodes or tonsil tissue. With the use of blocking antibody of the same species as the secondary antibodies and with our rigorous use of negative control slides, it was determined that isotype controls were not required in these experiments.

## 2.4 Microscopy

Images were acquired on a Nikon Eclipse Ti-E inverted microscope equipped with the Nikon A1R Si confocal imaging system and lasers that emitted light at the following wavelengths: 405nm, 488nm, 561nm, and 642nm. Low power images were obtained with a Pan Fluor x10 objective and high power images with a Pan Apo oil immersion x60 objective. In order to maintain consistency and to permit comparative analyses, all images were collected on the same microscope. Positively stained sections were imaged first and settings such as laser power, photo multiplier tube (PMT) gain, pixel dwell time, pin hole size, optical section thickness, laser offset, and filter settings were kept the same for analysis of any paired control slides. As far as possible these settings were maintained for analysis of all similarly stained sections but this was not always possible as small differences in thickness of tissue sections, the quality of the tissue fixation, the size of the biopsy specimen (which also affects the quality of fixation), and the age of the specimen all affect the strength of antibody binding and fluorescence. Accordingly, whilst some settings were always maintained the same for all samples (pin hole size, pixel dwell time, filter settings, and optical section thickness), the laser power, PMT gain, and laser offset had to be optimised for the particular section being imaged. Determining the appropriate settings was facilitated using the 'pixel saturation' function of the image acquisition software. Laser power and PMT gain were adjusted for each channel in turn to obtain the optimal image which is indicated when only a few pixels are shown to be over saturated. The laser offset could then be reduced until areas of negativity were indicated to be under-saturated. These settings were kept consistent for acquisition of separate images obtained from one slide, and for comparison of positive and negative controls but, as described above, settings usually had to be optimised for different slides.

Low power images (x10 objective) were captured first then immersion oil was applied to the coverslip for further acquisition of high power (x60 objective) images. In some images, an area of interest was digitally magnified. Where this has been performed it is indicated in the figure legend. Large, 'stitched' images of adjacent low-power fields could be obtained which were 'stitched' together by the image acquisition software, this was useful for showing a large field for example giving an overview of several GCs within one image.

The PMTs do not detect colour but the image acquisition and analysis software is able to generate colour for each channel. Any colour can be chosen for each channel but to maintain consistency the colours were kept the same for each channel in all images included in this thesis as detailed in Table 2-4. As most images were obtained with 4 colours it was necessary to use white to indicate the signal in one of the channels (channel 4, wavelength 640nm), this is important to note as an area where blue, green, and red overlap are sometimes shown as white in fluorescent microscopy images.

**Table 2-4 Allocation of colours to different channels and the associated fluorochromes**

| Channel number | Laser wavelength (nm) | Colour allocated | Fluorochromes |
|---|---|---|---|
| 1 | 405 | Blue | DAPI or Dy Light 405 |
| 2 | 488 | Green | FITC or Alexa Fluor 488 |
| 3 | 561 | Red | Alexa Fluor 555 |
| 4 | 640 | White | Alexa Fluor 647 |

One of the advantages of using a confocal microscope over a standard fluorescent microscope is that the field can be moved in 3 axes, X, Y and Z. By moving the stage vertically in the Z axis and capturing images at pre-defined intervals, Z-stacks (or Z-series) can be obtained. Reconstruction of Z-stacks permits the visualisation of the specimen in 3D which is particularly useful for investigating cellular interactions Figure 2-1. To obtain a Z-stack the focal plane was adjusted until the tissue was out of focus at the superior aspect of the tissue, the stage was then lowered until the section was out of focus at the inferior border of the tissue.

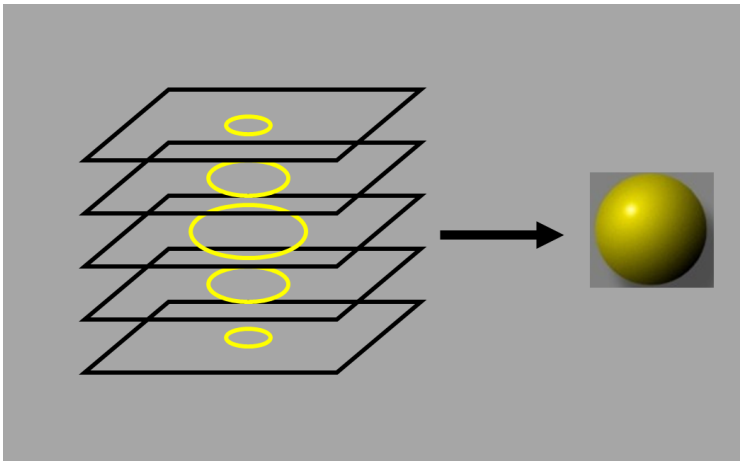

**Figure 2-1 Image indicating how a Z stack is formed.** A Z stack is a series of images taken at different planes in the z axis. Taking images through the section at different levels allows the images to be reconstructed in 3 dimensions.

The coordinates of the extremes of focal range were used by the operating system to define the upper and lower boundaries of the section. The stage was then automatically moved in the Z axis and a separate image acquired at each predefined step; a typical Z-stack of a 12µm section would consist of 15 images. Z-stacks were not routinely acquired for all sections as they were very time consuming and expensive to obtain, lead to bleaching of the area of tissue examined, and added little to the analysis of the proportions of cells expressing certain antigens in large fields. Z-stacks were acquired to investigate areas of cellular interaction especially the interaction between Ki67 positive tumour cells and PD1+ T-cells. Video reconstructions of the Z stacks could be generated which helped to appreciate the cellular interactions in 3 dimensions.

## 2.5 Image analysis

Images were analysed using Nikon elements NIS Advanced Research version 4.2 software. Images presented in this report have been optimised for contrast using Look Up Tables (LUTs) and, where appropriate, cropping or magnification has been performed but no further image enhancement or manipulation has been implemented. The image acquisition and analysis software stores the image files as ND2 files, these have been converted to tiff files and either inserted directly into this report or combined into figures using Microsoft PowerPoint.

The automated or semi-automated analysis of images obtained by immunofluorescent confocal microscopy forms an important part of this work and is paramount to its success. Since this is not a standard analytical technique, a detailed description of the image analysis method used in this report follows.

The first step in analysing images was to generate binary layers for the channels used. Binary layers are superimposed over the original image and do not affect the underlying image itself. A binary layer is essentially a 'mask' laid over the original image that indicates which areas of an image are considered as positive and which areas are negative in the channel(s) concerned. Generating binary layers for each channel permitted the accurate quantification of the amount of positive signal in an image, allowed the counting of cells as 'objects', and facilitated the analysis of co-localisation. As well as generating single channel binary layers it was possible to create binary layers where the signal in 2 or more channels overlaps, so-called 'intersection' binary layers. Binary layers could be allocated any colour and can be applied to standard 2D images as well as to 3D Z-stack reconstructions.

In most images in this report either 3 or 4 channels were used and binary layers needed to be generated for each channel except Channel 1 (405nm) if DAPI was used. A binary layer for DAPI was rarely generated as it was used as a nuclear counterstain only.

To generate a binary layer for a particular channel the thresholds for the image first had to be set. This was a crucial step in the image analysis as it determined which areas of the image would be considered as positive signal and therefore included in the binary layer, and which areas were negative, or background and therefore excluded from the binary layer and not included in analysis. Thresholding of an image was performed on the basis of intensity of fluorescence and a number of possible restrictions for example size, area, and circularity.

To set the threshold for a channel, representative areas considered positive were selected as reference points, these were selected using a 'picker' tool, this highlighted all other areas of the image

where the intensity measured in that channel was of the same or higher level, see Figure 2-2. Thresholds could also be set using histograms to define the upper and lower limits of the binary very precisely. Restrictions could be set to exclude areas below a certain size (e.g. <1.0µm) which were likely to be artefact, Figure 2-3, but this could also be performed mathematically on the data generated (by excluding all data from individual binary areas (or objects) below a certain size). Areas of autofluorescence or artefact such as formalin crystals or autofluorescing blood vessels could be deleted manually from the relevant binary layers. The use of a nuclear counterstain such as DAPI was helpful in determining whether signal detected was due to autofluorescence as it helped to define whether the signal was intracellular or not, areas of fluorescence that were not in a cellular area of the section were manually deleted, see Figure 2-4.

Once the thresholds had been set, the binary layer could be further refined for example to clean the binary (remove small objects), smooth (flatten the contours), fill holes (for example fill in a cell where its outline has been defined by the binary), or separate the binary where a number of closely packed cells had been counted as a single object in the binary layer. It was important to perform the separation of objects within the binary carefully when performing cell counts, although there was an automatic function for this within NIS Elements, we found that this did not reliably separate individual cells in closely packed tissue sections. Therefore, additional manual object separation had to be performed; this was very time consuming. Separation of clusters of cells into individual objects was facilitated by reference to the DAPI layer to identify individual cells, Figure 2-4.

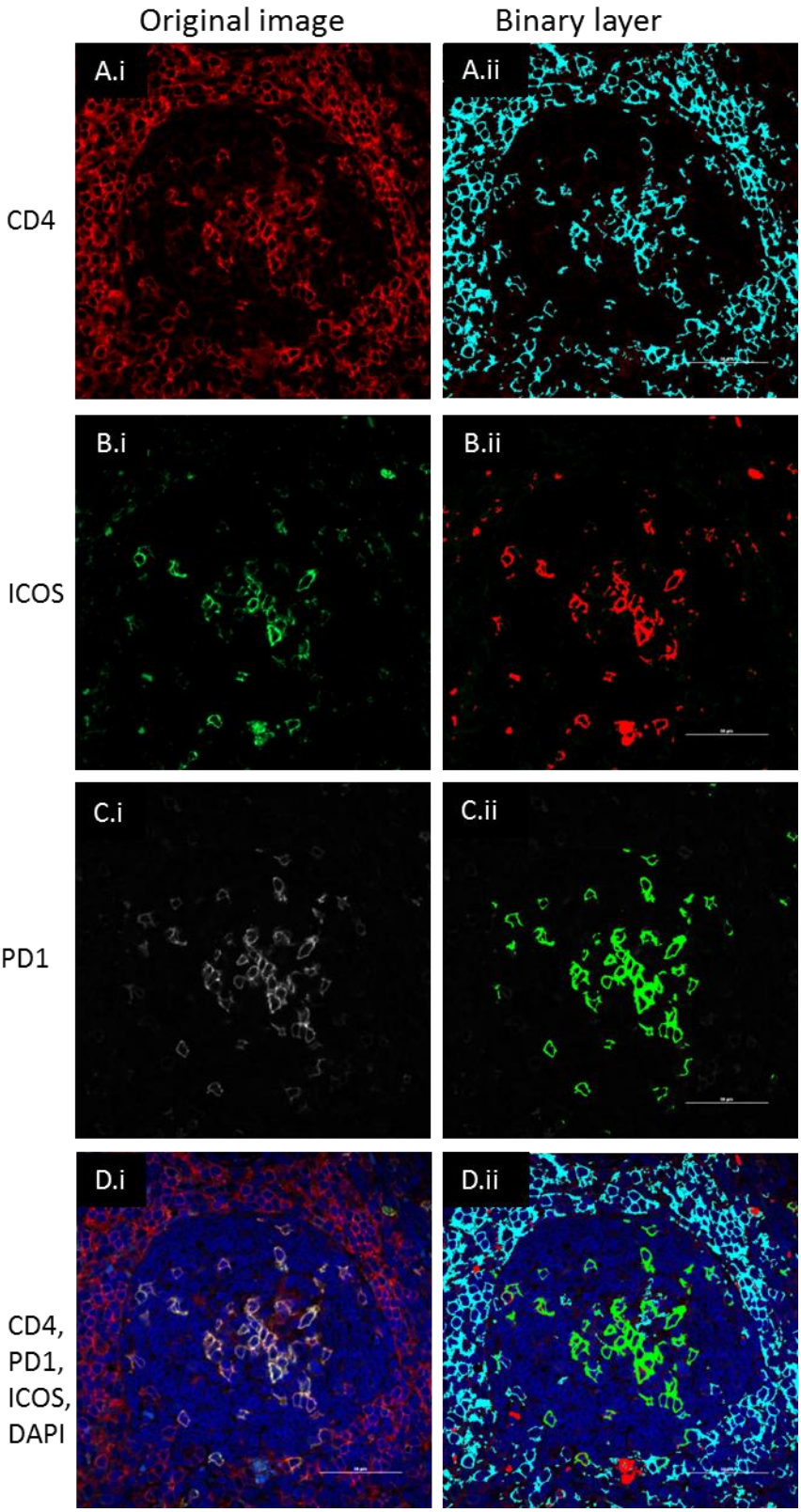


**Figure 2-2 Example of thresholding and setting binary layers.** x60 image of germinal centre labelled with **A.i** CD4 (**red**), **B.i** ICOS (**green**), **C.i** PD1 (**white**) and DAPI (**blue**). **D.i** All channels combined. To the right of each original image in **A.ii-C.ii** the thresholded binary layer for that channel is shown. **D.ii** shows all 3 binary layers superimposed over the original image.

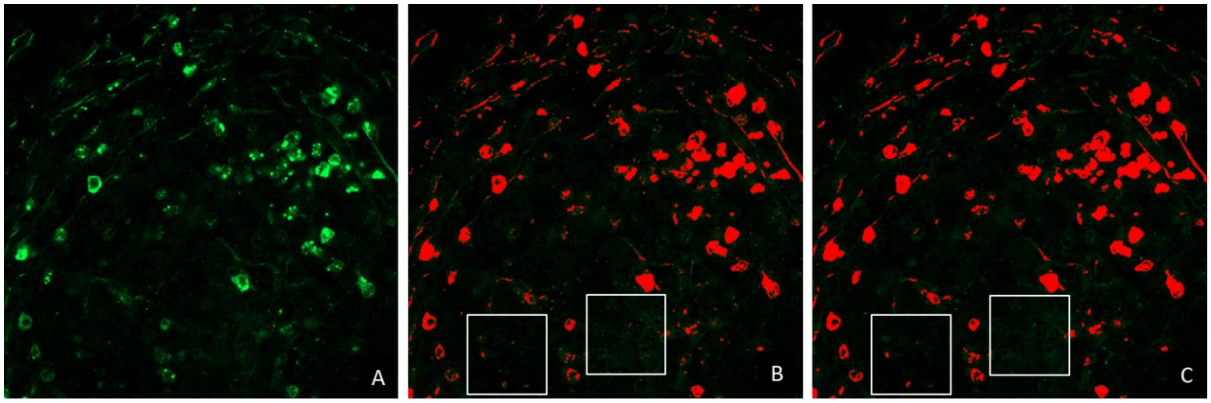


**Figure 2-3 Example of setting restrictions on a binary layer.** x60 image of FL labelled with Ki67 (green) **(A).** In **B** the threshold has been set and the binary is shown in red without restrictions, note multiple small areas of binary (red) within the 2 white rectangles which is artefact, not Ki67+ cells. In **C** size restriction (exclude items <1µm in size) and 'clean' x1 have been applied and the difference can be seen within the 2 white rectangles

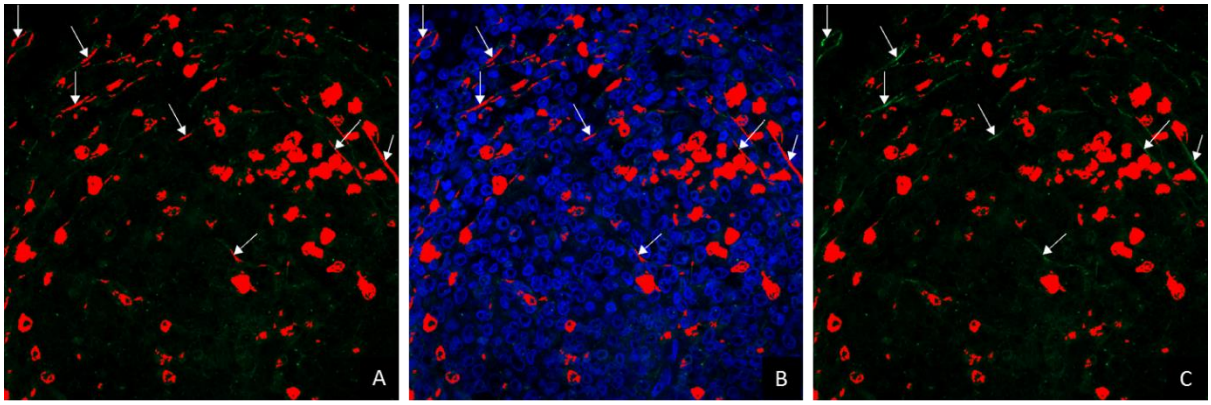


**Figure 2-4 Example of manually deleting areas of autofluorescence.** This section has been labelled with Ki67 (red) **(A)** which should be nuclear giving a characteristic staining pattern but in this case there are linear structures included in the binary (white arrows). By combining this with the DAPI channel image (blue) it can be confirmed that these areas are not cellular and may represent collagen or elastin in vessels. Since these are not thought to be Ki67+ cells, they can be manually deleted so giving a clean binary layer for Ki67 **(C)**

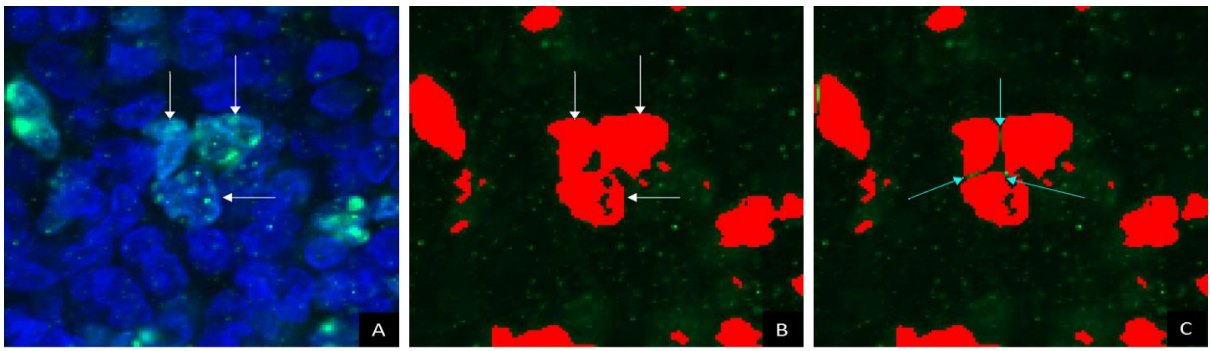


**Figure 2-5 Example of using automatic object separation.** In **A**, 3 separate Ki67 positive (green) cells can be identified (white arrows). In **B** the binary layer has included these 3 cells as one large object (red). By applying the 'separate' modification to the binary layer, the 3 cells are separated (blue arrows). This function can also be performed manually. (x60 zoomed image).

The threshold levels, restrictions and refinements, once set for all channels in an image, could be saved and the same thresholds applied to other acquired images. Whenever a negative control was analysed, the same thresholds were applied to determine whether any fluorescence detected met the criteria for being included as positive events.

To measure only a certain part of an image, a region of interest (ROI) could be set. This was useful for example when looking only at cells within, or outside of a GC in an image that contained both areas, see Figure 2-6.

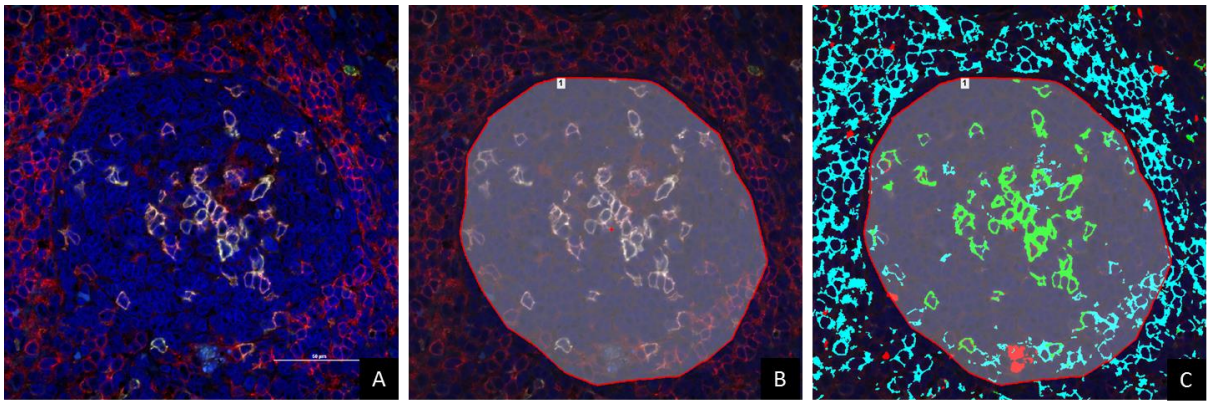


**Figure 2-6 x60 image of germinal centre** (**A**). In **B** a region of interest (ROI) has been drawn around the edge of the GC so that the binary layers (**C**) can be measured within and outside of the GC.

ROIs could also be used when measuring the amount of co-expression of antigens within cells, this worked best with a nuclear stain (e.g. Ki67 or FOXP3). The binary layer was set as described above and then converted into separate regions of interest. Each positive cell is then a separate ROI and interrogation of the amount of binary layers in each ROI (i.e. within each cell) could be performed. See section 3.4 below.

It was not possible to use exactly the same thresholds and settings for all images. As described in section 2.4 above, differences in thickness of tissue sections, the quality of the tissue fixation, the focal plane and other factors affect the strength of fluorescence, therefore whilst every effort was made to

keep acquisition and analysis settings the same, it was necessary to make fine adjustments to these settings for different specimens.

Further details about the specific image analysis method used are presented in the relevant sections of the results chapter.

## 2.6 Investigating the TCR repertoire

In order to investigate the antigen specificity of the CD4+ T cell compartment in FL lymph nodes we performed high throughput sequencing of DNA extracted from FFPE tumour samples.

An initial experiment was performed to determine if sufficient DNA could be extracted from FFPE samples to perform high-throughput sequencing of the CDR3 of the TCRβ subunits.

For this preliminary experiment, 2 separate lymph nodes biopsied simultaneously in the same patient at the time of original diagnosis were used.

For extraction of DNA from whole sections, 5 x 10μm thick 'rolls' of tissue were cut from the paraffin blocks (as described above) and collected directly into a DNase free Eppendorf tubes.

The sections were deparaffinised in xylene. Genomic DNA was then extracted from FFPE tissue using the QIAGEN miniDNA kit according to the manufacturer's instructions.

DNA quantification and quality assessment was performed using the NanoDrop spectrophotometer according to the manufacturer's instructions. The size of extracted DNA fragments was further assessed by gel electrophoresis.

The yield from this preliminary experiment was good and the samples were subsequently frozen and shipped to ImmunoSeq in Seattle, USA for high throughput deep sequencing of the CDR3 TCRβ subunits. Deep sequencing was successful and analysis revealed that there was overlap in the TCRβ repertoire between the two distant lymph nodes, lending support to the hypothesis that T cells

infiltrating the FL tumour microenvironment demonstrate antigen specificity, see results in section 3.9 below for further details.

This pilot project revealed that DNA could be successfully extracted from FFPE samples, the TCRβ repertoires could be sequenced, and that there was overlap between 2 distant lymph nodes biopsied at the same time.

We had previously identified that the phenotype of the T cells in FL depends on their location (whether follicular or interfollicular), and demonstrated that the interaction between $T_{FH}$ and proliferating neoplastic cells is restricted to the follicles. We therefore determined that to further understand the specificity, clonality and spatial heterogeneity of the T cell response in FL, it was necessary to dissect LN sections and interrogate the TCR repertoires in different compartments rather than sequencing the TCRs from entire LN sections.

We hypothesised that if CD4+ $T_{FH}$ cells are present in the follicles as a result of a specific response to antigen, the TCR repertoire between different follicles within the same LN would be similar. We therefore determined that it would be valuable to laser dissect follicles, extract DNA from separate follicles and perform comparisons of receptor repertoire between follicles.

We next performed some preliminary experiments to determine if this approach was feasible. Unfortunately, too little DNA could be extracted from individual follicles to permit analysis. We therefore experimented with the technique to determine if sequential sections from the same LN could be stained and the same follicle dissected from each section according to the schema depicted in Figure 2-7 below.

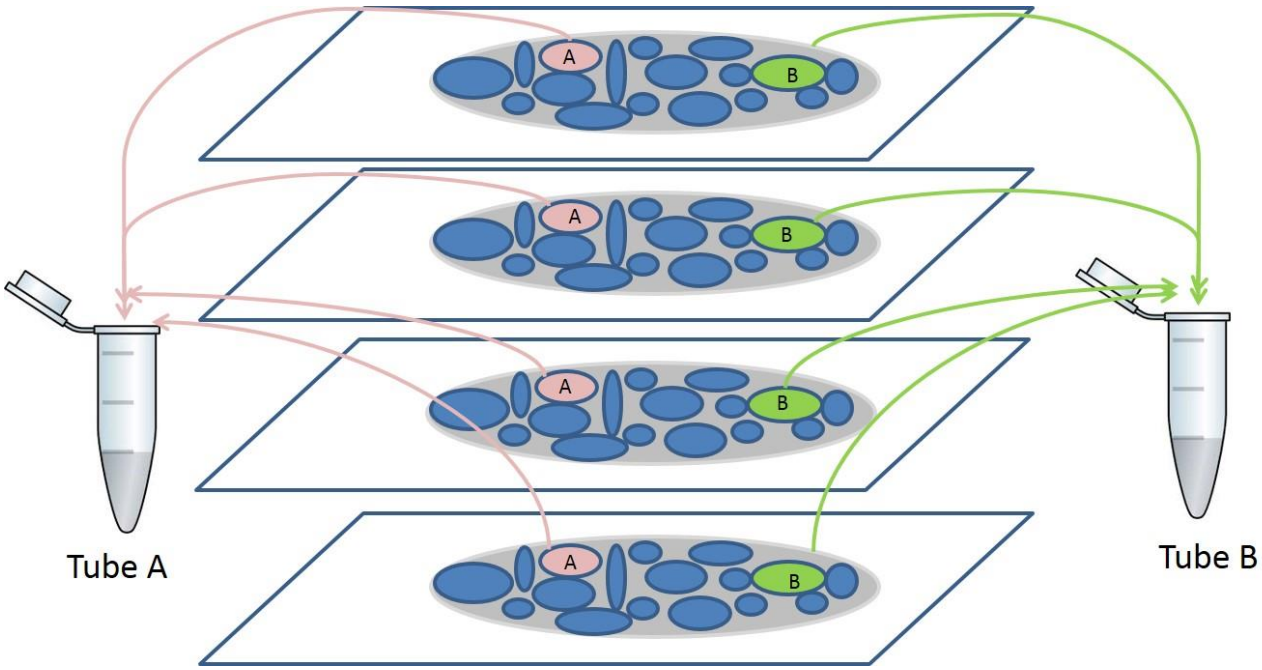


**Figure 2-7 Proposed method for comparing the TCRβ repertoire of 2 follicles.** Sequential sections of an FFPE lymph node biopsy were mounted onto slides. Serial sections of one malignant follicle (A) dissected using a laser capture microscope and specimens collected into tube A. Serial sections of a separate malignant follicle (B) from the same specimen micro-dissected and captured in tube B. DNA could then be extracted from the tissue in each collection tube and the TCRβ repertoire from follicle A could then be compared with that from follicle B

This proved to be technically unfeasible as it was not possible to reliably identify the same follicle in sequential sections and the yield of genomic DNA extracted was too low for sequencing even when sequential sections of the same follicle were able to be dissected.

We subsequently refined our approach by investigating if the TCR repertoire from the follicular areas of a FL LN was significantly different to the TCR repertoire of interfollicular areas from the same LN – see section 2.6.2 below.

Since we have identified that the T cells within the follicles are phenotypically significantly different to the T cells in the interfollicular areas, we hypothesised that the follicular TCR repertoire – where $T_{FH}$ are enriched – would be more restricted than the TCR from interfollicular areas.

### 2.6.1 Staining of samples for laser dissection

To distinguish between follicular and inter-follicular areas of tissue, sections were first stained with anti-BCL-6 by standard immunohistochemistry using the VECTASTAIN ABC system (Vector Laboratories, California, USA). The FFPE tissue block was cooled on ice prior to sectioning, thick sections (12µm) were cut from the block and floated onto sterile water at 40°C before mounting on to uncoated slides and drying as described in section 2.3.1 above. To reduce the risk of sample cross-contamination, all surfaces were cleaned with trisol detergent between specimens, the disposable microtome blade was changed after each section had been cut, the first 5 sections from each block were discarded, and strict aseptic technique precautions were observed.

Deparafinisation was carried out as per section 2.3.1 above. Endogenous peroxidase was then blocked in 0.5% hydrogen peroxidase (Sigma) for 10 minutes. Heat induced antigen retrieval was performed in pH 6.1 citrate buffer as per section 2.3.1 above. Subsequently sections were blocked in 3% horse serum with avidin for 1 hour at room temperature before biotin blocking (15 minutes at room temperature). Mouse anti-human BCL-6 monoclonal antibody was diluted in PBS to 1:50 and this was pipetted onto the specimens, slides were incubated overnight at 4°C. The primary antibody was thoroughly washed off and secondary antibody (biotinylated anti-mouse IgG, raised in horse, Vector Laboratories) diluted to 1:100 was added for 1 hour at room temperature. After washing, avidin-biotinylated enzyme complex (ABC) (Vector Laboratories) was prepared and added to the sections for 30 minutes at room temperature before further washing. The antibody labelling was then visualised using ImmPact Diaminobenzidine (DAB, Vector Laboratories). DAB was diluted according to the manufacturer's instructions and added to the tissue section which was observed directly under a light microscope until sufficient staining (brown colour) was observed, the slide was then immediately washed in water. Nuclear counterstaining was performed with haematoxylin which was added to the sections for 30 seconds before washing in running water. Sections were not dehydrated or mounted with coverslips.

### 2.6.2 Laser dissection of follicles and inter-follicular regions

Laser capture microscopy permits the non-contact capture of particular areas of tissue from samples for a variety of downstream applications including extraction and analysis of DNA or RNA from specific areas of tissue.

Laser dissection was performed using a Zeiss microscope fitted with the PALM Zeiss LCM system, see Figure 2-8. The PALM laser dissection system is operated according to the following principles. The areas to be captured are first highlighted using the software package. The lid of the collection tube is held in position by a clamp above the sample. The UV cutting laser is activated below the sample and the robotic stage moves the sample so that the areas demarcated by the software are cleanly cut. Once all highlighted areas are cut, a second pulse of laser at a different wave length to the cutting laser is directed through the sample to 'catapult' the dissected tissue into the collection cap which is held approximately 1mm above the sample. The collection caps have a self-adhesive coating so that areas of tissue catapulted upwards from the specimen are collected directly into the cap, Figure 2-8.

We experimented with a number of different techniques for the laser dissection and capture of follicles and inter-follicular regions of FFPE FL lymph node sections. The optimal yield would have been achieved by mounting the samples on to dedicated laser-capture membrane slides. These are slides made of a membrane that is easily 'cut' by the laser, the sample and the membrane so dissected are captured together using this method. Despite many attempts, it was not possible to overcome difficulties in fixing the samples to the membranes sufficiently strongly to withstand the IHC labelling process. We therefore had to mount the samples on standard glass slides. To optimise the easy cutting and catapulting of tissue from the glass slides, uncoated slides were used for this process as the tissue is too firmly attached to poly-L-lysine coated slides for capture. Compared to membrane slides, the yield of tissue was lower for each specimen as some parts of the demarcated tissue remained firmly adherent to the glass slides, nevertheless we had to pursue this technique due to the difficulties adhering samples to the membrane slides.

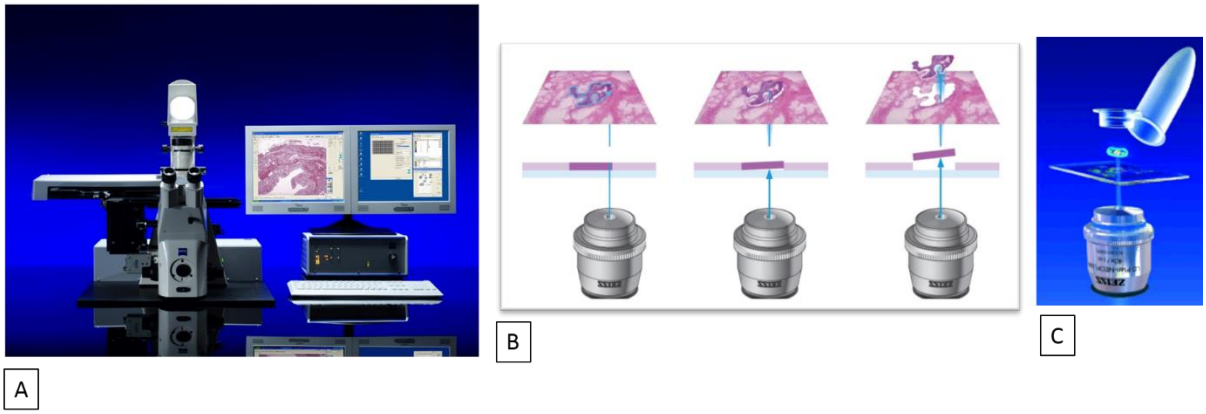


**Figure 2-8 Figure showing set up of laser dissection system. A.** The PALM Zeiss system consists of an inverted Axiovert Zeiss microscope, PALM robo laser system and stage, and PALM software package. **B.** Areas to be dissected are highlighted using the software system, a laser is then directed through the slide and specimen to cut out the area to be dissected. Pulses of laser are then directed through the sample to lift or 'catapult' the specimen into the collection tube cap (**C**). Note that samples must not be covered with a cover slip and that the sample is facing upwards on the slide with the lens of the inverted microscope below the glass slide. The pathway of the laser is through the inverted objective, through the glass slide and into the specimen **(B)**. Images adapted from ZEISS manual.

Dissection and collection of samples was according to the schema depicted in Figure 2-9. Firstly, areas identified as follicles – highlighted by BCL6 staining - were demarcated using the software package, the follicles were then circumscribed with the cutting laser before being 'catapulted' into the caps of the collection tubes.

It was observed that not all of the material 'cut' from the specimen and 'catapulted' towards the adhesive cap of the collection tube was captured in the adhesive material and some microscopic tissue fragments fell back onto the slide where it could then erroneously be catapulted into the incorrect tube e.g. follicular material could be collected into the interfollicular collection tube and vice versa. It was therefore necessary to dissect and collect follicular material from one section, and then collect interfollicular material from a separate, sequential section from the same sample to prevent cross-contamination of material into the relevant collection tubes.

To maximise the yield, six sequential sections from the same block were used for each sample. Equivalent areas of follicular and interfollicular tissue were collected from sequential sections from each of five separate FL LN specimens.

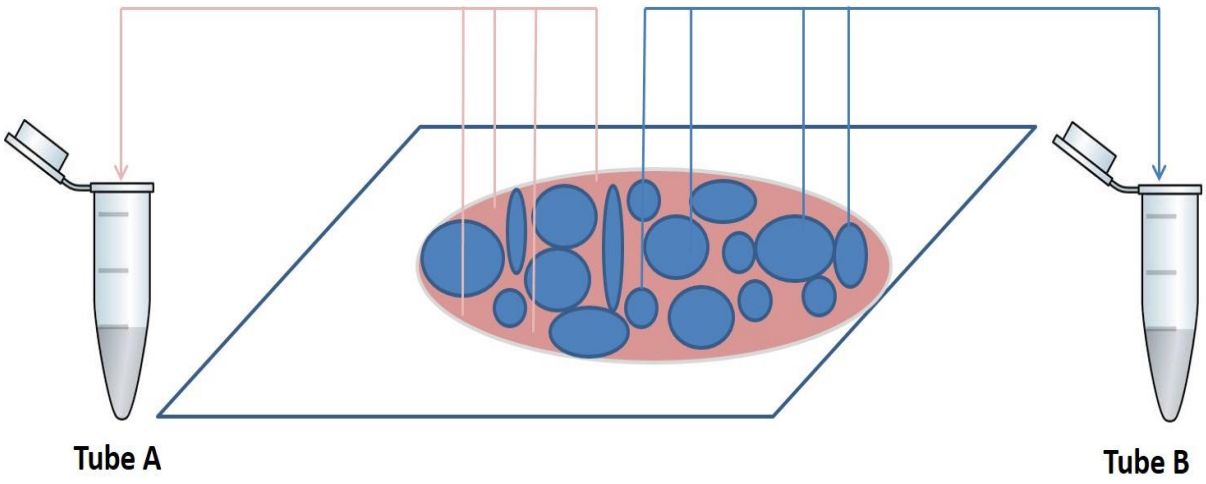


**Figure 2-9 Schema demonstrating method for comparing the TCRβ repertoire of follicular verus interfollicular T cells.** Sections of FFPE lymph node biopsy mounted onto slides. The inter-follicular areas (pink) dissected using a laser capture microscope and specimens catapulted into collection tube A. Follicular areas (blue) from the same specimen microdissected and catapulted into tube B. To maximise the yield, this was repeated for 6 sections from each sample (not depicted in this schema) and to minimise cross-contamination of inter-follicular and follicular areas, separate sections were used for Tube A and B (not depicted in this schema). The TCRβ repertoire of the inter-follicular area (A) was then compared with that of the follicles (B).

### 2.6.3 DNA extraction

DNA was extracted from the laser captured tissue using the QIAGEN miniDNA kit following the manufacturer's protocol. The yield of DNA was assessed using the NanoDrop spectrophotometer. Strict microbiological aseptic technique was followed at all steps of sample processing, dissection, DNA extraction and analysis to prevent sample contamination from external sources or cross-contamination from other samples.

### 2.6.4 TCR repertoire sequencing and analysis

After extraction, the DNA was shipped to Adaptive Biotechnolgies, Seattle, USA where TCRβ sequences were PCR amplified using consensus primers prior to next generation sequencing (NGS) using an Illumina platform (Adaptive Biotechnologies, Seattle, WA. USA).

Results from sequencing were released by Adaptive Biotechnologies through their proprietary software package, ImmunoSEQ. The immunoSEQ Platform permits quantification of TCRs, calculation of clonality and assessment of degree of overlap between specimens. Further description of the analysis of TCR repertoires, clonality and entropy are presented in the relevant results section 3.9.

## 2.7 Statistical analysis

Data generated in Nikon Elements NIS advanced research software were exported to Microsoft Excel and statistical analysis was performed using Graph Pad prism software version 5.0 (GraphPad Software Inc, La Jolla, California, USA).

Normally distributed values are presented as the mean (SD), non-normally distributed values are presented as median (IQR).

Normally distributed variables were compared using two-tailed Students unpaired t tests, non-normally distributed data were compared with the Mann Whitney test.

For comparison of paired data, Wilcoxon or Students paired t tests were used. Statistical significance was assumed when $P$ was $<0.05$.

Contingency tables were used to determine whether $Ki67^{pos}$ cells were more likely than non-proliferating cells to be in contact with $T_{FH}$. Fisher's exact test was used to compare individual samples, for comparing total numbers of cells in multiple samples, Fisher's exact test was used for GCs, and Chi squared for FL.

For correlations e.g. between number of Ki67$^{pos}$ cells and number of $T_{FH,}$ Spearman non-parametric correlation coefficient was used.

The calculation of TCR repertoire, clonality and entropy is described in the relevant results chapter.

# Chapter 3 Results

## 3.1 Specimens and clinical details

FFPE lymph node biopsy blocks were obtained from the archives of the department of histopathology at King's College Hospital, London from 8 patients with reactive lymphadenopathy, 2 excised tonsils (for control tissue only), 7 cases of CLL, and 25 cases of FL.

The clinical details for the patients with FL are detailed in Table 3-1. Of the FL samples, 18 were from biopsies taken at the time of initial presentation before any treatment had been administered, 7 were from biopsies taken at relapse, in all of these cases, no treatment had been given for FL for at least 12 months prior to biopsy. 17 samples were from patients with grade 1-2 FL, 5 samples were from patients with grade 3a disease and 3 were from patients with grade 3b disease. 8 patients have not received any treatment but are being managed under a 'watch and wait' approach which is the current standard of care in advanced stage asymptomatic disease.

Limited clinical details relating to the specimens from patients with reactive lymphadenopathy are presented in Table 3-2. Since FL has a mean age of presentation of 64 years and is very rare in childhood, and reactive lymphadenopathy can occur at any age, including in childhood, the median age of patients with reactive lymphadenopathy was younger than for the FL patients, 33.0 years versus 55.8 years.

**Table 3-1: Clinical Characteristics of FL Patients**

| Sample | Age (years) | Gender | Grade | Stage | Disease status at biopsy | Initial management (after current biopsy) |
|---|---|---|---|---|---|---|
| FL001 | 68 | Female | 1 | IV | relapse | R-CVP |
| FL002 | 88 | Female | 3b | I | untreated | not treated* |
| FL003 | 47 | Male | 2 | IV | untreated | R-CVP |
| FL004 | 56 | Male | 2 | IV | untreated | R-CHOP |
| FL005 | 45 | Female | 2 | IV | untreated | R-CVP |
| FL006 | 41 | Male | 2 | IV | untreated | R-CHOP + R |
| FL007 | 63 | Female | 3a | III | untreated | R-CHOP |
| FL008 | 60 | Female | 1 | III | untreated | W&W |
| FL009 | 34 | Female | 3b | I | untreated | R-CHOP + RT |
| FL010 | 70 | Female | 2 | III | relapse | R-CVP + R |
| FL011 | 58 | Male | 3b | III | untreated | R-CHOP |
| FL012 | 29 | Male | 2 | IV | untreated | R-CVP |
| FL013 | 47 | Female | 1 | IV | relapse | R-FC + ASCT |
| FL014 | 54 | Male | 2 | III | untreated | W&W |
| FL015 | 57 | Male | 1 | IV | untreated | R-CVP |
| FL016 | 32 | Male | 3a | IV | untreated | W&W |
| FL017 | 33 | Male | 1 - 2 | IV | relapse | W&W |
| FL018 | 52 | Male | 1 - 2 | IV | untreated | W&W |
| FL019 | 58 | Male | 3a | IV | relapse | R-bendamustine |
| FL020 | 38 | Female | 1 - 2 | III | untreated | W&W |
| FL021 | 63 | Female | 1 | III | untreated | W&W |
| FL022 | 88 | Female | 1 | IV | relapse | R-CVP |
| FL023 | 62 | Male | 1 - 2 | II | relapse | W&W |
| FL024 | 55 | Female | 3a | III | untreated | R-bendamustine |
| FL025 | 60 | Male | 3a | III | untreated | R-bendamustine |

* too frail to receive treatment and died due to ischemic heart disease and FL 5 months after diagnosis

R-CVP = rituximab, cyclophosphamide, vincristine, prednisolone. R-CHOP = rituximab, cyclophosphamide, doxorubicin, vincristine, prednisolone. W&W = watch and wait. RT = radiotherapy. R-FC = rituximab, fludarabine, cyclophosphamide. R = rituximab. CR = complete response. PR = partial response. HSCT = hematopoietic stem cell transplantation

**Table 3-2 Characteristics of patients with reactive lymphadenopathy**

| Sample | Age (years) | Gender | Histological diagnosis |
|---|---|---|---|
| rLN01 | 29 | Male | Reactive hyperplasia |
| rLN02 | 1 | Male | Reactive hyperplasia |
| rLN03 | 35 | Female | Reactive lymph node |
| rLN04 | 40 | Female | Reactive lymph node |
| rLN05 | 27 | Male | Reactive hyperplasia |
| rLN06 | 53 | Female | Reactive lymph node |
| rLN07 | 25 | Male | Reactive hyperplasia |
| rLN08 | 54 | Female | Reactive hyperplasia |

## 3.2 Optimising the multiple labelling technique

Before conducting multiple labelling experiments, it was first necessary to optimise the method of antigen retrieval and determine the contribution of tissue autofluorescence to any signal detected. It was then necessary to demonstrate that the primary antibodies could be used on FFPE material successfully without cross reacting and that they could be detected using fluorescently conjugated secondary antibodies without spectral overlap.

### 3.2.1 Antigen retrieval

Heat induced antigen retrieval was initially performed with pH 6.1 citrate buffer. Some primary antibodies gave rise to either non-specific labelling or no discernible labelling. In these instances, antigen retrieval with pH9.0 Tris-EDTA was attempted but this did not lead to an improvement in labelling in any cases and the primary antibodies were concluded to be incompatible with this experimental method and alternative antibodies were sourced.

Accordingly, all antigen retrieval was subsequently performed in pH 6.1 citrate buffer. The addition of Tween 20 to the citrate buffer gave rise to a slightly cleaner signal with less background although the difference was small (data not shown). Tween 20 (0.05%) was added to pH 6.1 citrate buffer solution in all labelling experiments.

### 3.2.2 Reducing autofluorescence and non-specific binding of secondary antibodies

For most combinations of antibodies, autofluorescence of the tissue sections was not a significant problem. Where autofluorescence was observed it was usually detected in channel 405 (blue) or 488 (green) with very little autofluorescence in the other two channels. It was found that using secondary antibodies conjugated to Alexa Fluor 488 rather than FITC gave a higher signal-to-background ratio, therefore Alexa Fluor 488 was the fluorochrome of choice for secondary antibodies detected in channel 488.

Blocking with normal serum from the species in which the secondary antibodies were raised reduces the cross reaction of the secondary antibody with endogenous immunoglobulins in the tissue and reduces Fc receptor binding of both primary and secondary antibodies. Optimal blocking was with 5% donkey serum for 1 hour at room temperature. No improvement in staining or reduction in non-specific secondary antibody staining was observed through additional blocking prior to incubation with the secondary antibodies or by diluting the antibodies in PBS with 5% blocking serum rather than PBS alone (data not shown).

Antibodies were diluted in PBS, there was no discernible difference in background staining when antibodies were diluted in Tris-buffered saline (TBS). It has been suggested that 0.025% Triton X-100 added to the PBS in which antibodies are diluted dissolves Fc receptors leading to reduced non-specific binding; we observed minimal reduction in background staining through the addition of Triton-X but it did reduce the surface tension of the antibody mixture which helped to ensure that the tissue sections were completely covered with antibody, this facilitated even staining and prevented areas of tissue from drying out during prolonged incubations.

### 3.2.3 Labelling with 3 antibodies simultaneously

To develop a multi-labelling experiment it was necessary to identify combinations of primary and secondary antibodies that would work together.

To reduce the risk of detecting a false signal through cross reactivity of antibodies, primary antibodies from 3 different species were used, mouse, goat, and rabbit, and secondary antibodies were from a different species (Donkey).

The first combinations tested were anti-CD4 (mouse) or anti-Ki67 (mouse), anti-PD1 (goat), and anti-ICOS (rabbit) antibodies. It was determined in single labelling experiments that the primary antibodies worked with this technique, and the optimal concentrations and incubation conditions were established. Next it was assessed whether these antibodies could be used in combination without cross reacting with each other and whether, when fluorescently labelled, they could be detected without significant spectral overlap or secondary antibody species cross reactivity. As shown previously in Figure 2-2, primary antibodies raised in mouse, goat and rabbit were successfully labelled and detected with the application of species-specific, fluorescently labelled secondary antibodies. This combination was successfully used with DAPI as a nuclear stain.

When slides were stained with only one primary antibody in turn but all secondary antibodies, no spectral overlap was detected, Figure 3-1.

A low level of autofluorescence was observed in most cases; where autofluorescence was detected, it was usually in the 488 (green) channel and was mostly identified in blood vessels (where elastin and collagen autofluoresce), or in formalin crystals. The level of background autofluorescence was usually low and easily distinguished from the positive signal.

Many different combinations of the primary antibodies listed in Table 2-2 were successfully used simultaneously. The primary antibodies used in all combinations were from different species, i.e. 2 or more antibodies raised in the same species were never used in the same staining experiment.

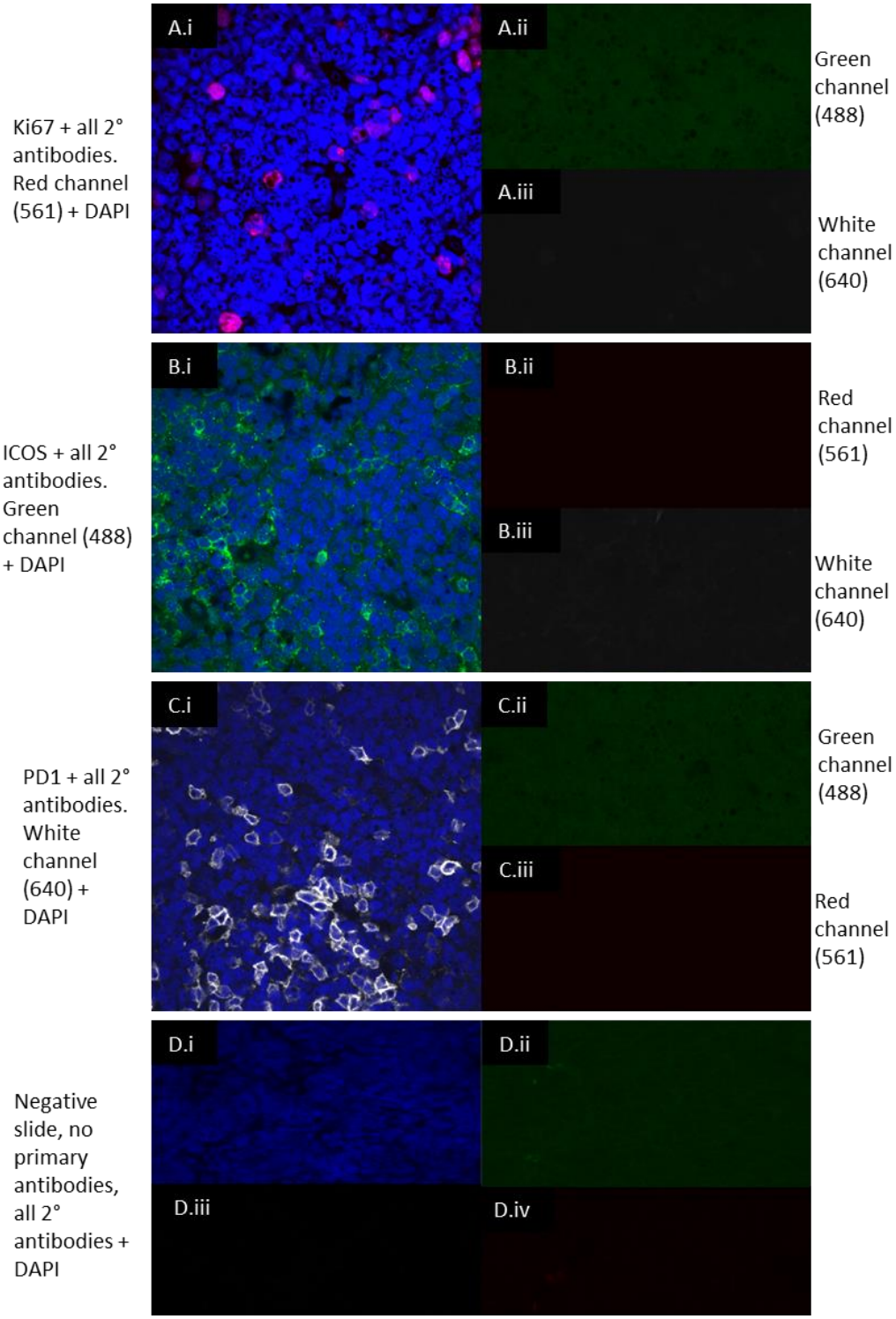


**Figure 3-1 Figure showing controls in multi-labelling experiments.** In **A-C,** 3 different fluorescently labelled donkey antibodies plus DAPI (**blue**) have been added to the slides. In **Ai, Bi,** and **Ci** only 1 primary antibody has been added to the slide (**red = Ki67**, **green = ICOS** and **white** = **PD1**), each one is shown in the channel where the signal is anticipated. In the images on the right, the other channels are shown demonstrating that there has been no spectral overlap or non-specific secondary antibody binding. There is background fluorescence seen in the green channel (488) in images **A.ii, C.ii.** This is confirmed in the double negative slide in which low-level non-specific green fluorescence is detected despite the addition of no primary antibodies to this specimen **(D.ii).**

### 3.2.4 Labelling with 4 antibodies simultaneously

In order to further develop the technique and to permit more refined distinction of cell types and their associations, a 4-antibody labelling protocol was developed. This was developed in particular so that an antibody against a T cell specific antigen (CD3) could be used in conjunction with an antibody against a B cell specific antigen (CD20) and 2 further antibodies for example Ki67 and PD1 to allow the investigation of co-localisation between proliferating B cells (Ki67, CD20) and PD1+ T-cells.

In this protocol the 405nm wavelength laser was used to excite a DyLight 405 conjugated secondary antibody rather than DAPI. The choice of primary antibodies that could be used in conjunction with 3 other antibodies raised in mouse, goat, and rabbit was limited, and no suitable anti-CD4 antibody could be identified but a monoclonal anti-CD3 antibody raised in rat that did not cross react with the other primary antibodies was sourced.

The antibodies used are listed in Table 3-3. The first attempts at 4-antibody labelling were unsuccessful as the level of background fluorescence in the 405 channel was too high to reliably detect the positive signal from the CD3 antibody, Figure 3-2A.

**Table 3-3 Initial antibody panel for 4 antibody labelling**

| Primary antibody | Secondary antibody |
|---|---|
| CD3 – rat | Donkey anti-rat DyLight 405 |
| CD20 – mouse | Donkey anti-mouse Alexa Fluor 555 |
| PD1 – goat | Donkey anti-goat Alexa Fluor 647 |
| Ki67 - rabbit | Donkey anti-rabbit Alexa Fluor 488 |

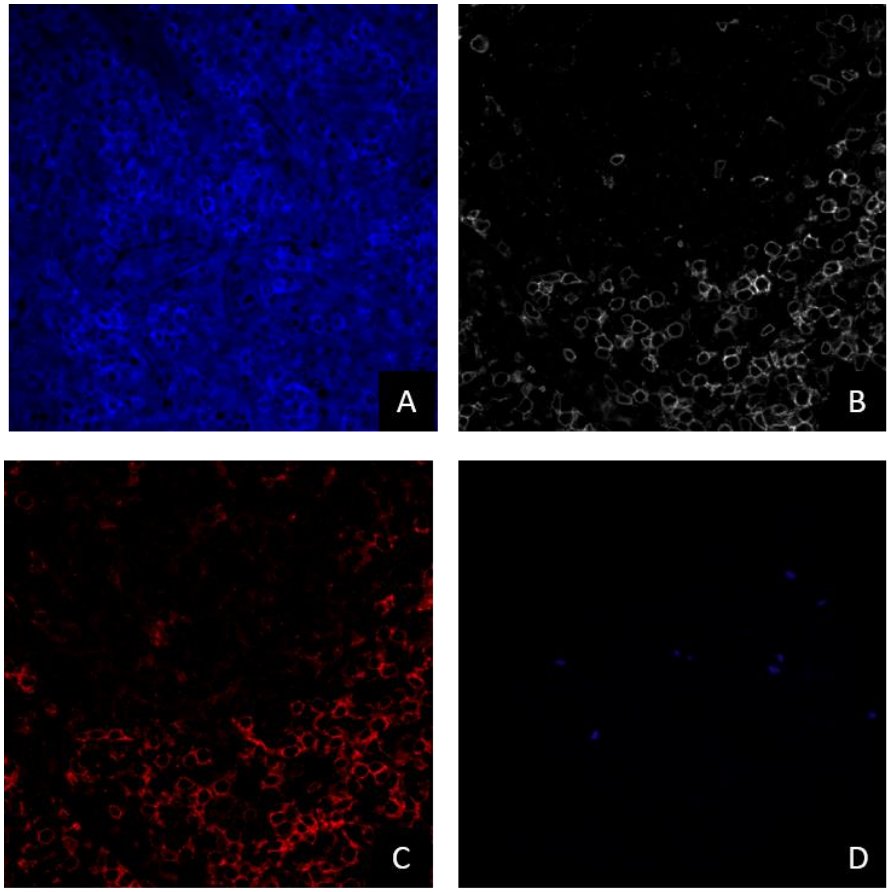


**Figure 3-2 Difficulties staining CD3 with donkey anti-rat DyLight 405. A:** CD3 (**blue**) has been stained but the positive signal is hard to appreciate above the high background signal. **B:** When the same CD3 antibody is detected with donkey anti-rat Alexa Fluor 647, a clean signal is obtained (**white**). **C:** The signal obtained in B is confirmed to be genuine by co-staining with anti-CD4 which shows a very similar pattern of staining (**red**). **D.** Double negative control (no primary or secondary antibody). This suggests that the primary anti-CD3 antibody works and is specific but it is not well detected above the high background signal in the 405 channel.

Possible causes for the high level of background in the 405 channel were non-specific binding of the primary antibody, tissue autofluorescence, non-specific binding of the secondary antibody, or spill-over (spectral overlap) from the other channels. All of these possibilities were investigated.

It was found that the primary antibody worked well when detected with alternative secondary antibodies (donkey-anti-rat Alexa Fluor 647, or donkey-anti-rat Alexa Fluor 488) and that the distribution of CD3+ cells closely matched the distribution of CD4+ cells in the same section, Figure 3-2B and C. Next it was demonstrated that, in a double negative control slide (no primary or secondary antibody), there was very minimal tissue autofluorescence seen in the 405 channel (Figure 3-3A), and

in single antibody controls, no spectral overlap from other channels was identified. It was therefore most likely that the high level of background fluorescence was due to non-specific binding of the secondary antibody to the tissue, indeed in the secondary antibody control slide (no primary antibody, donkey anti rat DyLight 405 secondary only) there was a very high background signal in the 405 channel (Figure 3-3B). To attempt to reduce this, the following steps were introduced: a second blocking step with 5% donkey serum prior to secondary antibody incubation, prolonged washing after the secondary antibody incubation, and further diluting the secondary antibody to 1:400. However, none of these steps led to an appreciable reduction in the high level of background in the 405 channel which made interpreting the pattern of CD3 staining very difficult due to the poor signal to background ratio.

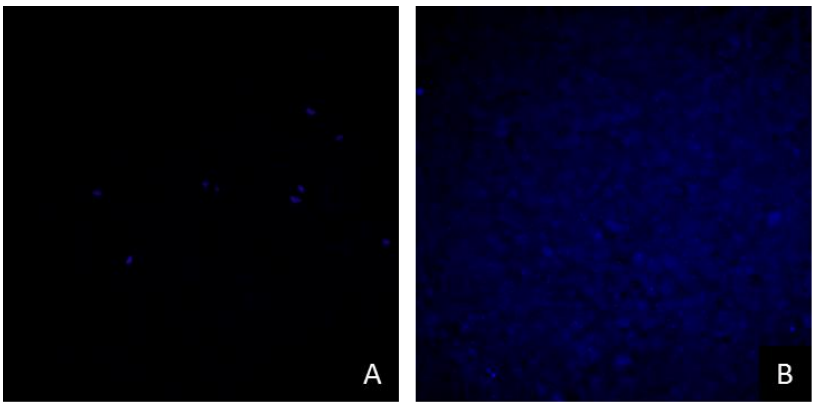


**Figure 3-3 Non-specific staining with DyLight 405 (blue).** When no primary or secondary antibodies are used there is minimal autofluorescence in the 405 channel **(A).** When the donkey anti-rat DyLight 405 secondary antibody is used alone with no primary antibodies, a high level of background fluorescence is obtained in the 405 channel **(B).**

Since this problem could not be resolved it was decided to change the secondary antibodies so that the primary antibody with the strongest and most distinctive pattern of staining (Ki67) was detected by labelling with the secondary antibody with the lowest signal to background ratio (DyLight 405) whilst the anti-CD3 antibody which does not have such a distinctive or characteristic staining pattern was detected with a stronger fluorescently conjugated secondary antibody (donkey anti-rat Alexa Fluor 488). This was found to give excellent results with Ki67 (detected with donkey anti-rabbit DyLight 405) clearly identified above the background signal in the 405 channel and very clear CD3 staining

detected in the 488 channel, Figure 3-4. Once this technique had been developed it permitted the investigation of further combinations with 4 simultaneously labelled antibodies, see Table 3-4.

**Table 3-4 Potential antibody combinations for 4 colour labelling experiments**

| Rat | Goat | Rabbit | Mouse |
|---|---|---|---|
| CD3 | PD1 | Ki67 | CD20 |
| CD3 | PD1 | Ki67 | AID |
| CD3 | PD1 | Ki67 | FOXP3 |

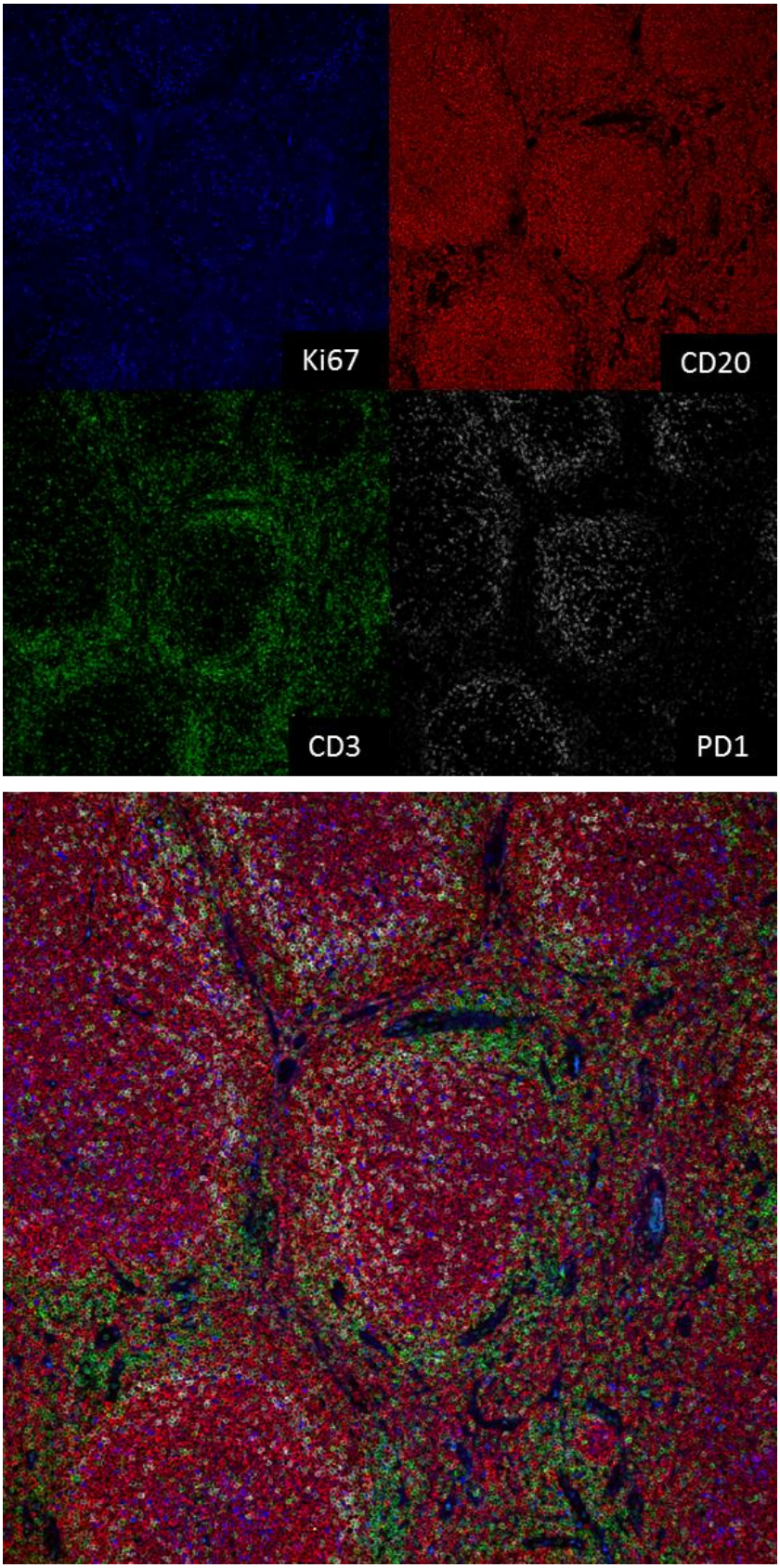


**Figure 3-4 Successful 4 antibody labelling of Ki67 (blue), CD20 (red), CD3 (green), and PD1 (white) in FL.** (Image acquired with x10 objective).

## 3.3 Distribution and phenotype of T Follicular Helper Cells in FL, reactive LN, and CLL

The phenotype and function of Follicular helper T cells ($T_{FH}$) are detailed in section 1.3 above. $T_{FH}$ cells have been described in FL by flow cytometry of disaggregated lymph nodes and single parameter IHC studies have revealed PD1+ cells to be limited mainly to the follicles where an increased number has been reported to be associated with better prognosis (see section 1.6.2). Limitations to previous research in this area are related to the methodology used; single parameter IHC is unable to accurately identify complex cellular subsets and flow cytometry on disaggregated LNs is unable to provide detailed information about the distribution and location of particular cell populations with regards to the follicles.

Thus, one of the key aims of this part of my research was to establish the phenotype and distribution of CD4+ T cells in FL and to make direct comparisons to the findings in GCs. This sophisticated method of analysing populations of cells in situ has not been previously performed in FL or GCs and accordingly novel insights into $T_{FH}$ in both FL and GCs have been attained.

Since PD1, ICOS, Bcl-6, and CXCR5 can be expressed by various T cell subsets and both Bcl-6 and PD1 can be identified in FL B cells, no single marker can be used to identify $T_{FH}$ cells and this is a problem of single parameter IHC studies that have used PD1 as a surrogate marker for $T_{FH}$ cells.

In this research we developed a protocol using antibodies against CD4, PD1, and ICOS simultaneously to identify $T_{FH}$ cells by confocal immunofluorescent microscopy. As detailed above, this combination of antibodies could be used with a nuclear counterstain (DAPI) without cross reaction and with well separated fluorescently labelled secondary antibodies. We investigated the proportion of CD4+ cells with a $T_{FH}$ phenotype within follicles (follicular) and outside follicles (interfollicular) in FL, within and outside of GCs in reactive lymph nodes, and for comparison with another lymphoproliferative disorder, in lymph nodes infiltrated with CLL.

### 3.3.1 Distribution and proportion of CD4+ T cells with $T_{FH}$ phenotype in FL

The distribution of CD4+ T cells in FL is striking; they were identified in all specimens analysed and were predominantly located in the interfollicular areas or at the border of the follicles where they often form dense infiltrates with relatively few scattered CD4+ T cells within the B cell rich malignant follicles. This predominantly interfollicular pattern of CD4+ T cell distribution was identified in 21/25 (84%) cases examined. In the remaining 4 cases, the pattern of CD4+ T cell infiltration was either indistinct (3/25 cases, 12%) or in one case (4%) the pattern appeared predominantly follicular (Case 004, a previously untreated male patient with Grade 2 FL). There was no clear association between histological grade and CD4 pattern of distribution. In the 4 cases not demonstrating the predominantly interfollicular CD4 pattern, the follicular structure was indistinct in the biopsy specimen as the follicles had become confluent with less distinction between follicular and interfollicular areas, Figure 3-5.

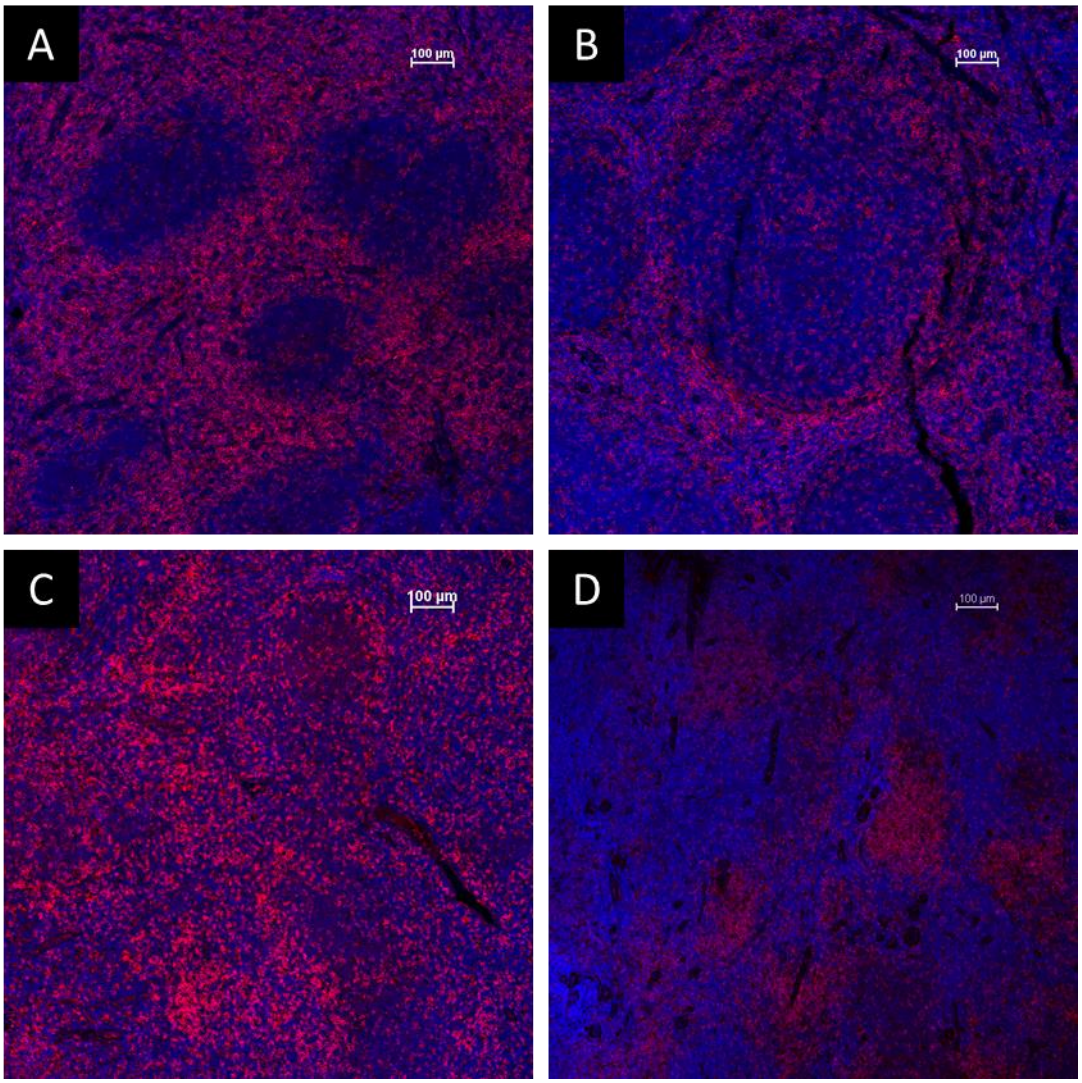


**Figure 3-5 The distribution of CD4+ T cells in FL.** CD4 (**red**) infiltration was interfollicular in 84% of samples **(A** and **B)** but can be mixed **(C),** or was predominantly follicular in one case **(D).** Nuclear counter stain is with DAPI (**blue**). (All images acquired with x10 objective, scale bars represent 100µm)

By measuring the proportion of CD4+ cells that co-expressed the surface antigens PD1 and ICOS it was possible to determine the proportion of CD4+ cells with a $T_{FH}$ phenotype in the follicular and interfollicular areas of infiltrated lymph nodes.

CD4+ PD1+ ICOS+ cells were identified within the follicles of all cases of FL examined (n=25).

Analysis of an average of 5 high power (x60 objective) fields from representative follicular areas per specimen revealed that the median proportion of follicular CD4+ cells co-expressing both PD1 and

ICOS was 25.0% (18.5-28.7). The CD4+ PD1+ ICOS+ cells were tightly restricted to the follicles with only 3.63% (1.89-6.15) of interfollicular CD4+ cells co-expressing PD-1 and ICOS. As discussed in section 3.3.1.3 on page 108 below, it was not possible to generate a reliable, reproducible, automated method of calculating the absolute number of CD4+ cells present in any given image.

The proportion of CD4+ T cells with a $T_{FH}$ phenotype within follicles was significantly higher than the proportion in interfollicular areas, p<0.001, (Mann-Whitney test), **Figure 3-6**. A representative high power field of a follicle showing the original image, the intersection of the CD4, PD1 and ICOS binary layers and how this relates to the CD4 layer is shown in Figure 3-7.

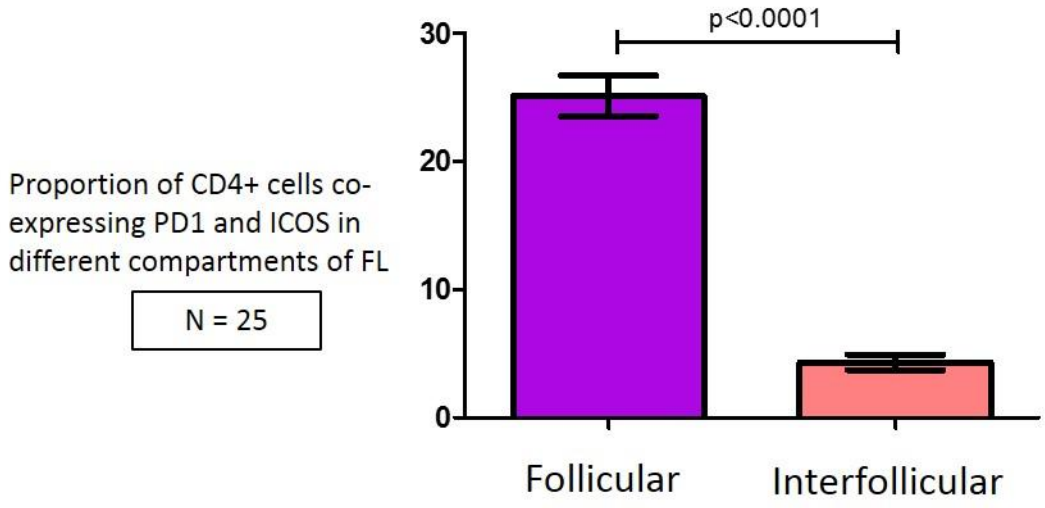


**Figure 3-6 The proportion of CD4+ cells with a TFH phenotype is significantly higher within FL follicles than in the interfollicular compartment. (Column heights represent mean, error bars SEM).**

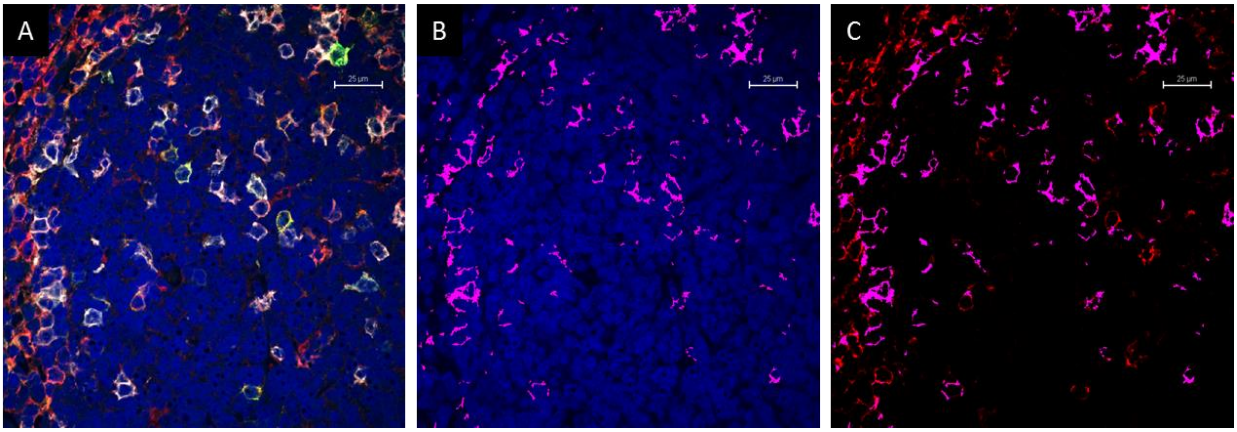


**Figure 3-7. $T_{FH}$ cells in FL. A.** The original image is shown with DAPI (**blue**) CD4 (**red**) ICOS (**green**) and PD1 (**white**). **B.** The intersection of the binary layers for CD4 PD1 and ICOS is shown in **pink** highlighting the $T_{FH}$ cells. **C.** The relationship of the intersecting binary layer to the CD4 (**red**) cells is shown. It can be seen that CD4+ cells (**red**) outside of the follicle (top left of image) do not co-express PD1 and ICOS (All images acquired with x60 objective, scale bars represent 25μm)

The distribution of $T_{FH}$ cells with regards to the follicles was variable; in 46% of cases there was a predominantly perifollicular distribution of $T_{FH}$ cells forming a 'halo' around the edge of the follicles. In 38% of cases the $T_{FH}$ cells were mainly concentrated in the centre of the follicles, and in the remaining cases (17%), the distribution was diffuse or mixed,

Figure 3-8. There may be a relationship between the pattern of distribution of $T_{FH}$ cells, histological grade and rate of proliferation; 6/9 (66%) of cases with a follicular pattern of $T_{FH}$ distribution were grade 3a or 3b disease whereas only 1/11 (9%) of cases with a perifollicular pattern of distribution had grade 3a disease. Not enough data has been generated to date to determine the significance of this observation.

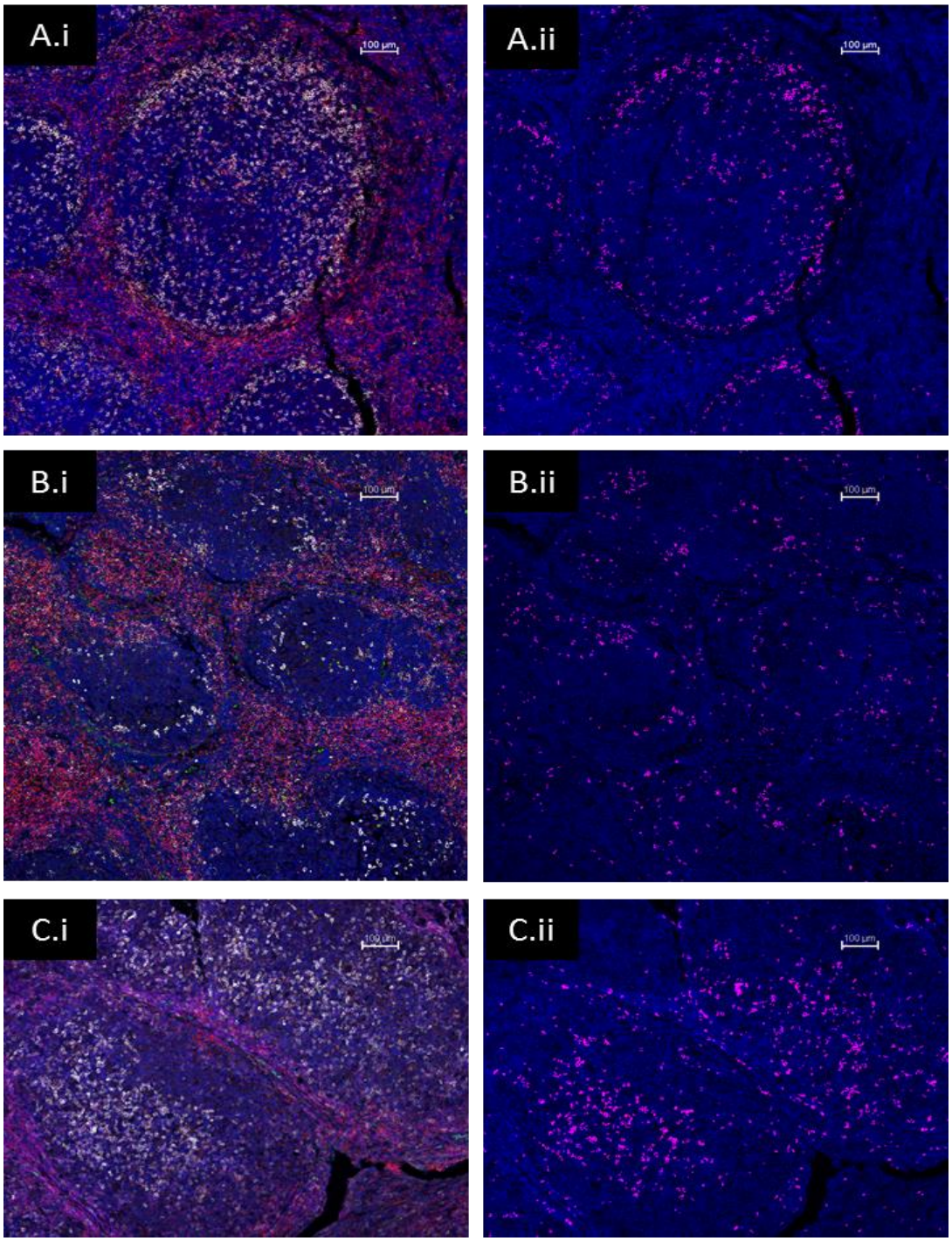


**Figure 3-8. Figure showing patterns of $T_{FH}$ location in FL.** CD4 (**red**), ICOS (**green**), PD1 (**white**), DAPI (**blue**). In **Ai, Bi** and **Ci** the original images are shown. In **Aii, Bii** and **Cii**, the DAPI layer (**blue**) is shown with superimposed binary layer of the intersection of CD4, PD1 and ICOS (**pink**). This highlights the mainly perifollicular location of $T_{FH}$ in **A** and **B** whilst in **C** the $T_{FH}$ are centrally located in the follicles. (All images acquired with x10 objective, scale bars represent 100μm)

The need for multi parameter labelling to identify the complex T cell subsets present in the FL microenvironment is highlighted by the observation that whilst 46.9% (34.7-51.9) of follicular CD4+ cells were positive for PD1, only 52.2% (45.7-61.9) of these co-expressed ICOS. In interfollicular areas, 9.3% (5.1-26.4) of CD4+ cells were positive for PD1 but almost two thirds of these (62% ± 4.8) did not co-express ICOS. Therefore, single staining for PD1 (or dual labelling for CD4 and PD1) would significantly overestimate the proportion of $T_{FH}$ cells as it would encompass two distinct populations of T cells, CD4+/PD1+/ICOS+ and CD4+/PD1+/ICOS- cells, as well as PD1+ B cells.

#### 3.3.1.1 Confirmation that CD4+ PD1+ ICOS+ cells are $T_{FH}$.

The complexity of phenotyping of CD4+ T cell subsets meant that it was necessary to perform further experiments to confirm that cells identified as CD4+, PD1+, ICOS+ were indeed $T_{FH}$.

A 4-antibody panel comprising CD3, BCL-6, PD1, and ICOS was developed in order to investigate whether the PD1+ ICOS+ T-cells expressed BCL-6, the transcription factors essential for $T_{FH}$ differentiation. Technical limitations meant that it was not possible to stain simultaneously with CD4, BCL6, PD1, and ICOS, hence CD3 was used in place of CD4. 15 images from 5 FL specimens were analysed using this technique. As expected, the FL B cells within follicles were strongly positive for BCL-6 and it was observed that a population of CD3+ T-cells within the follicles were also positive for BCL-6, Figure 3-9 and Figure 3-11. 89.6% (88.3-91.8) of PD-1+ ICOS+ CD3+ cells were BCL-6 positive strongly indicating that the majority of PD1+ ICOS+ T cells are $T_{FH}$.

This is the first time that BCL6 positive, CD4+ T cells with a $T_{FH}$ phenotype have been demonstrated in situ in FL.

Interestingly, the level of expression of BCL-6 was intermediate in $T_{FH}$; lower than in FL B-cells but significantly higher than in PD1- ICOS- T-cells, Figure 3-10.

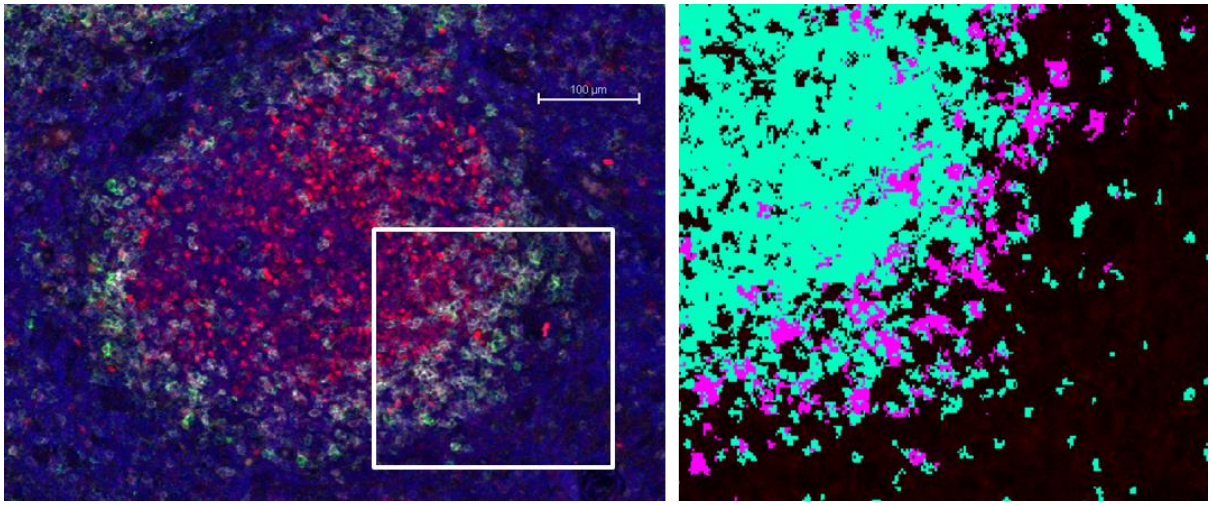


**Figure 3-9 BCL-6 is present in PD1+ ICOS+ cells.** Follicle in FL showing BCL-6 (**red**), ICOS (**green**), PD1 (**white**) and DAPI (**blue**). The area in the white rectangle has been magnified in the figure on the right and the binary layers for BCL6 (**turquoise**) and PD1/ICOS intersection (**pink**) are shown. This shows that most PD1+ ICOS+ cells (**pink**) are BCL6 positive. (Magnified area of image acquired with x10 objective, scale bar represents 100µm)

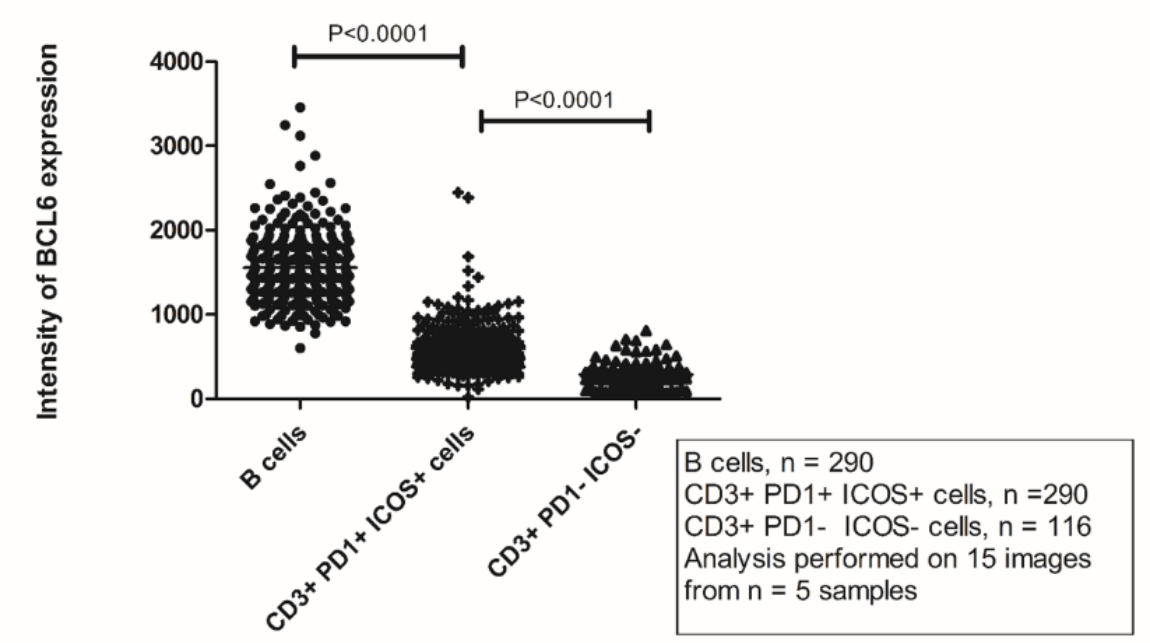


**Figure 3-10 Intensity of BCL-6 expression in FL: expression is significantly higher in $T_{FH}$ than other T-cells but is significantly lower than in the FL B-cells. (Horizontal bars represent mean).** Analysis performed on 15 images obtained from 5 samples. Individual dots represent intensity of expression on BCL6 in a given cell. Mean intensity compared by Mann Whitney Tests.

The analysis of these images could not be automated and required significant operator input to identify the cells in which BCL-6 expression was to be measured. This had the potential to introduce

bias to the system which was overcome by verifying the images with a second investigator, and was also very time consuming which prevented us from using this assay on more samples. Mean intensity of BCL6 expression within a given cell was measured using the automated intensity tool in the image analysis software.

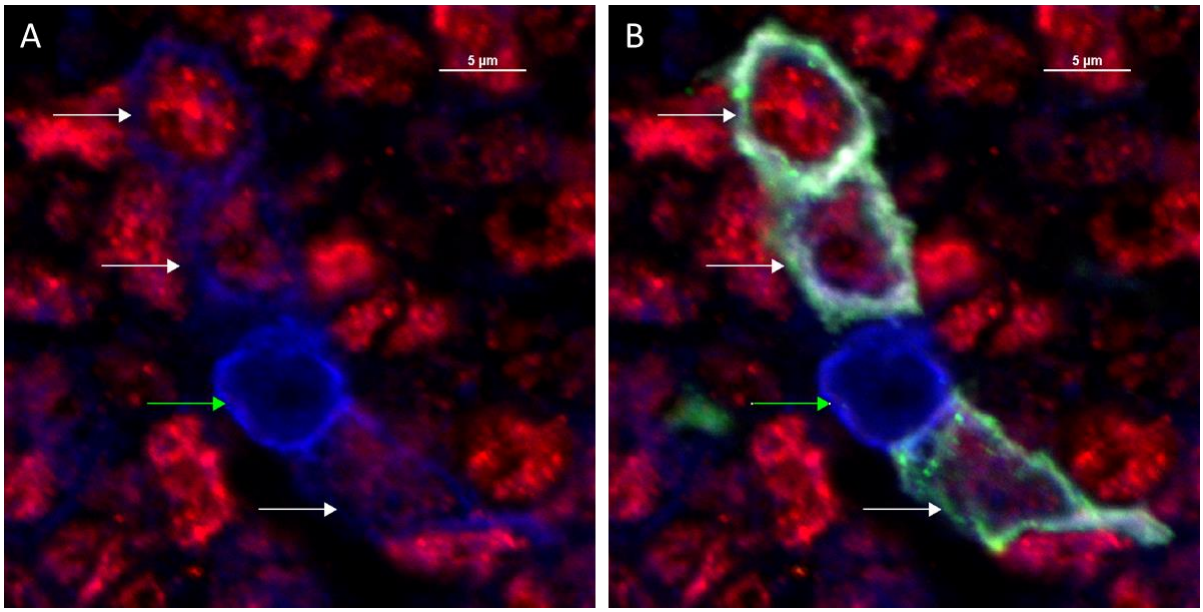


**Figure 3-11. PD1+ ICOS+ T cells express BCL-6. A.** 4 CD3+ T cells (**blue**) are seen in this highly magnified FL section. The 3 T cells labelled with white arrows are positive for BCL-6 (**red**). There is one T cell that is not positive for BCL-6 (green arrow). **B.** The 3 T cells that are positive for BCL-6 are also ICOS (**green**) and PD1 (**white**) positive confirming these as $T_{FH}$ cells. The BCL-6 negative T cell (green arrow) expresses neither PD1 or ICOS. The BCL-6+ (red) non-T-cells in this image are FL B cells. (Magnified area of image acquired with x60 objective, scale bar represents 5µm)

Since technical limitations meant that we had to stain with CD3 instead of CD4 in this panel, it was important to ascertain whether this was a valid substitution. In separate experiments we identified that there were no CD8+ BCL-6+ T-cells in FL, Figure 3-12, therefore we could assume that all CD3+ BCL-6+ T cells are CD4+ and this validated our panel of CD3, BCL-6, PD1 and ICOS for the identification and verification of $T_{FH}$.

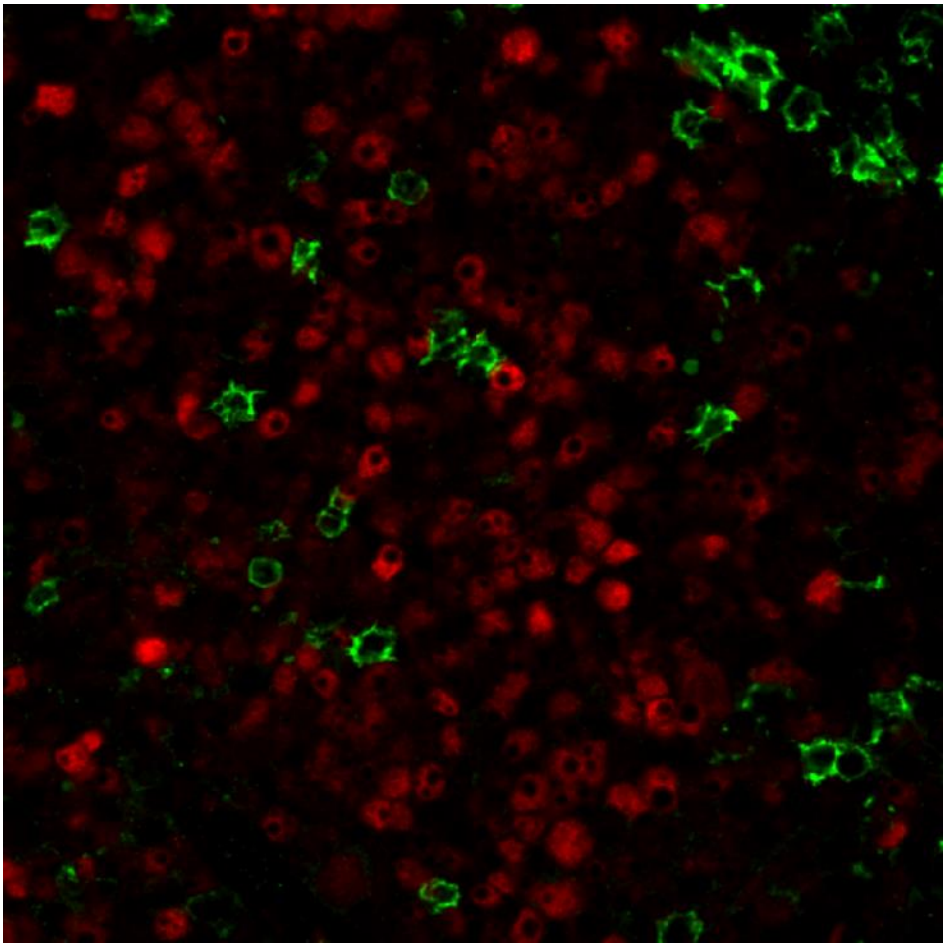

**Figure 3-12 CD8+ T cells (green) are not BCL-6+ (red) in FL.** Image acquired with x60 objective.

Furthermore, in additional staining experiments, we identified that PD1+ ICOS+ cells were CXCR5 positive, Figure 3-13. However, since most cells within the follicles and GCs are CXCR5+ this did not add further clarification that the cells we identified as being CD4+ PD1+ ICOS+ were indeed $T_{FH}$, CXCR5 was therefore not used to identify $T_{FH}$ in further experiments.

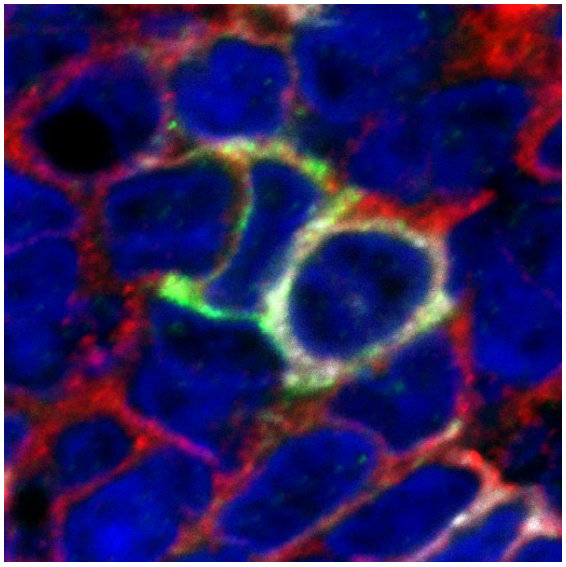

**Figure 3-13 PD1+ (white) ICOS+ (green) cells within follicles are also CXCR5+ (red).** Representative high power image. Note that CXCR5 does not specifically highlight the PD1+ ICOS+ cells but is expressed on many cells within the follicles. Magnified image acquired with x60 objective.

### 3.3.1.2 Intensity of expression of CD4 and PD1 depends on location of T-cells in FL

It was noted that the intensity of CD4 expression appeared to be lower amongst the follicular CD4+ cells than in interfollicular CD4+ cells, meanwhile PD1 appeared to be expressed at a high level in the follicular CD4+ cells but was present at a low level in a proportion of interfollicular CD4+ T cells.

The level of expression of CD4 and PD1 was formally measured in follicular and interfollicular areas in 5 FL samples. The intensity of CD4 expression was 30.7% lower in follicular CD4+ T-cells than in their interfollicular counterparts (mean intensity 846 ± 13.2 versus 1222 ± 17.5, P <0.0001). As CD4 is known to be internalised and degraded following activation, this finding suggests that these represent a distinct population of more activated T-cells.

The intensity of expression of PD-1 was significantly higher in follicular PD-1+ T-cells than in the interfollicular PD-1+ T-cells (1346 ± 55.2 versus 545 ± 13.7, P <0.0001). The high expression of PD-1 in the follicular T-cells is consistent with them being $T_{FH}$, which are characterized by very high PD-1

expression, meanwhile the interfollicular CD4+ PD1$^{low}$ ICOS- cells are unlikely to be $T_{FH}$ (Haynes, Allen et al. 2007), Figure 3-14.

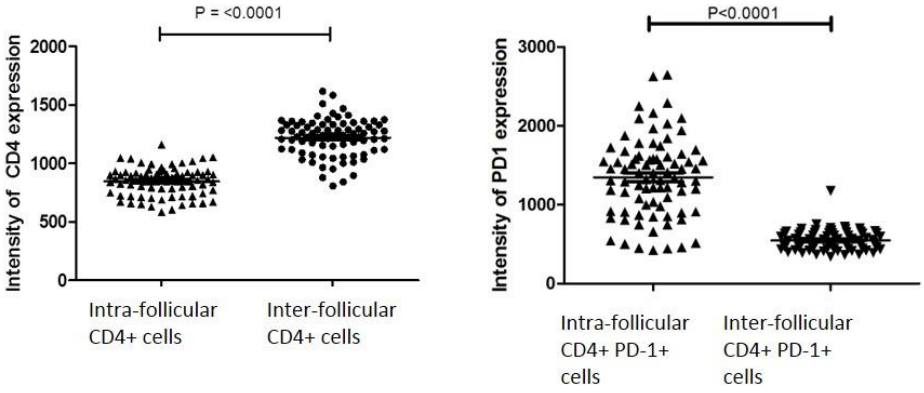


**Figure 3-14 (A) Mean intensity of CD4 expression was significantly lower in the follicular CD4+ T-cells in FL than in interfollicular CD4+ T-cells. (B) Mean intensity of PD-1 in follicular CD4+ PD1+ T-cells is significantly higher than in interfollicular CD4+PD1+ T-cells (n= 81 follicular areas and 81 interfollicular areas from n=5 FL cases).** Horizontal bars represent the mean, error bars = SEM**.**

As well as indicating that there are distinct populations of CD4+ and PD1+ T cells in the follicular and interfollicular regions, this observation highlighted the importance of carefully setting the threshold for CD4 and PD1. These thresholds were set on follicular regions and then the same thresholds were applied to the interfollicular area analysis so that the correct populations of cells were identified. This is similar to the way that gating strategies used in flow cytometry are based on level of expression in cells or beads known to be positive or negative for a particular antigen. Furthermore, a high level of PD1 expression (PD1$^{Hi}$) cells was used as a surrogate indicator of $T_{FH}$ in later experiments when ICOS or BCL6 could not be used in combination.

#### 3.3.1.3 Method of analysis for determining the proportion of $T_{FH}$ cells

Two methods of analysis were developed for determining the proportion of CD4+ T cells with a $T_{FH}$ phenotype, 'object' analysis and 'area' analysis. Object analysis divided the CD4 binary layer into 'objects' which broadly correlated with CD4+ cells. Each CD4+ 'object' (i.e. cell) was then interrogated

to determine whether it had any overlapping binary areas of PD1 and ICOS positivity so giving a count of the number of CD4+ cells that were $T_{FH}$. This method was severely compromised by the membrane pattern of staining of CD4 and the fact that in tissue sections, cells are very tightly packed together therefore it was difficult to automatically separate CD4+ cells into discrete objects and this process accordingly required a lot of manual object separation which was very time consuming, difficult to do accurately and, given that it could not be automated, introduced a possible element of user bias.

An alternative method of analysis was therefore developed, 'area' analysis. In area analysis, each binary layer is set as described in section 2.5 above and then the amount of the CD4 binary layer in which PD1 and ICOS are co-expressed is calculated as a proportion of this area. Whilst this has the advantage of being fully automated (once the thresholds had been set), and is therefore fast and has a reduced risk of user bias, it has a disadvantage that it does not give a cell count. Both methods were assessed and no significant difference in the percentage of CD4+ cells co-expressing PD1 and ICOS was detected between the two techniques (paired t test, p=0.487), Figure 3-15. Therefore, the area analysis was adopted for this analysis.

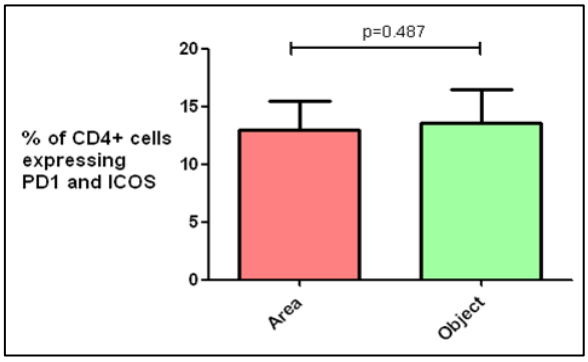


**Figure 3-15 Comparison of two different methods of image analysis:** There was no significant difference in the proportion of CD4+ T cells identified as having dual expression of PD1 and ICOS by the different methods of analysis.

### 3.3.2 Distribution and proportion of CD4+ T cells with $T_{FH}$ phenotype in reactive lymph nodes

Similar to FL, CD4+ T cells were also identified in all cases of reactive lymph nodes examined (n = 8). As in FL, the T cells were mainly located outside of the follicles and GCs but small distinct populations of CD4+ T cells were also present within the GCs.

$T_{FH}$ cells, identified by CD4, PD1, and ICOS staining were present in all reactive lymph nodes examined (n=8). They were very tightly restricted to the GCs where analysis of 5 high power fields (x60 magnification) per section revealed that a median of 33.05% (24.7-43.7) of CD4+ cells were dually positive for PD1 and ICOS with very few identified in the non-GC areas, median 0.34% (0.26-1.13), the difference between GCs and non-GCs was highly significant (Mann Whitney test, p = 0.0014), Figure 3-16. In representative sections from 4 cases of reactive lymphadenopathy, the GC PD1+/ICOS+ cells were also demonstrated to be BCL-6 positive and CXCR5 positive - as in FL – and are therefore highly likely to represent $T_{FH}$ cells.

The distribution of $T_{FH}$ cells within the GCs was variable, they were noted to be either centrally located or polarised to the light zone of the GC, Figure 3-17. As identified in FL, lower expression of CD4 and higher expression of PD1 were noted in the GC T cells than in the non-GC T cells but it has not been possible to formally quantify the difference in level of expression in reactive LNs retrospectively as adequate numbers of high quality images of non-GC areas of reactive LNs were not obtained at time of image acquisition.

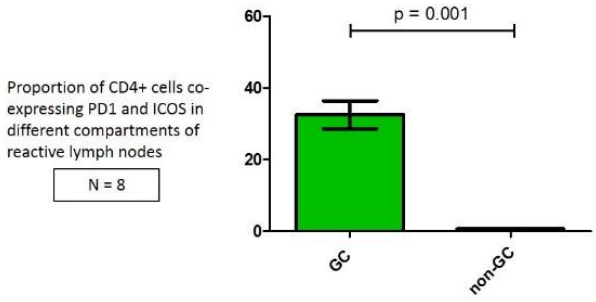


**Figure 3-16 Significantly more germinal centre than non-germinal centre CD4+ T cells have a $T_{FH}$ phenotype in reactive lymph nodes. (Column height represents mean with error bars indicating SEM).**

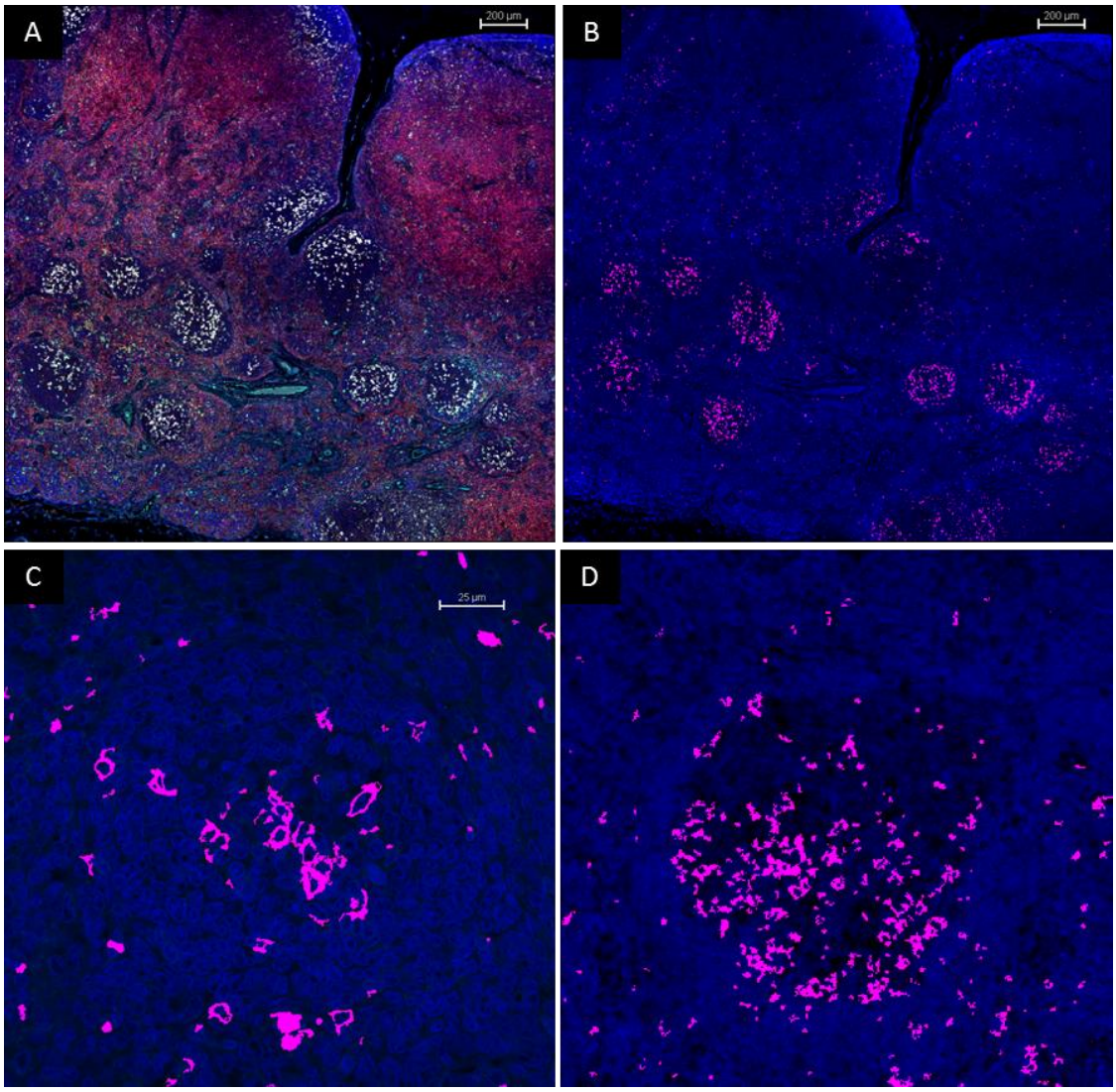


**Figure 3-17 Distribution of $T_{FH}$ cells in germinal centres of reactive lymph nodes. A.** Stitched image (4 x 10x magnification images joined together, scale bar represents 200µm) showing clear GCs with most CD4+ T cells located outside of the GCs, CD4 (**red**), ICOS (**green**), PD1 (white), DAPI (**blue**). **B.** The intersection of CD4, PD1 and ICOS is highlighted in **pink** showing $T_{FH}$ cells are restricted to the GCs. **C.** Distribution of $T_{FH}$ cells can be central or polarised to the light zone of the GC **(D).**

### 3.3.3 Distribution and proportion of CD4+ T cells with $T_{FH}$ phenotype in CLL

The presence and distribution of $T_{FH}$ cells were investigated in 7 cases of CLL as a comparison to FL and reactive lymph nodes. Although many cells in CLL expressed PD1, few were found to be $T_{FH}$. A median of 23% (17.9 – 33.7) of CD4+ cells in CLL expressed PD1, but only 2.8% (1.8 – 6.8) of CD4+ cells co-expressed PD1 and ICOS and very few BCL-6+ T cells could be identified. The PD1+ CD4+ $ICOS^{neg}$ T cells are unlikely to represent $T_{FH}$ cells but could perhaps be exhausted T cells. The pattern of distribution of the few $T_{FH}$ cells in CLL was diffuse and it was beyond the scope of this research to determine whether they were present in proliferation centres.

### 3.3.4 $T_{FH}$ comparison between FL, reactive GCs and CLL

There was no significant difference in the proportion of CD4+ T cells with a $T_{FH}$ phenotype in the follicles of FL and normal GCs (medians 25.0 versus 33.0 respectively, Mann Whitney test, p = 0.06). There were slightly more interfollicular $T_{FH}$ in FL than in reactive lymph nodes but the numbers were low in both situations and the slight increase in the interfollicular area of FL may reflect the sometimes diffuse nature of the follicles and subsequent difficulty distinguishing the follicular border in FL whereas the GCs of reactive LNs were always clearly demarcated (medians 3.63 versus 0.34, Mann Whitney test, p = 0.003). The proportion of CD4+ T cells that were $T_{FH}$ in CLL was significantly lower than either FL follicles or reactive GCs but was not significantly different to the interfollicular region of FL (Mann Whitney test, p = 0.61), Figure 3-18, and Table 3-5.

**Table 3-5 Proportion of CD4+ T cells co-expressing PD1 and ICOS in different compartments**

| | FL follicles | GCs | Interfollicular area of FL | Interfollicular area of reactive LNs | CLL |
|---|---|---|---|---|---|
| Median % (IQR) | 25 (18.5 – 28.75) | 33 (24.7 – 43.7) | 3.63 (1.89 – 6.15) | 0.34 (0.26 – 1.13) | 4.14 (1.45 – 6.8) |

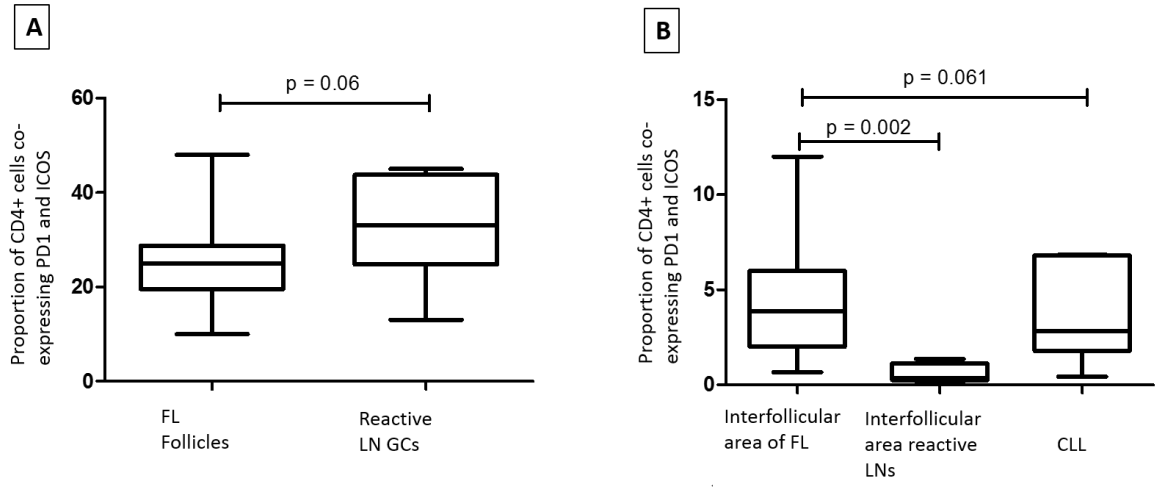


**Figure 3-18 Graphs showing differences in proportion of $T_{FH}$ between different compartments. A.** No difference in proportion of $T_{FH}$ between follicles of FL and GCs of reactive LNs. **B.** A small but significant difference between the interfollicular regions of FL and non-GC areas of reactive LNs, and a non-significant difference between the interfollicular area of FL and CLL. (n = 115 images from 25 FL samples, n = 39 images from 8 reactive LNs, n = 28 images from 7 CLL samples). Boxes represent interquartile range, horizontal bars show median, 'whiskers' show minimum and maximum values.

## 3.4 Association of $T_{FH}$ cells with proliferating B cells

It has previously been identified that proliferating B cells in CLL are frequently in close contact with CD4+ T cells indicating a role of the CLL microenvironment in influencing proliferation in this disease (Patten, Buggins et al. 2008). Such an association has never previously been reported in FL, and whilst it is accepted that $T_{FH}$ are important in determining GC size and B cell proliferation within GCs, co-localisation of GC B cells with $T_{FH}$ has not previously been demonstrated. Here, we investigated whether there was any spatial correlation between proliferating B cells in FL and $T_{FH}$ cells and explored to what extent this is the same in reactive lymph nodes.

### 3.4.1 Association of $T_{FH}$ cells with proliferating B cells in FL

Proliferation was identified by Ki67 staining whilst simultaneously co-staining with CD4 and PD1; in separate sections Ki67, ICOS and PD1 were co-stained. Later, once a 4-colour staining protocol was developed it was possible to simultaneously stain for CD20, Ki67, PD1 and CD3. Ki67 is commonly used in IHC to identify cells in cycle. Ki67 expression can be detected by IHC at all stages of cellular proliferation, Ki67 expression is highest in $G_2$ but it is not expressed at the protein level in $G_0$ (Williams and Stoeber 2007).

As previously reported by others, proliferation – as identified by Ki67 staining - was found to be highly variable both within different follicles of the same section and between cases (Samols, Smith et al. 2013, Kedmi, Hedvat et al. 2014) but, as expected, $Ki67^{pos}$ cells were more frequent in high grade disease samples (Grade 3a and 3b) than in low grade disease (Grade 1-2).

Ki67 had a similar pattern of distribution as $T_{FH}$ cells; in cases where the $T_{FH}$ cells were located at the follicular border, $Ki67^{pos}$ cells were predominantly at the follicular border too, but when $T_{FH}$ cells were more diffusely located, the distribution of $Ki67^{pos}$ cells was diffuse too, Figure 3-19.

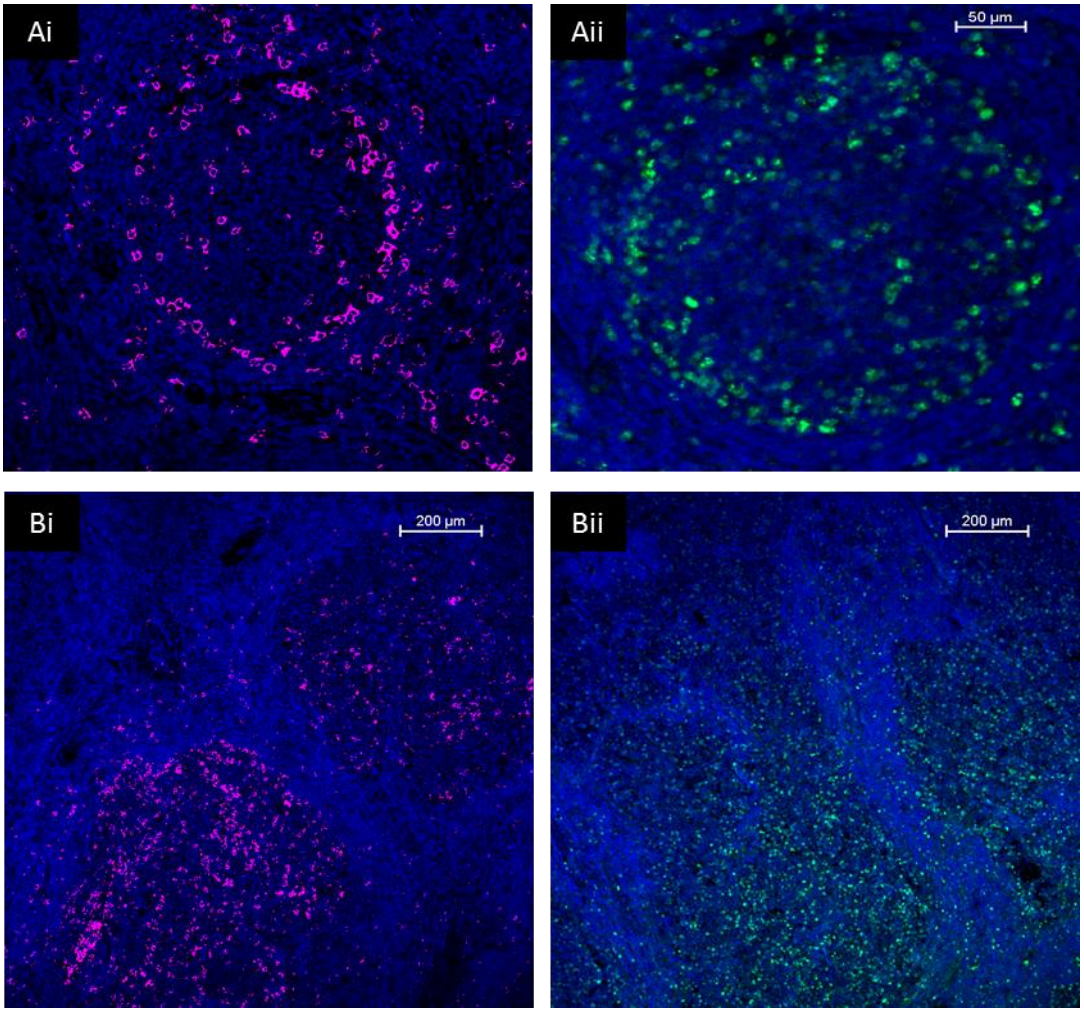


**Figure 3-19 Distribution of Ki67 positive cells is similar to $T_{FH}$ distribution in FL. Ai** shows peripheral location of $T_{FH}$ (**pink** intersection binary of CD4/PD1/ICOS) and in a separate section of the same specimen when Ki67 is stained (**green**) **(Aii)** it is shown to have a similar perifollicular distribution. **Bi** shows follicular location of $T_{FH}$ (**pink** intersection of CD4/PD1/ICOS) and in the same specimen when Ki67 is stained **(Bii)** it is shown to have a similar follicular distribution.

A high proportion of proliferating cells were found to be in close contact with $T_{FH}$ cells. In 23 FL cases examined, a mean of 41% ± 13.6 of $Ki67^{pos}$ cells were in direct contact with CD4+ $PD\text{-}1^{Hi}$ cells (n=100 images from 23 samples). Staining for Ki67 PD-1 and ICOS in separate sections revealed that 84.7% ± 1.7 (n=43 images from 13 samples) of the $PD\text{-}1^{Hi}$ CD4+ cells in contact with $Ki67^{pos}$ cells were dually positive for ICOS and therefore likely to be $T_{FH}$, Figure 3-20 & Figure 3-21.

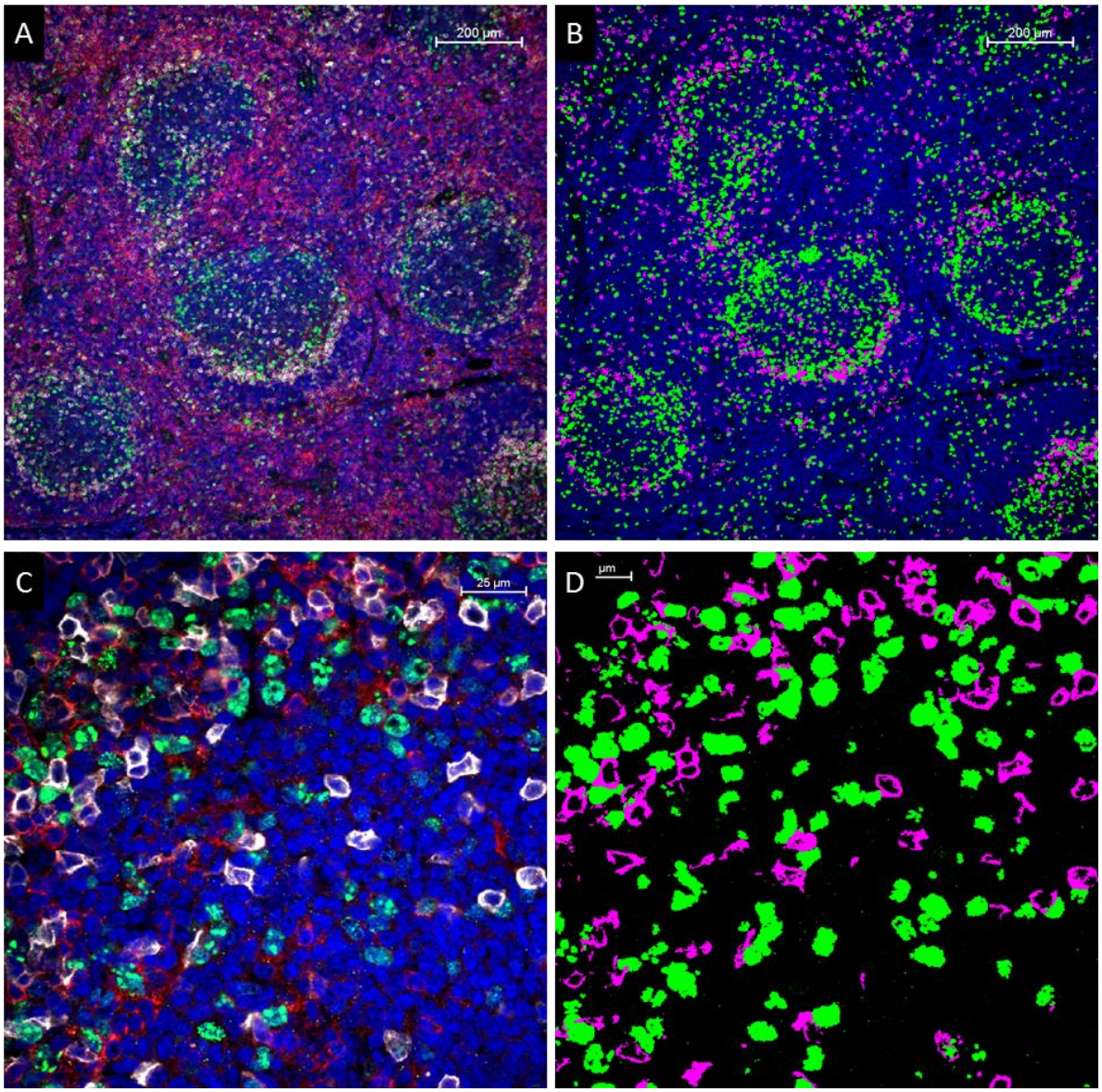


**Figure 3-20 Ki67$^{pos}$ cells are in close proximity to CD4+ PD1+ cells in FL. A.** low power view showing Ki67 (**green**), CD4 (**red**) PD1 (**white**), and DAPI (**blue**). **B.** The binary layers of Ki67 (**green**) and CD4-PD1 intersections (**pink**) are shown highlighting the close proximity of Ki67$^{pos}$ cells to PD1$^{Hi}$ T cells. **C and D.** High power views showing the same as A and B. >40% of Ki67$^{pos}$ cells are in direct contact with PD1$^{Hi}$ CD4+ cells.

3D reconstruction of Z-stacks allowed closer visualisation of the often intimate interaction of these cells and revealed more interactions than were identified in 2D images. It was sometimes found that proliferating cells were in contact with more than one $T_{FH}$ simultaneously, Figure 3-21 and Figure 3-29.

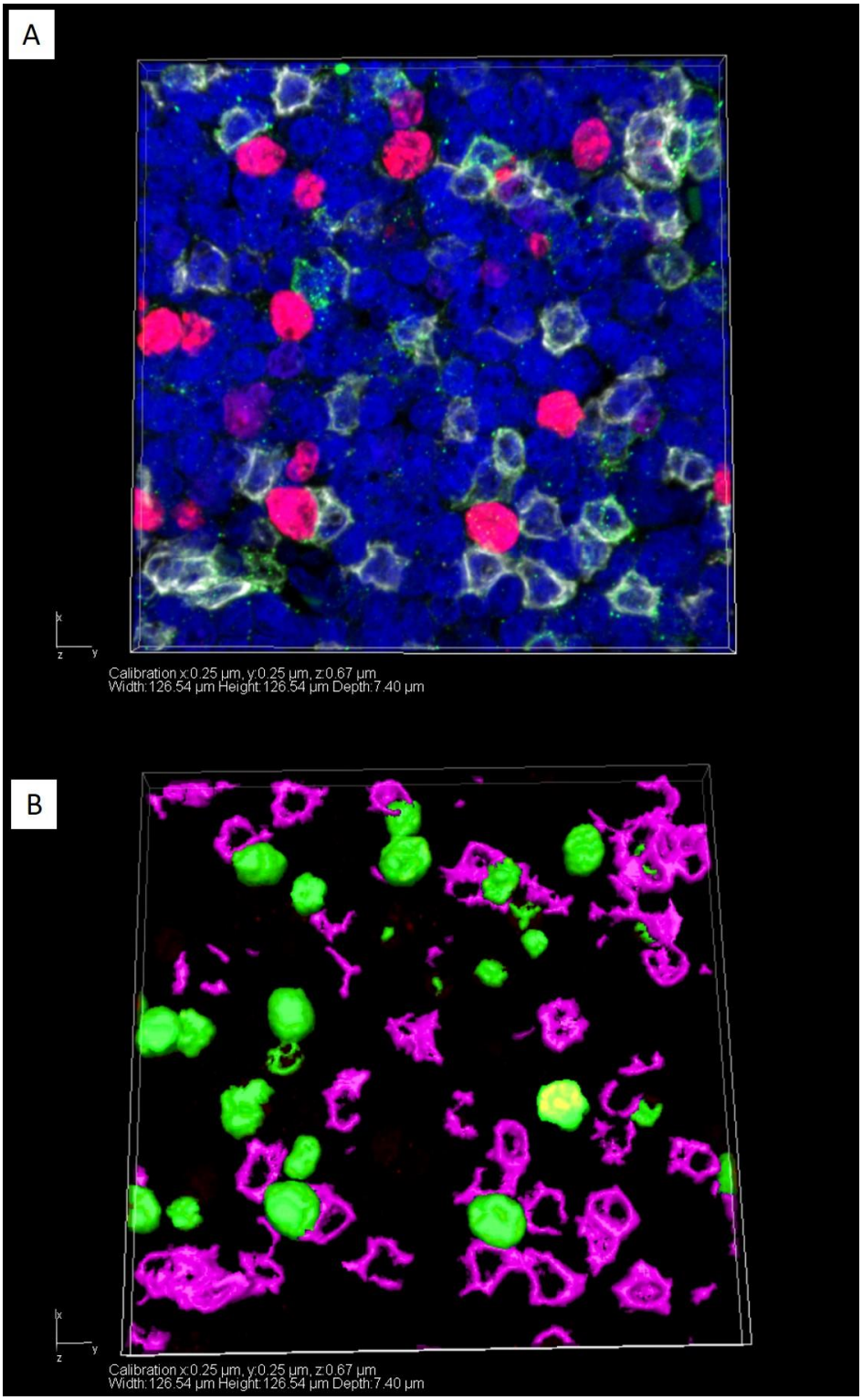


**Figure 3-21 PD1$^{Hi}$ cells in contact with Ki67$^{pos}$ cells are ICOS+ A.** Ki67 (**red**), PD1 (white), ICOS (**green**) z series 3D reconstruction. **B.** When the binary layers are shown (Ki67 **green**, PD1-ICOS intersection **pink**) close apposition can be seen.

The development of a 4-antibody staining method permitted co-staining with CD20 to confirm that proliferating cells were B cells whilst still keeping PD1 and a T cell marker (although it was necessary to replace CD4 with CD3 for these experiments). A small proportion of Ki67+ cells were found to be CD3+/CD20- T-cells (3.5% ± 0.86, n = 12 images from 4 samples), but the majority were B-cells and $Ki67^{pos}$ T-cells were easily identified and excluded from the binary layers during analysis, see Figure 3-22.

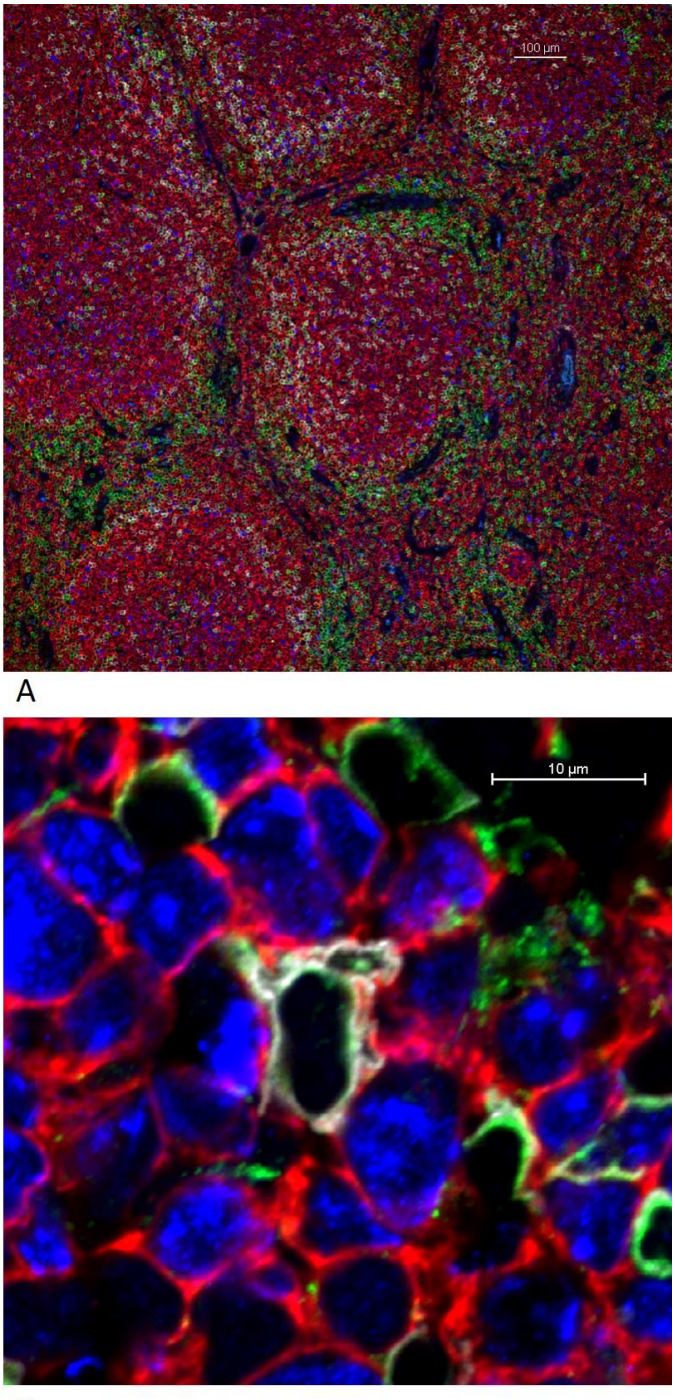


**Figure 3-22 Ki67$^{pos}$ cells are CD20+ B-cells. Ki67 = blue, CD20 = red, PD1 = white, CD3 = green.** Representative low power (A) and magnified high power (B) images of 4 colour labelling in FL. 96% of Ki67$^{pos}$ cells are CD20+ B cells. Scale bars, A = 100µm, B = 10µm**.**

Another benefit of using this method is that, as CD20 is located in the membrane whereas Ki67 is nuclear, it permits further analysis of the close spatial correlation of these cells. This is discussed in further detail later and shown in, Figure 3-29 and Figure 3-31.

#### 3.4.1.1 Method for analysing co-localisation of Ki67$^{pos}$ cells with $T_{FH}$ cells

The automated analysis of images was very important to this part of the research as visual analysis would be difficult to standardise, overly time consuming, and open to bias.

To analyse the proportion of Ki67$^{pos}$ cells that were in direct contact with $T_{FH}$ cells the binary layers for Ki67, PD1 and CD4 (or ICOS) were set. The binary layer for Ki67 was then carefully 'cleaned' so that only Ki67$^{pos}$ cells were included in the binary; since Ki67 was usually detected in the 488 channel which is where there was most autofluorescence, manual deletion of areas of Ki67 positivity that were not cellular was necessary. Since manual deletion was time consuming and open to user variability, a mathematical model was also introduced which excluded any object in the Ki67 binary layer with an area <10µm$^2$ as analysis revealed that these did not correlate with cells, nevertheless, additional manual deletions were still required. The Ki67 binary layer was then 'separated' so that all discrete Ki67$^{pos}$ cells were identified in the binary layer as separate 'objects', the automated 'separate' function of the software was not always able to distinguish individual cells when they were closely packed and so manual separation was necessary too, cross referencing the DAPI layer was helpful for this. The CD4 and PD1 (or PD1 and ICOS) binary layers were combined as an intersection layer to highlight $T_{FH}$ cells. Since Ki67 is nuclear and both CD4 and PD1 are located in the membrane it was necessary to dilate the Ki67 binary by 1µm in all directions to calculate the number of Ki67 cells in contact with $T_{FH}$.

Next, the Ki67 binary layer was converted into individual regions of interest (ROI). It was then possible to calculate the number of ROIs (Ki67$^{pos}$ cells measuring >10µm$^2$) that were overlapping with CD4+/PD1$^{Hi}$ cells (or PD1$^{Hi}$/ICOS+). A $T_{FH}$-Ki67 co-localisation score was generated by dividing the number of Ki67 cells touching $T_{FH}$ by the total number of Ki67 cells. This was repeated on 5 high power images per section to generate a score for each sample. Correlation with visual analysis confirmed that this approach yielded accurate measurement.

It should be noted that this method only counted Ki67$^{pos}$ cells as being in contact with a $T_{FH}$ if there was some overlap between the area of the Ki67 binary layer and the CD4/PD1 or PD1/ICOS

intersecting binary layers, many more Ki67$^{pos}$ cells were in very close proximity to $T_{FH}$ but not counted as 'in contact' by this strict, semi-automated method. Furthermore, as described above, Ki67 can be detected by IHC throughout the cell cycle except in $G_0$ and there is little data on how long Ki67 remains detectable for after a cell has completed division (Gerdes, Lemke et al. 1984, Williams and Stoeber 2007).

### 3.4.2 Association between Ki67, histological grade, and number of $T_{FH}$ in FL

Next we investigated if there was any association between the number of $T_{FH}$ cells and the rate of cellular proliferation (i.e. the number of Ki67$^{pos}$ B cells) and histological grade, this had not previously been investigated in FL or other lymphoproliferative disorders to the best of our knowledge. The hypothesis was that there would be more $T_{FH}$ cells in cases where there was higher rate of cellular proliferation but that in more aggressive cases, e.g. grade 3a and grade 3b disease, there may be less dependence on $T_{FH}$ cells for B cell proliferation so there may be a lower level of $T_{FH}$-Ki67 co-localisation in the highly proliferative cases.

As expected, the total area of the Ki67 binary layer and the corresponding number of Ki67$^{pos}$ cells counted by automated analysis increased with histological grade (Spearman non-parametric correlation coefficient r = 0.90, P<0.0001, n=99 images from 23 samples), Figure 3-23 A & B. As well as being an expected finding, this further validated the method of semi-automated counting of Ki67+ cells.

The area of the PD-1$^{Hi}$ ICOS+ intersection binary was strongly correlated with the number of Ki67$^{pos}$ cells and with grade (Spearman non-parametric correlation coefficient r = 0.79, P<0.0001, n=42 images from 13 samples), demonstrating that the absolute number of $T_{FH}$ cells is increased in cases with higher proliferation, Figure 3-23C & D.

There was only weak correlation between the number of $Ki67^{pos}$ cells and amount of co-localization with $T_{FH}$ cells ($r = 0.47$, $p = 0.001$, n=42 images from 13 samples) and no significant difference in the level of Ki67-$T_{FH}$ co-localization and histological grade.

Thus, in cases with low Ki67 there were relatively few $T_{FH}$ cells and in cases with high proliferation there were more $T_{FH}$ cells but the level of co-localization remained relatively constant regardless of grade or the number of $Ki67^{pos}$ cells, Figure 3-23E and F.

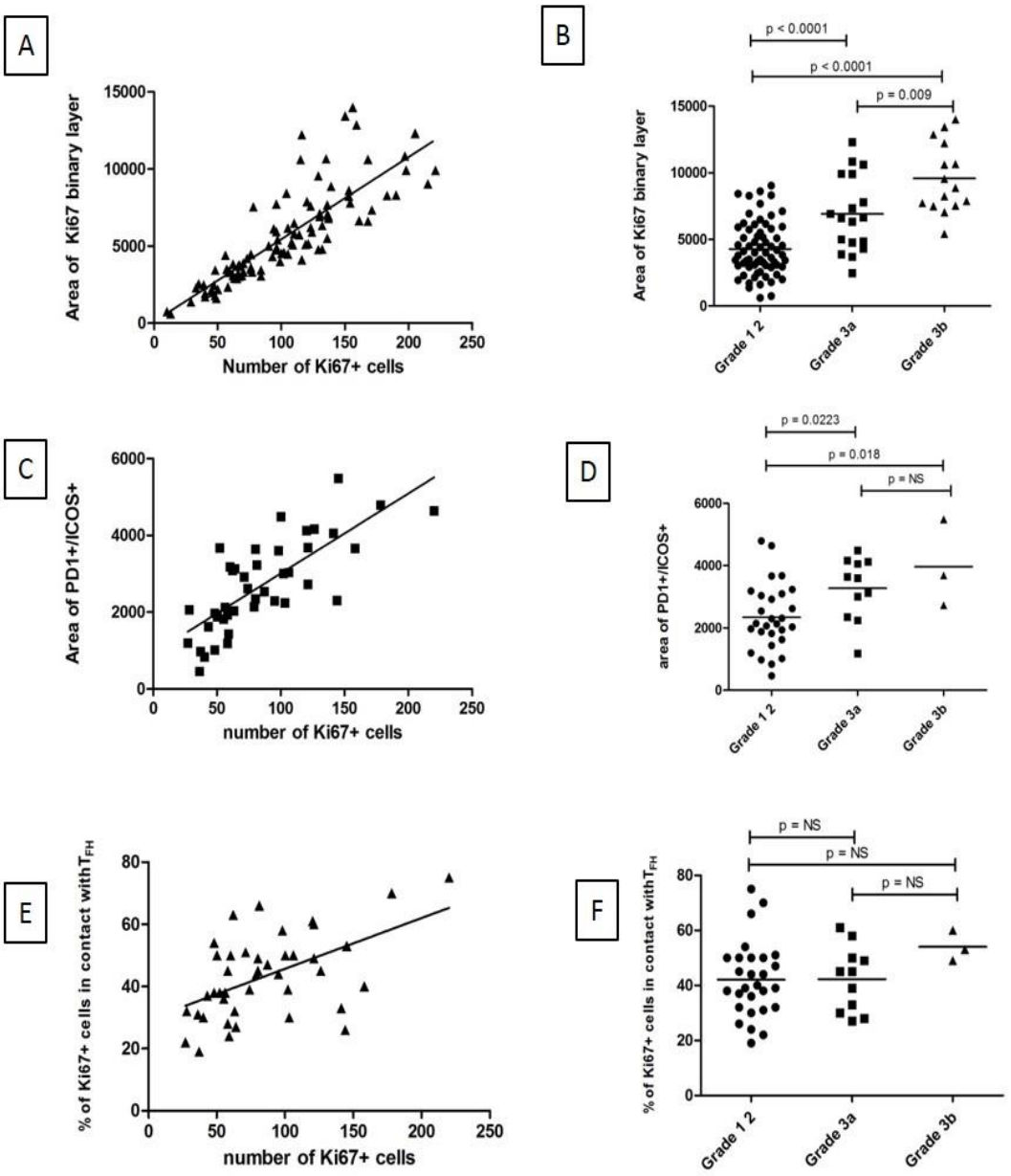


**Figure 3-23 Correlation between number of $T_{FH}$, histological grade and number of $Ki67^{pos}$ cells in FL. A**. The area of the Ki67 binary layer correlates closely with the number of $Ki67^{pos}$ cells automatically counted (r = 0.90 (Spearman correlation), P<0.0001) (n=23 samples, 99 images). **B**. The area of the Ki67 binary layer is significantly higher in grade 3a or 3b disease than in grade 1-2 disease (n=23 samples, 99 images). **C**. The number of $Ki67^{pos}$ cells correlates closely with the number of $PD1^{Hi}$/ICOS+ cells (r = 0.79 (Spearman correlation), p < 0.0001) (n=13 samples, 42 images). **D**. There are significantly more $T_{FH}$ cells (as represented by increased area of PD1/ICOS) in grade 3a and 3b disease than in grade 1-2 disease (n=13 samples, 42 images). **E**. The degree of $T_{FH}$ – Ki67 interactions is only weakly associated with the number of $Ki67^{pos}$ cells (r = 0.47, p = 0.001). **F**. The proportion of $Ki67^{pos}$ cells in contact with $T_{FH}$ does not significantly differ according to histological grade disease.

### 3.4.3 Are Ki67$^{pos}$ FL B cells in contact with $T_{FH}$ cells by chance?

Having identified a very close spatial relationship between $T_{FH}$ cells and Ki67$^{pos}$ FL B cells, and a correlation between the number of $T_{FH}$ and the rate of B cell proliferation, we next investigated whether these cells were in close spatial proximity by chance or because the $T_{FH}$ are involved in promoting FL B cell proliferation.

To investigate this we used the 4-colour labelling technique (see section 3.2.4) to simultaneously stain CD20, Ki67, CD3 and PD1. As described previously, it was not possible to simultaneously stain with CD20, Ki67, PD1, and CD4 but we determined that CD3 was an acceptable substitute in this situation. Furthermore, it was not possible to add a further marker of $T_{FH}$ cells e.g. ICOS or BCL6 but earlier work identified that setting a high threshold to include only T cells strongly expressing PD1 (PD1$^{Hi}$) meant that we could be confident that the CD3+ PD1$^{Hi}$ cells in close proximity to B cells were $T_{FH}$ cells.

The null hypothesis was that if $T_{FH}$ cells were in contact with Ki67$^{pos}$ cells by chance, then the proportion of CD20+ Ki67$^{neg}$ cells in contact with $T_{FH}$ cells would not be significantly different to the proportion of CD20+ Ki67$^{pos}$ cells in contact with $T_{FH}$ cells.

Initial observation showed that within follicles there were areas of high proliferation (high number of Ki67$^{pos}$ CD20+ B cells) and areas where there were many CD20+ B cells but low numbers of Ki67$^{pos}$ cells. It was observed that $T_{FH}$ cells were more frequent within areas of high proliferation, and in areas where the proliferation rate was low, few $T_{FH}$ were identified, Figure 3-24. This suggested that $T_{FH}$ are not randomly distributed but this observation alone couldn't exclude the possibility that the spatial relationship was due to chance. Further analysis was therefore required to establish if the null hypothesis could be rejected.

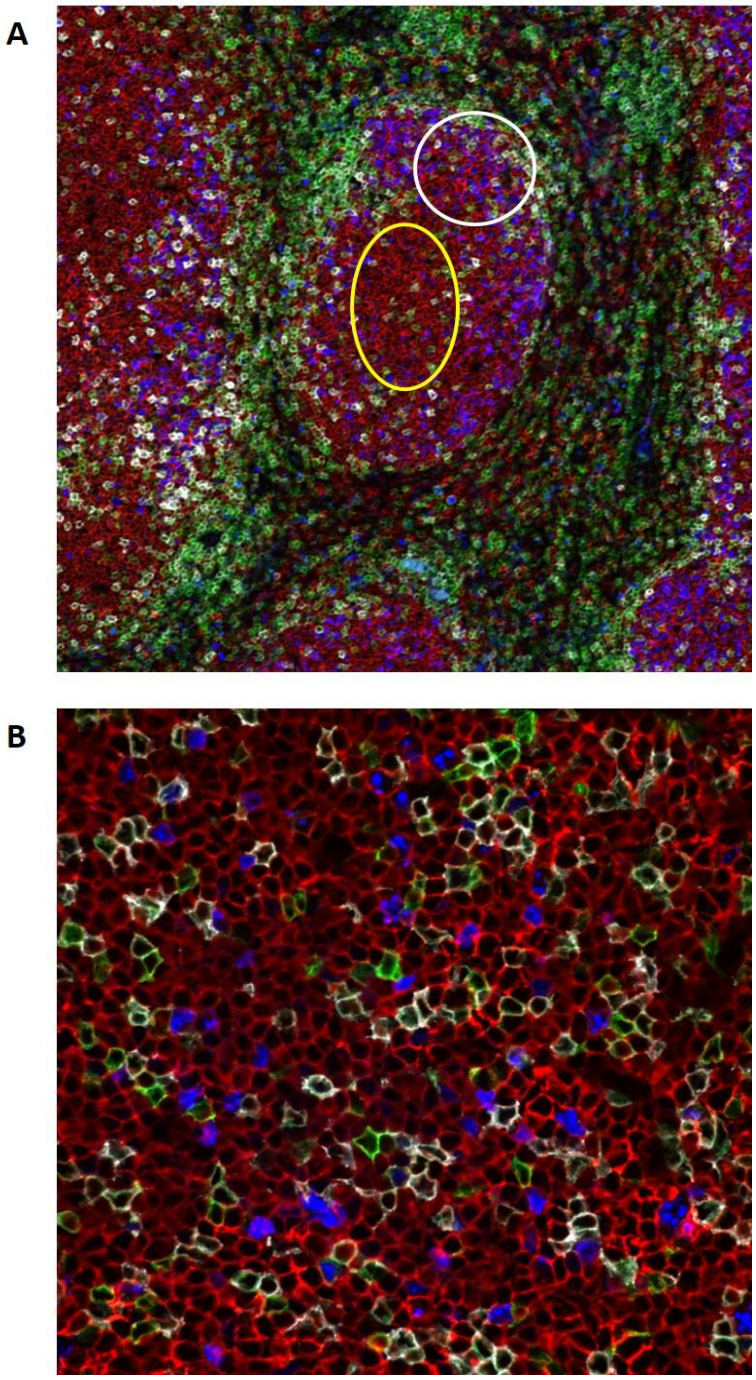


**Figure 3-24 $T_{FH}$ cells are more often located near proliferating CD20+ cells than non-proliferating cells. Ki67 = blue, CD20 = red, PD1 = white, CD3 = green.** Image showing 4 colour staining to analyse $Ki67^{pos}$ and $Ki67^{neg}$ CD20+ B cell co-localisation with $PD1^{Hi}$ CD3+ T cells in FL. **A.** Low power image (x10), it can be seen that within the follicles there are areas of low cellular proliferation (low Ki67 - blue) where there are few $PD1^{Hi}$ (white) CD3+ T cells (green) (area highlighted by yellow oval), whereas in areas where there is high Ki67, there are more $PD1^{Hi}$, CD3+ T cells (area highlighted by white circle) and they are frequently in contact with $Ki67^{pos}$ CD20+ FL B cells. **B.** High power image (x60) in which the close correlation of $Ki67^{pos}$ (blue) B cells with $PD1^{Hi}$ (white) CD3+ (green) cells can be seen, whilst the CD20+ (red), $Ki67^{neg}$ cells are less frequently in contact with $T_{FH}$ cells. This indicates that FL B cells are more likely to be in contact with $T_{FH}$ if they are $Ki67^{pos}$ than if they are $Ki67^{neg}$.

We analysed 25 images from 7 different samples for this analysis. Due to the diffuse pattern of CD20 staining, the automated analysis software was unable to reliably distinguish CD20+ cells that were not $Ki67^{pos}$. In the automated analyses described earlier, the nuclear pattern of staining of Ki67 permitted reliable automated analysis but the membrane pattern of staining of CD20 meant that when there are many closely packed CD20+ B cells, as in the follicles of FL, the software could not reliably identify individual cells. For this analysis we therefore had to resort to manual, visual assessment.

To perform this, images were thresholded according to the method described above in section 2.5 and intersections of the CD3+/$PD1^{Hi}$ binary layer were created. The image was then opened with the binary layers hidden from view. A grid was superimposed over the image to assist in visual assessment and to help ensure that each area of the image was inspected. A 'taxonomy tool' within the NIS elements software package was used to facilitate the manual counting of different cells.

First, $Ki67^{pos}$ CD20+ B cells were marked with the taxonomy tool and the sum of $Ki67^{pos}$ B cells was recorded. All $Ki67^{pos}$ B cells in the image that were not touching the edges of the image were marked and counted by systematically working through each box in the superimposed grid. Cells touching the edge of the image were excluded as it could not be certain if they were or were not in contact with a $T_{FH}$ beyond the boundaries of the image.

The CD3+/$PD1^{Hi}$ intersection binary layer was then shown and the taxonomy tool was used to mark each $Ki67^{pos}$ cell if it was assessed as touching an area of CD3/$PD1^{Hi}$ intersection, i.e. if it was touching a $T_{FH}$. The number of $Ki67^{pos}$ B cells touching $T_{FH}$ cells was recorded and from this, the number of $Ki67^{pos}$ B cells not in contact with a $T_{FH}$ cell was derived.

The channels for PD1 and CD3 were then hidden so only Ki67 and CD20 were showing and the taxonomy tool was used to mark and count non-proliferating $Ki67^{neg}$ CD20+ B cells. PD1 and CD3 layers were hidden from view during this step in the process to prevent inadvertent bias e.g. not including CD20+ $Ki67^{neg}$ cells that could be seen to be close to T cells.

Finally, the $PD1^{Hi}$/CD3 intersection binary was again shown and the taxonomy tool was used to highlight and count all of the marked $Ki67^{neg}$ CD20+ B cells that were in contact with an area of CD3/PD1 positivity i.e. $T_{FH}$ cells. The number of $Ki67^{neg}$ CD20+ B cells not in contact with $T_{FH}$ was derived from these numbers.

The number of $Ki67^{pos}$ B cells contacting $T_{FH}$ cells was then compared with the number of $Ki67^{neg}$ B cells contacting $T_{FH}$ cells for each sample and the statistical significance was determined using contingency tables and either Chi Squared or Fisher's exact tests.

Due to the manual visual assessment of these images rather than the automated image analysis employed in the other sections of this thesis, two investigators analysed a subset of these images in order to identify and reduce operator bias. The two investigators were blinded to each other's results. We identified no significant difference in number of $Ki67^{pos}$ cells counted by observer, the number of cells in contact with $T_{FH}$ was also concordant between operators. Therefore, whilst this visual assessment was not considered to be as robust as the automated analysis used elsewhere in this research, we are confident that the results presented below are an accurate representation of the co-localisation of $T_{FH}$ cells to $Ki67^{pos}$ and $Ki67^{neg}$ CD20+ FL B cells as shown in Figure 3-24 above.

In total, 25 images stained with Ki67, CD20, PD1 and CD3 acquired from 7 FL specimens were analysed, 1481 $Ki67^{pos}$ B cells were counted and 877 (59%) of these were assessed to be in contact with $T_{FH}$ by the method described above. 2597 $Ki67^{neg}$ CD20+ B cells were counted from the same images and 552 (21%) were in contact with $T_{FH}$. This difference is highly significant, Chi Squared 595, $P<0.0001$, see Table 3-6.

For individual samples, Fisher's exact test was applied as cell numbers were too low for Chi Squared test, by Fisher's exact test, P was <0.0001 for each sample analysed, Table 3-7.

**Table 3-6 Contingency table for <u>all samples combined</u>.** Number of Ki67$^{pos}$ FL B cells in contact with $T_{FH}$ cells are compared with the number of Ki67$^{neg}$ B cells. Ki67$^{pos}$ B cell are significantly more likely to be in contact with $T_{FH}$ than Ki67$^{neg}$ FL B cells. (n=25 images from n=7 specimens)

| | KI67$^{POS}$ B CELLS | KI67$^{NEG}$ B CELLS | TOTAL |
|---|---|---|---|
| **IN CONTACT WITH $T_{FH}$** | 877 | 552 | 1429 |
| **NOT IN CONTACT WITH $T_{FH}$** | 604 | 2045 | 2649 |
| **TOTAL** | 1481 | 2597 | 4078 |

**CHI SQUARED 595, P<0.0001**

**Table 3-7 Contingency tables for each FL sample analysed (n=7).** Number of Ki67$^{pos}$ FL B cells in contact with $T^{FH}$ cells are compared with the number of Ki67$^{neg}$ B cells for each sample. Ki67$^{pos}$ B cell are significantly more likely to be in contact with $T_{FH}$ than Ki67$^{neg}$ FL B cells in each sample analysed.

| **<u>Sample ID FL012</u>** | **Ki67$^{pos}$ cells** | **Ki67$^{neg}$ cells** | **Total** |
|---|---|---|---|
| **In contact with $T_{FH}$** | 83 | 26 | 109 |
| **Not in contact with $T_{FH}$** | 75 | 263 | 338 |
| **Total** | 158 | 289 | 447 |

**Fisher's exact test for sample FL012, P < 0.0001**

| **<u>Sample ID FL018</u>** | **Ki67$^{pos}$ cells** | **Ki67$^{neg}$ cells** | **Total** |
|---|---|---|---|
| **In contact with $T_{FH}$** | 76 | 49 | 125 |
| **Not in contact with $T_{FH}$** | 60 | 251 | 311 |
| **Total** | 136 | 300 | 436 |

**Fisher's exact test for sample FL018, P < 0.0001**

| **<u>Sample ID FL020</u>** | **Ki67$^{pos}$ cells** | **Ki67$^{neg}$ cells** | **Total** |
|---|---|---|---|
| **In contact with $T_{FH}$** | 168 | 94 | 262 |
| **Not in contact with $T_{FH}$** | 133 | 406 | 539 |
| **Total** | 301 | 500 | 801 |

**Fisher's exact test for sample FL020, P < 0.0001**

| Sample ID FL010 | Ki67$^{pos}$ cells | Ki67$^{neg}$ cells | Total |
|---|---|---|---|
| **In contact with $T_{FH}$** | 229 | 57 | 286 |
| **Not in contact with $T_{FH}$** | 133 | 314 | 447 |
| **Total** | 362 | 371 | 733 |

**Fisher's exact test for sample FL010, P < 0.0001**

| Sample ID FL004 | Ki67$^{pos}$ cells | Ki67$^{neg}$ cells | Total |
|---|---|---|---|
| **In contact with $T_{FH}$** | 113 | 63 | 176 |
| **Not in contact with $T_{FH}$** | 39 | 139 | 178 |
| **Total** | 152 | 202 | 354 |

**Fisher's exact test for sample FL004, P < 0.0001**

| Sample ID FL013 | Ki67$^{pos}$ cells | Ki67$^{neg}$ cells | Total |
|---|---|---|---|
| **In contact with $T_{FH}$** | 17 | 17 | 34 |
| **Not in contact with $T_{FH}$** | 18 | 124 | 142 |
| **Total** | 35 | 141 | 176 |

**Fisher's exact test for sample FL013, P < 0.0001**

| Sample ID FL014 | Ki67$^{pos}$ cells | Ki67$^{neg}$ cells | Total |
|---|---|---|---|
| **In contact with $T_{FH}$** | 191 | 198 | 389 |
| **Not in contact with $T_{FH}$** | 126 | 596 | 722 |
| **Total** | 317 | 794 | 1111 |

**Fisher's exact test for sample FL014, P < 0.0001**

This finding means that Ki67$^{pos}$ FL B cells are significantly more likely to be in contact with $T_{FH}$ cells than non-proliferating FL B cells. It is therefore highly unlikely that the close spatial relationship between

Ki67$^{pos}$ FL B cells and $T_{FH}$ cells is due to chance. This is further evidence that FL B cells may be dependent on interaction with $T_{FH}$ for inducing or sustaining proliferation.

Although 21% of Ki67$^{neg}$ FL B cells were in contact with $T_{FH}$ cells, it is possible that this is due to chance. As seen in Figure 3-24, the closely packed nature of CD20+ B cells within the FL follicles means that any given cell is in contact with approximately 6 other cells and therefore there is a chance of a Ki67$^{neg}$ B cell being adjacent to a $T_{FH}$ cell randomly. However, the statistical difference between the proportion of Ki67$^{pos}$ and Ki67$^{neg}$ FL B cells in contact with $T_{FH}$ cells is so great that we can infer that the Ki67$^{pos}$ cells are not in contact with $T_{FH}$ cells by chance. The null hypothesis was therefore rejected.

These results confirm the observation in low power images that there were areas of follicles with low proliferation (low Ki67), and in these areas there were few $T_{FH}$ cells whereas in areas of high numbers of Ki67$^{pos}$ FL B cells, there were more $T_{FH}$, Figure 3-24. This also supports the finding that in cases of high proliferation there were higher numbers of $T_{FH}$, Figure 3-23A & C.

### 3.4.4 Association of $T_{FH}$ cells with proliferating B cells in germinal centres

As in FL, proliferating B cells within the GCs of reactive LNs were frequently found to be in close contact with CD4+ PD1$^{Hi}$ T cells. Unlike the follicles of FL there was striking zonal demarcation within the GCs and a marked difference between the dark and light zones was observed.

In the light zones, where proliferation of B cells was relatively low, as in FL, many proliferating cells were found to be in close contact with CD4+ PD1$^{Hi}$ cells. In the dark (highly proliferative) zones there was substantially less interaction between proliferating B cells and T cells perhaps indicating that B cell proliferation in the dark zone does not require $T_{FH}$ help whereas it is required for proliferation in the light zone and in FL, Figure 3-25 & Figure 3-26. The distinction between dark and light zones was made subjectively based on area of highest number of Ki67$^{pos}$ cells as shown by the superimposed dashed line in Figure 3-25.

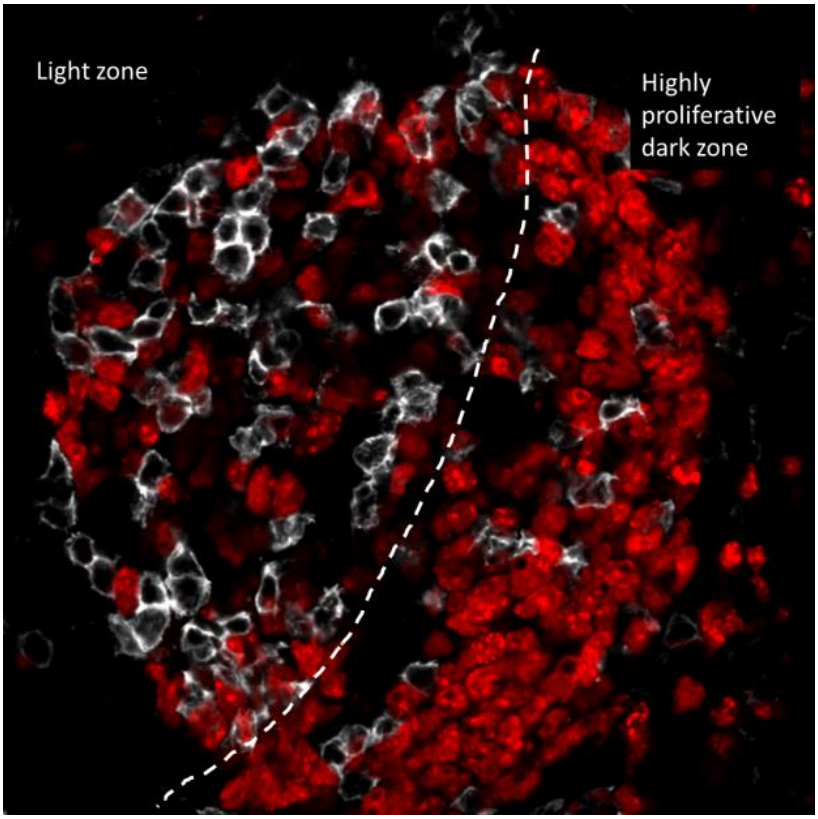


**Figure 3-25. Proliferation and association with PD1$^{Hi}$cells in a normal germinal centre. Ki67 = red, PD1 = white.** Proliferation (Ki67, red) can be seen to be considerably higher in the dark zone than the light zone. In the dark zone there are very few PD1$^{Hi}$ cells (white). In the light zone proliferation rate is lower but there is a close association with PD1$^{Hi}$ cells. (Image acquired with x60 objective, dotted line highlights boundary of dark and light zones).

Quantification of the level of co-localisation between $T_{FH}$ cells and Ki67$^{pos}$ B cells in the GCs of reactive lymph nodes was challenging because the very high number of closely packed Ki67$^{pos}$ cells made identification and separation of the Ki67 binary layer into discrete cells difficult. Accordingly this analysis required a time consuming effort to separate the Ki67 binary layer into individual cells. The analysis of this was otherwise the same as for the FL samples.

Analysis of Ki67 – $T_{FH}$ co-localisation within the light zones revealed that 63.1% ± 15.9 Ki67$^{pos}$ cells (n=13 images from 4 reactive LN samples) were in direct contact with CD4+ PD-1$^{Hi}$ cells, and visual inspection revealed that almost all Ki67$^{pos}$ cells were very close to (within one cell's width), but not touching $T_{FH}$ cells. Many Ki67$^{pos}$ cells were in contact with more than one $T_{FH}$ cell simultaneously, and

due to the closely packed nature of proliferating cells and $T_{FH}$, many $T_{FH}$ were in contact with more than one $Ki67^{pos}$ cell simultaneously, Figure 3-27B.

The majority of the $PD\text{-}1^{Hi}$ T cells in close proximity to $Ki67^{pos}$ cells were also ICOS+ with 53.9% ± 14.2 of $Ki67^{pos}$ cells in contact with $PD\text{-}1^{Hi}$ ICOS+ cells (n=12 images from 4 samples).

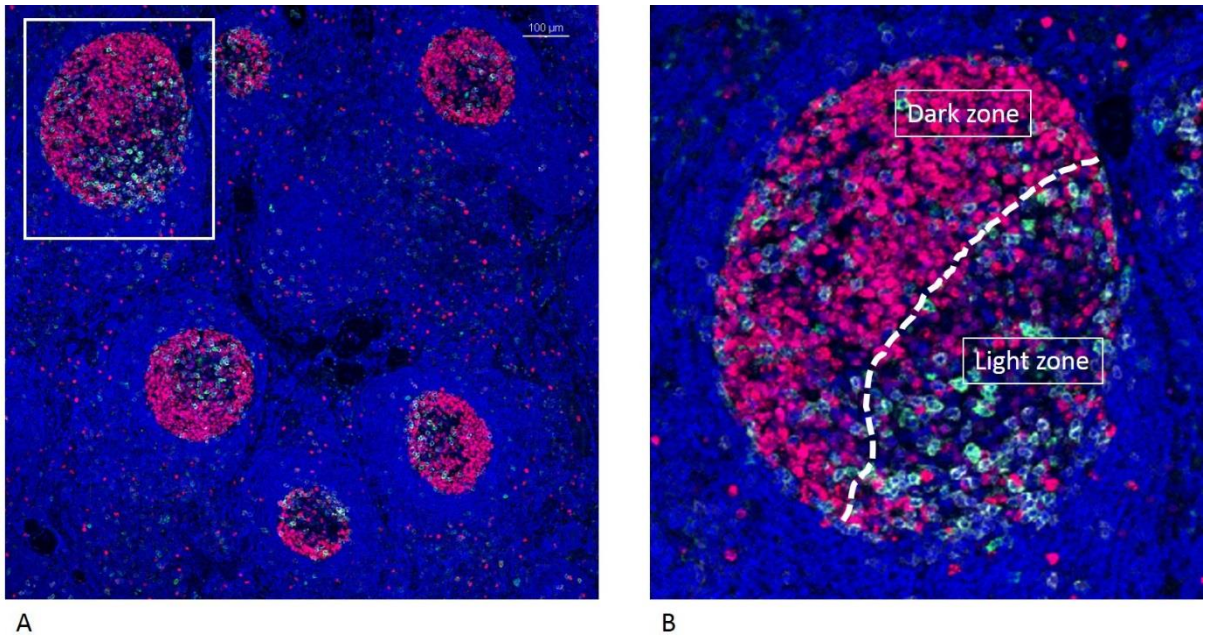


**Figure 3-26 $Ki67^{pos}$ cells co-localise with $PD1^{Hi}$ ICOS+ T Cells within the light zone of GCs. Ki67 = red, PD1 = white, ICOS = green, DAPI = blue. A.** Low power (x10) image of reactive LN showing six GCs. The GCs can clearly be seen to be demarcated into highly proliferative dark zones with high Ki67 (red) and light zones with much lower rate of proliferation. **B.** The GC highlighted by the white rectangle in **A** is enlarged. Here it can be seen that within the light zones, $Ki67^{pos}$ cells are often in contact with $PD1^{Hi}$ ICOS+ cells. In the dark zone there are relatively few $PD1^{Hi}$ ICOS+ cells. Scale bar = 100µm

In the highly proliferative dark zones, the level of Ki67 was too high to reliably distinguish individual $Ki67^{pos}$ cells even after extensive manual 'separation' of the binary layer. Therefore, formal quantification of the proportion of $Ki67^{pos}$ cells in contact with $T_{FH}$ in this compartment could not be performed but, since the number of $Ki67^{pos}$ cells was higher in the dark zones and few $T_{FH}$ were present in this compartment, the level of spatial correlation was markedly lower than in the light zones.

,

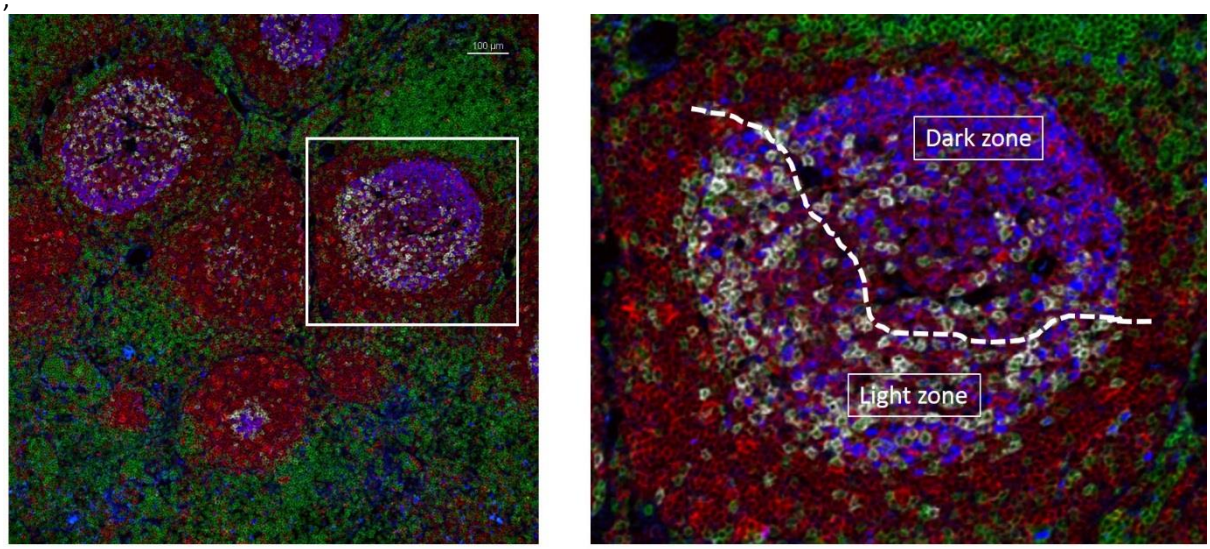


**Figure 3-27 Germinal centres in reactive LN showing proliferation of CD20+ B cells and zonal demarcation. Ki67 = blue, CD20 = red, CD3 = green, PD1 = white. A.** Low power (x10) image of GCs in a reactive LN, 4 colour staining with Ki67, CD20, PD1, and CD3. Scale bar = 100µm. **B**. Magnification of the area highlighted by the white rectangle in **A** highlighting that most cells within the follicles are CD20+ (**red**) B cells. In the dark zones where there is high proliferation (**Ki67, blue**) there are few $PD1^{Hi}$ CD3+ T cells ($T_{FH}$). In the light zones $Ki67^{pos}$ CD20+ B cells are frequently in contact with $PD1^{Hi}$ CD3+ T cells.

The high number of $T_{FH}$ cells in the light zones of reactive GCs meant that even $Ki67^{neg}$ CD20+ B cells were often in contact with one or more $T_{FH}$ cell. Additionally, the closely packed nature of the cells within the GCs, relative scarcity of $Ki67^{neg}$ CD20+ B cells and high number of $T_{FH}$ cells meant that it was technically challenging to perform the same analysis as we performed in FL to ascertain if the $T_{FH}$ cells were in proximity to CD20+ $Ki67^{pos}$ B cells by chance or not.

Nevertheless we were able to analyse images acquired from 5 GCs from images of 2 separate reactive LNs stained with the 4-antibody labelling method for Ki67, CD20, CD3 and PD1, Table 3-8. These images were analysed visually rather than automatically as described for FL above, in section 3.4.3. Only the light zones were analysed. Within the dark zones, CD20+ $Ki67^{neg}$ B cells were very few or not present, and therefore this analysis was not possible for the dark zones.

**Table 3-8 Contingency tables for Light Zones of GCs (n=5 GCs from n=2 samples). Number of $Ki67^{pos}$ FL B cells in contact with $T_{FH}$ cells are compared with the number of $Ki67^{neg}$ B cells for each sample. $Ki67^{pos}$ B cell are significantly more likely to be in contact with $T_{FH}$ than $Ki67^{neg}$ B cells**

| **Sample ID LN03** | $Ki67^{pos}$ cells | $Ki67^{neg}$ cells | Total |
|---|---|---|---|
| **In contact with $T_{FH}$** | 39 | 17 | 56 |
| **Not in contact with $T_{FH}$** | 12 | 23 | 35 |
| **Total** | 51 | 40 | 91 |

**Fisher's exact test for sample LN03, P < 0.0012**

| **Sample ID LN008** | **$Ki67^{pos}$ cells** | **$Ki67^{neg}$ cells** | **Total** |
|---|---|---|---|
| **In contact with $T_{FH}$** | 86 | 50 | 136 |
| **Not in contact with $T_{FH}$** | 37 | 49 | 86 |
| **Total** | 123 | 99 | 222 |

**Fisher's exact test for sample LN08, P < 0.0037**

Whilst a higher proportion of $Ki67^{neg}$ B cells were in contact with $T_{FH}$ cells in the light zones of GCs than in the malignant follicles of FL, there was still a significantly higher chance of $Ki67^{pos}$ cells being in contact with one or more $T_{FH}$ cell than the non-proliferating cells. Whilst the numbers of samples analysed for this are too low to draw firm conclusions, this is preliminary evidence that the $T_{FH}$ cells are not in contact with proliferating B cells in the light zones of GCs by chance.

Furthermore, analysis of the area of $T_{FH}$ and area of Ki67 positivity – surrogate indicators of the number of $T_{FH}$ cells and $Ki67^{pos}$ cells respectively, in GCs revealed a positive correlation in reactive LNs, although the correlation was not as strong as that identified in FL, Figure 3-28 (r = 0.55, P = 0.019, n=17 GCs from n=4 samples). Again, the number of samples analysed for this is too low to draw firm conclusions but this supports the evidence of others that GC size is determined at least in part by the number of $T_{FH}$ (Allen, Okada et al. 2007, Rolf, Bell et al. 2010).

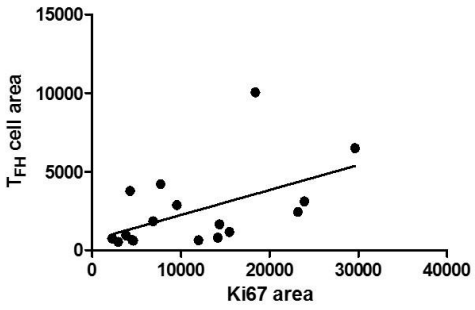


**Figure 3-28 Association between area of Ki67 and $T_{FH}$ in reactive GCs.** r = 0.55, P = 0.019, n=17 GCs from n=4 samples

## 3.5 Synapse formation between $T_{FH}$ cells and proliferating B cells in FL

As described above, we found that a high proportion of proliferating B cells are in close contact with $T_{FH}$ cells in the follicles of FL and in the light zones of GCs. We also found evidence that it is unlikely that this close spatial relationship is due to chance with significantly higher co-localisation of $T_{FH}$ cells with $Ki67^{pos}$ B cells than $Ki67^{neg}$ B cells in both the malignant follicles of FL and the light zones of reactive GCs. It was also noted that the $T_{FH}$ are often very closely apposed to the proliferating cells. This led us to investigate if there is evidence of the formation of immunological synapses between these cells.

Immunological synapses are points of physical contact between a T cell and an antigen presenting cell that may serve a number of functions including facilitating T cell activation, T cell signalling, and the delivery of secretory granules (e.g. cytotoxic T cells secreting perforin granules).

The immunological synapse is also known as the supramolecular activation cluster (SMAC) which is composed of 2 parts, the central (c-SMAC) and peripheral (p-SMAC) (Dustin 2011). There are a number of morphological and molecular features that identify immunological synapses. Morphological features include close apposition of cells, the formation of projections that encompass other cells, and distortion of the T cell nucleus due to rearrangement of the cytoskeleton. Molecular features are the presence of components of the c-SMAC (e.g. components of the TCR, protein kinase C-theta (PKC-θ),

CD3, and co-stimulatory receptors) and p-SMAC (e.g. leucocyte function-associated antigen-1 - LFA-1). The formation of central and peripheral components of the SMAC gives rise to a characteristic bull's eye appearance of the synapse (Kupfer and Kupfer 2003, Barcia, Thomas et al. 2006, Dustin 2011).

Whilst immunological synapses are well described *in vitro* they have rarely been visualised *in situ.* We used the multicolour confocal microscopy method described above to investigate whether there was evidence of immunological synapse formation between proliferating FL B cells and $T_{FH}$ cells in FL *in situ* in FFPE tissue.

In FL, it has previously been reported that tumour infiltrating T cells form impaired synapses with FL B cells compared to healthy B cells and that PD1+ T cells in FL are globally dysfunctional with impaired response to cytokines (Ramsay, Clear et al. 2009, Myklebust, Irish et al. 2013). However, previous work on this area has been performed in vitro and this work represents the first time that synapses have investigated in situ in FL and our results provide some findings that are counter to the previous work in this field.

We identified features of immunological synapses including the formation of cell membrane projections, distortion of the cell nucleus in T cells adherent to proliferating cells, and concentration of the membrane antigens PD1, and CD3 at points of contact, Figure 3-29, Figure 3-30, and Figure 3-31. Staining for components of the c-SMAC and p-SMAC such as PKC-θ, f-actin and LFA-1 were also attempted but yielded poor staining and high background which precluded analysis (data not shown).

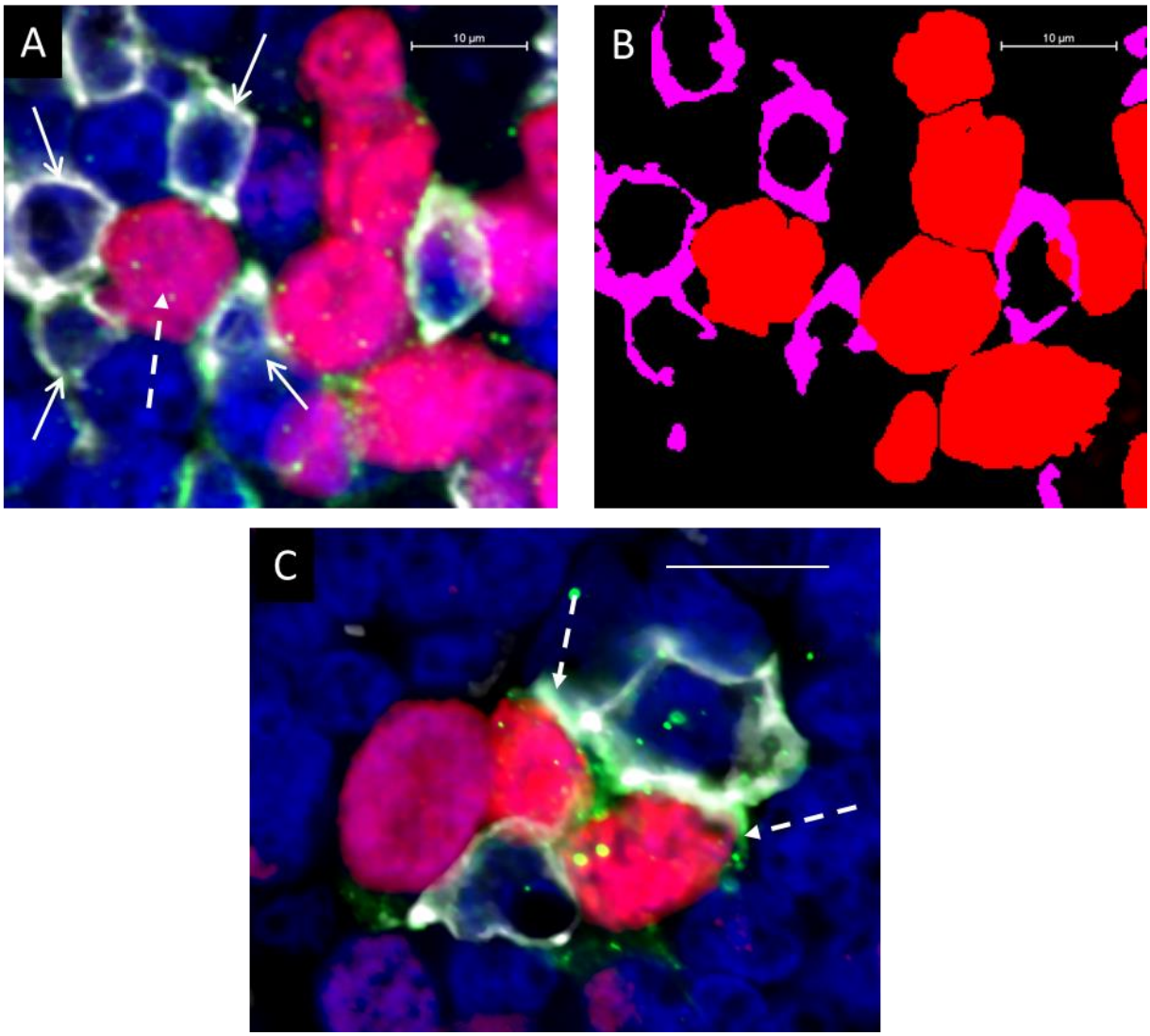


**Figure 3-29. Close contact between Ki67$^{pos}$ cells and $T_{FH}$ in FL: Evidence of synapse formation. A & C: Ki67 = red, ICOS = green, PD1 = white, and DAPI = blue. B: Ki67 binary layer = red, PD1/ICOS intersecting binary layer = pink. A.** A ki67$^{pos}$ cell (red) (dashed arrow) is seen to be in contact with 4 PD1$^{Hi}$ (white) ICOS+ cells (green) (white arrows). The PD1$^{Hi}$ ICOS+ cells are closely adherent with the Ki67$^{pos}$ cell **B.** The binary layers of Ki67 (**red**) and PD1/ICOS intersection (**pink**) are shown highlighting this close association. **C.** The $T_{FH}$ cells form projections encompassing the Ki67$^{pos}$ cell (white arrows). PD1 and ICOS appear more concentrated at site of cell contact. (Magnified images acquired with x60 objective, scale bars = 10µm)

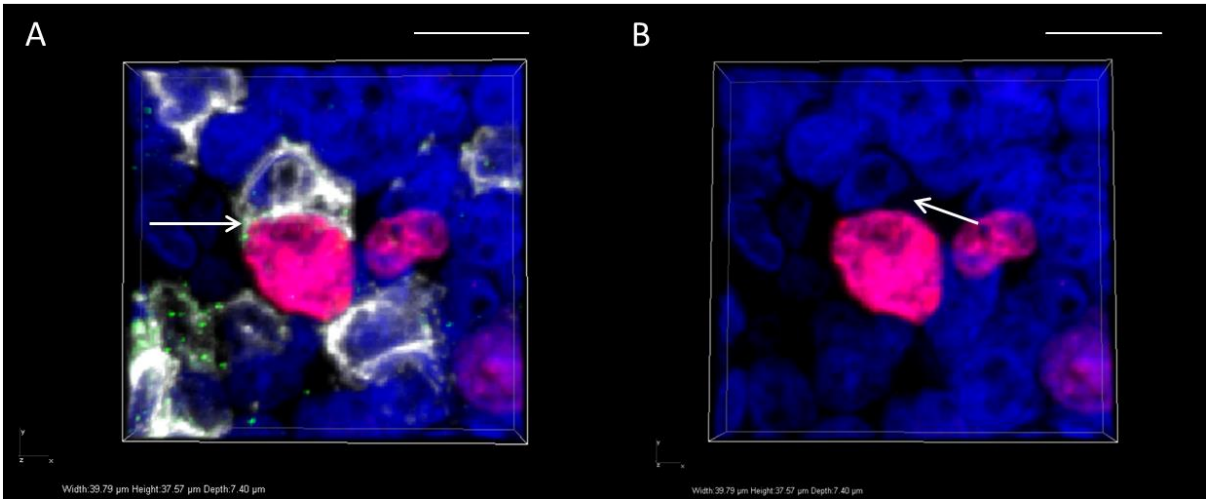


**Figure 3-30. Evidence of synapse formation. Ki67 = red, ICOS = green, PD1 = white, and DAPI = blue. A.** A Ki67$^{pos}$ cell (red) is in contact with a PD1$^{Hi}$ (white) ICOS+ (green) cell; PD1 appears more concentrated at site of cell contact and there are projections encompassing the Ki67$^{pos}$ cell. **B.** Only DAPI and Ki67 are shown and the T cell nucleus can be seen to be distorted which is a feature of synapses (white arrow). (3D reconstructions of magnified Z-stacks acquired with x60 objective, scale bars = 10µm)

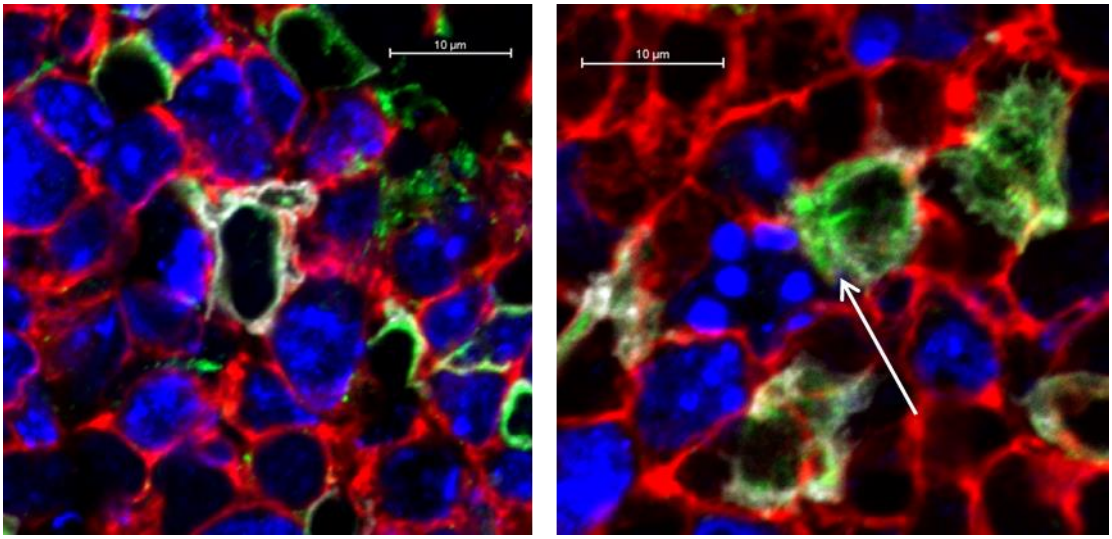


**Figure 3-31 Four colour labelling allows better appreciation of cellular contact. Ki67 = blue, CD20 = red, CD3 = green, PD1 = white**. The proliferating cells are demonstrated to be CD20+ and there is overlap of the B cell and T cell membranes with concentration of CD3 at the point of contact (white arrow). (Magnified images acquired with x60 objective, scale bars = 10µm)

To formally quantify if there was concentration of T cell membrane proteins at the points of cell contact with proliferating B cells, a novel analytical technique was developed. High definition, highly magnified images were captured from representative areas of tissue, these images were technically difficult to generate and required lengthy acquisition times on the confocal microscope.

The images so generated were thresholded and binary layers generated as previously described. The T cell membrane was then defined manually on the image and the intensity of fluorescence could then be automatically measured at each pixel around the perimeter of the T cell membrane, Figure 3-32.

A graph representing intensity was generated from this data and the area under the curve for a defined length of T cell membrane in contact with a Ki67+ cell was compared to the area under the curve for an identical length of cell membrane at the opposite pole of the cell, Figure 3-33.

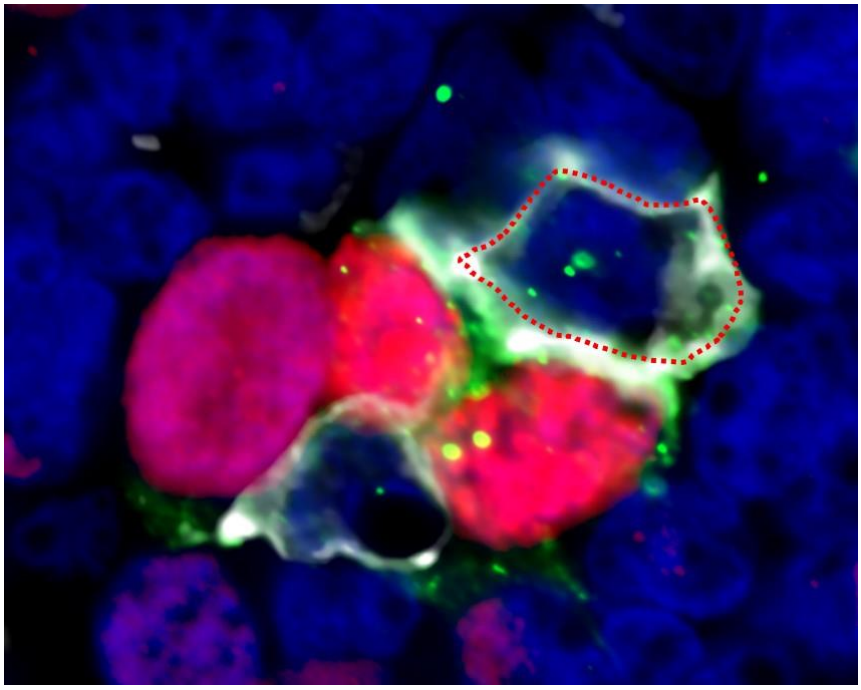

**Figure 3-32 Measuring intensity of expression of cell membrane proteins at immunological synapses. Ki67 = red, ICOS = green, PD1 = white, and DAPI = blue.** Highly magnified image showing a $T_{FH}$ cell in contact with Ki67pos FL cell. The T cell membrane has been delineated manually by the red dotted line. The intensity of expression of PD1 and ICOS can then be measured at each pixel around this line.

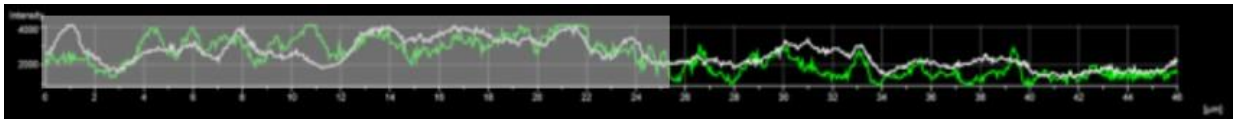

**Figure 3-33 Graph showing the level of intensity of PD1 (white line) and ICOS (green line) around the T cell membrane**. The area under the curve (AUC) for the segment of T cell membrane in contact with the Ki67+ cell

(highlighted by the grey box) is compared to the AUC for the opposite pole. In this representative graph the AUC for the area of contact was greater than at the opposite pole for both PD1 and ICOS.

This technique was used to investigate 61 cell contacts in images from 9 FL samples. Results show that the intensity of expression of CD3, PD1, and ICOS were all significantly higher at points of cell contact than at the opposite pole indicating polarisation of the T cell membrane and the formation of an immunological synapse, Figure 3-34.

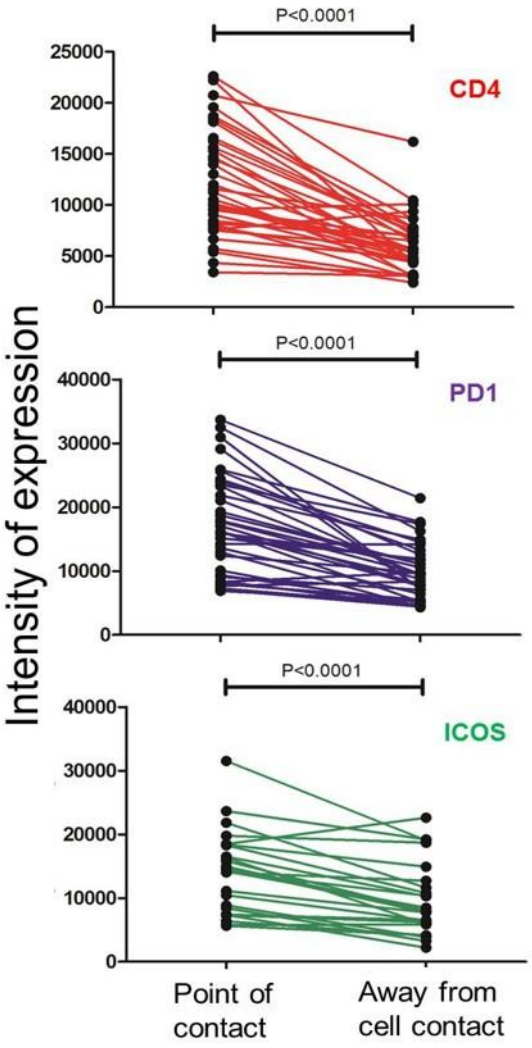


**Figure 3-34 CD4, PD1, and ICOS all have significantly higher intensity of expression at the sites of cell contact than at the opposite pole.** Paired t tests, n=61 cell contacts, from highly magnified images in 9 FL specimens stained with either CD4/PD-1/Ki67, or PD-1/ICOS/Ki67.

The time consuming nature of the microscopy required to generate appropriate images for this analytical technique prevented us from being able to perform this on a greater number of samples within the confines of the current research.

We attempted to investigate if there was a difference in the number of cell contacts with features consistent with synapse formation in FL and GCs however technical difficulties described in the paragraph below, precluded this.

In the reactive LN samples, the number of $Ki67^{pos}$ cells was so high, even in the light zones of the GCs that most $T_{FH}$ were found to be in contact with more than one $Ki67^{pos}$ cell simultaneously. It was therefore not possible to employ the same analysis technique in the reactive LN specimens as had been used in the FL specimens as we could not delineate clear areas of T cell membrane that were not in contact with $Ki67^{pos}$ cells.

Although formal quantitative assessment of the formation of immunological synapses could not be performed in GCs, morphological assessment revealed that it appears that the formation of immunological synapses between $T_{FH}$ and $Ki67^{pos}$ B cells in FL was at least as good as in GCs.

## 3.6 PD-L1 expression in FL and GCs

As described above in the introduction, section 1.4, there are two known endogenous ligands for PD-1, PD-L1 (CD274) and PD-L2 (CD273). PD-L1 has previously been reported to be absent from the surface of FL B-cells (Andorsky, Yamada et al. 2011), but, given the high level of PD1 expression in some T cells in FL, we sought to investigate whether there was any co-localisation between T cells with high PD1 expression and cells expressing PD-L1.

We obtained a monoclonal antibody against PD-L1 raised in rabbit from Spring Bioscience and performed multiple-labelling experiments to determine if there was evidence of PD-L1 expression on the surface of the proliferating malignant cells in contact with $T_{FH}$ in FL. Additionally, co-staining with CD23 was performed by a colleague in the laboratory, Dr Beth Phillips to determine if PD-L1 was present on follicular dendritic cells.

We found no evidence that PD-L1 was strongly expressed on the Ki67+ cells that were in contact with PD-1$^{Hi}$ cells, Figure 3-35. Instead, PD-L1 appeared to be expressed mainly on CD23 negative cells in the interfollicular areas, Figure 3-36.

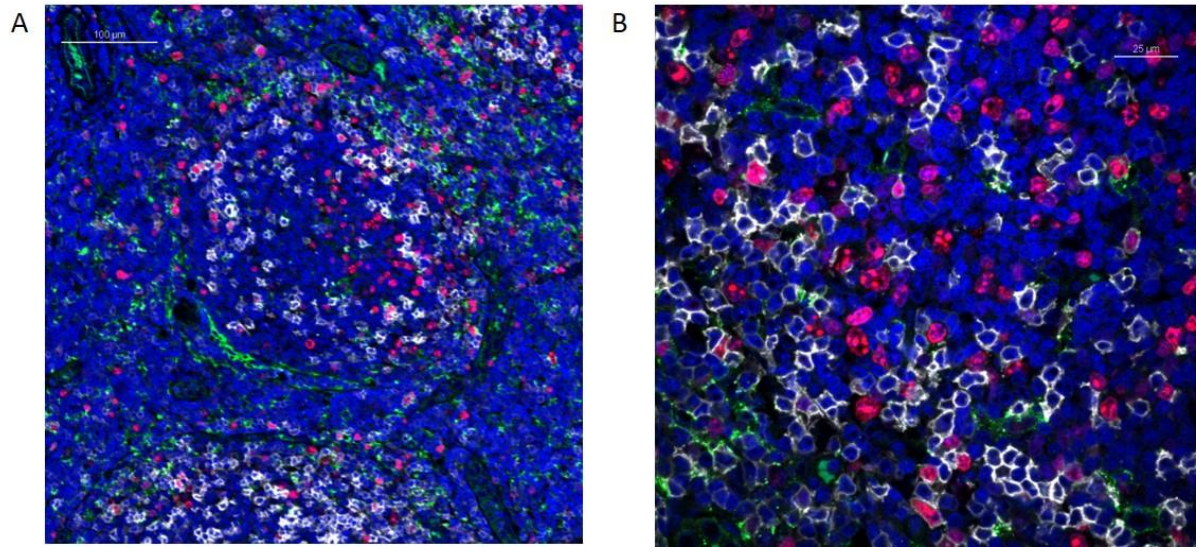


**Figure 3-35 PD-L1 staining in FL. PD-L1 = green, Ki67 = red, PD1 = white, DAPI = blue.** PD-L1 is not present on the Ki67+ cells in contact with PD1$^{Hi}$ cells. Representative low power (A) and high power (B) images of FL showing that PD-L1 (green) is not highly expressed on the Ki67+ cells (red) that are in contact with PD-1$^{Hi}$ cells (white). Scale bars represent 100µm (A) and 25 µm (B).

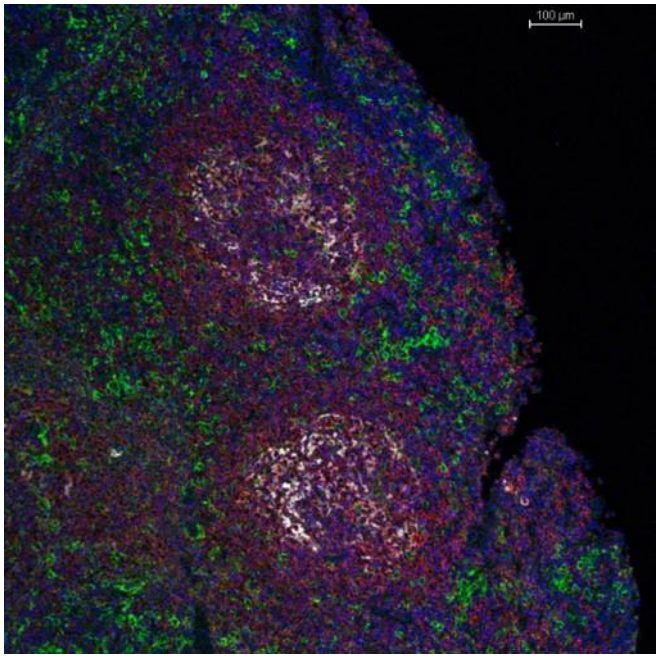


**Figure 3-36 PD-L1 is mainly found outside of the follicles and is not present on CD23+ follicular dendritic cells. PD-L1 = green. CD23 = white. CD20 = red.** Scale bar represents 100µm. Staining and image acquisition for this image was performed by Dr Beth Philips.

The pattern of PD-L1 staining in reactive lymph nodes was also investigated and no discernible co-localisation between PD-L1 expressing cells and $PD1^{Hi}$, presumed $T_{FH}$ cells could be identified, in particular, expression of PD-L1 could not be clearly established on the $Ki67^{pos}$ cells in contact with $T_{FH}$ in the light zones of GCs, Figure 3-37.

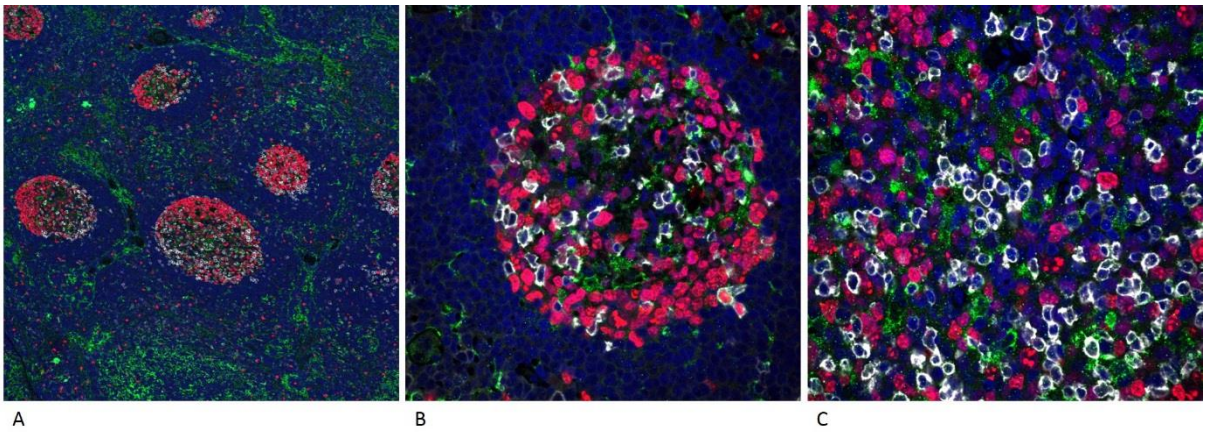


**Figure 3-37 PD-L1 staining in germinal centres. PD-L1 = green, Ki67 = red, PD1 = white, DAPI = blue.** PD-L1 is not present on the $Ki67^{pos}$ cells in contact with $PD1^{Hi}$ cells in germinal centres. Representative low power (A&B) and high power (C) images of GCs showing that PD-L1 (green) is not highly expressed on the $Ki67^{pos}$ cells (red) that are in contact with $PD\text{-}1^{Hi}$ cells (white).

## 3.7 AID expression in proliferating B cells

AID is a tightly controlled DNA modifying enzyme required for class switch recombination and somatic hypermutation. It is present exclusively in GC B cells as they undergo the processes required to generate highly specific BCRs. The expression of AID is induced by T cell – B cell interactions in the GC. AID has been implicated in the pathogenesis of GC derived lymphomas such as FL perhaps through errors in AID-induced BCR rearrangements in B cells that are protected from apoptosis through the upregulation of *BCL-2*. In mouse models lacking AID, it has been demonstrated that BCL-6 dependent GC derived lymphomas do not develop (Pasqualucci, Bhagat et al. 2008), see introduction section 1.2.

We investigated the expression of AID in FL B cells and the association of AID with proliferation and T cells with the hypothesis that AID expression may be induced following interaction with $T_{FH}$ cells and there may therefore be a spatial relationship between $T_{FH}$ cells and $AID^{pos}$ cells.

Staining for AID was technically difficult and required testing a number of different antibodies at different concentrations, different incubation conditions and different antigen retrieval methods. Reliable staining was achieved with monoclonal mouse anti-AID clone ZA001 (Invitrogen) at a dilution of 1:200 and overnight incubation using citrate antigen retrieval.

The pattern of staining was predominantly cytoplasmic and there was a high level of background staining but positive signal restricted to the GCs in reactive lymph nodes or follicles in FL samples could be clearly detected above the background signal.

### 3.7.1 Distribution of AID in FL: association with proliferation and $T_{FH}$

AID positivity was found to be restricted exclusively to the follicles of 7/7 cases of FL examined and simultaneous co-staining with Ki67 revealed that it was positive predominantly in proliferating cells.

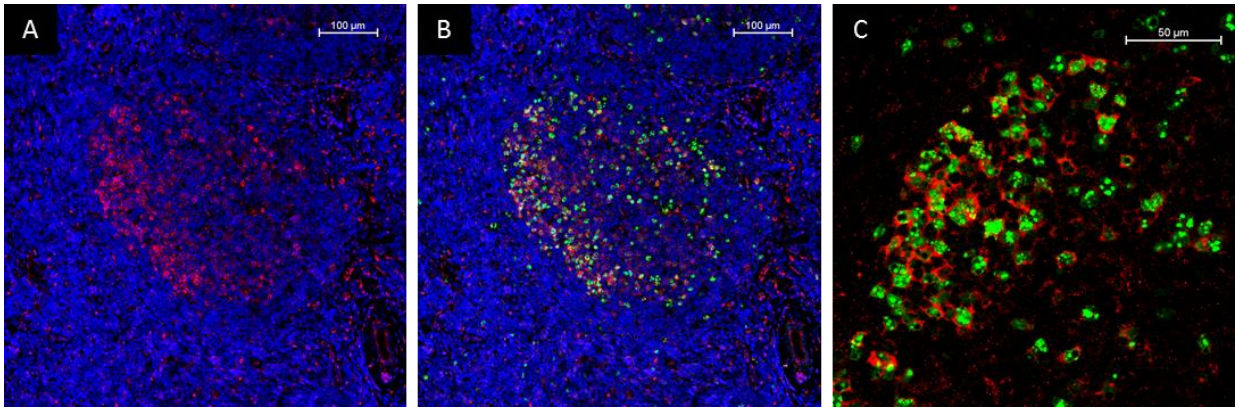


**Figure 3-38 Expression of AID is restricted to the follicles in FL where it is present only in proliferating cells. AID = red, Ki67 = green, PD1 = white, DAPI = blue. A.** AID (red) is shown to be limited to the follicle. **B and C.** co-staining with Ki67 (green) shows that AID is predominantly expressed in proliferating cells within the follicles. (A and B acquired with x10 objective, scale bars = 100µm, C acquired with x60 objective, scale bar = 50µm)

In FL, 63% ± 8.8 of $Ki67^{POS}$ cells were positive for AID (n=16 images from 6 samples, 1 sample was not assessable due to high background staining), Figure 3-38.

As we had earlier identified that proliferating B cells in FL are frequently found to be in close contact with $T_{FH}$ cells, we next investigated whether $T_{FH}$ cells are implicated in regulating AID by assessing whether AID expressing cells were in close spatial relationship with $T_{FH}$ cells. Limitations in the antibodies available meant that we could only use PD1 to label the T cells.

We found that 39.8% ±9.7 of $AID^{pos}Ki67^{pos}$ cells were in direct contact with $PD\text{-}1^{Hi}$ cells, Figure 3-39. As we had previously identified that 84.7% ± 1.7 of $PD\text{-}1^{Hi}$ cells in direct contact with Ki67+ cells were ICOS+, we can predict that the majority of $PD\text{-}1^{Hi}$ cells in contact with $AID^{pos}$ $Ki67^{pos}$ cells were $T_{FH}$. A limited number of 4-colour staining experiments confirmed that the $PD1^{Hi}$ cells in close contact with $Ki67^{pos}$ $AID^{pos}$ cells were CD3+ T cells (data not shown).

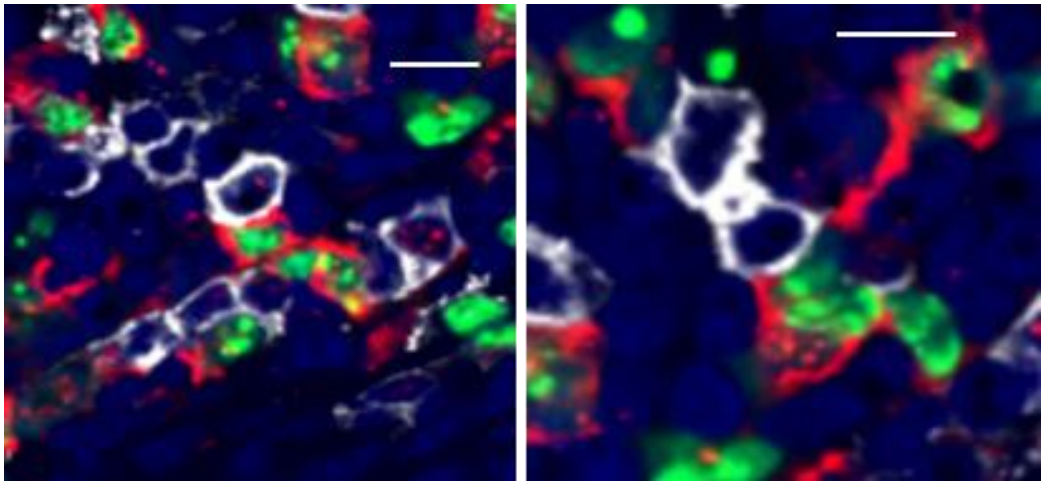

**Figure 3-39 Proliferating cells expressing AID are often in contact with PD1+ cells in FL. AID = red, Ki67 = green, PD1 = white, DAPI = blue.** Highly magnified images showing Ki67+ (green) AID+ (red) cells in close contact with PD1+ (white) cells. (Images acquired with x60 objective, scale bars = 10µm)

### 3.7.2 Distribution of AID in reactive lymph nodes: association with proliferation and $T_{FH}$

As in FL, the AID distribution was limited to proliferating cells in the GCs of reactive lymph nodes, Figure 3-40. In contrast to FL, in reactive LNs, there was evidence of polarisation of the GCs; in the highly proliferative dark zones there were more $Ki67^{pos}$ cells and corresponding AID staining compared to the less proliferative light zones. Whilst it was hard to appreciate any relationship between AID and $PD1^{Hi}$ cells in the dark zones, in the light zones there was a similar association to that observed in FL, i.e. $Ki67^{pos}$ $AID^{pos}$ cells were found to be closely associated with $PD1^{Hi}$ cells, which may be $T_{FH}$,

Figure 3-41.

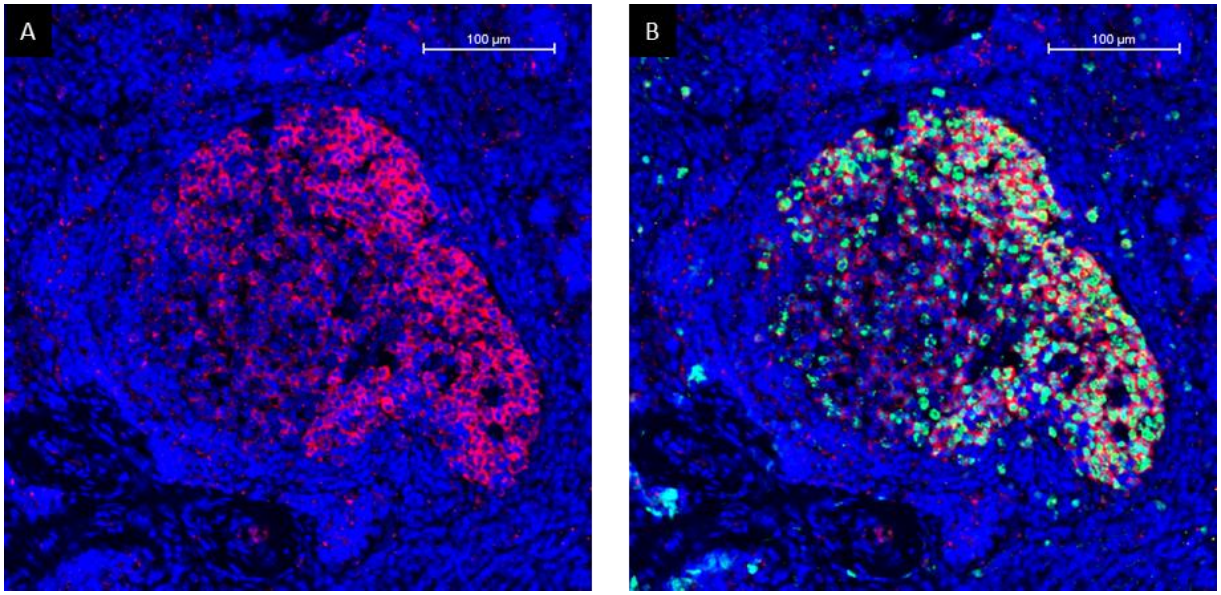


**Figure 3-40. AID expression is limited to proliferating cells in germinal centres. AID = red, Ki67 = green, PD1 = white, DAPI = blue A.** AID (red) can be seen to be more prominent at one pole of the GC. **B.** When Ki67 is simultaneously visualised it can be seen that AID is present mainly in proliferating cells and is highest in the dark zone. (Image captured with x10 objective, scale bar = 100µm)

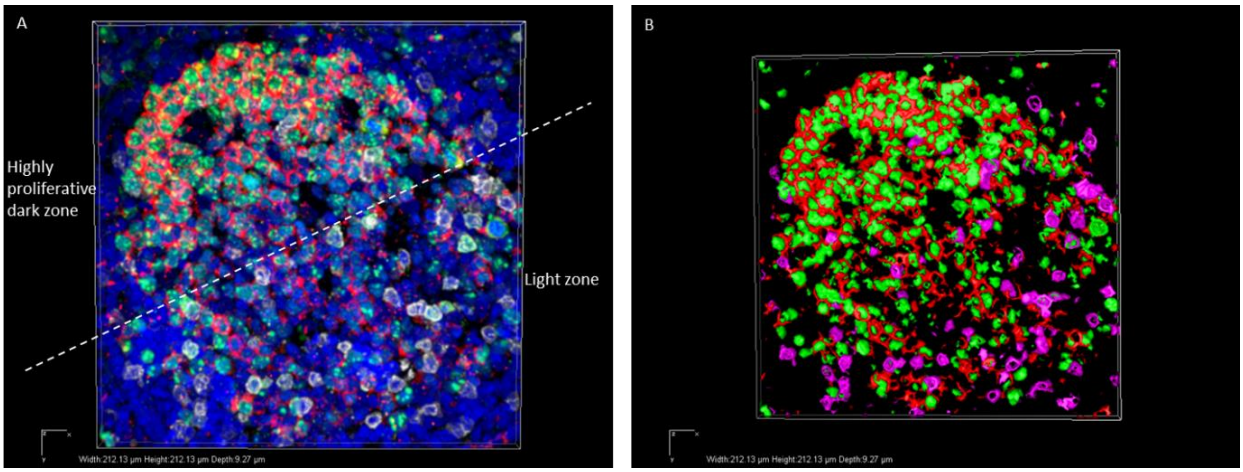


**Figure 3-41. 3D reconstruction of Z series showing AID in the proliferating cells of the dark zone and association with PD1 in the light zone. A. AID = red, Ki67 = green, PD1 = white, DAPI = blue** In the dark zone there are many proliferating $AID^{pos}$ cells but few $PD1^{Hi}$ cells. In the light zone $PD1^{Hi}$ cells (white) can be seen to be in contact with proliferating $AID^{pos}$ cells (the dotted line shows the demarcation between dark and light zone). **B.** In this image only the binary layers are shown (**Ki67 green, AID red, PD1 pink**).

## 3.8 FOXP3+ T cells in reactive LN and FL

FOXP3 is a transcription factor usually associated with T regulatory cells ($T_{regs}$) but it has also recently been demonstrated to be present in a subset of cells that express ICOS and have a phenotype between $T_{FH}$ and $T_{regs}$, so called T follicular regulatory cells ($T_{FR}$) which have been identified in secondary lymphoid tissue and in the FL tumour microenvironment (Ame-Thomas, Le Priol et al. 2012, Sage, Francisco et al. 2013).

$T_{regs}$ have been associated with adverse outcome in FL especially if distributed in a follicular or peri-follicular pattern, and it is thought that this may be through inhibition of the anti-tumour response (Farinha, Al-Tourah et al. 2010).

Although the primary aim of our research was to thoroughly investigate the $T_{FH}$ cells present in the FL tumour microenvironment, it was important to investigate whether the PD1+ ICOS+ T cells that we have identified as $T_{FH}$ express FOXP3. We pursued this line of investigation for two reasons, firstly to ensure that the cells we have described as $T_{FH}$ are genuinely $T_{FH}$, in which case they should not express the transcription factor FOXP3, and secondly to explore if there is a subset of $FOXP3^{pos}$ $T_{FH}$-like cells for example $T_{FR}$ that can be identified using the techniques we developed.

Three different anti-FOXP3 antibodies were assessed; no successful labelling was achieved with the first 2 antibodies despite attempting different antigen retrieval and incubation conditions. Finally, monoclonal mouse anti-FOXP3 clone 236A/E7 (Abcam) was found to work well with standard pH6.1 citrate antigen retrieval and overnight incubation at 4°C.

Since this was a mouse antibody, it could not be used simultaneously with the mouse CD4 antibody but could be used with rat anti-CD3 antibody.

### 3.8.1 Distribution and phenotype of FOXP3$^{pos}$ CD3+ T cells in FL

Nuclear FOXP3 was identified exclusively in CD3+ cells in 4/4 FL cases examined. FOXP3 staining was not identified in any non-T cells, Figure 3-42.

Although apparently lower in number than $T_{FH}$ cells, the distribution of FOXP3 positive T cells within the follicles was similar to the pattern of distribution of $T_{FH}$ cells; FOXP3$^{pos}$ cells were found mostly in a perifollicular distribution with some scattered through the follicles, Figure 3-42 and Figure 3-43A and B. Unlike $T_{FH}$ cells which were rarely identified outside the follicles, FOXP3+ T cells were also found in the interfollicular areas of FL. Since this was not the primary focus of the research, limited numbers of samples were stained for FOXP3 (n=4) and formal quantification of the number of FOXP3$^{pos}$ cells and comparison to number of $T_{FH}$ has not been performed.

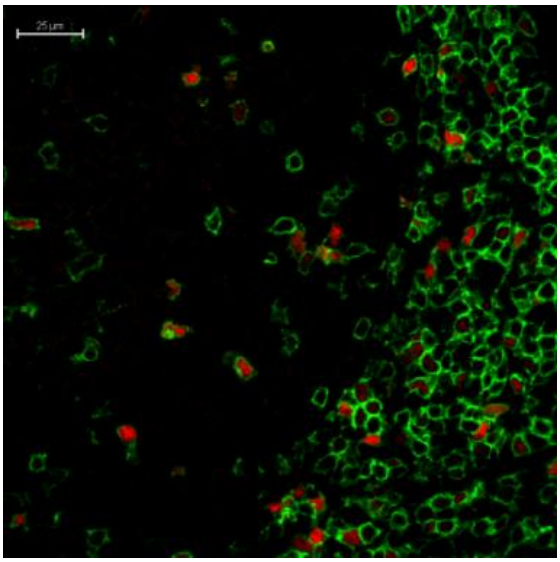


**Figure 3-42. FOXP3 is limited to T cells. FOXP3 = red, CD3 = green.** FOXP3 is identified in a proportion of CD3+ T cells (green) at the follicular border and is never identified in non-CD3+ cells. (Image acquired with x60 objective, scale bar = 25µm)

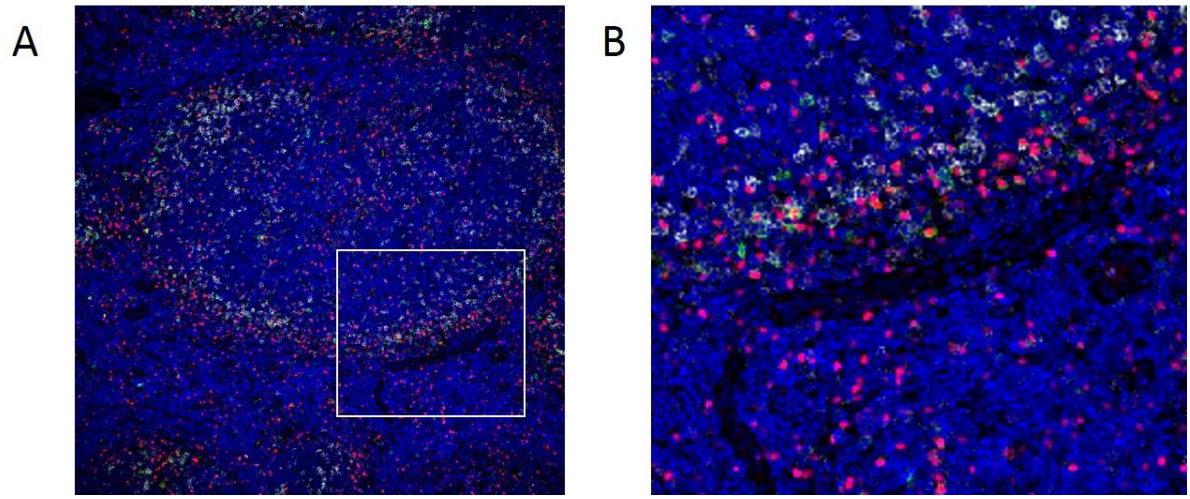


**Figure 3-43 Distribution and phenotype of FOXP3$^{pos}$ cells in FL. FOXP3 = red, PD1 = white, ICOS = green, DAPI = blue. A.** FOXP3$^{pos}$ cells are distributed mainly around the border of the follicle in a similar pattern to PD1 and ICOS but there are also scattered FOXP3$^{pos}$ cells in the interfollicular areas (acquired with x10 objective). **B.** The area in the white rectangle in **A** has been enlarged. Some FOXP3$^{pos}$ cells can be seen to express either ICOS or PD1.

Co-staining with PD1, ICOS, and FOXP3 was next performed to determine if FOXP3$^{pos}$ cells co-expressed either or both of PD1 and ICOS. Only 4 samples were stained with this combination and one stained sample was not analysable due to a high level of background signal. Results are therefore based on analysis of n=12 images from 3 samples. Analysis of FOXP3 images was performed manually.

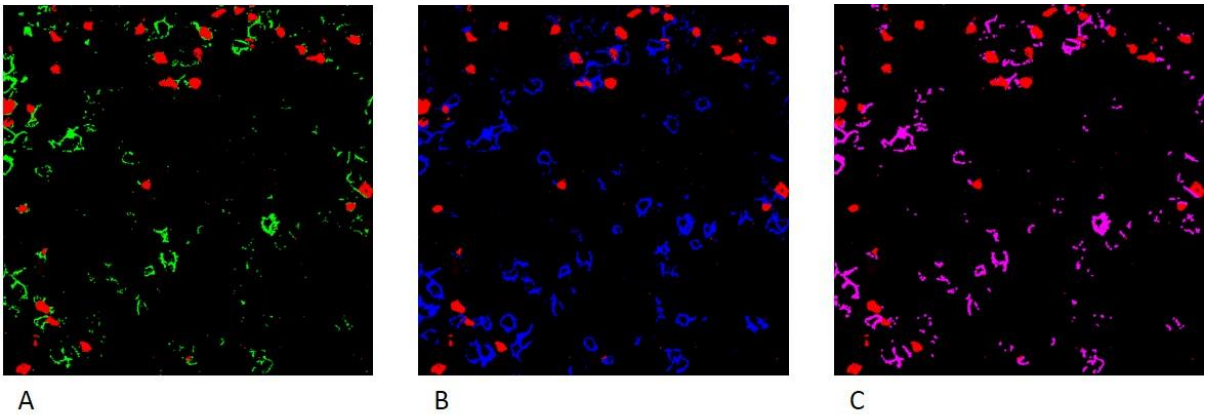


**Figure 3-44 Phenotype of FOXP3$^{pos}$ cells in FL. FOXP3 = red, ICOS = green, PD1 = blue, PD1-ICOS intersection = pink.** Separate binary layers of the same high power (x60) image of a FL follicle are shown in each panel. **A,** some ICOS+ (green) cells are seen to be FOXP3$^{pos}$ (**red**). **B.** some PD1$^{Hi}$ (**blue**) cells are FOXP3$^{pos}$, but in **C** it can be seen that few FOXP3$^{pos}$ cells are dually positive for both PD1 and ICOS (**pink**).

In FL, a median of 25% (6.0-28.0) of ICOS+ cells were positive for FOXP3, and a median of 4.0% (1.0 – 8.0) of PD1+ cells were FOXP3$^{pos}$. However, when the intersection binary layer of PD1 and ICOS was

created, it was found that only a very small proportion of dual positive PD-1+/ICOS+ cells were $FOXP3^{pos}$, median 5%, (1.0 – 8.0), n= 3 FL samples, 12 images, Figure 3-44.

Thus, whist $PD1^{Hi}$ $FOXP3^{pos}$ cells and ICOS+ $FOXP3^{pos}$ cells were relatively frequent, the majority of $PD1^{Hi}$/ICOS+ cells were negative for FOXP3. This is supportive of the majority of $PD1^{Hi}$ ICOS+ T cells being $T_{FH}$ rather than $T_{regs}$.

In the sections stained for FOXP3, PD1 and ICOS, it was noted there were some PD1+/ICOS+ cells adjacent to $FOXP3^{pos}$ cells, Figure 3-44. Too few sections have been stained and analysed with this combination to draw conclusions about this and line of enquiry requires further investigation to determine if $FOXP3^{pos}$ $T_{regs}$, may regulate $T_{FH}$ in FL as discussed in the introductory section 1.3.4.

Similarly, when staining simultaneously for Ki67, PD1, and FOXP3 in 2 preliminary experiments we found that there appear to be some $FOXP3^{pos}$ cells in close proximity to $Ki67^{pos}$ cells, Figure 3-45. This area also requires further investigation for example to determine if the ratio of $T_{FH}$-$T_{reg}$, or the proportion of $Ki67^{pos}$ cells in contact with $T_{FH}$ cells compared to $T_{regs}$ is important in predicting prognosis in FL. This was beyond the scope of the current research but may be investigated further at a later time.

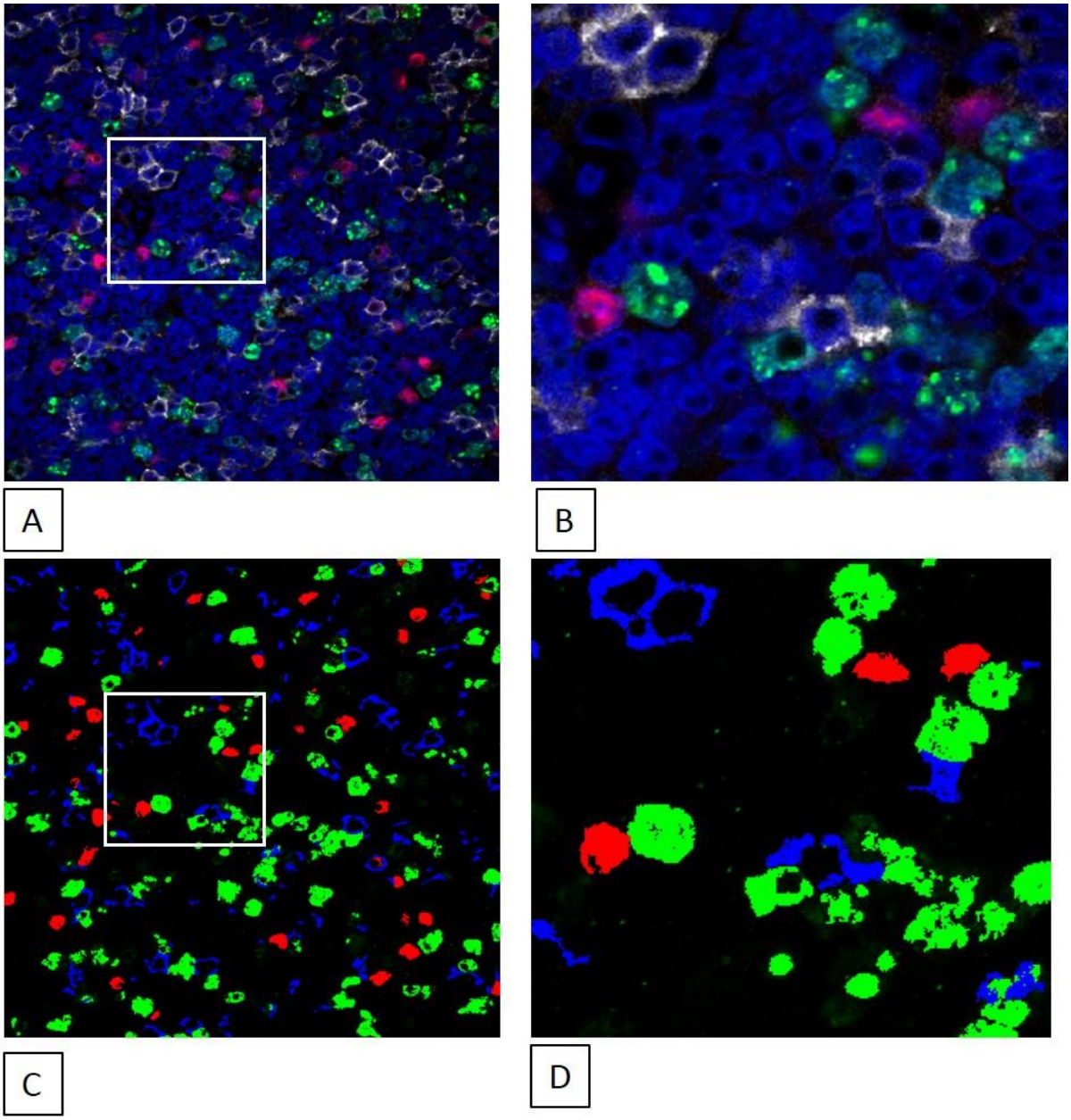


**Figure 3-45 FOXP3$^{pos}$ cells sometimes co-localise with Ki67$^{pos}$ cells in FL. FOXP3 = red, Ki67 = green, PD1 = white, DAPI = blue. A,** some FOXP3$^{pos}$ cells can be seen to co-localise with Ki67$^{pos}$ cells in the area highlighted by the white rectangle. **B.** This area is magnified in **B. C & D** show the same images in the binary layers only (**FOXP3 = red, Ki67 = green, PD1 = blue).**

### 3.8.2 Distribution and phenotype of FOXP3$^{pos}$ CD3+ T cells in reactive lymph nodes

There was a notable difference in distribution of FOXP3 between FL and reactive LNs. In reactive LNs FOXP3$^{pos}$ cells were almost exclusively located outside of the GCs with very few located within GCs.

Co-staining with PD1, ICOS, and FOXP3 was next performed to determine if FOXP3$^{pos}$ cells co-expressed PD1 and ICOS in normal GCs. 3 reactive LNs were stained with this combination.

Within the GCs, there were too few FOXP3$^{pos}$ cells to generate meaningful data regarding the proportion of FOXP3$^{pos}$ cells co-expressing PD1 and ICOS but visual inspection revealed that no FOXP3$^{pos}$ PD1+ ICOS+ cells were identified within GCs, Figure 3-46.

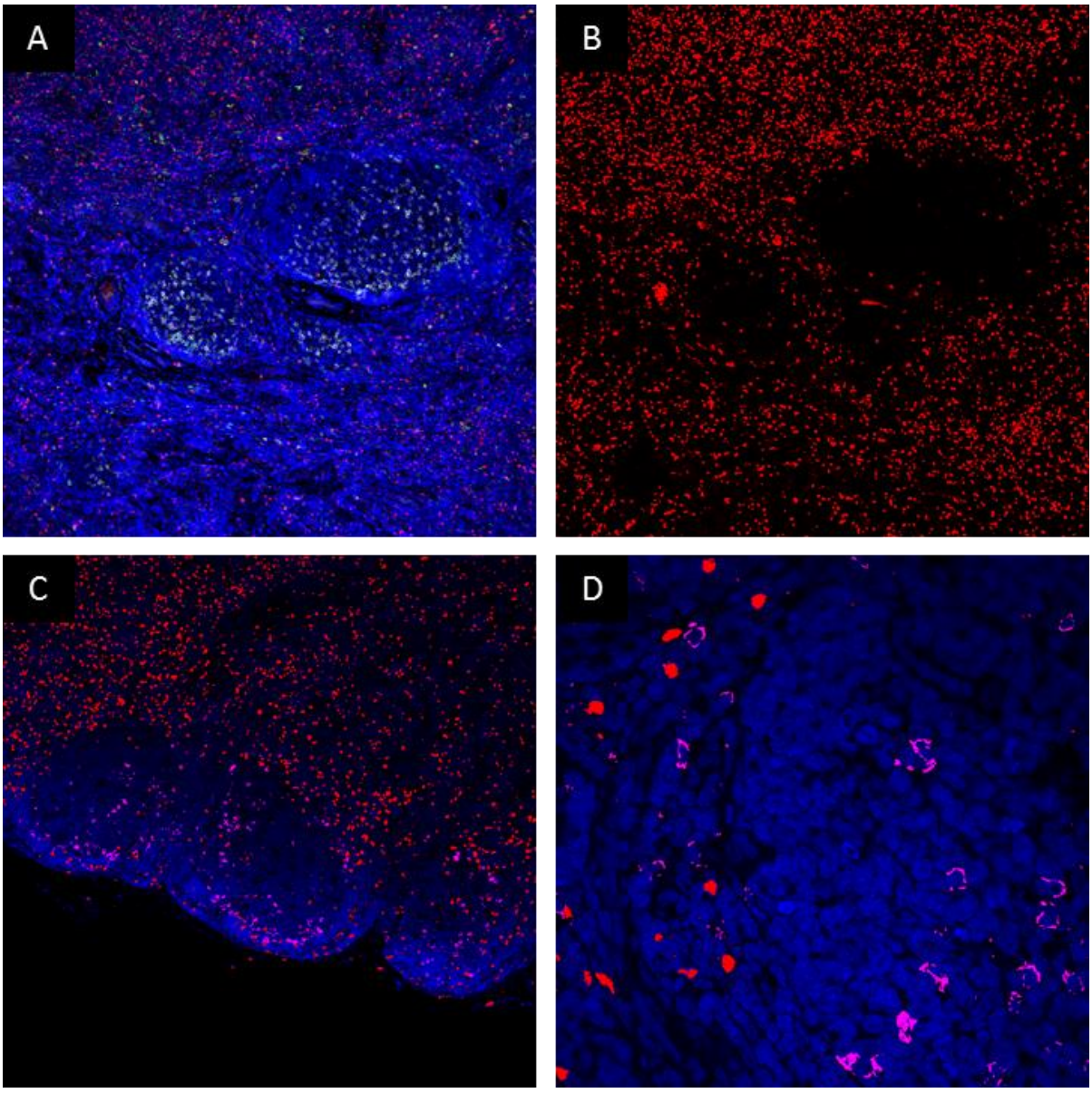


**Figure 3-46. FOXP3 in reactive germinal centres. FOXP3 = red, PD1 = white, ICOS = green, DAPI = blue A.** FOXP3 is seen to be located almost exclusively outside the GCs. **B.** The same image as **A** showing only the FOXP3 binary layer (**red**) highlighting its exclusion from the GCs. **C.** Only the FOXP3 (**red**) binary and the intersection of PD1/ICOS (**pink**) are shown demonstrating their different distributions. **D.** At the border of this GC it can be seen that no PD1+/ICOS+ cells (**pink**) are FOXP3$^{pos}$ (**red**). (Images A, B, and C acquired with x10 objective. Image D acquired with x60 objective).

## 3.9 Investigating the TCR repertoire of T cells in FL

As described in the introduction, section 1.8, we hypothesised that, if the T cells within the malignant follicles of FL are present in response to antigen, there may be skewing of their TCR repertoire compared to those in the inter-follicular areas of FFPE LN biopsy specimens. The TCR repertoire of T cells in the FL microenvironment has not previously been reported.

The methods for processing and dissecting sections, DNA extraction and sequencing of the TCRs are described in section 2.6. To briefly re-cap, it was first ascertained that genomic DNA could be extracted from archived FFPE LN specimens for TCR sequencing. Subsequently, the research question was refined to determine whether the TCR repertoire of T cells within the follicles was different to the TCR repertoire of interfollicular T cells.

The methodology was influenced by the results of preliminary experiments and by the practical problems encountered in laser dissection as described in the methods chapter.

### 3.9.1 Sequencing technique and calculation of clonality

Next generation sequencing (NGS) of T-cell receptor β (TCR) repertoires and initial data analysis and processing were performed by Adaptive Biotechnologies, Seattle, USA (Robins, Campregher et al. 2009). Additional analyses were performed by Dr Marta Pasikowska and Prof Stephen Devereux at KCL.

Sequence reads were aligned to V, D and J sequences, insertions and deletions were identified and productive CDR3 sequences extracted. Clonotypes were considered significant if two or more copies of the same sequences were obtained, importantly, no clones of size n=1 (singletons) were reported.

The degree of restriction of the TCR Vβ repertoires was assessed using a clonality index which derives from Shannon's entropy. This is a measure of the certainty with which the identity of a species selected randomly from a population of different species can be predicted, and is normalised for the number of productive sequences present. The calculation takes in to consideration, and accounts for

differences in the number of cells in different samples. In this research, although there were likely to be different numbers of T cells analysed in different areas of tissue dissected from the specimens, this is corrected for by expressing diversity as a function of the number of unique sequences present (Robins, Campregher et al. 2009, Sherwood, Emerson et al. 2013).

The entropy calculation is influenced by both the total number of different species and the diversity of the population. A population or sample containing only one clone would have an entropy of 0 whilst a completely polyclonal population, in which all clones are equally frequent, would have a Shannon's entropy equal to the logarithm of the number of unique sequences. To allow populations containing different numbers of unique clones to be compared, the entropy was normalized by dividing by the logarithm of the number of unique reads present. The clonality index corresponds to the reciprocal of the normalized entropy so that a monoclonal population gives a value of 1 and a polyclonal population 0.

### 3.9.2 TCR sequencing from whole LN sections

In the preliminary experiment to ascertain the feasibility of DNA extraction and TCR sequencing from FFPE tissue (see section 2.6 above), 175ug/ul DNA was extracted from 2 separate FFPE LNs excised synchronously from a patient with newly diagnosed, untreated FL. The DNA was frozen and shipped to ImmunoSeq in Seattle, USA for NGS sequencing of the CDR3 TCRβ subunits.

It is important to note that in this preliminary experiment, whole LN sections were used for DNA extraction and TCR repertoire analysis with no dissection performed. Analysis revealed 2806 unique TCR reads from lymph node 1, and 2989 unique reads from lymph node 2 with 152 sequences common to both lymph nodes, this is depicted in Figure 3-47 below. In this figure, sequences unique to LN1 are represented as green dots on the Y axis, with the frequency with which each clone occurs displayed on a logarithmic scale. Sequences unique to LN2 are represented as red dots on the x axis (with frequency of occurrence displayed on a logarithmic scale), and sequences found in both LNs are displayed as blue dots.

It can be seen that while most clones are unique to one of the LNs (green and red dots), there is a population found in both LNs, and many of these shared TCR sequences (blue dots) are present at high frequency in both LNs possibly indicating the presence of a population of antigen restricted T cells present in 2 separate lymph nodes biopsied simultaneously.

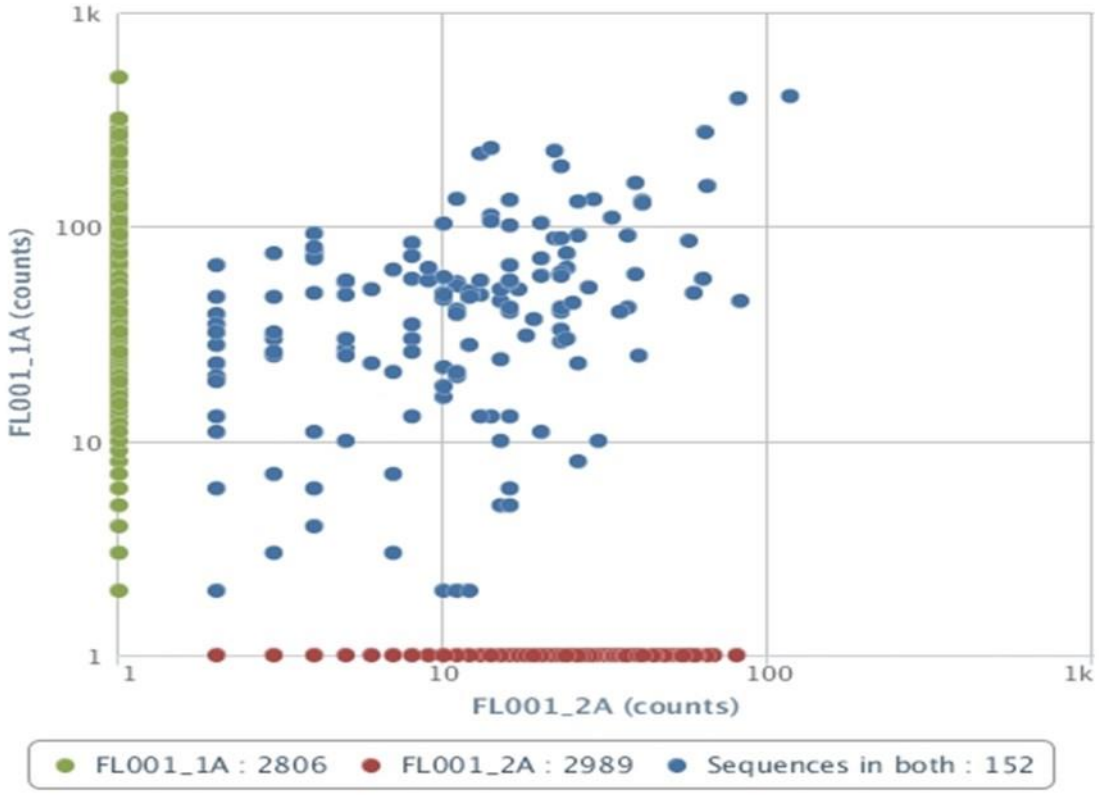


**Figure 3-47 Results of TCR sequencing from 2 lymph nodes biopsied simultaneously from a patient with newly diagnosed FL.** On the Y axis, green dots represent, 2806 TCR sequences unique to LN 1 are shown. On the X axis, red dots represent 2989 TCR sequences unique to LN 2. Sequences found in both lymph nodes are represented by blue dots. Scales represent frequency of occurrence of sequences, displayed on a log scale.

This provided preliminary evidence to support the theory that there may be TCR restriction in the T cells infiltrating lymph nodes in FL. However, as detailed above, this preliminary experiment did not distinguish between T cells located in the follicular and interfollicular compartments and led to the subsequent experiments examining differences in TCR repertoire between these compartments.

### 3.9.3 Comparison of TCR repertoire between follicular and interfollicular regions of FL

Since we identified that the phenotype of the T cells within the follicles of FL was markedly different to those located in the interfollicular areas, and that interaction between $T_{FH}$ and proliferating FL B cells was restricted predominantly to the follicles, we next investigated if there was a difference in the TCR repertoire between these different compartments.

Equivalent areas of tissue were laser dissected from follicular and interfollicular areas of 5 FL LN samples. Following refinements of the technique, an adequate yield of DNA was obtained using the method described in section 2.6.2 and Figure 2-9.

There was no significant difference in the quantity of DNA extracted from follicular and interfollicular areas, mean 415µg (range 310-764µg). The DNA was frozen and shipped to ImmunoSeq in Seattle, USA for NGS of the CDR3 TCRβ subunits.

The TCR repertoire of tissue dissected from the malignant follicles of FL was more restricted with greater clonality than the TCRs of the interfollicular areas in each of the 5 cases examined (median clonality of follicular areas 0.062, median clonality of interfollicular areas 0.049, Mann Whitney, $p = 0.0317$), Figure 3-48A. This finding was consistent in all cases examined and suggests that the T-cells within neoplastic follicles are antigen restricted.

As expected from their different phenotypes, the clonotypes present in the follicular and interfollicular areas of the same sample were markedly different with <20% overlap in all cases (median overlap 0.16), indicating that the TCR repertoires of the follicular and interfollicular areas are different, Figure 3-48B.

When only the top 100 most frequent clones were considered, the difference between the follicular and interfollicular regions was especially marked with a predominance of more frequent clones in the follicles and very little overlap with the interfollicular areas.

These data indicate that high-frequency T-cell clones of restricted repertoire dominate the TCRVβ repertoire of neoplastic follicles in FL whereas the interfollicular regions contain more distinct clones occurring at lower frequency Figure 3-48C.

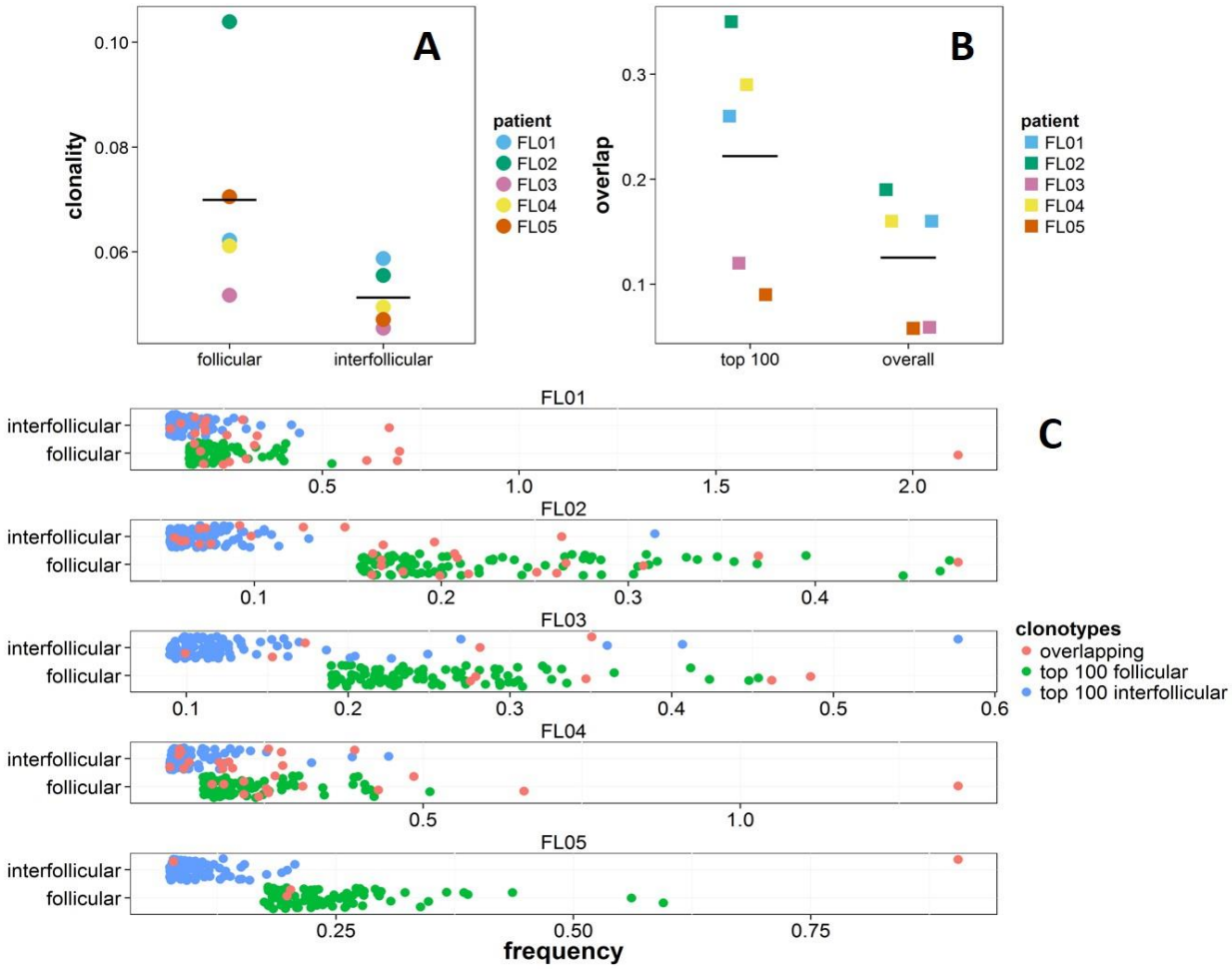


**Figure 3-48 Evidence of TCR restriction in FL.** (A) The clonality of the TCRs in intrafollicular areas was higher than in the interfollicular compartment in all cases examined, horizontal bars represent mean of all samples. (B) The level of overlap of clonotypes between follicular and interfollicular compartments for all clonotypes in paired samples (overall) and for top 100 clonotypes (top 100), horizontal bars represent mean of all samples. (C) The frequency of the top 100 clonotypes in each sample from follicular (green dots) and interfollicular compartments (blue dots) are shown highlighting greater restriction in the follicular TCRs. Sequences present in both compartments are shown as red dots, very few sequences are present in both follicular and interfollicular areas (range 2-15) demonstrating that there is little overlap in repertoire between the two compartments.

In order to look at this data another way, we next calculated the proportion of high frequency productive reads/clones in the follicular and interfollicular areas (Nazarov, Pogorelyy et al. 2015). Consistent with the previous analysis, this showed that compared to the interfollicular areas, the

follicular TCR repertoire was dominated by high frequency clones Figure 3-49. The top 50 most frequent clones made up a mean of 19% of all clones in the follicular areas (95% CI 17-21) compared to 9.8% (95% CI 6.1-13.4) in the interfollicular region (p=0.0002).

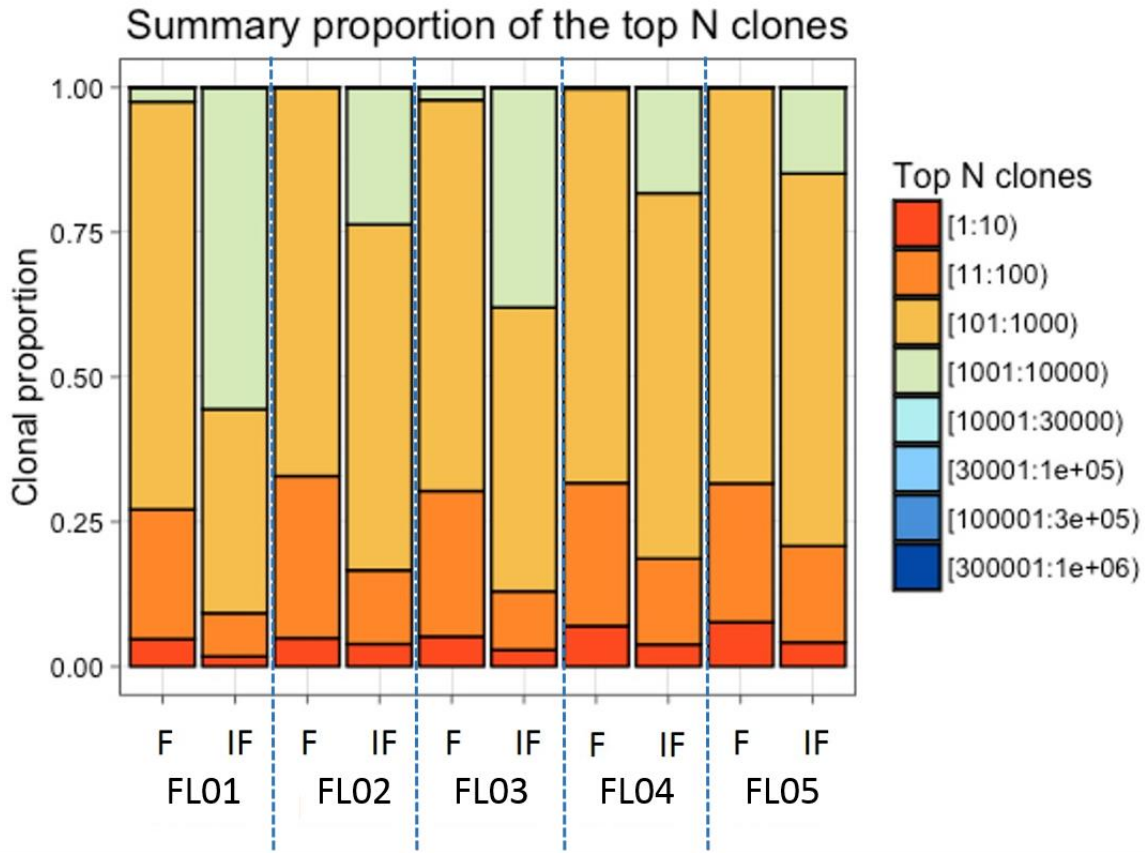


**Figure 3-49 Summary of TCR data showing the proportion of the total population accounted for by high frequency clones in the follicular (F) and interfollicular (IF) regions of FL lymph nodes.** Each case is presented as a pair of column representing the follicular (F) and interfollicular regions (IF) side-by-side. In each case it can be seen that the follicular regions are dominated by larger populations of more frequently occurring clones (orange and red colours) whereas the interfollicular regions have higher proportions of low frequency clones (pale green colour)

# Chapter 4 Discussion

We have revealed a number of important and novel findings in this research that extend our understanding of the composition of the FL microenvironment and how a specialised subset of T cells, $T_{FH}$, interact with the malignant cells. We have also gained greater understanding of $T_{FH}$ in the normal GC reaction and in doing so have identified many parallels between FL and GCs.

In this research we have demonstrated some powerful techniques that can be used on readily available, archived, formalin fixed paraffin embedded tissue sections. Coupled with this, we developed a unique semi-automated image analysis algorithm that permitted the detailed analysis of multiple images with minimal manual interference and therefore with reduced scope for operator error or bias. The techniques used in this research overcome some of the limitations of other approaches that have previously been used to study the microenvironment in FL and other lymphoproliferative disorders.

The pivotal new findings generated in this research include the following:

- $T_{FH}$ have been visualised in situ in FL and GCs for the first time using multi-colour immunofluorescent confocal microscopy that included simultaneous co-staining with BCL6, PD1, ICOS, and CD3.
- Many similarities between the phenotype, proportion, and location of $T_{FH}$ were identified in FL and GCs indicating that $T_{FH}$ may play a similar role in the FL microenvironment as they do in GCs.
- For the first time, a correlation between the number of $T_{FH}$ and the number of $Ki67^{pos}$ FL B cells was identified. Associated with this, a correlation between the number of $T_{FH}$ and histological grade was identified.
- In GCs a very close spatial relationship between $Ki67^{pos}$ B cells and $T_{FH}$ was identified in the light zones for the first time and a correlation between number of $T_{FH}$ and number of $Ki67^{pos}$

B cells was revealed supporting the theory that $T_{FH}$ control GC size and rate of B cell proliferation.

- $AID^{pos}$ $Ki67^{pos}$ B cells were found to be in close proximity to $T_{FH}$ suggesting that $T_{FH}$ may be important in regulating AID which could be important in the pathogenesis of FL or the development of histological transformation.
- Contrary to previous reports of impaired synapse formation, we identified in situ evidence that $T_{FH}$ form immunological synapses with FL B cells.
- The TCR repertoire of T cells in the FL microenvironment has not been previously studied. Our experiments in this area yielded fascinating insights that show TCR repertoire skewing in the follicular areas indicating that T cells within the follicles may be present in response to antigen.

These and other findings are discussed in more detail below.

## 4.1 Techniques used in this research: advantages, disadvantages and applicability

One of the key and most widely applicable findings of this work is that multi-parameter confocal immunofluorescent microscopy can be performed on archived FFPE lymph node tissue sections without undue autofluorescence, and that quantitative analysis of the images acquired can be performed.

This builds on research techniques developed in our laboratory over a number of years and has been refined to allow up to 4 antigens or proteins to be simultaneously labelled (Patten, Buggins et al. 2008). The semi-automated quantitative image analysis described in this thesis was developed specifically for this research and represents a significant advance over previous work using similar techniques and overcomes some of the difficulties of interpreting standard IHC (Sander, de Jong et al. 2014).

Previous research has demonstrated that the microenvironment has a very important role in the pathogenesis of FL but when the composition of the microenvironment has been correlated with

prognosis, vastly disparate results have been reported from different groups (Lee, Clear et al. 2006, Glas, Knoops et al. 2007, Carreras, Lopez-Guillermo et al. 2009, Wahlin, Aggarwal et al. 2010, Richendollar, Pohlman et al. 2011).

There are many reasons for these discrepant findings. One of the reasons for this disparity is the use of single parameter IHC in much of the published research which is not sufficiently sensitive to precisely define the subsets of cells implicated in the pathogenesis of the disease (Carreras, Lopez-Guillermo et al. 2009, Wahlin, Aggarwal et al. 2010, Richendollar, Pohlman et al. 2011). This is highlighted in our research where 46.9% (34.7-51.9) of follicular CD4+ cells were positive for PD1, but only 52.2% (45.7-61.9) of these co-expressed ICOS. Therefore, if we had used non-quantitative PD1 positivity as a surrogate marker for $T_{FH}$ cells we would have considerably overestimated the proportion of this important T cell subset. We occasionally had to use PD1 and CD4 alone to identify $T_{FH}$ but were able to set a very high threshold for PD1 in these instances ($PD1^{Hi}$) and only used this method when specifically investigating T cells in direct contact with FL B cells which we had earlier identified to be predominantly $T_{FH}$.

One of the many reasons therefore for the disparity in the reported influence of PD1 expression on prognosis in FL is that it may be important to know not only how many cells in the microenvironment are PD1+, but more precisely, how many $PD1^{Hi}$ $T_{FH}$ are there in relation to incompetent, exhausted PD1+ T cells? Additional reasons for discrepant results include heterogeneously treated patient populations, and subjective interpretation of IHC (Sander, de Jong et al. 2014).

Other high quality research into the FL microenvironment has used multiparameter flow cytometry on disaggregated lymph node samples (Pangault, Ame-Thomas et al. 2010, Ame-Thomas, Le Priol et al. 2012, Ame-Thomas, Hoeller et al. 2015). This powerful technique permits simultaneous labelling of numerous cell markers and therefore precise identification of T cell subsets can be performed, but a drawback to this approach is that it does not allow architectural information or cellular co-localisations to be assessed.

The technique that we developed and used therefore offers advantages over both standard IHC on tissue sections and flow cytometry on disaggregated LNs for investigating the lymphoma microenvironment.

There were, however, some disadvantages to our technique. Firstly, the antibody panels were more limited than if using flow cytometry. Only 3 or 4 antibodies could be used simultaneously and all primary antibodies had to be raised in different species. Whilst 3-4 antibodies permits more sophisticated investigation of cellular subsets than single parameter IHC, we sometimes had to make compromises in selection of antibodies. For example, in some experiments CD3 had to be used as a surrogate for CD4, and in some circumstances we had to make assumptions based on earlier experiments, for example that $PD1^{Hi}$ cells in contact with FL B cells were $T_{FH}$. Again, the quantitative approach of the image analysis that we used compared to standard IHC lent validity to this approach. It was also found that some antigens were best detected in certain channels which had a bearing on which combinations of antibodies could be successfully combined. It was necessary to carry out regular control experiments to ensure that there was no tissue autofluorescence that could be misinterpreted as positive signal, spectral overlap, or non-specific binding of either primary or secondary antibodies.

Acquisition time on the confocal microscope was long and expensive which is a potential barrier to using this technique more widely or on larger cohorts of samples. Similarly, whilst the semi-automated image analysis technique that we developed offered many advantages over the subjective analysis of IHC images, it was time consuming and labour intensive to set up, and there was still some scope for operator-bias for example at the stage of setting the binary layers.

Another potential disadvantage of the research presented in this thesis is that it was performed on archived tissue from patients treated heterogeneously from a single centre over a number of years. This prevents meaningful application of the results to the population level. However, it will be possible for future research to be performed on tissue samples collected from patients enrolled in large

prospective clinical trials which will permit the investigation of correlations between the composition of the microenvironment and clinical outcomes in homogenous cohorts of patients treated with the same interventions.

The latter part of this research, focusing on the TCR repertoire of T cells infiltrating the tumour microenvironment, also used novel techniques including laser dissection of FFPE samples, extraction of DNA from very small amounts of tissue and deep sequencing of the DNA obtained by this method. The results of this are further discussed below but, once again, this shows that valuable information can be obtained from archived FFPE tissue. This is important as FFPE tissue is the most common form in which diagnostic lymphoma biopsies are processed and stored, it is easy to store, does not significantly degrade over time, and is often routinely collected in clinical trials.

It should however be noted that most of the samples that we analysed were from whole lymph node excisions. A few core biopsies were analysed by confocal fluorescent microscopy and whilst they yielded adequate results they were not as good as whole sections and not as many whole follicles per specimen could be inspected. We did not attempt DNA extraction from core biopsies. There is an increasing tendency to use core biopsies for the diagnosis of lymphoma in the UK which can have significant clinical and patient-centred benefits over whole node excisions but, since they yield smaller tissue volumes, they may not be as valuable for correlative translational research. This is an area that we need to consider as a research and clinical community.

## 4.2 $T_{FH}$ in GCs and the FL microenvironment

FL is derived from GC B cells and in this research we have demonstrated some important similarities between normal GCs and the follicles of FL especially with regards to the presence of $T_{FH}$ cells and their close spatial relationship with proliferating B cells.

We found that 25.0% (18.5-28.7) of CD4+ T cells within the follicles co-express the surface markers PD1 and ICOS and, in separate sections have shown that these cells are positive for the transcription

factor BCL6, the chemokine receptor CXCR5, and negative for the transcription factors FOXP3 and TBET. These can therefore be considered with a high degree of certainty to be $T_{FH}$ cells.

Their proportion, relative to the total number of CD4+ T cells was not significantly different from GCs of reactive lymph nodes where 33.05% (24.7-43.7) CD4+ cells were $T_{FH}$. In the interfollicular regions, where the majority of T cells in a lymph node are located, very few had a $T_{FH}$ phenotype, 3.63% (1.89-6.15); which was significantly higher than in the non-GC areas of reactive lymph nodes although the proportion was very low in both cases. One reason for the slightly higher proportion of inter-follicular $T_{FH}$ cells in FL than in reactive LNs may have been because it was sometimes difficult to accurately delineate the follicular border in FL whereas the border of GCs was very clear in reactive LNs.

Of note, we made a comparison with the proportion of $T_{FH}$ in CLL and whilst there were many PD1+ T cells in CLL, very few T cells dually expressed ICOS and PD1 and the proportion of $T_{FH}$ was significantly lower than in either FL follicles or GCs. This highlights the need to use more than one antibody to identify $T_{FH}$ and demonstrates that PD1 expression on T cells in CLL is likely to be due the presence of exhausted T cells rather than functional $T_{FH}$.

Although the proportion of $T_{FH}$ was not different between FL follicles and GCs, their distribution was different; in GCs there was clear demarcation between the dark and light zones with most $T_{FH}$ found in the light zones or at the interface between dark and light zones. In FL meanwhile the $T_{FH}$ were often in a peri-follicular pattern or sometimes distributed throughout the follicles. The distribution of $T_{FH}$ in FL was later shown to mirror the distribution of $Ki67^{pos}$ tumour cells.

Thus, although are many striking similarities between follicles of FL and normal GCs, the lack of zonal demarcation in FL is a clear difference. The reasons for this difference and its implication is not clear at present but warrants further investigation.

$T_{FH}$ have previously been reported to constitute 24-35% of all CD4+ T cells assessed by flow cytometry in whole disaggregated FL lymph nodes (Pangault, Ame-Thomas et al. 2010, Ame-Thomas, Le Priol et

al. 2012, Myklebust, Irish et al. 2013). Given that we identified that 25% of CD4+ T cells within the follicles were $T_{FH}$ and very few $T_{FH}$ were present in interfollicular areas where there are proportionally more CD4+ T cells, this translates to a lower proportion of $T_{FH}$ in the lymph node as a whole in our research than the previous reports but, the use of different techniques makes it difficult to make direct comparisons.

The authors of previous research identified a significantly lower proportion of $T_{FH}$ in whole reactive lymph nodes than in FL lymph nodes which led them to conclude that FL nodes are enriched by $T_{FH}$ relative to normal reactive LNs. However, this did not account for the extensive contribution of interfollicular tissue in whole disaggregated nodes. In our research, in the interfollicular area of reactive nodes <1% of CD4+ T cells were $T_{FH}$ and this area is more extensive than the corresponding interfollicular component of FL where the lymph node is effaced by large follicles with relatively less interfollicular tissue than reactive LNs. This will therefore have caused an underestimate of the proportion of T cells with a $T_{FH}$ phenotype located specifically within the GCs in the previous research leading to their conclusion that $T_{FH}$ are enriched in FL compared to reactive LNs (Ame-Thomas, Le Priol et al. 2012). Conversely, one of the novel findings of our research, only possible due to the techniques used, was the findings that there was no significant difference in the proportion of $T_{FH}$ within FL follicles and reactive GCs. This suggests that this important feature of normal GCs is recapitulated in the follicles of the FL microenvironment.

Thus, our findings add to previous research into $T_{FH}$ in both FL and GCs. We confirm their presence and phenotype which is broadly in keeping with the studies performed by flow cytometry yet we add to these findings by being able to describe their distribution with regard to the follicles and, as discussed below, their interactions with other cells.

### 4.2.1 Image analysis for identifying $T_{FH}$

Although our method of image analysis is robust and has many advantages over traditional IHC image analysis, there were disadvantages to it too.

We developed a technique that measured the total area of CD4 positivity and then calculated the proportion of this area that had co-expression of one or more antigens (e.g. PD1 and ICOS) as defined by the binary layers. Once the binary layers were established, this technique was fast and reliable and not subject to user bias or interference, but we were limited to describing the proportion of the CD4+ area that co-expressed other antigens rather than the absolute number of cells.

However, we validated this approach by demonstrating that results of the 'area' based analysis were not significantly different to a semi-automated, cell-based 'object' analysis. 'Object' analysis was a more operator-dependent, time consuming approach that was open to more user bias. One reason for the difficulty in using an automated 'object' based image analysis approach to define the number of CD4+ cells expressing different antigens is the membrane pattern of CD4 staining which makes it difficult to automatically count individual cells when packed closely together in a tissue section. This problem was not encountered when $Ki67^{pos}$ cells were counted as this is a nuclear stain and it is easier for the automated analysis software to count individual cells with a nuclear stain than when they are only defined by their membranes.

Developing the image analysis approach further to include a reliable measure of actual cell counts would be an important advance if this approach is to be used in larger cohorts of patients to investigate a prognostic tool.

## 4.3 Co-localisation between $Ki67^{pos}$ cells and $T_{FH}$ in GCs and FL

It is known that $T_{FH}$ are vital in providing B cell help in the GC reaction where they are implicated in promoting SHM, differentiation to memory or plasma cells, and B cell proliferation (Fazilleau, Mark et al. 2009). However there is a scarcity of published research detailing the phenotype and location of $T_{FH}$ in situ in normal human GCs.

Previous studies of $T_{FH}$ in FL have identified that they express high levels of IL-4 which may promote B cell survival through phosphorylation of STAT6. Furthermore, *in vitro* work has demonstrated that co-

culture of FL B cells with $T_{FH}$ cells rescued them from apoptosis (Pangault, Ame-Thomas et al. 2010, Ame-Thomas, Le Priol et al. 2012).

The interaction of $T_{FH}$ with tumour cells in situ has not previously been investigated.

In this work we identified that $T_{FH}$ and $Ki67^{pos}$ B cells have a similar pattern of distribution in FL and we demonstrated for the first time an extraordinarily close association between $Ki67^{pos}$ B cells and $T_{FH}$. We found that 40% of $Ki67^{pos}$ CD20+ B cells are in direct contact with one or more $T_{FH}$, and many more are in very close proximity to $T_{FH}$ although not in direct contact as calculated using our strict, automated image analysis algorithm. This suggests that the $T_{FH}$ may be directly providing a pro-tumour signal, perhaps inducing or supporting FL B cell proliferation.

Interestingly, we found that in cases with high proliferation (Ki67) there were more $T_{FH}$ with a strong correlation between the two, and proportionately more $T_{FH}$ were identified as histological grade increased. In addition, CD20+ FL B cells were significantly more likely to be in contact with $T_{FH}$ if $Ki67^{pos}$ than if $Ki67^{neg}$ in each case examined meaning that the co-localisation between $T_{FH}$ and proliferating FL B cells was unlikely to be due to chance. These findings are further evidence to support the theory that $T_{FH}$ are important in driving FL B cell proliferation.

We hypothesised that in higher grade FL (grade 3a / 3b), proliferation would be less dependent on T cell help, perhaps due to additional genetic events intrinsic to the tumour cells driving proliferation in more aggressive disease. Interestingly however, we identified that the close spatial association between $Ki67^{pos}$ cells and $T_{FH}$ was present in grade 3a and 3b FL as well as in grade 1-2 disease. The degree of co-localisation between $T_{FH}$ and $Ki67^{pos}$ B cells remained relatively constant as grade and Ki67 increased suggesting that support from the microenvironment in the form of $T_{FH}$ help remains important even in more histologically aggressive disease.

Importantly, we also assessed co-localisation between $T_{FH}$ and $Ki67^{pos}$ B cells in GCs and this work represents one of the most detailed assessments of such co-localisation in GCs to date. In GCs a

marked difference between the light and dark zones was observed. In the dark zones, where proliferation is very high, there were few $T_{FH}$ and little interaction or co-localisation was identified. However, in the light zones 63.1% of $Ki67^{pos}$ cells were in contact with $T_{FH}$. As in FL, there was a correlation between rate of proliferation and the number of $T_{FH}$. Similarly, CD20+ B cells were significantly more likely to be in contact with $T_{FH}$ if they were $Ki67^{pos}$. These findings support the theory that $T_{FH}$ are vital in the GC reaction and that GC size is determined by the availability of $T_{FH}$ help (Allen, Okada et al. 2007, Rolf, Bell et al. 2010).

If GC B cell proliferation is dependent on $T_{FH}$ help then it is interesting to consider why the spatial correlation is limited to the light zones where the rate of cellular proliferation is lower. There is now good evidence from multiphoton imaging in live animal models that GCs are dynamic environments with movement of B and T cells in and out of the GCs (Victora and Nussenzweig 2012). The images presented here are therefore a static representation of this highly dynamic process and it is possible that B cells receive their signal to start proliferating in the light zone under the influence of $T_{FH}$ help which is then $T_{FH}$ independent when the B cells migrate to the dark zone. This is highly speculative and is an area for possible further work especially since we have identified that proliferation – as indicated by Ki67 – is not limited to the dark zones.

Although there has been much work in recent years using very advanced imaging techniques to investigate the GC reaction (Victora and Nussenzweig 2012), to the best of our knowledge this is the first time that this close association between $T_{FH}$ and $Ki67^{pos}$ B cells has been demonstrated in GCs in human tissue.

The close association between CD20+ GC B cells and $T_{FH}$ in the light zones therefore represents a significant finding that supports previous work that suggests $T_{FH}$ are important in driving GC B cell proliferation and GC size.

### 4.3.1 Method of analysing co-localisation

Automated image analysis for assessing co-localisation was essential to the success of this part of the research. The nuclear pattern of Ki67 staining made it relatively easy to automatically identify $Ki67^{pos}$ cells and we developed a system that automatically calculated the number of $Ki67^{pos}$ cells that overlapped with $T_{FH}$ (defined in different experiments as either CD4+/$PD1^{Hi}$ or ICOS+/ $PD1^{Hi}$). The only situation in which this method was not successful was in the dark zones of GCs where there were too many tightly packed $Ki67^{pos}$ cells for the software to automatically detect individual cells.

Whilst quadruple labelling experiments allowed us to confirm that the $Ki67^{pos}$ cells were CD20+, the image analysis software was unable to define individual CD20+ cells due to the extraordinarily high number of tightly packed CD20+ cells in both FL follicles and GCs and the membrane pattern of CD20 staining. The assessment of whether CD20+ B cells were more likely to be in direct contact with $T_{FH}$ if $Ki67^{pos}$ than if $Ki67^{neg}$ was hampered by this difficulty and we had to resort to manual, visual assessment of this according to a strict method and using 2 investigators blinded to each other's results to reduce the influence of operator bias in this analysis.

### 4.3.2 Co-localisation between $Ki67^{pos}$ B cells and $T_{FH}$: interpretations and drawbacks

These findings highlight that the number of $T_{FH}$ and the availability of $T_{FH}$ help to FL B cells may be critical in determining the rate of B cell proliferation in FL as they are in the normal GC reaction.

Further work is necessary to investigate this important observation in greater detail as it is conceivable that accurately assessing the number if $T_{FH}$ in FL may have prognostic importance and interrupting the interaction between these cells may be a viable therapeutic target.

The nature of our research was observational and, whilst one of the strengths is that this is the first time that these interactions have been visualised in situ in human tissue, one of the drawbacks is that we can't be sure that $T_{FH}$ are really driving B cell proliferation. An alternative interpretation of these findings could be that the number of $T_{FH}$ is determined by the rate of proliferation and that $T_{FH}$ are

attracted to proliferating B cells rather than that the rate of proliferation is determined by the availability of $T_{FH}$ help as we have hypothesised.

Given that other groups have reported pSTAT6 expression in FL B-cells following exposure to $T_{FH}$ derived IL-4, we performed some experiments to see if we could demonstrate pSTAT6 in FL B cells that were in close contact with $T_{FH}$ (Pangault, Ame-Thomas et al. 2010). Unfortunately the pSTAT6 antibodies available did not work well with the multiple labelling immunofluorescent method and we were unable to reliably identify $pSTAT6^{pos}$ cells – data not shown.

An investigation into the feasibility of performing co-culture studies to research the impact of $T_{FH}$ on B cell proliferation and survival was beyond the scope of this research project, available funding, and patient material. However, the results of the work presented in this thesis have led to the generation of grant income for a subsequent student to perform these further studies.

## 4.4 Clinical correlations

We did not investigate associations between clinical features or outcome and either the proportion of $T_{FH}$ or the degree of co-localisation as the small number of patients included in this study and the heterogeneous nature of the cohort meant that it was beyond the scope of the current research.

## 4.5 Demonstration of synapse formation between $T_{FH}$ and $Ki67^{pos}$ FL B cells

It has been previously reported that tumour infiltrating T cells in FL form impaired synapses with FL B cells compared to healthy B cells and that PD1+ T cells in FL are globally dysfunctional with impaired response to cytokines (Ramsay, Clear et al. 2009, Myklebust, Irish et al. 2013).

Given the close proximity between $T_{FH}$ and proliferating FL B cells and the correlation between them that we revealed, we investigated if we could identify evidence of synapse formation between these cells in FFPE tissue.

We attempted to identify molecular components of the cSMAC or pSMAC that constitute the immunological synapse (PKC-θ, f-actin and LFA-1) but this proved technically difficult and staining was not of sufficiently good enough standard to enable analysis - data not shown. We did however identify morphological features that strongly suggest the formation of immune synapses between $T_{FH}$ and proliferating B cells in FL.

Morphological findings included overlapping of B- and T cell membranes, distortion of the T cell nuclei away from the point of cell contact and the presence of T cell 'processes' that encompass $Ki67^{pos}$ B cells. Furthermore, we developed and employed a highly innovative method of formally quantifying cell surface expression of CD4, PD1 and ICOS. This demonstrated significantly higher levels of expression at the pole of cell contact than at the opposite pole which strongly suggests polarisation of the membrane and synapse formation.

It is intriguing to consider why our results should be discrepant with previous reports of impaired synapse formation (Ramsay, Clear et al. 2009, Myklebust, Irish et al. 2013). One explanation is that, as demonstrated in our work there are likely to be at least 2 subsets of CD4+ PD1+ cells; CD4+/PD1+/ICOS+ $T_{FH}$ cells and CD4+/PD1+/ICOS- cells, the latter of which may perhaps represent dysfunctional or exhausted T cells, this is supported by the work of others (Ame-Thomas, Hoeller et al. 2015, Yang, Grote et al. 2015). It is possible that the $T_{FH}$ are able to form synapses with FL B cells and provide them with a survival or proliferative advantage, meanwhile, the exhausted T cells may be dysfunctional and unable to form normal synapses.

Another explanation is that the previous work describing impaired synapses was performed in an artificial experimental model that bears little resemblance to the human physiological state. One of the advantages of our research is that it was performed in situ on human tissue. The results can't therefore be ignored and the dogma that T cells in the lymphoma microenvironment form impaired synapses should be challenged. This contradictory finding serves to highlight the complexity of the FL microenvironment.

Unfortunately, one of the disadvantages of the work presented in this thesis is that we were unable to undertake the same quantitative analysis of synapse formation in normal GCs due to technical difficulties as described in the results section 3.5. Despite being unable to perform quantitative assessments in GCs, very similar morphological features suggesting immune synapse formation were identified in GCs.

## 4.6 Expression of AID in $Ki67^{pos}$ B cells in contact with $T_{FH}$

It is known that AID is important in the pathogenesis of the GC derived lymphomas including FL and has also been implicated in histological transformation. The mechanism by which AID plays a role in lymphomagenesis is thought to be through inducing the accumulation of additional mutations as B cells - that are resistant to apoptosis due to the t(14;18) translocation - undergo repeated GC reactions during which they are exposed to the DNA modifying enzyme AID (Pasqualucci, Bhagat et al. 2008, Roulland, Sungalee et al. 2013, Pasqualucci, Khiabanian et al. 2014).

In this research we demonstrated that AID is expressed predominantly in proliferating B cells in FL and for the first time that these cells are often found to be in close contact with $PD1^{Hi}$ T cells. Limitations of our antibody panels meant that we were unable to confirm that the $PD1^{Hi}$ T cells in contact with $AID^{pos}$ $Ki67^{pos}$ were $T_{FH}$ in the same sections but earlier results suggest that these are very likely to be $T_{FH}$.

Although this aspect of the work is limited by low numbers of specimens assessed with this combination of antibodies, the spatial relationship between $AID^{pos}$ $Ki67^{pos}$ B cells and $T_{FH}$ in FL is striking and suggests that $T_{FH}$ may induce AID expression in FL B cells as they are proposed to do in normal GC B cells where it is essential for CSR and SHM.

It can therefore be hypothesised that interaction between $T_{FH}$ cells and B cells is important in the pathogenesis of FL by inducing the expression of the DNA modifying enzyme AID, off-target action of

which may contribute to the accumulation of additional mutations necessary for the disease to develop, progress and undergo histological transformation.

## 4.7 FOXP3$^{pos}$ T cells in FL and GCs

The primary focus of our research was to describe the phenotype, distribution and possible roles of $T_{FH}$ in FL. As part of the work to define the phenotype of these cells it was necessary to demonstrate that the cells that we identified as $T_{FH}$ did not express FOXP3, the transcription factor associated with $T_{regs}$. Additionally, since FOXP3+ $T_{FR}$ cells with an immunophenotype between that of $T_{FH}$ and $T_{regs}$ have been described in FL, it was important to ascertain if we could identify these cells using the techniques we developed (Linterman, Pierson et al. 2011, Ame-Thomas, Le Priol et al. 2012).

Whereas $T_{FH}$ distribution was very similar between GCs and FL – with the exception that there was zonal demarcation between the dark and light zones in GCs – it was found that FOXP3$^{pos}$ T cell distribution was quite different between FL and normal LNs. In FL, FOXP3$^{pos}$ T cells were found within the follicles predominantly in a perifollicular distribution similar to $T_{FH}$, in reactive LNs meanwhile, there was a striking absence of FOXP3$^{pos}$ cells from the GCs with the FOXP3$^{pos}$ T cells instead located mainly in the interfollicular areas.

In FL, although a high proportion of FOXP3$^{pos}$ T cells were positive for ICOS (25%), triple positive PD1$^{Hi}$, ICOS+, FOXP3$^{pos}$ that may represent $T_{FR}$ were rare (5% of all CD4+ T cells). This confirms that most PD1$^{Hi}$ ICOS+ CD4+ T cells are indeed $T_{FH}$ and that there is a small population of $T_{FR}$ in the FL microenvironment, additional antibodies including anti-CD25 would need to be used to further characterise and quantify these cells.

Intriguingly, in the few samples stained with this combination of antibodies (n=3), it was noted that FOXP3$^{pos}$ cells were sometimes located in close proximity to PD1$^{Hi}$ ICOS+ T cells, i.e. in close proximity to $T_{FH}$. Additionally, 2 sections were stained with the FOXP3, Ki67, PD1 combination and some FOXP3$^{pos}$ cells were noted to be in contact with Ki67$^{pos}$ cells. We were unable to investigate these interesting

findings further but given that $T_{FR}$ cells are reported to regulate $T_{FH}$ function, this is an area that requires further study in this disease as well as in other diseases where both $T_{FH}$ and $T_{FR}$ are present.

Others have proposed that it is the balance of different cells in the tumour microenvironment that may impart prognostic significance (Ame-Thomas and Tarte 2014). It is possible that the balance between $T_{FH}$ and $T_{FR}$, or the spatial relationships between these CD4+ T cells subsets with regards to each other and in relation to tumour cells is important. This area requires more study and the techniques that we have described herein are ideally suited to taking this forward.

## 4.8 PD-L1 expression

Reliable IHC staining for the main ligand of PD1, PD-L1 has been difficult to achieve with reports of variable staining in the literature (Hawkes, Grigg et al. 2015, Gibney, Weiner et al. 2016). We sourced an anti-PD-L1 antibody that worked reliably with our immunofluorescent technique. Despite PD1 being expressed highly on the surface of $T_{FH}$ cells in direct contact with tumour cells and evidence of concentration of this protein at points of cell contact, we were unable to identify high levels of PD-L1 expression on the surface of the $Ki67^{pos}$ tumour cells that were in contact with $T_{FH}$.

This is in keeping with the findings of others who have not identified PD-L1 expression on FL tumour cells unlike in Hodgkin Lymphoma, some subtypes of DLBCL and other EBV-driven lymphoproliferative disorders, especially those with the 9p24 mutation, which have high PD-L1 expression on the tumour cells (Green, Rodig et al. 2012, Hawkes, Grigg et al. 2015).

In diseases in which PD-L1 is upregulated on the tumour cells, this is proposed to be a mechanism by which the tumour can subvert its microenvironment into suppressing the anti-tumour immune response so conferring a survival advantage for the tumour cells (Hawkes, Grigg et al. 2015). In FL however, PD1 is expressed highly on $T_{FH}$ as demonstrated in this research. We do not fully understand the role of PD1 expression in normal $T_{FH}$ cells at present but it has been speculated that it's role is to regulate the number of $T_{FH}$ as, in the absence of PD1 expression, $T_{FH}$ cells could potentially proliferate

uncontrollably on stimulation which could lead to an exaggerated immune response (Crotty 2014). Additionally, there are other ligands for PD1 including PD-L2 and, theoretically at least, there may be others that are not yet identified to which PD1 may bind.

Thus PD-L1 may not have been identified on the proliferating cells for a number of reasons: it may genuinely not be present, there may be an alternative ligand to PD1 on the proliferating cells, or the assay may have been insufficiently sensitive to detect PD-L1 at low levels by the immunofluorescent technique.

Recognising that PD1 is highly expressed on $T_{FH}$ in FL and that PD-L1 is not present on the malignant cells with which the $T_{FH}$ are interacting are important observations as we enter the era of immune checkpoint inhibition with drugs that block the PD1 PD-L1 axis.

Whilst blocking PD1 on exhausted tumour infiltrating T cells may reduce or reverse tumour-mediated immune suppression, we also need to consider the effect of PD1 blockade on $PD1^{Hi}$ tumour infiltrating $T_{FH}$. There is a lack of experimental data to describe what happens to the number of $T_{FH}$ when PD1 is blocked. If, as described above, PD1 expression by $T_{FH}$ reduces their proliferation, blockade of PD1 may lead to a rise in $T_{FH}$ number in FL which may in turn lead to tumour flare if, as postulated in this research, they provide the tumour cells with a proliferative advantage. The techniques described in this thesis would be a valuable tool to investigate this.

This hypothesis (that PD1 inhibition may in some instances lead to tumour progression through expansion of $T_{FH}$ number) is not supported by the provisional early phase clinical trial data that demonstrated some evidence of activity of PD1 inhibition in FL (Westin, Chu et al. 2014). Correlative studies using biopsies pre- and during treatment will be essential to answer this question. Intriguingly, new data on the drug Pidilizumab now suggests that it does not in fact act by blocking PD1, and development of this drug is on hold while its mechanism of action is further defined, there is therefore very little clinical data on the use of PD1 inhibition in FL. Furthermore, given the lack of PD-L1

expression on the tumour cells, it is uncertain whether PD-L1 inhibition – which has been demonstrated to be a useful therapeutic approach in some solid organ malignancies and in Hodgkin Lymphoma (Hawkes, Grigg et al. 2015, Ansell 2016) - will be beneficial in FL although it should be noted that PD-L1 expression does not always correlate with the clinical efficacy of these drugs (Gibney, Weiner et al. 2016).

## 4.9 The T cell receptor repertoire in FL

We have demonstrated that the TCR repertoire of T-cells within the follicles of FL is significantly more restricted than that of interfollicular T-cells and that, as expected from their different phenotypes, there is little repertoire overlap between these two compartments. These findings suggest that, within the neoplastic FL follicles there is an antigen-driven oligoclonal expansion of T-cells. There is no published literature on the TCR repertoire in FL, however, restricted repertoires have been reported in colonic cancer where little overlap between normal and neoplastic tissue was identified (Sherwood, Emerson et al. 2013).

This part of the work suffered from technical challenges that firstly had to be overcome. The main challenge was in capturing adequate amounts of tissue using the laser capture microscope. As a result of the difficulties experienced with this we had to adapt our research questions and techniques. It would have been informative to compare the TCR repertoire of two distinct follicles within the same LNs for example but it wasn't possible to extract sufficient DNA from individual follicles to do this. Furthermore, we captured areas of tissue containing many different subtypes of T cells rather than selecting only $T_{FH}$. This was a limitation of the technique that we used but it would be possible to form cell suspensions from fresh LN biopsies or FNAs and perform cell sorting to investigate the TCR repertoire of the $T_{FH}$ only. If we used this technique however, it would be difficult to investigate differences in clonality between follicles unless a patient had more than one lesion amenable to biopsy at the same time.

Another limitation of the TCR repertoire studies is that, although we compared similar areas of tissue in each comparison, the number of T cells, and in particular the number of $T_{FH}$ will have varied between samples. This was accounted for in the calculations used to determine clonality and although cell numbers analyzed differed between samples, the fact that follicles contained consistently fewer, larger clones and inter-follicular areas contained a larger number of smaller clones suggests that these differences were real.

PCR-based analysis of TCR repertoire also suffers from the limitation that errors introduced during amplification may lead to apparent skewing of the repertoire (Best, Oakes et al. 2015). Whilst it is not possible to completely exclude this possibility, we minimized the risk by direct, intra-patient comparison in the same assay runs, and our findings were consistent in all cases studied.

This is the first time that the TCR repertoire of T cells infiltrating the FL microenvironment has been studied and as such represents preliminary evidence that there is an antigen-driven T-cell response in FL. This is a novel finding that poses many questions about the pathogenesis of the disease. Further research into the TCR repertoire of FL is warranted as described below in section 4.11.

## 4.10 Final summary and implications

In summary, we used multicolour confocal immunofluorescent microscopy to define CD4+ T cell subsets in the FL microenvironment and made comparisons with GCs in reactive lymph nodes.

$T_{FH}$ cells were present in equal proportions in the follicles of FL as in GCs and were tightly restricted to the follicles and GCs. There was marked zonal demarcation in GCs with the $T_{FH}$ cells mostly present in the light zones, in FL follicles however this zonal demarcation was lost.

We identified a remarkable co-localisation between $T_{FH}$ and $Ki67^{pos}$ B cells in both the follicles of FL and light zones of GCs. The observation that CD20+ B cells were significantly more likely to be in contact with a $T_{FH}$ if $Ki67^{pos}$ means that this co-localisation is unlikely to be due to chance, and together with the evidence that the number of $T_{FH}$ is correlated with Ki67 in both FL and GCs, suggests that $T_{FH}$ have a pivotal role in supporting B cell proliferation in both situations. In addition, we identified that $T_{FH}$ are co-localised with $AID^{pos}$ B cells in FL suggesting that they may also contribute to lymphomagenesis through the induction of AID which may lead to the acquisition of additional mutations. Finally, we revealed for the first time provisional evidence of antigen restriction amongst the tumour infiltrating T cells.

The results of this research come at an important time. There is much interest in immune checkpoints and their inhibition in the treatment of solid organ malignancies and lymphomas. Our findings highlight the complexity of PD1 expression in FL. To understand how best to use new treatments that block PD1 in FL, a greater understanding of which cells express it and its ligands is required This research goes some way to understanding why PD1 inhibition in FL may be more complex than in other malignancies.

There is an unmet need for novel biomarkers in FL to allow us to better predict outcome and to identify which patients stand to benefit most from particular therapeutic strategies. Whilst we have not identified a prognostic biomarker in the research performed to date, we have developed a technique

that may be used to do so in future studies. Given their apparent importance in FL as in GCs, accurate quantification of $T_{FH}$, their location and proportion relative to other T cell subsets (e.g. $T_{FR}$) may have prognostic value and interrupting the interaction between $T_{FH}$ and FL B cells may be a useful therapeutic target. Further investigation of these areas is warranted.

## 4.11 Areas for future work

Building on the work presented in this thesis, suggested areas for future work include the following:

- Conduct similar work on a larger cohort of patients treated homogeneously in a clinical trial and develop the image analysis protocol to calculate actual cell counts (rather than proportions) and compare numbers of $T_{FH}$ with $T_{regs}$ in the same specimens to ascertain if this has prognostic significance.
    - This could be performed on samples from patients enrolled in the UK 'Watch and Wait' trial in which patients were randomised to rituximab only or observation.
    - It would be informative to investigate differences in composition of the CD4+ compartment of patients in the observation arm who never required treatment compared to patients who progressed rapidly.
- Further analyse interaction of $FOXP3^{pos}$ T cells with $T_{FH}$ and with proliferating B cells in FFPE tissue using the techniques described in this thesis.
- In trials of PD1 / PD-L1 inhibitors, utilise the experimental approach detailed in this thesis to investigate pre- and post- (or during) therapy co-localisation of PD1+ cells to malignant cells and ascertain if $T_{FH}$ number changes while on PD1 inhibitor therapy
    - These experiments will be necessary to determine which patients stand to benefit most from immune checkpoint inhibition
    - This is important given the theoretical possibility of causing an expansion in $T_{FH}$ number through PD1 inhibition which could in turn lead to tumour flare in some cases.
- It would be very informative to validate the findings presented in this thesis by investigating in in vitro co-culture systems whether rate of FL B cell proliferation is determined by the presence of $T_{FH}$.
- Investigate the TCR repertoires in greater depth. Future research questions in this area include:

- Is the TCR repertoire of GCs more restricted than that of the inter-follicular area of reactive LNs as we found in FL?
- Compare the TCR repertoire of PB with that of the follicular and interfollicular areas in FL.
- Identify patients who have had multiple biopsies during the course of their disease and investigate if the TCR repertoire changes over time. Make simultaneous comparisons with peripheral blood TCR repertoire.
- Future work could also make use of fine needle aspirates or fresh disaggregated lymph nodes which would permit the sorting of cells according to phenotype and may permit specific assessment of the TCR repertoire of $T_{FH}$ cells to determine if it is these cells that are most restricted.

## References


Advani, R. H., J. J. Buggy, J. P. Sharman, S. M. Smith, T. E. Boyd, B. Grant, K. S. Kolibaba, R. R. Furman, S. Rodriguez, B. Y. Chang, J. Sukbuntherng, R. Izumi, A. Hamdy, E. Hedrick and N. H. Fowler (2013). "Bruton tyrosine kinase inhibitor ibrutinib (PCI-32765) has significant activity in patients with relapsed/refractory B-cell malignancies." J Clin Oncol **31**(1): 88-94.

Ahearne, M. J., R. L. Allchin, C. P. Fox and S. D. Wagner (2014). "Follicular helper T-cells: expanding roles in T-cell lymphoma and targets for treatment." Br J Haematol **166**(3): 326-335.

Ai, W. Z., J. Z. Hou, R. Zeiser, D. Czerwinski, R. S. Negrin and R. Levy (2009). "Follicular lymphoma B cells induce the conversion of conventional CD4+ T cells to T-regulatory cells." Int J Cancer **124**(1): 239-244.

Allen, C. D., T. Okada and J. G. Cyster (2007). "Germinal-center organization and cellular dynamics." Immunity **27**(2): 190-202.

Allen, R. C., R. J. Armitage, M. E. Conley, H. Rosenblatt, N. A. Jenkins, N. G. Copeland, M. A. Bedell, S. Edelhoff, C. M. Disteche, D. K. Simoneaux and et al. (1993). "CD40 ligand gene defects responsible for X-linked hyper-IgM syndrome." Science **259**(5097): 990-993.

Alvaro, T., M. Lejeune, M. T. Salvado, C. Lopez, J. Jaen, R. Bosch and L. E. Pons (2006). "Immunohistochemical patterns of reactive microenvironment are associated with clinicobiologic behavior in follicular lymphoma patients." J Clin Oncol **24**(34): 5350-5357.

Ame-Thomas, P., S. Hoeller, C. Artchounin, J. Misiak, M. S. Braza, R. Jean, J. Le Priol, C. Monvoisin, N. Martin, P. Gaulard and K. Tarte (2015). "CD10 delineates a subset of human IL-4 producing follicular helper T cells involved in the survival of follicular lymphoma B cells." Blood **125**(15): 2381-2385.

Ame-Thomas, P., J. Le Priol, H. Yssel, G. Caron, C. Pangault, R. Jean, N. Martin, T. Marafioti, P. Gaulard, T. Lamy, T. Fest, G. Semana and K. Tarte (2012). "Characterization of intratumoral follicular helper T cells in follicular lymphoma: role in the survival of malignant B cells." Leukemia **26**(5): 1053-1063.

Ame-Thomas, P. and K. Tarte (2014). "The yin and the yang of follicular lymphoma cell niches: role of microenvironment heterogeneity and plasticity." Semin Cancer Biol **24**: 23-32.

Andorsky, D. J., R. E. Yamada, J. Said, G. S. Pinkus, D. J. Betting and J. M. Timmerman (2011). "Programmed death ligand 1 is expressed by non-hodgkin lymphomas and inhibits the activity of tumor-associated T cells." Clin Cancer Res **17**(13): 4232-4244.

Ansell, S. M. (2016). "Where Do Programmed Death-1 Inhibitors Fit in the Management of Malignant Lymphoma?" J Oncol Pract **12**(2): 101-106.

Ansell, S. M., A. M. Lesokhin, I. Borrello, A. Halwani, E. C. Scott, M. Gutierrez, S. J. Schuster, M. M. Millenson, D. Cattry, G. J. Freeman, S. J. Rodig, B. Chapuy, A. H. Ligon, L. Zhu, J. F. Grosso, S. Y. Kim, J. M. Timmerman, M. A. Shipp and P. Armand (2015). "PD-1 blockade with nivolumab in relapsed or refractory Hodgkin's lymphoma." N Engl J Med **372**(4): 311-319.

Ardeshna, K. M., W. Qian, P. Smith, N. Braganca, L. Lowry, P. Patrick, J. Warden, L. Stevens, C. F. E. Pocock, F. Miall, D. Cunningham, J. Davies, A. Jack, R. Stephens, J. Walewski, B. Ferhanoglu, K. Bradstock and D. C. Linch (2014). "Rituximab versus a watch-and-wait approach in patients with

advanced-stage, asymptomatic, non-bulky follicular lymphoma: an open-label randomised phase 3 trial." The Lancet Oncology **15**(4): 424-435.

Ardeshna, K. M., P. Smith, A. Norton, B. W. Hancock, P. J. Hoskin, K. A. MacLennan, R. E. Marcus, A. Jelliffe, G. Vaughan, Hudson and D. C. Linch (2003). "Long-term effect of a watch and wait policy versus immediate systemic treatment for asymptomatic advanced-stage non-Hodgkin lymphoma: a randomised controlled trial." Lancet **362**(9383): 516-522.

Armand, P., A. Nagler, E. A. Weller, S. M. Devine, D. E. Avigan, Y. B. Chen, M. S. Kaminski, H. K. Holland, J. N. Winter, J. R. Mason, J. W. Fay, D. A. Rizzieri, C. M. Hosing, E. D. Ball, J. P. Uberti, H. M. Lazarus, M. Y. Mapara, S. A. Gregory, J. M. Timmerman, D. Andorsky, R. Or, E. K. Waller, R. Rotem-Yehudar and L. I. Gordon (2013). "Disabling immune tolerance by programmed death-1 blockade with pidilizumab after autologous hematopoietic stem-cell transplantation for diffuse large B-cell lymphoma: results of an international phase II trial." J Clin Oncol **31**(33): 4199-4206.

Bachy, E., P. Brice, R. Delarue, N. Brousse, C. Haioun, S. Le Gouill, A. Delmer, D. Bordessoule, H. Tilly, B. Corront, C. Allard, C. Foussard, A. Bosly, B. Coiffier, C. Gisselbrecht, P. Solal-Celigny and G. Salles (2010). "Long-term follow-up of patients with newly diagnosed follicular lymphoma in the prerituximab era: effect of response quality on survival--A study from the groupe d'etude des lymphomes de l'adulte." J Clin Oncol **28**(5): 822-829.

Baldo, P., M. Rupolo, A. Compagnoni, R. Lazzarini, A. Bearz, R. Cannizzaro, S. Spazzapan, I. Truccolo and L. Moja (2010). "Interferon-alpha for maintenance of follicular lymphoma." Cochrane Database Syst Rev(1): CD004629.

Barber, D. L., E. J. Wherry, D. Masopust, B. Zhu, J. P. Allison, A. H. Sharpe, G. J. Freeman and R. Ahmed (2006). "Restoring function in exhausted CD8 T cells during chronic viral infection." Nature **439**(7077): 682-687.

Barcia, C., C. E. Thomas, J. F. Curtin, G. D. King, K. Wawrowsky, M. Candolfi, W. D. Xiong, C. Liu, K. Kroeger, O. Boyer, J. Kupiec-Weglinski, D. Klatzmann, M. G. Castro and P. R. Lowenstein (2006). "In vivo mature immunological synapses forming SMACs mediate clearance of virally infected astrocytes from the brain." J Exp Med **203**(9): 2095-2107.

Berger, R., R. Rotem-Yehudar, G. Slama, S. Landes, A. Kneller, M. Leiba, M. Koren-Michowitz, A. Shimoni and A. Nagler (2008). "Phase I safety and pharmacokinetic study of CT-011, a humanized antibody interacting with PD-1, in patients with advanced hematologic malignancies." Clin Cancer Res **14**(10): 3044-3051.

Best, K., T. Oakes, J. M. Heather, J. Shawe-Taylor and B. Chain (2015). "Computational analysis of stochastic heterogeneity in PCR amplification efficiency revealed by single molecule barcoding." Sci Rep **5**: 14629.

Bindea, G., B. Mlecnik, M. Tosolini, A. Kirilovsky, M. Waldner, A. C. Obenauf, H. Angell, T. Fredriksen, L. Lafontaine, A. Berger, P. Bruneval, W. H. Fridman, C. Becker, F. Pages, M. R. Speicher, Z. Trajanoski and J. Galon (2013). "Spatiotemporal dynamics of intratumoral immune cells reveal the immune landscape in human cancer." Immunity **39**(4): 782-795.

Blank, C., T. F. Gajewski and A. Mackensen (2005). "Interaction of PD-L1 on tumor cells with PD-1 on tumor-specific T cells as a mechanism of immune evasion: implications for tumor immunotherapy." Cancer Immunol Immunother **54**(4): 307-314.

Byers, R. J., E. Sakhinia, P. Joseph, C. Glennie, J. A. Hoyland, L. P. Menasce, J. A. Radford and T. Illidge (2008). "Clinical quantitation of immune signature in follicular lymphoma by RT-PCR-based gene expression profiling." Blood **111**(9): 4764-4770.

Campbell, B. A., N. Voss, R. Woods, R. D. Gascoyne, J. Morris, T. Pickles, J. M. Connors and K. J. Savage (2010). "Long-term outcomes for patients with limited stage follicular lymphoma: involved regional radiotherapy versus involved node radiotherapy." Cancer **116**(16): 3797-3806.

Canioni, D., G. Salles, N. Mounier, N. Brousse, M. Keuppens, F. Morchhauser, T. Lamy, A. Sonet, M. C. Rousselet, C. Foussard and L. Xerri (2008). "High numbers of tumor-associated macrophages have an adverse prognostic value that can be circumvented by rituximab in patients with follicular lymphoma enrolled onto the GELA-GOELAMS FL-2000 trial." J Clin Oncol **26**(3): 440-446.

Carbone, A., A. Gloghini, A. Cabras and G. Elia (2009). "The Germinal centre-derived lymphomas seen through their cellular microenvironment." Br J Haematol **145**(4): 468-480.

Carlotti, E., D. Wrench, J. Matthews, S. Iqbal, A. Davies, A. Norton, J. Hart, R. Lai, S. Montoto, J. G. Gribben, T. A. Lister and J. Fitzgibbon (2009). "Transformation of follicular lymphoma to diffuse large B-cell lymphoma may occur by divergent evolution from a common progenitor cell or by direct evolution from the follicular lymphoma clone." Blood **113**(15): 3553-3557.

Carreras, J., A. Lopez-Guillermo, G. Roncador, N. Villamor, L. Colomo, A. Martinez, R. Hamoudi, W. J. Howat, E. Montserrat and E. Campo (2009). "High numbers of tumor-infiltrating programmed cell death 1-positive regulatory lymphocytes are associated with improved overall survival in follicular lymphoma." J Clin Oncol **27**(9): 1470-1476.

Cartron, G., S. de Guibert, M. S. Dilhuydy, F. Morschhauser, V. Leblond, J. Dupuis, B. Mahe, R. Bouabdallah, G. Lei, M. Wenger, E. Wassner-Fritsch and M. Hallek (2014). "Obinutuzumab (GA101) in relapsed/refractory chronic lymphocytic leukemia: final data from the phase 1/2 GAUGUIN study." Blood.

Chen, B. J., B. Chapuy, J. Ouyang, H. H. Sun, M. G. Roemer, M. L. Xu, H. Yu, C. D. Fletcher, G. J. Freeman, M. A. Shipp and S. J. Rodig (2013). "PD-L1 expression is characteristic of a subset of aggressive B-cell lymphomas and virus-associated malignancies." Clin Cancer Res **19**(13): 3462-3473.

Coelho, V., S. Krysov, A. M. Ghaemmaghami, M. Emara, K. N. Potter, P. Johnson, G. Packham, L. Martinez-Pomares and F. K. Stevenson (2010). "Glycosylation of surface Ig creates a functional bridge between human follicular lymphoma and microenvironmental lectins." Proc Natl Acad Sci U S A **107**(43): 18587-18592.

Colombat, P., G. Salles, N. Brousse, P. Eftekhari, P. Soubeyran, V. Delwail, E. Deconinck, C. Haioun, C. Foussard, C. Sebban, A. Stamatoullas, N. Milpied, F. Boue, B. Taillan, P. Lederlin, A. Najman, C. Thieblemont, F. Montestruc, A. Mathieu-Boue, A. Benzohra and P. Solal-Celigny (2001). "Rituximab (anti-CD20 monoclonal antibody) as single first-line therapy for patients with follicular lymphoma with a low tumor burden: clinical and molecular evaluation." Blood **97**(1): 101-106.

Conchello, J. A. and J. W. Lichtman (2005). "Optical sectioning microscopy." Nat Methods **2**(12): 920-931.

Craig, M., W. T. Hanna, F. Cabanillas, C. S. Chen, D. L. Esseltine, R. Neuwirth and O. A. O'Connor (2014). "Phase II study of bortezomib in combination with rituximab, cyclophosphamide and prednisone with or without doxorubicin followed by rituximab maintenance in patients with relapsed or refractory follicular lymphoma." Br J Haematol **166**(6): 920-928.

Crotty, S. (2014). "T follicular helper cell differentiation, function, and roles in disease." Immunity **41**(4): 529-542.

Czuczman, M. S., L. Fayad, V. Delwail, G. Cartron, E. Jacobsen, K. Kuliczkowski, B. K. Link, L. Pinter-Brown, J. Radford, A. Hellmann, E. Gallop-Evans, C. G. DiRienzo, N. Goldstein, I. Gupta, R. C. Jewell, T. S. Lin, S. Lisby, M. Schultz, C. A. Russell and A. Hagenbeek (2012). "Ofatumumab monotherapy in rituximab-refractory follicular lymphoma: results from a multicenter study." Blood **119**(16): 3698-3704.

Czuczman, M. S., G. Hess, O. V. Gadeberg, L. M. Pedersen, N. Goldstein, I. Gupta, R. C. Jewell, T. S. Lin, S. Lisby, C. Strange, K. Windfeld and A. Viardot (2012). "Chemoimmunotherapy with ofatumumab in combination with CHOP in previously untreated follicular lymphoma." Br J Haematol **157**(4): 438-445.

Dave, S. S., G. Wright, B. Tan, A. Rosenwald, R. D. Gascoyne, W. C. Chan, R. I. Fisher, R. M. Braziel, L. M. Rimsza, T. M. Grogan, T. P. Miller, M. LeBlanc, T. C. Greiner, D. D. Weisenburger, J. C. Lynch, J. Vose, J. O. Armitage, E. B. Smeland, S. Kvaloy, H. Holte, J. Delabie, J. M. Connors, P. M. Lansdorp, Q. Ouyang, T. A. Lister, A. J. Davies, A. J. Norton, H. K. Muller-Hermelink, G. Ott, E. Campo, E. Montserrat, W. H. Wilson, E. S. Jaffe, R. Simon, L. Yang, J. Powell, H. Zhao, N. Goldschmidt, M. Chiorazzi and L. M. Staudt (2004). "Prediction of survival in follicular lymphoma based on molecular features of tumor-infiltrating immune cells." N Engl J Med **351**(21): 2159-2169.

de Jong, D. and T. Fest (2011). "The microenvironment in follicular lymphoma." Best Pract Res Clin Haematol **24**(2): 135-146.

de Jong, D., A. Koster, A. Hagenbeek, J. Raemaekers, D. Veldhuizen, S. Heisterkamp, J. P. de Boer and M. van Glabbeke (2009). "Impact of the tumor microenvironment on prognosis in follicular lymphoma is dependent on specific treatment protocols." Haematologica **94**(1): 70-77.

Dustin, M. L. (2011). "Visualization of Cell-Cell Interaction Contacts: Synapses and Kinapses." Self Nonself **2**(2): 85-97.

Emerson, R. O., A. M. Sherwood, M. J. Rieder, J. Guenthoer, D. W. Williamson, C. S. Carlson, C. W. Drescher, M. Tewari, J. H. Bielas and H. S. Robins (2013). "High-throughput sequencing of T-cell receptors reveals a homogeneous repertoire of tumour-infiltrating lymphocytes in ovarian cancer." J Pathol **231**(4): 433-440.

Evens, A. M., M. R. Smith, I. S. Lossos, I. Helenowski, M. Millenson, J. N. Winter, S. T. Rosen and L. I. Gordon (2014). "Frontline bortezomib and rituximab for the treatment of newly diagnosed high tumour burden indolent non-Hodgkin lymphoma: a multicentre phase II study." Br J Haematol **166**(4): 514-520.

Eyre, T. A. and G. P. Collins (2015). "Immune checkpoint inhibition in lymphoid disease." Br J Haematol **170**(3): 291-304.

Farinha, P., A. Al-Tourah, K. Gill, R. Klasa, J. M. Connors and R. D. Gascoyne (2010). "The architectural pattern of FOXP3-positive T cells in follicular lymphoma is an independent predictor of survival and histologic transformation." Blood **115**(2): 289-295.

Farinha, P., H. Masoudi, B. F. Skinnider, K. Shumansky, J. J. Spinelli, K. Gill, R. Klasa, N. Voss, J. M. Connors and R. D. Gascoyne (2005). "Analysis of multiple biomarkers shows that lymphoma-associated macrophage (LAM) content is an independent predictor of survival in follicular lymphoma (FL)." Blood **106**(6): 2169-2174.

Fazilleau, N., L. Mark, L. J. McHeyzer-Williams and M. G. McHeyzer-Williams (2009). "Follicular helper T cells: lineage and location." Immunity **30**(3): 324-335.

Federico, M., M. Bellei, L. Marcheselli, S. Luminari, A. Lopez-Guillermo, U. Vitolo, B. Pro, S. Pileri, A. Pulsoni, P. Soubeyran, S. Cortelazzo, G. Martinelli, M. Martelli, L. Rigacci, L. Arcaini, F. Di Raimondo, F. Merli, E. Sabattini, P. McLaughlin and P. Solal-Celigny (2009). "Follicular lymphoma international prognostic index 2: a new prognostic index for follicular lymphoma developed by the international follicular lymphoma prognostic factor project." J Clin Oncol **27**(27): 4555-4562.

Federico, M., S. Luminari, A. Dondi, G. Rossi, C. Boccomini, F. di Raimondo, L. Rigacci, A. Carella, A. Pulsoni, F. Merli, L. Arcaini, L. Marcheselli, M. Brugiatelli and U. Vitolo (2011). "R-CVP vs R-CHOP vs R-FM for the initial treatment of patients with advanced stage follicular lymphoma. Preliminary results of FOLL05 IIL trial." Annals of Oncology **22**(Supplement 4): 135.

Ferrari, S., S. Giliani, A. Insalaco, A. Al-Ghonaium, A. R. Soresina, M. Loubser, M. A. Avanzini, M. Marconi, R. Badolato, A. G. Ugazio, Y. Levy, N. Catalan, A. Durandy, A. Tbakhi, L. D. Notarangelo and A. Plebani (2001). "Mutations of CD40 gene cause an autosomal recessive form of immunodeficiency with hyper IgM." Proc Natl Acad Sci U S A **98**(22): 12614-12619.

Fowler, N. and E. Davis (2013). "Targeting B-cell receptor signaling: changing the paradigm." Hematology Am Soc Hematol Educ Program **2013**: 553-560.

Gerdes, J., H. Lemke, H. Baisch, H. H. Wacker, U. Schwab and H. Stein (1984). "Cell cycle analysis of a cell proliferation-associated human nuclear antigen defined by the monoclonal antibody Ki-67." J Immunol **133**(4): 1710-1715.

Ghielmini, M., S. F. Schmitz, S. B. Cogliatti, G. Pichert, J. Hummerjohann, U. Waltzer, M. F. Fey, D. C. Betticher, G. Martinelli, F. Peccatori, U. Hess, E. Zucca, R. Stupp, T. Kovacsovics, C. Helg, A. Lohri, M. Bargetzi, D. Vorobiof and T. Cerny (2004). "Prolonged treatment with rituximab in patients with follicular lymphoma significantly increases event-free survival and response duration compared with the standard weekly x 4 schedule." Blood **103**(12): 4416-4423.

Gibney, G. T., L. M. Weiner and M. B. Atkins (2016). "Predictive biomarkers for checkpoint inhibitor-based immunotherapy." Lancet Oncol **17**(12): e542-e551.

Gigoux, M., J. Shang, Y. Pak, M. Xu, J. Choe, T. W. Mak and W. K. Suh (2009). "Inducible costimulator promotes helper T-cell differentiation through phosphoinositide 3-kinase." Proc Natl Acad Sci U S A **106**(48): 20371-20376.

Glas, A. M., L. Knoops, L. Delahaye, M. J. Kersten, R. E. Kibbelaar, L. A. Wessels, R. van Laar, J. H. van Krieken, J. W. Baars, J. Raemaekers, P. M. Kluin, L. J. van't Veer and D. de Jong (2007). "Gene-expression and immunohistochemical study of specific T-cell subsets and accessory cell types in the transformation and prognosis of follicular lymphoma." J Clin Oncol **25**(4): 390-398.

Good-Jacobson, K. L., C. G. Szumilas, L. Chen, A. H. Sharpe, M. M. Tomayko and M. J. Shlomchik (2010). "PD-1 regulates germinal center B cell survival and the formation and affinity of long-lived plasma cells." Nat Immunol **11**(6): 535-542.

Gopal, A. K., B. S. Kahl, S. de Vos, N. D. Wagner-Johnston, S. J. Schuster, W. J. Jurczak, I. W. Flinn, C. R. Flowers, P. Martin, A. Viardot, K. A. Blum, A. H. Goy, A. J. Davies, P. L. Zinzani, M. Dreyling, D. Johnson, L. L. Miller, L. Holes, D. Li, R. D. Dansey, W. R. Godfrey and G. A. Salles (2014). "PI3Kdelta inhibition by idelalisib in patients with relapsed indolent lymphoma." N Engl J Med **370**(11): 1008-1018.

Green, M. R., A. J. Gentles, R. V. Nair, J. M. Irish, S. Kihira, C. L. Liu, I. Kela, E. S. Hopmans, J. H. Myklebust, H. Ji, S. K. Plevritis, R. Levy and A. A. Alizadeh (2013). "Hierarchy in somatic mutations arising during genomic evolution and progression of follicular lymphoma." Blood **121**(9): 1604-1611.

Green, M. R., S. Monti, S. J. Rodig, P. Juszczynski, T. Currie, E. O'Donnell, B. Chapuy, K. Takeyama, D. Neuberg, T. R. Golub, J. L. Kutok and M. A. Shipp (2010). "Integrative analysis reveals selective 9p24.1 amplification, increased PD-1 ligand expression, and further induction via JAK2 in nodular sclerosing Hodgkin lymphoma and primary mediastinal large B-cell lymphoma." Blood **116**(17): 3268-3277.

Green, M. R., S. Rodig, P. Juszczynski, J. Ouyang, P. Sinha, E. O'Donnell, D. Neuberg and M. A. Shipp (2012). "Constitutive AP-1 activity and EBV infection induce PD-L1 in Hodgkin lymphomas and posttransplant lymphoproliferative disorders: implications for targeted therapy." Clin Cancer Res **18**(6): 1611-1618.

Gregoire, M., F. Guilloton, C. Pangault, F. Mourcin, P. Sok, M. Latour, P. Ame-Thomas, E. Flecher, T. Fest and K. Tarte (2015). "Neutrophils trigger a NF-kappaB dependent polarization of tumor-supportive stromal cells in germinal center B-cell lymphomas." Oncotarget **6**(18): 16471-16487.

Gu-Trantien, C., S. Loi, S. Garaud, C. Equeter, M. Libin, A. de Wind, M. Ravoet, H. Le Buanec, C. Sibille, G. Manfouo-Foutsop, I. Veys, B. Haibe-Kains, S. K. Singhal, S. Michiels, F. Rothe, R. Salgado, H. Duvillier, M. Ignatiadis, C. Desmedt, D. Bron, D. Larsimont, M. Piccart, C. Sotiriou and K. Willard-Gallo (2013). "CD4(+) follicular helper T cell infiltration predicts breast cancer survival." J Clin Invest **123**(7): 2873-2892.

Haematological Malignancy Research Network. (2014). "Incidence of follicular lymphoma." Retrieved 24/09/2014, 2014, from https://www.hmrn.org/statistics/incidence.

Hamid, O., C. Robert, A. Daud, F. S. Hodi, W. J. Hwu, R. Kefford, J. D. Wolchok, P. Hersey, R. W. Joseph, J. S. Weber, R. Dronca, T. C. Gangadhar, A. Patnaik, H. Zarour, A. M. Joshua, K. Gergich, J. Elassaiss-Schaap, A. Algazi, C. Mateus, P. Boasberg, P. C. Tumeh, B. Chmielowski, S. W. Ebbinghaus, X. N. Li, S. P. Kang and A. Ribas (2013). "Safety and tumor responses with lambrolizumab (anti-PD-1) in melanoma." N Engl J Med **369**(2): 134-144.

Hanahan, D. and L. M. Coussens (2012). "Accessories to the crime: functions of cells recruited to the tumor microenvironment." Cancer Cell **21**(3): 309-322.

Hanahan, D. and R. A. Weinberg (2011). "Hallmarks of cancer: the next generation." Cell **144**(5): 646-674.

Harris, N., S. Swerdlow, E. Jaffe, G. Ott, B. Nathwani, D. De Jong, T. Yoshino and D. Spagnolo (2008). WHO Classification of Tumours of Haematopoietic and Lymphoid Tissues, 4th edn. Lyon, International Agency for Research on Cancer.

Hawkes, E. A., A. Grigg and G. Chong (2015). "Programmed cell death-1 inhibition in lymphoma." Lancet Oncol **16**(5): e234-245.

Haynes, N. M., C. D. C. Allen, R. Lesley, K. M. Ansel, N. Killeen and J. G. Cyster (2007). "Role of CXCR5 and CCR7 in Follicular Th Cell Positioning and Appearance of a Programmed Cell Death Gene-1High Germinal Center-Associated Subpopulation." The Journal of Immunology **179**(8): 5099-5108.

Herold, M., A. Haas, S. Srock, S. Neser, K. H. Al-Ali, A. Neubauer, G. Dolken, R. Naumann, W. Knauf, M. Freund, R. Rohrberg, K. Hoffken, A. Franke, T. Ittel, E. Kettner, U. Haak, U. Mey, C. Klinkenstein, M. Assmann and U. von Grunhagen (2007). "Rituximab added to first-line mitoxantrone, chlorambucil,

and prednisolone chemotherapy followed by interferon maintenance prolongs survival in patients with advanced follicular lymphoma: an East German Study Group Hematology and Oncology Study." J Clin Oncol **25**(15): 1986-1992.

Hiddemann, W., M. Kneba, M. Dreyling, N. Schmitz, E. Lengfelder, R. Schmits, M. Reiser, B. Metzner, H. Harder, S. Hegewisch-Becker, T. Fischer, M. Kropff, H. E. Reis, M. Freund, B. Wormann, R. Fuchs, M. Planker, J. Schimke, H. Eimermacher, L. Trumper, A. Aldaoud, R. Parwaresch and M. Unterhalt (2005). "Frontline therapy with rituximab added to the combination of cyclophosphamide, doxorubicin, vincristine, and prednisone (CHOP) significantly improves the outcome for patients with advanced-stage follicular lymphoma compared with therapy with CHOP alone: results of a prospective randomized study of the German Low-Grade Lymphoma Study Group." Blood **106**(12): 3725-3732.

Hino, R., K. Kabashima, Y. Kato, H. Yagi, M. Nakamura, T. Honjo, T. Okazaki and Y. Tokura (2010). "Tumor cell expression of programmed cell death-1 ligand 1 is a prognostic factor for malignant melanoma." Cancer **116**(7): 1757-1766.

Hirt, C., K. Weitmann, F. Schuler, T. Kiefer, C. S. Rabkin, W. Hoffmann and G. Dolken (2013). "Circulating t(14;18)-positive cells in healthy individuals: association with age and sex but not with smoking." Leuk Lymphoma.

Hochster, H., E. Weller, R. D. Gascoyne, T. M. Habermann, L. I. Gordon, T. Ryan, L. Zhang, N. Colocci, S. Frankel and S. J. Horning (2009). "Maintenance rituximab after cyclophosphamide, vincristine, and prednisone prolongs progression-free survival in advanced indolent lymphoma: results of the randomized phase III ECOG1496 Study." J Clin Oncol **27**(10): 1607-1614.

Horning, S. J. and S. A. Rosenberg (1984). "The natural history of initially untreated low-grade non-Hodgkin's lymphomas." N Engl J Med **311**(23): 1471-1475.

Hoskin, P. J., A. A. Kirkwood, B. Popova, P. Smith, M. Robinson, E. Gallop-Evans, S. Coltart, T. Illidge, K. Madhavan, C. Brammer, P. Diez, A. Jack and I. Syndikus (2014). "4 Gy versus 24 Gy radiotherapy for patients with indolent lymphoma (FORT): a randomised phase 3 non-inferiority trial." The Lancet Oncology **15**(4): 457-463.

Ishida, Y., Y. Agata, K. Shibahara and T. Honjo (1992). "Induced expression of PD-1, a novel member of the immunoglobulin gene superfamily, upon programmed cell death." EMBO J **11**(11): 3887-3895.

Johnson, P. W., A. Z. Rohatiner, J. S. Whelan, C. G. Price, S. Love, J. Lim, J. Matthews, A. J. Norton, J. A. Amess and T. A. Lister (1995). "Patterns of survival in patients with recurrent follicular lymphoma: a 20-year study from a single center." J Clin Oncol **13**(1): 140-147.

Johnson, P. W., S. M. Watt, D. R. Betts, D. Davies, S. Jordan, A. J. Norton and T. A. Lister (1993). "Isolated follicular lymphoma cells are resistant to apoptosis and can be grown in vitro in the CD40/stromal cell system." Blood **82**(6): 1848-1857.

Johnston, R. J., A. C. Poholek, D. DiToro, I. Yusuf, D. Eto, B. Barnett, A. L. Dent, J. Craft and S. Crotty (2009). "Bcl6 and Blimp-1 are reciprocal and antagonistic regulators of T follicular helper cell differentiation." Science **325**(5943): 1006-1010.

Kedmi, M., C. V. Hedvat, J. Maragulia, Z. Zhang and A. D. Zelenetz (2014). "Association of quantitative assessment of the intrafollicular proliferation index with outcome in follicular lymphoma." Br J Haematol **164**(5): 646-652.

Kiaii, S., A. J. Clear, A. G. Ramsay, D. Davies, A. Sangaralingam, A. Lee, M. Calaminici, D. S. Neuberg and J. G. Gribben (2013). "Follicular lymphoma cells induce changes in T-cell gene expression and function: potential impact on survival and risk of transformation." J Clin Oncol **31**(21): 2654-2661.

King, C. (2009). "New insights into the differentiation and function of T follicular helper cells." Nat Rev Immunol **9**(11): 757-766.

Kridel, R., L. H. Sehn and R. D. Gascoyne (2012). "Pathogenesis of follicular lymphoma." J Clin Invest **122**(10): 3424-3431.

Kroenke, M. A., D. Eto, M. Locci, M. Cho, T. Davidson, E. K. Haddad and S. Crotty (2012). "Bcl6 and Maf cooperate to instruct human follicular helper CD4 T cell differentiation." J Immunol **188**(8): 3734-3744.

Kupfer, A. and H. Kupfer (2003). "Imaging immune cell interactions and functions: SMACs and the Immunological Synapse." Semin Immunol **15**(6): 295-300.

Kuppers, R. (2005). "Mechanisms of B-cell lymphoma pathogenesis." Nat Rev Cancer **5**(4): 251-262.

Laurent, C., S. Muller, C. Do, T. Al-Saati, S. Allart, L. M. Larocca, S. Hohaus, S. Duchez, A. Quillet-Mary, G. Laurent, P. Brousset and S. Valitutti (2011). "Distribution, function, and prognostic value of cytotoxic T lymphocytes in follicular lymphoma: a 3-D tissue-imaging study." Blood **118**(20): 5371-5379.

Lee, A. M., A. J. Clear, M. Calaminici, A. J. Davies, S. Jordan, F. MacDougall, J. Matthews, A. J. Norton, J. G. Gribben, T. A. Lister and L. K. Goff (2006). "Number of CD4+ cells and location of forkhead box protein P3-positive cells in diagnostic follicular lymphoma tissue microarrays correlates with outcome." J Clin Oncol **24**(31): 5052-5059.

Leich, E., G. Ott and A. Rosenwald (2011). "Pathology, pathogenesis and molecular genetics of follicular NHL." Best Pract Res Clin Haematol **24**(2): 95-109.

Lenz, G., G. Wright, S. S. Dave, W. Xiao, J. Powell, H. Zhao, W. Xu, B. Tan, N. Goldschmidt, J. Iqbal, J. Vose, M. Bast, K. Fu, D. D. Weisenburger, T. C. Greiner, J. O. Armitage, A. Kyle, L. May, R. D. Gascoyne, J. M. Connors, G. Troen, H. Holte, S. Kvaloy, D. Dierickx, G. Verhoef, J. Delabie, E. B. Smeland, P. Jares, A. Martinez, A. Lopez-Guillermo, E. Montserrat, E. Campo, R. M. Braziel, T. P. Miller, L. M. Rimsza, J. R. Cook, B. Pohlman, J. Sweetenham, R. R. Tubbs, R. I. Fisher, E. Hartmann, A. Rosenwald, G. Ott, H. K. Muller-Hermelink, D. Wrench, T. A. Lister, E. S. Jaffe, W. H. Wilson, W. C. Chan and L. M. Staudt (2008). "Stromal gene signatures in large-B-cell lymphomas." N Engl J Med **359**(22): 2313-2323.

Limpens, J., R. Stad, C. Vos, C. de Vlaam, D. de Jong, G. J. van Ommen, E. Schuuring and P. M. Kluin (1995). "Lymphoma-associated translocation t(14;18) in blood B cells of normal individuals." Blood **85**(9): 2528-2536.

Linterman, M. A., A. Liston and C. G. Vinuesa (2012). "T-follicular helper cell differentiation and the co-option of this pathway by non-helper cells." Immunol Rev **247**(1): 143-159.

Linterman, M. A., W. Pierson, S. K. Lee, A. Kallies, S. Kawamoto, T. F. Rayner, M. Srivastava, D. P. Divekar, L. Beaton, J. J. Hogan, S. Fagarasan, A. Liston, K. G. Smith and C. G. Vinuesa (2011). "Foxp3+ follicular regulatory T cells control the germinal center response." Nat Med **17**(8): 975-982.

Lister, T. A., D. Crowther, S. B. Sutcliffe, E. Glatstein, G. P. Canellos, R. C. Young, S. A. Rosenberg, C. A. Coltman and M. Tubiana (1989). "Report of a committee convened to discuss the evaluation and staging of patients with Hodgkin's disease: Cotswolds meeting." J Clin Oncol **7**(11): 1630-1636.

Lossos, I. S. and R. D. Gascoyne (2011). "Transformation of follicular lymphoma." Best Pract Res Clin Haematol **24**(2): 147-163.

Ma, J., C. Zhu, B. Ma, J. Tian, S. E. Baidoo, C. Mao, W. Wu, J. Chen, J. Tong, M. Yang, Z. Jiao, H. Xu, L. Lu and S. Wang (2012). "Increased frequency of circulating follicular helper T cells in patients with rheumatoid arthritis." Clin Dev Immunol **2012**: 827480.

Maloney, D. G., A. J. Grillo-Lopez, C. A. White, D. Bodkin, R. J. Schilder, J. A. Neidhart, N. Janakiraman, K. A. Foon, T. M. Liles, B. K. Dallaire, K. Wey, I. Royston, T. Davis and R. Levy (1997). "IDEC-C2B8 (Rituximab) anti-CD20 monoclonal antibody therapy in patients with relapsed low-grade non-Hodgkin's lymphoma." Blood **90**(6): 2188-2195.

Marafioti, T., C. Copie-Bergman, M. Calaminici, J. C. Paterson, V. H. Shende, H. Liu, M. Baia, A. D. Ramsay, C. Agostinelli, J. Briere, A. Clear, M. Q. Du, P. P. Piccaluga, N. Masir, E. P. Nacheva, P. Sujobert, K. Shanmugam, T. M. Grogan, S. P. Brooks, A. Khwaja, K. Ardeshna, W. Townsend, S. A. Pileri, C. Haioun, D. Linch, J. G. Gribben, P. Gaulard and P. G. Isaacson (2013). "Another look at follicular lymphoma: immunophenotypic and molecular analyses identify distinct follicular lymphoma subgroups." Histopathology **62**(6): 860-875.

Marcus, R., A. Davies, K. Ando, W. Klapper, S. Opat, C. Owen, E. Phillips, R. Sangha, R. Schlag, J. F. Seymour, W. Townsend, M. Trneny, M. Wenger, G. Fingerle-Rowson, K. Rufibach, T. Moore, M. Herold and W. Hiddemann (2017). "Obinutuzumab for the First-Line Treatment of Follicular Lymphoma." N Engl J Med **377**(14): 1331-1344.

Marcus, R., K. Imrie, A. Belch, D. Cunningham, E. Flores, J. Catalano, P. Solal-Celigny, F. Offner, J. Walewski, J. Raposo, A. Jack and P. Smith (2005). "CVP chemotherapy plus rituximab compared with CVP as first-line treatment for advanced follicular lymphoma." Blood **105**(4): 1417-1423.

Marcus, R., K. Imrie, P. Solal-Celigny, J. V. Catalano, A. Dmoszynska, J. C. Raposo, F. C. Offner, J. Gomez-Codina, A. Belch, D. Cunningham, E. Wassner-Fritsch and G. Stein (2008). "Phase III study of R-CVP compared with cyclophosphamide, vincristine, and prednisone alone in patients with previously untreated advanced follicular lymphoma." J Clin Oncol **26**(28): 4579-4586.

Martinelli, G., S. F. Schmitz, U. Utiger, T. Cerny, U. Hess, S. Bassi, E. Okkinga, R. Stupp, R. Stahel, M. Heizmann, D. Vorobiof, A. Lohri, P. Y. Dietrich, E. Zucca and M. Ghielmini (2010). "Long-term follow-up of patients with follicular lymphoma receiving single-agent rituximab at two different schedules in trial SAKK 35/98." J Clin Oncol **28**(29): 4480-4484.

McDonnell, T. J. and S. J. Korsmeyer (1991). "Progression from lymphoid hyperplasia to high-grade malignant lymphoma in mice transgenic for the t(14; 18)." Nature **349**(6306): 254-256.

Meignan, M., S. Barrington, E. Itti, A. Gallamini, C. Haioun and A. Polliack (2014). "Report on the 4th International Workshop on Positron Emission Tomography in Lymphoma held in Menton, France, 3-5 October 2012." Leuk Lymphoma **55**(1): 31-37.

Merli, M., A. Ferrario, C. Basilico, M. Maffioli, D. Caramazza, L. Appio, L. Arcaini and F. Passamonti (2013). "Novel agents in indolent lymphomas." Ther Adv Hematol **4**(2): 133-148.

Montoto, S., P. Corradini, M. Dreyling, M. Ghielmini, E. Kimby, A. Lopez-Guillermo, S. Mackinnon, R. E. Marcus, G. Salles, H. C. Schouten, A. Sureda and P. Dreger (2013). "Indications for hematopoietic stem cell transplantation in patients with follicular lymphoma: a consensus project of the EBMT-Lymphoma Working Party." Haematologica **98**(7): 1014-1021.

Montoto, S., A. J. Davies, J. Matthews, M. Calaminici, A. J. Norton, J. Amess, S. Vinnicombe, R. Waters, A. Z. Rohatiner and T. A. Lister (2007). "Risk and clinical implications of transformation of follicular lymphoma to diffuse large B-cell lymphoma." J Clin Oncol **25**(17): 2426-2433.

Morschhauser, F., J. F. Seymour, P. Feugier, F. Offner, A. Lopez-Guillermo, R. Bouabdallah, L. M. Pedersen, P. Brice, D. Belada, L. Xerri and G. Salles (2011). "Impact of induction chemotherpay regimen on response, safety and outcome in the PRIMA study." Annals of Oncology **22**(Supplement 4): iv89.

Mossner, E., P. Brunker, S. Moser, U. Puntener, C. Schmidt, S. Herter, R. Grau, C. Gerdes, A. Nopora, E. van Puijenbroek, C. Ferrara, P. Sondermann, C. Jager, P. Strein, G. Fertig, T. Friess, C. Schull, S. Bauer, J. Dal Porto, C. Del Nagro, K. Dabbagh, M. J. Dyer, S. Poppema, C. Klein and P. Umana (2010). "Increasing the efficacy of CD20 antibody therapy through the engineering of a new type II anti-CD20 antibody with enhanced direct and immune effector cell-mediated B-cell cytotoxicity." Blood **115**(22): 4393-4402.

Myklebust, J. H., J. M. Irish, J. Brody, D. K. Czerwinski, R. Houot, H. E. Kohrt, J. Timmerman, J. Said, M. R. Green, J. Delabie, A. Kolstad, A. A. Alizadeh and R. Levy (2013). "High PD-1 expression and suppressed cytokine signaling distinguish T cells infiltrating follicular lymphoma tumors from peripheral T cells." Blood **121**(8): 1367-1376.

Nazarov, V. I., M. V. Pogorelyy, E. A. Komech, I. V. Zvyagin, D. A. Bolotin, M. Shugay, D. M. Chudakov, Y. B. Lebedev and I. Z. Mamedov (2015). "tcR: an R package for T cell receptor repertoire advanced data analysis." BMC Bioinformatics **16**: 175.

Ng, S. Y. and M. S. Davids (2014). "Selective Bcl-2 inhibition to treat chronic lymphocytic leukemia and non-Hodgkin lymphoma." Clin Adv Hematol Oncol **12**(4): 224-229.

Nomi, T., M. Sho, T. Akahori, K. Hamada, A. Kubo, H. Kanehiro, S. Nakamura, K. Enomoto, H. Yagita, M. Azuma and Y. Nakajima (2007). "Clinical significance and therapeutic potential of the programmed death-1 ligand/programmed death-1 pathway in human pancreatic cancer." Clin Cancer Res **13**(7): 2151-2157.

Nussenzweig, A. and M. C. Nussenzweig (2010). "Origin of chromosomal translocations in lymphoid cancer." Cell **141**(1): 27-38.

Nutt, S. L. and D. M. Tarlinton (2011). "Germinal center B and follicular helper T cells: siblings, cousins or just good friends?" Nat Immunol **131**(6): 472-477.

Okosun, J., C. Bodor, J. Wang, S. Araf, C. Y. Yang, C. Pan, S. Boller, D. Cittaro, M. Bozek, S. Iqbal, J. Matthews, D. Wrench, J. Marzec, K. Tawana, N. Popov, C. O'Riain, D. O'Shea, E. Carlotti, A. Davies, C. H. Lawrie, A. Matolcsy, M. Calaminici, A. Norton, R. J. Byers, C. Mein, E. Stupka, T. A. Lister, G. Lenz, S. Montoto, J. G. Gribben, Y. Fan, R. Grosschedl, C. Chelala and J. Fitzgibbon (2014). "Integrated genomic analysis identifies recurrent mutations and evolution patterns driving the initiation and progression of follicular lymphoma." Nat Genet **46**(2): 176-181.

Pangault, C., P. Ame-Thomas, P. Ruminy, D. Rossille, G. Caron, M. Baia, J. De Vos, M. Roussel, C. Monvoisin, T. Lamy, H. Tilly, P. Gaulard, K. Tarte and T. Fest (2010). "Follicular lymphoma cell niche: identification of a preeminent IL-4-dependent T(FH)-B cell axis." Leukemia **24**(12): 2080-2089.

Pardoll, D. and C. Drake (2012). "Immunotherapy earns its spot in the ranks of cancer therapy." J Exp Med **209**(2): 201-209.

Pardoll, D. M. (2012). "The blockade of immune checkpoints in cancer immunotherapy." Nat Rev Cancer **12**(4): 252-264.

Pasqualucci, L., G. Bhagat, M. Jankovic, M. Compagno, P. Smith, M. Muramatsu, T. Honjo, H. C. Morse, 3rd, M. C. Nussenzweig and R. Dalla-Favera (2008). "AID is required for germinal center-derived lymphomagenesis." Nat Genet **40**(1): 108-112.

Pasqualucci, L., H. Khiabanian, M. Fangazio, M. Vasishtha, M. Messina, A. B. Holmes, P. Ouillette, V. Trifonov, D. Rossi, F. Tabbo, M. Ponzoni, A. Chadburn, V. V. Murty, G. Bhagat, G. Gaidano, G. Inghirami, S. N. Malek, R. Rabadan and R. Dalla-Favera (2014). "Genetics of follicular lymphoma transformation." Cell Rep **6**(1): 130-140.

Pastore, A., V. Jurinovic, R. Kridel, E. Hoster, A. M. Staiger, M. Szczepanowski, C. Pott, N. Kopp, M. Murakami, H. Horn, E. Leich, A. A. Moccia, A. Mottok, A. Sunkavalli, P. Van Hummelen, M. Ducar, D. Ennishi, H. P. Shulha, C. Hother, J. M. Connors, L. H. Sehn, M. Dreyling, D. Neuberg, P. Moller, A. C. Feller, M. L. Hansmann, H. Stein, A. Rosenwald, G. Ott, W. Klapper, M. Unterhalt, W. Hiddemann, R. D. Gascoyne, D. M. Weinstock and O. Weigert (2015). "Integration of gene mutations in risk prognostication for patients receiving first-line immunochemotherapy for follicular lymphoma: a retrospective analysis of a prospective clinical trial and validation in a population-based registry." Lancet Oncol **16**(9): 1111-1122.

Patten, P. E., A. G. Buggins, J. Richards, A. Wotherspoon, J. Salisbury, G. J. Mufti, T. J. Hamblin and S. Devereux (2008). "CD38 expression in chronic lymphocytic leukemia is regulated by the tumor microenvironment." Blood **111**(10): 5173-5181.

Postow, M. A., J. Chesney, A. C. Pavlick, C. Robert, K. Grossmann, D. McDermott, G. P. Linette, N. Meyer, J. K. Giguere, S. S. Agarwala, M. Shaheen, M. S. Ernstoff, D. Minor, A. K. Salama, M. Taylor, P. A. Ott, L. M. Rollin, C. Horak, P. Gagnier, J. D. Wolchok and F. S. Hodi (2015). "Nivolumab and ipilimumab versus ipilimumab in untreated melanoma." N Engl J Med **372**(21): 2006-2017.

Pyo, J. S., G. Kang and J. Y. Kim (2016). "Prognostic role of PD-L1 in malignant solid tumors: a meta-analysis." Int J Biol Markers: 0.

Quezada, S. A. and K. S. Peggs (2013). "Exploiting CTLA-4, PD-1 and PD-L1 to reactivate the host immune response against cancer." Br J Cancer **108**(8): 1560-1565.

Rabkin, C. S., C. Hirt, S. Janz and G. Dolken (2008). "t(14;18) Translocations and risk of follicular lymphoma." J Natl Cancer Inst Monogr(39): 48-51.

Radford, J., A. Davies, G. Cartron, F. Morschhauser, G. Salles, R. Marcus, M. Wenger, G. Lei, E. Wassner-Fritsch and U. Vitolo (2013). "Obinutuzumab (GA101) plus CHOP or FC in relapsed/refractory follicular lymphoma: results of the GAUDI study (BO21000)." Blood **122**(7): 1137-1143.

Ramsay, A. G., A. J. Clear, G. Kelly, R. Fatah, J. Matthews, F. Macdougall, T. A. Lister, A. M. Lee, M. Calaminici and J. G. Gribben (2009). "Follicular lymphoma cells induce T-cell immunologic synapse dysfunction that can be repaired with lenalidomide: implications for the tumor microenvironment and immunotherapy." Blood **114**(21): 4713-4720.

Richendollar, B. G., B. Pohlman, P. Elson and E. D. Hsi (2011). "Follicular programmed death 1-positive lymphocytes in the tumor microenvironment are an independent prognostic factor in follicular lymphoma." Hum Pathol **42**(4): 552-557.

Robert, C., G. V. Long, B. Brady, C. Dutriaux, M. Maio, L. Mortier, J. C. Hassel, P. Rutkowski, C. McNeil, E. Kalinka-Warzocha, K. J. Savage, M. M. Hernberg, C. Lebbe, J. Charles, C. Mihalcioiu, V. Chiarion-Sileni, C. Mauch, F. Cognetti, A. Arance, H. Schmidt, D. Schadendorf, H. Gogas, L. Lundgren-Eriksson, C. Horak, B. Sharkey, I. M. Waxman, V. Atkinson and P. A. Ascierto (2015). "Nivolumab in previously untreated melanoma without BRAF mutation." N Engl J Med **372**(4): 320-330.

Robertson, D., K. Savage, J. S. Reis-Filho and C. M. Isacke (2008). "Multiple immunofluorescence labelling of formalin-fixed paraffin-embedded (FFPE) tissue." BMC Cell Biol **9**: 13.

Robins, H. S., P. V. Campregher, S. K. Srivastava, A. Wacher, C. J. Turtle, O. Kahsai, S. R. Riddell, E. H. Warren and C. S. Carlson (2009). "Comprehensive assessment of T-cell receptor beta-chain diversity in alphabeta T cells." Blood **114**(19): 4099-4107.

Rolf, J., S. E. Bell, D. Kovesdi, M. L. Janas, D. R. Soond, L. M. Webb, S. Santinelli, T. Saunders, B. Hebeis, N. Killeen, K. Okkenhaug and M. Turner (2010). "Phosphoinositide 3-kinase activity in T cells regulates the magnitude of the germinal center reaction." J Immunol **185**(7): 4042-4052.

Roulland, S., M. Faroudi, E. Mamessier, S. Sungalee, G. Salles and B. Nadel (2011). "Early steps of follicular lymphoma pathogenesis." Adv Immunol **111**: 1-46.

Roulland, S., R. S. Kelly, E. Morgado, S. Sungalee, P. Solal-Celigny, P. Colombat, N. Jouve, D. Palli, V. Pala, R. Tumino, S. Panico, C. Sacerdote, J. R. Quiros, C. A. Gonzales, M. J. Sanchez, M. Dorronsoro, C. Navarro, A. Barricarte, A. Tjonneland, A. Olsen, K. Overvad, F. Canzian, R. Kaaks, H. Boeing, D. Drogan, A. Nieters, F. Clavel-Chapelon, A. Trichopoulou, D. Trichopoulos, P. Lagiou, H. B. Bueno-de-Mesquita, P. H. Peeters, R. Vermeulen, G. Hallmans, B. Melin, S. Borgquist, J. Carlson, E. Lund, E. Weiderpass, K. T. Khaw, N. Wareham, T. J. Key, R. C. Travis, P. Ferrari, I. Romieu, E. Riboli, G. Salles, P. Vineis and B. Nadel (2014). "t(14;18) Translocation: A predictive blood biomarker for follicular lymphoma." J Clin Oncol **32**(13): 1347-1355.

Roulland, S., S. Sungalee, E. Morgado, E. Mamessier, E. Gregoire, G. Debroas, N. Jouve, C. Menard, P. Ruminy, E. Jaffe, C. Schiff, J. Hardwigsen, K. Tarte and B. Nadel (2013). "Iterative germinal centre re-entries of memory B cells with t(14;18) translocation and early steps of follicular lymphoma progression." Haematological Oncology **31** (S1): 97.

Rowley, J. D. (1988). "Chromosome studies in the non-Hodgkin's lymphomas: the role of the 14;18 translocation." J Clin Oncol **6**(5): 919-925.

Rummel, M. J., N. Niederle, G. Maschmeyer, G. A. Banat, U. von Grünhagen, C. Losem, D. Kofahl-Krause, G. Heil, M. Welslau, C. Balser, U. Kaiser, E. Weidmann, H. Dürk, H. Ballo, M. Stauch, F. Roller, J. Barth, D. Hoelzer, A. Hinke and W. Brugger (2013). "Bendamustine plus rituximab versus CHOP plus rituximab as first-line treatment for patients with indolent and mantle-cell lymphomas: an open-label, multicentre, randomised, phase 3 non-inferiority trial." The Lancet **381**(9873): 1203-1210.

Sage, P. T., L. M. Francisco, C. V. Carman and A. H. Sharpe (2013). "The receptor PD-1 controls follicular regulatory T cells in the lymph nodes and blood." Nat Immunol **14**(2): 152-161.

Salaverria, I. and R. Siebert (2011). "Follicular lymphoma grade 3B." Best Pract Res Clin Haematol **24**(2): 111-119.

Salles, G., N. Mounier, S. de Guibert, F. Morschhauser, C. Doyen, J. F. Rossi, C. Haioun, P. Brice, B. Mahe, R. Bouabdallah, B. Audhuy, C. Ferme, C. Dartigeas, P. Feugier, C. Sebban, L. Xerri and C. Foussard (2008). "Rituximab combined with chemotherapy and interferon in follicular lymphoma patients: results of the GELA-GOELAMS FL2000 study." Blood **112**(13): 4824-4831.

Salles, G., J. F. Seymour, F. Offner, A. Lopez-Guillermo, D. Belada, L. Xerri, P. Feugier, R. Bouabdallah, J. V. Catalano, P. Brice, D. Caballero, C. Haioun, L. M. Pedersen, A. Delmer, D. Simpson, S. Leppa, P. Soubeyran, A. Hagenbeek, O. Casasnovas, T. Intragumtornchai, C. Ferme, M. G. da Silva, C. Sebban, A. Lister, J. A. Estell, G. Milone, A. Sonet, M. Mendila, B. Coiffier and H. Tilly (2011). "Rituximab maintenance for 2 years in patients with high tumour burden follicular lymphoma responding to rituximab plus chemotherapy (PRIMA): a phase 3, randomised controlled trial." Lancet **377**(9759): 42-51.

Salles, G. A., F. Morschhauser, P. Solal-Celigny, C. Thieblemont, T. Lamy, H. Tilly, E. Gyan, G. Lei, M. Wenger, E. Wassner-Fritsch and G. Cartron (2013). "Obinutuzumab (GA101) in patients with relapsed/refractory indolent non-Hodgkin lymphoma: results from the phase II GAUGUIN study." J Clin Oncol **31**(23): 2920-2926.

Samols, M. A., N. E. Smith, J. M. Gerber, M. Vuica-Ross, C. D. Gocke, K. H. Burns, M. J. Borowitz, T. C. Cornish and A. S. Duffield (2013). "Software-automated counting of Ki-67 proliferation index correlates with pathologic grade and disease progression of follicular lymphomas." Am J Clin Pathol **140**(4): 579-587.

Sander, B., D. de Jong, A. Rosenwald, W. Xie, O. Balague, M. Calaminici, J. Carreras, P. Gaulard, J. Gribben, A. Hagenbeek, M. J. Kersten, T. J. Molina, A. Lee, S. Montes-Moreno, G. Ott, J. Raemaekers, G. Salles, L. Sehn, C. Thorns, B. E. Wahlin, R. D. Gascoyne and E. Weller (2014). "The reliability of immunohistochemical analysis of the tumor microenvironment in follicular lymphoma: a validation study from the Lunenburg Lymphoma Biomarker Consortium." Haematologica **99**(4): 715-725.

Sant, M., P. Minicozzi, M. Mounier, L. A. Anderson, H. Brenner, B. Holleczek, R. Marcos-Gragera, M. Maynadié, A. Monnereau, G. Osca-Gelis, O. Visser and R. De Angelis (2014). "Survival for haematological malignancies in Europe between 1997 and 2008 by region and age: results of EUROCARE-5, a population-based study." The Lancet Oncology **15**(9): 931-942.

Schuler, F., L. Dolken, C. Hirt, T. Kiefer, T. Berg, G. Fusch, K. Weitmann, W. Hoffmann, C. Fusch, S. Janz, C. S. Rabkin and G. Dolken (2009). "Prevalence and frequency of circulating t(14;18)-MBR translocation carrying cells in healthy individuals." Int J Cancer **124**(4): 958-963.

Shaffer, A. L., 3rd, R. M. Young and L. M. Staudt (2012). "Pathogenesis of human B cell lymphomas." Annu Rev Immunol **30**: 565-610.

Sherwood, A. M., R. O. Emerson, D. Scherer, N. Habermann, K. Buck, J. Staffa, C. Desmarais, N. Halama, D. Jaeger, P. Schirmacher, E. Herpel, M. Kloor, A. Ulrich, M. Schneider, C. M. Ulrich and H. Robins (2013). "Tumor-infiltrating lymphocytes in colorectal tumors display a diversity of T cell receptor sequences that differ from the T cells in adjacent mucosal tissue." Cancer Immunol Immunother **62**(9): 1453-1461.

Shulman, Z., A. D. Gitlin, S. Targ, M. Jankovic, G. Pasqual, M. C. Nussenzweig and G. D. Victora (2013). "T follicular helper cell dynamics in germinal centers." Science **341**(6146): 673-677.

Simpson, N., P. A. Gatenby, A. Wilson, S. Malik, D. A. Fulcher, S. G. Tangye, H. Manku, T. J. Vyse, G. Roncador, G. A. Huttley, C. C. Goodnow, C. G. Vinuesa and M. C. Cook (2010). "Expansion of circulating T cells resembling follicular helper T cells is a fixed phenotype that identifies a subset of severe systemic lupus erythematosus." Arthritis Rheum **62**(1): 234-244.

Smith, S. M. (2013). "Dissecting follicular lymphoma: high versus low risk." Hematology Am Soc Hematol Educ Program **2013**: 561-567.

Solal-Celigny, P., P. Roy, P. Colombat, J. White, J. O. Armitage, R. Arranz-Saez, W. Y. Au, M. Bellei, P. Brice, D. Caballero, B. Coiffier, E. Conde-Garcia, C. Doyen, M. Federico, R. I. Fisher, J. F. Garcia-Conde, C. Guglielmi, A. Hagenbeek, C. Haioun, M. LeBlanc, A. T. Lister, A. Lopez-Guillermo, P. McLaughlin, N. Milpied, P. Morel, N. Mounier, S. J. Proctor, A. Rohatiner, P. Smith, P. Soubeyran, H. Tilly, U. Vitolo, P. L. Zinzani, E. Zucca and E. Montserrat (2004). "Follicular lymphoma international prognostic index." Blood **104**(5): 1258-1265.

Specht, L. (2014). "Radiotherapy for indolent lymphomas: how much is enough?" The Lancet Oncology **15**(4): 372-374.

Sungalee, S., E. Mamessier, E. Morgado, E. Gregoire, P. Z. Brohawn, C. A. Morehouse, N. Jouve, C. Monvoisin, C. Menard, G. Debroas, M. Faroudi, V. Mechin, J. M. Navarro, C. Drevet, F. C. Eberle, L. Chasson, F. Baudimont, S. J. Mancini, J. Tellier, J. M. Picquenot, R. Kelly, P. Vineis, P. Ruminy, B. Chetaille, E. S. Jaffe, C. Schiff, J. Hardwigsen, D. A. Tice, B. W. Higgs, K. Tarte, B. Nadel and S. Roulland (2014). "Germinal center reentries of BCL2-overexpressing B cells drive follicular lymphoma progression." J Clin Invest **124**(12): 5337-5351.

Taskinen, M., M. L. Karjalainen-Lindsberg, H. Nyman, L. M. Eerola and S. Leppa (2007). "A high tumor-associated macrophage content predicts favorable outcome in follicular lymphoma patients treated with rituximab and cyclophosphamide-doxorubicin-vincristine-prednisone." Clin Cancer Res **13**(19): 5784-5789.

Topalian, S. L., F. S. Hodi, J. R. Brahmer, S. N. Gettinger, D. C. Smith, D. F. McDermott, J. D. Powderly, R. D. Carvajal, J. A. Sosman, M. B. Atkins, P. D. Leming, D. R. Spigel, S. J. Antonia, L. Horn, C. G. Drake, D. M. Pardoll, L. Chen, W. H. Sharfman, R. A. Anders, J. M. Taube, T. L. McMiller, H. Xu, A. J. Korman, M. Jure-Kunkel, S. Agrawal, D. McDonald, G. D. Kollia, A. Gupta, J. M. Wigginton and M. Sznol (2012). "Safety, activity, and immune correlates of anti-PD-1 antibody in cancer." N Engl J Med **366**(26): 2443-2454.

Tuscano, J. M., M. Dutia, K. Chee, A. Brunson, C. Reed-Pease, M. Abedi, J. Welborn and R. T. O'Donnell (2014). "Lenalidomide plus rituximab can produce durable clinical responses in patients with relapsed or refractory, indolent non-Hodgkin lymphoma." Br J Haematol **165**(3): 375-381.

van Oers, M. H., M. Van Glabbeke, L. Giurgea, R. Klasa, R. E. Marcus, M. Wolf, E. Kimby, M. van t Veer, A. Vranovsky, H. Holte and A. Hagenbeek (2010). "Rituximab maintenance treatment of relapsed/resistant follicular non-Hodgkin's lymphoma: long-term outcome of the EORTC 20981 phase III randomized intergroup study." J Clin Oncol **28**(17): 2853-2858.

Victora, G. D. and M. C. Nussenzweig (2012). "Germinal centers." Annu Rev Immunol **30**: 429-457.

Wahlin, B. E., M. Aggarwal, S. Montes-Moreno, L. F. Gonzalez, G. Roncador, L. Sanchez-Verde, B. Christensson, B. Sander and E. Kimby (2010). "A unifying microenvironment model in follicular lymphoma: outcome is predicted by programmed death-1--positive, regulatory, cytotoxic, and helper T cells and macrophages." Clin Cancer Res **16**(2): 637-650.

Wahlin, B. E., O. E. Yri, E. Kimby, H. Holte, J. Delabie, E. B. Smeland, C. Sundstrom, B. Christensson and B. Sander (2012). "Clinical significance of the WHO grades of follicular lymphoma in a population-based cohort of 505 patients with long follow-up times." Br J Haematol **156**(2): 225-233.

Wang, M., N. Fowler, N. Wagner-Bartak, L. Feng, J. Romaguera, S. S. Neelapu, F. Hagemeister, M. Fanale, Y. Oki, B. Pro, J. Shah, S. Thomas, A. Younes, C. Hosing, L. Zhang, K. J. Newberry, M. Desai, N. Cheng, M. Badillo, M. Bejarano, Y. Chen, K. H. Young, R. Champlin, L. Kwak and L. Fayad (2013). "Oral

lenalidomide with rituximab in relapsed or refractory diffuse large cell, follicular and transformed lymphoma: a phase II clinical trial." Leukemia **27**(9): 1902-1909.

Westin, J. R., F. Chu, M. Zhang, L. E. Fayad, L. W. Kwak, N. Fowler, J. Romaguera, F. Hagemeister, M. Fanale, F. Samaniego, L. Feng, V. Baladandayuthapani, Z. Wang, W. Ma, Y. Gao, M. Wallace, L. M. Vence, L. Radvanyi, T. Muzzafar, R. Rotem-Yehudar, R. E. Davis and S. S. Neelapu (2014). "Safety and activity of PD1 blockade by pidilizumab in combination with rituximab in patients with relapsed follicular lymphoma: a single group, open-label, phase 2 trial." The Lancet Oncology **15**(1): 69-77.

Williams, G. H. and K. Stoeber (2007). "Cell cycle markers in clinical oncology." Curr Opin Cell Biol **19**(6): 672-679.

Wu, C., Y. Zhu, J. Jiang, J. Zhao, X. G. Zhang and N. Xu (2006). "Immunohistochemical localization of programmed death-1 ligand-1 (PD-L1) in gastric carcinoma and its clinical significance." Acta Histochem **108**(1): 19-24.

Xerri, L., B. Chetaille, N. Serriari, C. Attias, Y. Guillaume, C. Arnoulet and D. Olive (2008). "Programmed death 1 is a marker of angioimmunoblastic T-cell lymphoma and B-cell small lymphocytic lymphoma/chronic lymphocytic leukemia." Hum Pathol **39**(7): 1050-1058.

Yang, Z. Z., D. M. Grote, S. C. Ziesmer, B. Xiu, A. J. Novak and S. M. Ansell (2015). "PD-1 expression defines two distinct T-cell sub-populations in follicular lymphoma that differentially impact patient survival." Blood Cancer J **5**: e281.

Yang, Z. Z., A. J. Novak, M. J. Stenson, T. E. Witzig and S. M. Ansell (2006). "Intratumoral CD4+CD25+ regulatory T-cell-mediated suppression of infiltrating CD4+ T cells in B-cell non-Hodgkin lymphoma." Blood **107**(9): 3639-3646.

Yang, Z. Z., A. J. Novak, S. C. Ziesmer, T. E. Witzig and S. M. Ansell (2006). "Attenuation of CD8(+) T-cell function by CD4(+)CD25(+) regulatory T cells in B-cell non-Hodgkin's lymphoma." Cancer Res **66**(20): 10145-10152.

Zou, W. (2005). "Immunosuppressive networks in the tumour environment and their therapeutic relevance." Nat Rev Cancer **5**(4): 263-274.